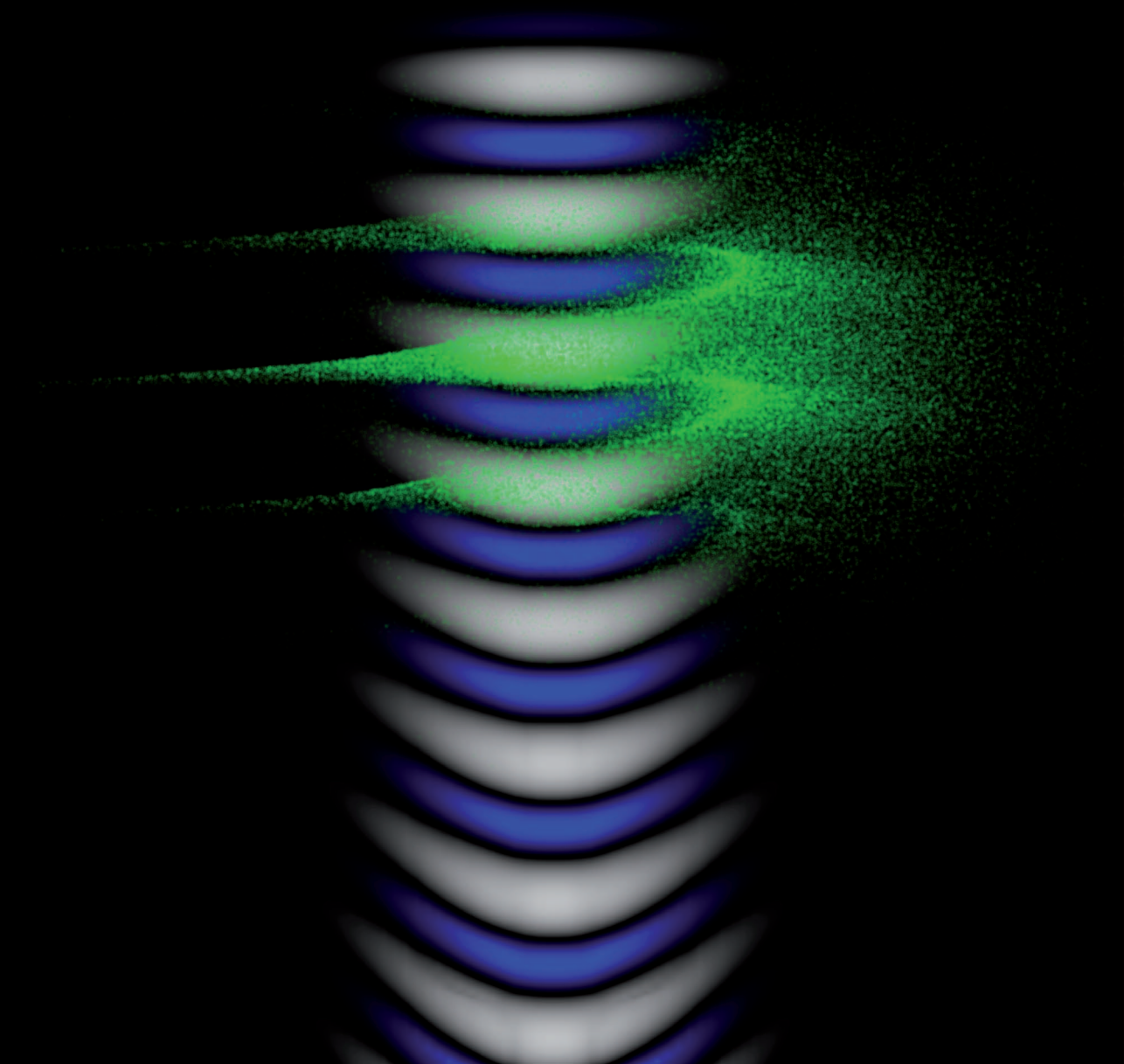# Mark J.H. Luttikhof

Theoretical investigation of external injection schemes for laser wakefield acceleration

Theoretical investigation of external injection schemes for laser wakefield acceleration

by

Mark Jan Hendrik Luttikhof

Samenstelling van de promotiecommissie:

Voorzitter & secretaris:

prof. dr. ir. W.P.M. van Swaaij   University of Twente, The Netherlands

Promotor:

prof. dr. K.-J. Boller   University of Twente, The Netherlands

Assistent-promotor:

dr. A.G. Khachatryan   University of Twente, The Netherlands

Leden:

prof. dr. J.L. Herek   University of Twente, The Netherlands
prof. dr. F. Bijkerk   University of Twente, The Netherlands
prof. dr. ir. H.J.W. Zandvliet   University of Twente, The Netherlands
prof. dr. W.J. Briels   University of Twente, The Netherlands
prof. dr. S. Brandenburg   University of Groningen, The Netherlands

Front cover illustration: Injection at an angle (see chapter 4)
Back cover illustration: Injection behind the laser pulse (see chapter 3)

Theoretical investigation of external injection schemes for laser wakefield acceleration

Proefschrift

ter verkrijging van
de graad van doctor aan de Universiteit Twente,
op gezag van de rector magnificus,
prof. dr. H. Brinksma
volgens besluit van het College voor Promoties
in het openbaar te verdedigen
op vrijdag 17 september 2010 om 15.00 uur

door

Mark Jan Hendrik Luttikhof
geboren op 31 oktober 1980
te Hellendoorn

Dit proefschrift is goedgekeurd door:

De promotor: prof. dr. K.-J. Boller
De assistent-promotor: dr. A.G. Khachatryan

List of publications

Journals

M.J.H. Luttikhof, A.G. Khachatryan, F.A. van Goor and K.-J. Boller, *Ultra-relativistic attosecond electron bunches from laser wakefield accelerators*, Physical Review Letters, accepted for publication

R.A. Loch, T. Ceccotti, F. Quéré, H. George, F. Reau, P.D'Oliveira, M.J.H. Luttikhof, F. Bijkerk, Ph. Martin and K.-J. Boller, *Ion acceleration in the transparent regime and the critical influence of the plasma scale length*, in preparation

M.J.H. Luttikhof, A.G. Khachatryan, F.A. van Goor and K.-J. Boller, *Generation of stable ultra-relativistic attosecond electron bunches via the laser wakefield acceleration mechanism*, arXiv:0906.3372 (2009)

M.J.H. Luttikhof, A.G. Khachatryan, F.A. van Goor, K.-J. Boller and P. Mora, *Electron bunch injection at an angle into a laser wakefield*, Laser and Particle Beams 27, 69 (2009)

A. Irman, M.J.H. Luttikhof, A.G. Khachatryan, F.A. van Goor, J.W.J. Verschuur, H.M.J. Bastiaens and K.-J. Boller, *Design and simulation of laser wakefield acceleration with external bunch injection in front of the laser pulse*, Journal of Applied Physics 102, 024513 (2007)

M.J.H. Luttikhof, A.G. Khachatryan, F.A. van Goor and K.-J. Boller, *The effect of the vacuum-plasma transition and an injection angle on electron-bunch injection into a laser wakefield*, Physics of Plasmas 14, 083101 (2007)

A.G. Khachatryan, M.J.H. Luttikhof, F.A. van Goor and K.-J. Boller, *Effect of the ponderomotive scattering and injection position on electron-bunch injection into a laser wakefield*, Applied Physics B 86, 41 (2007)

A.G. Khachatryan, M.J.H. Luttikhof, A. Irman, F.A. van Goor, J.W.J. Verschuur, H.M.J. Bastiaens and K.-J. Boller, *Conceptual design of a laser wakefield acceleration experiment with external bunch injection*, Nuclear Instruments and Methods in Physical Research Section A 566, 244 (2006)

Conferences

M.J.H. Luttikhof, A.G. Khachatryan, F.A. van Goor and K.-J. Boller, *Attosecond electron bunches from laser wakefield accelerators*, Oral presentation, Conference on Laser and Electro-Optics / International Quantum Electronics Conference (CLEO/QELS), San Jose, United States of America, 16-21 May 2010

M.J.H. Luttikhof, A.G. Khachatryan, A. Irman, F.A. van Goor and K.-J. Boller, *Attosecond electron bunches from a laser wakefield accelerator*, Poster presentation, Physics@FOM, Veldhoven, The Netherlands, 19-20 January 2010

M.J.H. Luttikhof, A.G. Khachatryan, A. Irman, F.A. van Goor and K.-J. Boller, *Attosecond electron bunch formation in a laser wakefield accelerator*, Poster presentation, Mesa+ Meeting, Enschede, The Netherlands, 22 September 2009

M.J.H. Luttikhof, A.G. Khachatryan, A. Irman, F.A. van Goor and K.-J. Boller, *On the theory of channel-guided laser wakefield accelerators*, Oral presentation, Laser and Plasma Accelerators Workshop, Kardamili, Greece, 22-26 June 2009

B. Zandt, M.W. Hendrikx, R.A. Loch, H.M.J. Bastiaens, A. Irman, M.J.H. Luttikhof, F.A. van Goor, A.G. Khachatryan, F. Bijkerk and K.-J. Boller, *Enhancement of high harmonic generation in a helium-xenon gas mixture*, Poster presentation, 21st NNV/CPS - Plasma Physics & Radiation Technology Symposium, Lunteren, The Netherlands, 3-4 March 2009

M.J.H. Luttikhof, A.G. Khachatryan, A. Irman, F.A. van Goor and K.-J. Boller, *A novel way of external injection of electrons into a laser wakefield*, Poster presentation, Physics@FOM, Veldhoven, The Netherlands, 20-21 January 2009

M.J.H. Luttikhof, A. Irman, A.G. Khachatryan, F.A. van Goor, K.-J. Boller, *External injection: The effects of the vacuum-plasma transition, laser pulse dynamics and an injection angle*, Oral and poster presentation, EuroLEAP annual meeting, Eindhoven, The Netherlands, 10-11 april 2008

M.J.H. Luttikhof, A. Irman, W.O. Rekers, A.G. Khachatryan, F.A. van Goor, R.A. Loch, J.W.J. Verschuur, H.M.J. Bastiaens, F. Bijkerk and K.-J. Boller, *Recent progress of theory and experiments on laser wakefield acceleration at the University of Twente*, Poster presentation, 20th NNV/CPS - Plasma Physics & Radiation Technology Symposium, Lunteren, The Netherlands, 4-5 March, 2008

M.W. Hendrikx, R.A. Loch, H.M.J. Bastiaens, A. Irman, M.J.H. Luttikhof, F.A. van Goor, A.G. Khachatryan, P.J.M. Peters, F. Bijkerk and K.-J. Boller, *Enhanced high harmonic generation from gas mixtures*, Poster presentation, 20th NNV/CPS - Plasma Physics & Radiation Technology Symposium, Lunteren, The Netherlands, 4-5 March 2008

R.A. Loch, M.J.H. Luttikhof, M.W. Hendrikx, A. Irman, A.G. Khachatryan, F.A. van Goor, H.M.J. Bastiaens, P.J.M. Peters, F. Bijkerk and K.-J. Boller, *Ultra-high intensity laser-plasma interactions*, Poster presentation, 1st International Conference on Ultra-intense Laser Interaction Sciences, Bordeaux, France, 1-5 October 2007

M.J.H. Luttikhof, R.A. Loch, M.W. Hendrikx, A. Irman, A.G. Khachatryan, F.A. van Goor, H.M.J. Bastiaens, P.J.M. Peters, F. Bijkerk and K.-J. Boller, *High energy particles and coherent X-rays for high resolution observations*, Poster presentation, Mesa+ Meeting, Enschede, The Netherlands, 11 September 2007

A. Irman, M.J.H. Luttikhof, A.G. Khachatryan, F.A. van Goor, J.W.J. Verschuur, H.M.J. Bastiaens and K.-J. Boller, *Design and simulation of laser wakefield acceleration with external electron bunch injection in front of the laser pulse*, Poster presentation, Laser and plasma accelerators workshop, Azores, Portugal, 9-13 July 2007

A. Irman, M.J.H. Luttikhof, A.G. Khachatryan, F.A. van Goor, J.W.J. Verschuur, H.M.J. Bastiaens and K.-J. Boller, *Design and simulation of laser wakefield acceleration with external bunch injection in front of the laser pulse*, Poster presentation, Emerging sources workshop, Lund, Sweden, 11-13 June 2007

A. Irman, M.J.H. Luttikhof, A.G. Khachatryan, F.A. van Goor, J.W.J. Verschuur, H.M.J. Bastiaens and K.-J. Boller, *Design and simulation of laser wakefield acceleration with external bunch injection in front of the laser pulse*, Poster presentation, 19th NNV/CPS - Plasma Physics & Radiation Technology Symposium, Lunteren, The Netherlands, 7-8 March 2007

A. Irman, M.J.H. Luttikhof, A.G. Khachatryan, F.A. van Goor, J.W.J. Verschuur, H.M.J. Bastiaens and K.-J. Boller, *Electron bunch transportation for a laser wakefield experiment at the University of Twente*, Poster presentation, 18th NNV/CPS - Plasma Physics & Radiation Technology Symposium, Lunteren, The Netherlands, 22-23 March 2006

A.G. Khachatryan, F.A. van Goor, M.J.H. Luttikhof, A. Irman, J.W.J. Verschuur, H.M.J. Bastiaens and K.-J. Boller, *Conceptual design of a laser wakefield experiment with external bunch injection in front of the laser pulse*, Oral presentation, International Workshop "High energy electron acceleration using plasmas (HEEAUP)", Paris, France, 18 June 2005

Summary

The strength of the maximum electric field available in state-of-the-art particle accelerators using radio-frequency (rf) technology is constrained to a fundamental limit of 100 MV/m at most. Therefore, increasing the length of the accelerator is the only way to scale the energy to higher values. This is why state-of-the-art rf accelerators are many kilometers in size with little potential for further increases in energy. Because of these limitations, researchers are now investigating fundamentally different concepts of particle acceleration which would allow the reduction of the size and complexity of particle accelerators.

Laser wakefield acceleration [1–3] is a radically new approach for particle acceleration, that builds on the huge electric fields that a plasma wave can provide. In this approach, an ultra-short laser pulse of high intensity is sent through an ionized, plasma medium. At sufficient laser intensity, the radiation pressure of the pulse expels a significant number of plasma electrons from the beam path while the ions remain at an almost fixed position due to their higher mass. This leads to a traveling charge separation wave, also called the plasma wave, driven by the laser pulse. Associated with the charge separation wave is a traveling electric field distribution called the laser wakefield, that provides huge field strengths of up to hundreds of GV/m. Such field strengths offer the potential to accelerate particles thousands of times more quickly, over much shorter distances, or towards much higher energies, than that which is currently possible with conventional rf accelerators.

However, current experiments demonstrating the basic working of laser wakefield acceleration suffer from a fundamental lack of control, large shot-to-shot fluctuations and also poor scalability. This is due to the fact that in all of the current schemes the injection of electrons and their subsequent acceleration is intrinsically coupled, because these schemes are based on nonlinear dynamics such as wavebreaking in order to inject electrons from the plasma background itself. This is why there is now a growing perception that electron bunches need to be injected from a separate external accelerator, so that the injection can be controlled and laser wakefield accelerators can live up to their potential.

This thesis provides a theoretical investigation into the injection of electron bunches from an external accelerator and studies the influence of the timing and direction of the injection on laser wakefield acceleration. To investigate situations that lie in the range of current technological feasibility, we focus on

injection from conventional rf accelerators. We present and investigate three methods in which the relatively long bunches from rf accelerators can be injected into a wakefield in such a way that the accelerated bunches attain a high quality. These schemes differ in their timing and thus in the position of the injected bunch with regard to the laser pulse. We investigated electron bunch injection behind the drive laser pulse, at an angle with the laser's propagation direction, and in front of the laser pulse.

For the first method, we consider that the electron bunch from the rf accelerator is focused and injected with several MeV initial kinetic energy into a plasma channel, immediately behind the drive laser pulse. In this approach, generally considered as the only suitable standard injection method, the electron bunch enters the plasma, where it immediately experiences the wakefield trailing the drive laser pulse. Once in the wakefield, the bunch will be sliced into several smaller bunches, each with a duration of a few femtoseconds and a transverse size of a few micrometer. Our investigations, while reproducing the standard approach, show that this scheme can suffer from two problems which have been overlooked thus far and which we address for the first time. The first problem is ponderomotive scattering of the bunch off the drive laser pulse in the vacuum in front of the plasma channel, i.e., before the bunch has even entered the plasma. The second problem arises from the circumstance that, other than has been assumed in all of the previous calculations, the plasma at the entrance of the accelerator does not form an infinitely sharp boundary with the surrounding vacuum. In reality, there is always a transition region of finite length within which the plasma density is varying from zero (in vacuum) to its full value (in the plasma channel). We have taken this transition region into account and have observed that the injected electrons experience an altering wakefield, due to a continuous change in the plasma wavelength with regard to the plasma density. We show that, especially for high laser intensities and low injection energies, ponderomotive scattering and the vacuum-plasma transition can strongly scatter the injected bunch before it even reaches the regular wakefield. From these investigations it can be concluded that moderate laser intensities and higher electron injection energies are required to obtain high quality accelerated bunches using this standard approach.

As a novel alternative to bunch injection behind the laser pulse, we propose a scheme where the bunch is injected into the wakefield at a small angle immediately behind the laser pulse. Thereby one effectively avoids any overlap of the bunch with the wakefield in the transition region. This avoids both the undesired effects of the ponderomotive scattering and of the vacuum-plasma transition region. In this scheme the wakefield will, as in the standard scheme, slice the injected, longer bunch into a train of smaller bunches separated by the plasma wavelength. An important advantage of this scheme is that it enables the injection of electron bunches with a wider transverse size. With standard injection behind the pulse (with zero angle), wider bunches can only be trapped in a smaller part, because the electrons injected farther away from the wakefield axis do not propagate through the transversely focusing regions of the

wakefield. On the other hand, the trapping of the electrons after injection at an angle requires higher laser intensities in the weakly nonlinear regime, and electrons that are injected with a higher energy.

A special case of injection at an angle is collinear injection (with zero angle, on the propagation axis of the drive laser), but with the electron bunch injected in front of the laser pulse. Temporally, the electron bunch is injected first and, due to its high group velocity, the laser pulse overtakes the electron bunch inside the plasma. In this case the wakefield compensates for the ponderomotive scattering. We show that when the laser pulse overtakes the electron bunch, a large fraction of the electrons can be trapped immediately behind the laser pulse at the accelerating slope of the wake. These electrons are all collected in the first accelerating phase of the wakefield where a compressed bunch builds up. Unlike the other schemes, a single bunch is formed. But otherwise the electron dynamics are very similar to those found in the injection at an angle, where the electrons move gradually into the wakefield. A demonstration experiment for injection in front of the laser pulse is currently being prepared at the University of Twente. Our calculations for the conceptual design predict that electron bunches with an energy of up to 0.7 GeV can be generated with an energy spread as low as 1%.

The final part of the thesis describes novel, ultrafast dynamics in laser wakefield accelerators. Previous experimental observations and theoretical investigations have shown that electron bunches can be generated with durations as short as a few femtoseconds. However, we predict that wakefield acceleration can generate significantly shorter bunches, with durations in the sub-femtosecond (attosecond) range. We have identified the fact that the radius of a femtosecond bunch undergoes ultrafast betatron oscillations with a higher frequency in the front of the bunch than in its tail as being the mechanism responsible for this phenomenon. Attosecond bunches were found to be formed over a broad range of parameters and their formation appeared to be independent of the selected injection mechanism. We investigated the bunch dynamics over a wider range of parameters and concluded that the formation of attosecond bunches is a very general, intrinsic feature of laser wakefield accelerators. As important precondition enabling the attosecond bunches to be applied we show that, after the formation, the bunches propagate over appreciable distances of many tens of centimeters without losing their attosecond structure.

Samenvatting

De sterkte van het maximale elektrische veld dat beschikbaar is in moderne deeltjesversnellers, die gebruik maken van radiofrequentie (rf) technologie, is beperkt tot een fundamentele limiet van 100 MV/m. Daarom is het langer maken van de versneller de enige mogelijkheid om de energie van de deeltjes te laten toenemen. Dit is de reden dat moderne rf versnellers vele kilometers lang zijn en maar weinig potentie hebben om de energie nog verder te laten groeien. Onderzoekers proberen fundamenteel nieuwe concepten te vinden voor het versnellen van deeltjes die niet gelimiteerd zijn en die het mogelijk maken de afmeting en complexiteit van deeltjesversnellers te verminderen.

Laser hekgolf versnelling (Engels: Laser wakefield acceleration) [1–3] is een radicaal nieuwe benadering voor het versnellen van deeltjes, die gebruik maakt van de reusachtige velden veroorzaakt door een plasma golf. Bij deze methode wordt een ultrakorte laserpuls met een hoge intensiteit door een geïoniseerd plasmamedium gestuurd. Wanneer de intensiteit van de laser hoog genoeg is wordt, door de stralingsdruk van de puls, een beduidende hoeveelheid elektronen in het plasma van het pad van de puls verdreven, terwijl de ionen praktisch op dezelfde positie blijven vanwege hun grotere massa. Dit leidt tot een voortbewegende golf van gescheiden lading, ook wel plasma golf genoemd, die door de laserpuls wordt aangedreven. Met deze golf gaat een propagerende elektrisch veld distributie gepaard, de laser hekgolf, met enorme veldsterktes tot wel honderd GV/m. Dergelijke veldsterktes zijn potentieel bruikbaar om deeltjes duizend maal sneller en over een veel kortere afstand dan standaard rf versnellers te versnellen naar hoge energieën.

Echter, de experimenten die op dit moment de basiswerking van laser hekgolf versnelling demonstreren hebben fundamentele problemen met de controle, met schot-tot-schot fluctuaties en ook met een slechte schaalbaarheid. De reden is dat, in alle huidige methoden, de injectie van de elektronen en hun verdere versnelling intrinsiek gekoppeld zijn, omdat de methoden gebaseerd zijn op niet-lineaire dynamica zoals het breken van de plasmagolven om elektronen van het plasma zelf te injecteren. Daarom begint men zich nu te realiseren dat, om laser hekgolf versnellers te laten voldoen aan de behoefte, elektronen van een aparte, externe versneller moeten worden geïnjecteerd, zodat de injectie kan worden gecontroleerd.

Dit proefschrift biedt een theoretisch onderzoek naar de injectie van elektronenbundels van een externe versneller om de invloed van de timing en de richting van injectie op laser hekgolf versnelling te onderzoeken. Om situaties te

onderzoeken die op dit moment technisch haalbaar zijn, richten we ons onderzoek op de injectie van elektronen afkomstig van een conventionele versneller. Wij presenteren en onderzoeken drie methodes om de relatief lange bundels van elektronen van rf versnellers te injecteren in een hekgolf, zodanig dat de versnelde bundels een hoge kwaliteit krijgen. De methodes zijn te onderscheiden aan de hand van de positie van injectie met betrekking tot de laserpuls. Wij hebben de injectie van elektronenbundels achter de laserpuls, met een hoek ten opzichte van de propagatie richting van de laser en voor de laserpuls onderzocht.

Bij de eerste methode wordt de bundel elektronen, afkomstig van een rf versneller, gefocusseerd en geïnjecteerd in een plasma kanaal met een energie van enkele MeV's, direct achter de aandrijvende laserpuls. Bij deze aanpak, die in het algemeen werd gezien als de enige geschikte standaard injectie methode, ziet de elektronenbundel opeens de hekgolf achter de aandrijvende laserpuls zodra hij het plasma binnenkomt. Zodra de elektronenbundel in de hekgolf is, wordt hij opgedeeld in enkele kleinere bundels, elk met een duur van een aantal femtosecondes en een transversale grootte van enkele micrometers. Ons onderzoek liet, bij het reproduceren van deze standaard aanpak, zien dat deze methode twee problemen heeft, die tot nu toe over het hoofd zijn gezien en die wij hier voor de eerste keer bespreken. Het eerste probleem is ponderomotieve verstrooiing van de bundel in het vacuüm door de laserpuls voor het plasma kanaal, dus voordat de te injecteren bundel het plasma is binnengegaan. Het tweede probleem komt doordat, anders dan wat werd aangenomen in alle voorgaande berekeningen, het plasma aan het begin van de versneller geen oneindig scherpe overgang met het vacuüm maakt. In werkelijkheid is er altijd een gebied met een eindige lengte waar een overgang is waar de plasmadichtheid varieert van nul (in vacuüm) tot zijn volledige waarde (in het plasma kanaal). Wij houden rekening met deze overgangsregio en observeren dat de geïnjecteerde elektronen een veranderende hekgolf ondervinden vanwege een continu veranderende plasmagolflengte met de plasmadichtheid. Wij laten zien dat, vooral voor hoge intensiteiten en lage injectie energieën, ponderomotieve verstrooiing evenals de vacuüm-plasma overgang, de geïnjecteerde bundel sterk kunnen verstrooien, zelfs voordat de bundel de normale hekgolf bereikt. Uit dit onderzoek kan worden geconcludeerd dat gematigde laser intensiteiten en hogere injectie energieën van de elektronen nodig zijn om hoge kwaliteit versnelde bundels te verkrijgen met deze standaard aanpak.

Als een compleet nieuw alternatief voor de injectie van bundels van elektronen achter de laserpuls, stellen wij een methode voor waarbij de bundel met een kleine hoek wordt geïnjecteerd in de hekgolf, direct achter de laserpuls. Daardoor vermijdt men enige overlapping van de bundel met de hekgolf in de overgangsregio, waardoor beide ongewenste effecten, de ponderomotieve verstrooiing en de vacuüm-plasma overgang, worden vermeden. De hekgolf zal in dit mechanisme, net als in het standaard mechanisme, de geïnjecteerde lange bundel elektronen opdelen in kleinere bundels gescheiden door de plasma golflengte. Een belangrijk voordeel van deze methode is dat het mogelijk is om elektronenbundels met een bredere transversale grootte te injecteren. Met de standaard

methode, waarbij de elektronenbundel achter de puls wordt geïnjecteerd (met een hoek van nul graden), kan maar een klein gedeelte van de elektronen in bredere bundels worden gevangen, omdat de elektronen die ver van de as van de hekgolf worden geïnjecteerd niet door de transversaal focuserende regio's propageren. Hiertegenover staat dat voor het vangen van elektronen bij injectie onder een hoek grotere laser intensiteiten nodig zijn, in het zwakke niet lineaire regime en dat de elektronen geïnjecteerd moeten worden met een hogere energie.

Een speciaal geval van injectie onder een hoek is colineaire injectie (met een hoek van nul graden, op de propagatie as van de aandrijvende laser), maar met injectie van de elektronenbundel aan de voorzijde van de laserpuls. In de tijd wordt de elektronenbundel eerst geïnjecteerd en, vanwege zijn grote groepsnelheid, zal de laserpuls de elektronenbundel inhalen in het plasma. In dit geval wordt ponderomotieve verstrooiing gecompenseerd door de hekgolf. Wij laten zien dat, wanneer de laserpuls de elektronenbundel inhaalt, een groot gedeelte van de elektronen kan worden gevangen, direct achter de laserpuls, op de versnellende helling van de hekgolf. Deze elektronen worden allemaal verzameld in de eerste versnellende fase van de hekgolf, waar een gecomprimeerde bundel van elektronen wordt opgebouwd. Vergeleken met de andere methodes wordt hier slechts een bundel gevormd. Verder is de elektronendynamica erg vergelijkbaar met die van injectie onder een hoek, waar de elektronen, na de injectie, geleidelijk in de hekgolf bewegen. Een demonstratie experiment voor injectie voor de laserpuls wordt op dit moment voorbereid op de Universiteit Twente. Onze berekeningen voor het conceptuele ontwerp voorspellen dat elektronenbundels met een energie tot 0.7 GeV kunnen worden geformeerd met een lage energiespreiding van 1%.

Het laatste gedeelte van het proefschrift beschrijft een nieuwe, ultrasnelle dynamica in laser hekgolf versnellers. Eerdere experimentele observaties en theoretische onderzoeken hebben laten zien dat elektronenbundels met een duur van slechts enkele femtosecondes geformeerd kunnen worden. Echter, wij voorspellen dat laser hekgolf versnellers zelfs veel kortere elektronenbundels kunnen genereren, met een duur in het sub-femtoseconde (attoseconde) gebied. Het mechanisme dat verantwoordelijk is voor dit verschijnsel zijn de ultrasnelle betatron oscillaties van de straal van de femtoseconde bundel, met een frequentie die voorin de bundel groter is dan achterin. Attoseconde bundels worden gevormd in een breed scala aan parameters en hun formatie lijkt onafhankelijk te zijn van het gebruikte injectie mechanisme. We hebben de dynamica van de elektronenbundels onderzocht voor een groot bereik van parameters en concluderen dat de formatie van attoseconde bundels een erg algemeen en intrinsiek kenmerk van laser hekgolf versnellers is. Wij laten zien dat de geformeerde bundels kunnen propageren over aanmerkelijke afstanden van enkele tientallen centimeters zonder hun attoseconde structuur te verliezen, wat een eerste vereiste is voor eventuele toepassingen.

Contents

1

Introduction

1.1 Particle accelerators

Particle accelerators have become indispensable instruments for investigating the fundamental structure of matter and energy, which can revolutionize our understanding of some of the most profound questions about the universe. In addition to fundamental research, particle accelerators are also used for dozens of other applications, including radiation treatment for cancer patients, treating materials used in industry, producing isotopes used for diagnostic imaging, sterilizing food, and disposing of nuclear waste. It is estimated that more than 17,000 particle accelerators are in operation around the world.

At the beginning of last century, particle accelerators were still humble devices. As particle physics advanced, researchers sought machines of ever higher energy. Unfortunately the acceleration field of current radio-frequency (rf) technology is constrained by a fundamental upper limit of around 100 MV/m. Beyond this point the acceleration field becomes unstable due to vacuum breakdown. This is the reason why increasing the size of the accelerators seemed to be the only viable way to increase the energy. The current generation of particle accelerators using existing rf technology are many kilometers in size and cost billions of euros. The most prominent example is the Large Hadron Collider (LHC) at the Conseil Européen pour la Recherche Nucléaire (CERN) on the French-Swiss border near Geneva. This is currently the largest accelerator with a length of 27 km, producing the highest particle energy and costing about 2.9 billion euro. The LHC is an immensely complex machine, which can only be built and maintained by a collaboration of thousands of highly specialized engineers and scientists.

Such particle accelerators will have a strong impact on our understanding of nature and solve longstanding questions. Nevertheless, the enormous size and complexity of such devices may also set a limit towards further increasing the particle energy and restrict the use of such facilities to a small number of exclusive users. As a result, researchers are striving for an alternative accelerator concept to push the fundamental limit in particle energy beyond what is currently possible. Laser wakefield acceleration (LWFA) is such an accelerator concept. The goal of this thesis is to pursue the various options and the potential of laser wakefield acceleration via a theoretical analysis. The findings from such an investigation may then be considered a valuable basis for further development of experimental methods.

1.2   Laser wakefield acceleration

As described above, a fundamental revision of accelerator technology is necessary as scaling up the current technology is becoming complicated and exorbitantly expensive. Laser researchers have long recognized the enormous transverse field amplitudes that can be provided by a laser and have tried to realign a fraction of this field to point along the longitudinal direction in order to accelerate particles. More than thirty years ago, in 1979, at the University of California, Los Angeles (UCLA), Tajima and Dawson published a theoretical article in which they suggested that this conversion could be done efficiently in a plasma [1]. Plasmas are an attractive medium that can sustain enormous electric fields, because plasmas are not subject to the electrical breakdown that limits conventional accelerators. Tajima and Dawson proposed two schemes, which are now called laser wakefield acceleration (LWFA) and plasma beat wave acceleration (PBWA) [4].

To explain the basic working principle, in laser wakefield acceleration [1–3] of electrons, positrons and ions, a plasma wave is driven by an ultra-short high-intensity laser (at intensities of 10^{18}-10^{19} W/cm^2) sent through a suitable plasma. The radiation pressure of such a laser pulse, at sufficient intensity, expels a large amount of the plasma electrons, while the ions will remain at an almost fixed position due their higher mass. This leads to charge separation. When the laser pulse moves on and the electrons do not feel its field anymore, they are pulled back to their original position by the ions. However the electrons overshoot their original position and create an oscillating electron density modulation behind the pulse. The changing electron density can result in fields of hundreds of gigavolt-per-meter that accelerate particles thousands of times more quickly over a distance that is thousands of times shorter than conventional accelerators.

Plasma beat wave acceleration was another concept proposed by Tajima and Dawson [1] as an alternative to laser wakefield acceleration, which had to be done in the relativistic regime where high intensity lasers, unavailable at that time, would be needed. The plasma beat wave accelerator requires two long laser pulses (≤ 100 ps) with moderate intensity ($I \simeq 10^{15}$ W/cm^2) that are

spatially overlapped in the plasma and have slightly different frequencies such that the difference between the two frequencies, their beat frequency, equals the plasma frequency. In this way the beat-wave can resonantly excite the plasma wave in which electrons can be accelerated.

A few years after the publication by Tajima and Dawson [1], Chen *et al.* [5] suggested that, instead of a laser pulse, an electron beam could be used as the driver for the wakefield; this scheme is now called plasma wakefield acceleration (PWFA). Soon after the publication by Chen *et al.*, plasma wakefield acceleration was demonstrated by Rosenzweig *et al.* [6], with the production of a considerable amount of accelerated particles.

In 1985 Donna Strickland and Gerard Mourou [7, 8] provided a breakthrough in generating ultrashort laser pulses with very high intensities reaching the petawatt level. They invented a technique for amplifying an ultrashort laser pulse to enormous intensities called chirped pulse amplification (CPA). In CPA, the broadband spectrum of an ultrashort pulse is sent through a strongly dispersive delay line, such that the carrier wave becomes time dependent (dispersed) and the pulse is temporally stretched to a much longer duration. This can be done by a grating pair or a long fiber, for example. Stretching of the pulse reduces the peak power, which would otherwise destroy the gain medium used for the next step of amplification. Behind the gain medium, a second element with an opposite dispersion (normally a grating pair) is used, which removes the chirp and temporally compresses the pulse to a duration which is comparable to the input pulse duration. Chirped pulse amplification made compact table-top sources of intense, high power, ultrashort pulses available. These sources with energies up to several joules and femtosecond durations fulfilled the formerly unreachable intensity requirements for the laser wakefield acceleration scheme.

1.3 The "plasma bubble" accelerator

Prior to 2004, several experiments demonstrated the high potential of the laser-plasma accelerator [9–18], by showing the presence of the expected huge electric fields of the order of 100 GV/m and accelerated electrons with energies of more than 100 MeV. However the accelerated electron bunches were of a poor quality. The latter meant that only a few electrons achieved the named high energy, while the majority part of the energy spectrum of the generated electron bunches consisted of low energy electrons (< 10 MeV) with only a small tail towards the high energy (> 100 MeV). The energy spread observed was around 100% which came from the trapping of electrons from the background plasma in all the accelerating phases of the wakefield, similar to how whitewater is trapped and accelerated in an ocean wave. Although the maximum or average energy in such bunches with high spread may look attractive, such bunches are actually undesired, because most applications require bunches with a low energy spread. The situation changed radically in 2004, when three independent groups from Laboratoire d'Optique Appliquée (LOA) [19], Lawrence Berkeley
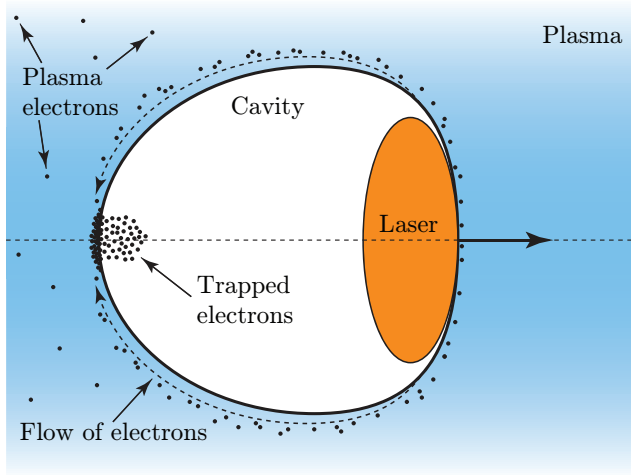
Figure 1.1: Schematic diagram of self-injection in the "bubble" regime

National Laboratory (LBNL) [20] and Imperial College [21] produced quasi-monoenergetic electron bunches. By choosing a particular combination of laser and plasma parameters, the researchers were able to generate electron bunches accelerated to energies of the order of 100 MeV with a relatively small energy spread of only a few percent. For the first time, electron bunches accelerated with a laser wakefield accelerator became comparable to conventional sources. These results were an immense step for the development of plasma accelerators and were reproduced by several groups worldwide [22–27].

The new parameter regime used, which is now called the "blowout" or "bubble" regime, was already predicted to obtain such progress in 2002 by Pukhov and Meyer ter Vehn [28]. In this regime, by self-focusing, the laser pulse intensity becomes so high that the plasma electrons are completely expelled by the ponderomotive force of the laser pulse (see figure 1.1). Instead of a periodic plasma wave, the pulse creates a cavity or bubble cleared of plasma electrons with a strong positive charge, because the positive ions are left behind. The expelled plasma electrons stream around the generated bubble thereby forming a sort of sheath around it. Behind the bubble the electrons become collected and form a strongly concentrated negative charge. When the electron density in this region increases beyond a critical value, some electrons are expelled back into the bubble in the form of a small bunch, which is also called self-injection. This self-generated and self-injected bunch may then be accelerated with a relatively small energy spread in the longitudinal accelerating field present in the bubble.

In 2006 Leemans *et al.* [29] were able to increase the accelerated energy of the electrons to 1 GeV by channeling a laser pulse with a peak power of 40 TW in a 3.3 cm long capillary discharge waveguide. The bunches maintained

a relatively low energy spread (2.5%), however, the scheme suffered from a considerable shot-to-shot fluctuation of the energy.

The stability of laser wakefield acceleration was noticeably improved in 2006 by Faure et al. [30], when they experimentally demonstrated, what is now called, the colliding-pulse regime. This scheme makes use of two counter-propagating laser pulses, an idea that was first proposed by Umstadter *et al.* [31] and further developed by Esarey *et al.* [32]. The first pulse drives a plasma wave, but is not strong enough to break the wave in order to inject electrons. The injection is done by a second, weaker, counter-propagating pulse with the same wavelength and polarization as the first one. When the two pulses meet (also named "collide"), interference creates a standing wave pattern with intensity fringes, which are separated by a length of the order of the wavelength. The ponderomotive force associated with these fringes is very large and can pre-accelerate plasma electrons. Some of these pre-accelerated electrons can be trapped in the wakefield and accelerated to relativistic energies. This regime turned out to have a much higher shot-to-shot reproducibility than the bubble regime, something that can be attributed to the operation in the linear or weakly non-linear regime.

In 2008 Geddes *et al.* [33] first demonstrated particle trapping in a laser wakefield accelerator using plasma density gradients in a gas jet. This method had been proposed [34–36] to further improve control in the trapping of the plasma electrons, further reduce shot-to-shot fluctuations and decrease the energy spread. This approach works as follows. When the laser pulse propagates through a sharp downward density transition, which is formed by the back side of a gas jet, the plasma wavelength increases. This causes a decrease of the phase velocity of the wake and a reduction in the trapping threshold for the injection velocity of the plasma electrons. The trapped bunches in that experiment showed a 10- to 100-fold lower momentum spread and the stability was better than in previous experiments. However the average energy of the bunches was rather low, only at the 1 MeV level. A second wakefield accelerator stage would be necessary to accelerate such a bunch to ultra-relativistic energies, i.e., the range beyond a few hundred MeV.

The electron bunches produced by current laser wakefield accelerators have unique properties that are well beyond what can be achieved by using conventional acceleration techniques. They typically have an extremely small size with a duration of just a few femtosecond and a transverse size of a few micrometers and peak currents in the order of 10 kA [20]. In this thesis we show that even shorter bunch durations (in the attosecond range) should become possible. The generation and control of such bunches will open new fields of research and applications and make laser wakefield acceleration highly promising for breakthroughs in the field of particle and radiation physics. Irrespective of this huge potential, up to now laser wakefield experiments still fail to provide the most basic properties that any novel accelerator concept needs to possess, namely controllability, stability and scalability of the output parameters. In the following, we describe the mechanism responsible for such essential prob-

lems and, within this thesis, we describe a possible solution based on external bunch injection from a standard rf accelerator.

1.4   External injection

So far most of the laser wakefield experiments have focused on the self-injection of electrons from the plasma wave, which is also called internal injection. The problems observed with such approaches, such as, lack of control, large shot-to-shot fluctuations and poor scalability, are due to the fact that the injection and acceleration of the electrons are coupled. On the one hand a combination of high plasma densities and high laser intensities is required to obtain bubble formation via a strongly nonlinear laser pulse and plasma dynamics. On the other hand, it is the nonlinearity in the dynamics that makes it difficult to control the outcome, this hinders its scaling, and makes this approach sensitive to all fluctuations of the input parameters.

To better illustrate this problem, it is instructive to compare it with conventional rf accelerators. All rf accelerators are based on two basic physical processes, which can be independently controlled and which aim to achieve linear bunch dynamics. The first process generates and injects electron bunches with free and precise adjustable timing, e.g., a photocathode gun. The second process is designed solely for optimum acceleration, typically in high-Q rf cavities driven by pulsed microwaves. Of central importance is that the injection can be timed with regard to the acceleration such that the bunches from the photocathode are injected into the optimum phase of the microwave field, e.g., to maximize the output energy or imply a certain energy chirp that can later be used for compression.

Currently used internal injection schemes do not possess the required separation of the injection and acceleration process. This is why there is now a growing conviction that bringing laser wakefield acceleration to controllability and scalability requires electrons to be generated, pre-accelerated and injected from separate external source. Our approach is to externally inject electrons from a conventional rf linear accelerator. In this thesis, we investigate how external injection, with its separation of the injection of the electrons from the excitation of the wakefield, improves the fundamental controllability and stability of the acceleration. It is also essential for the achievement of the highest kinetic energy, best controllability and scalability that the plasma density and the laser intensity are low enough, to operate close to the linear wakefield regime and to avoid nonlinearities in the drive laser pulse propagation dynamics. This is why this thesis concentrates on moderate drive intensities in the so called weakly relativistic regime.

When one realizes that the plasma wavelength is of the order of 100 µm, while the sizes of electron bunches from a conventional accelerator are typically much larger, it might sound surprising that high quality bunches can be obtained by injecting such a long and wide bunch, because electrons would be injected into all phases of the accelerating wakefield. This is why it was long

believed that only the injection of a bunch with a duration much smaller than the plasma wavelength, precisely phased within the plasma wave, could deliver high quality bunches from a wakefield accelerator. In this case the injected electron bunch would need to possess a duration in the order of femtoseconds and be synchronized with the drive laser pulse within a few femtoseconds precision. Such extremely short bunches are not available from standard accelerators yet and the synchronization is a technical challenge. However, it has been shown theoretically that the injection of a long bunch, longer than the plasma wavelength, under suitably chosen conditions, can lead to the generation of ultra-relativistic electron bunches with a surprisingly low energy spread [37–39]. This also makes the requirements for the synchronization less stringent and could be the key to experimentally demonstrating the first laser wakefield accelerator with external bunch injection.

1.5 Outline of the thesis

In this thesis we will show that there are three different schemes, that can deliver high quality bunches for the external injection of a long electron bunch from a conventional accelerator into a laser wakefield. These schemes differ with regard to the position of injection of the bunch relative to the laser pulse. Specifically, the electron bunch can be injected behind, in front or at an angle in relation to the drive laser pulse.

The thesis is organized as follows. Chapter 2 gives a basic introduction to the theory of the excitation of a wakefield in a plasma by a high intensity laser pulse. The following three chapters each discuss one of the external injection schemes. Chapter 3 investigates injection behind the drive laser pulse and discusses two important perturbing effects that have been overlooked so far, namely bunch scattering by the laser pulse in vacuum [40] and in the inhomogeneous laser wakefield in the vacuum-plasma transition at the entrance of the plasma channel [41]. In chapter 4, we introduce a novel external injection scheme for which the electron bunch is injected at a small angle into the laser wakefield [39]. In this chapter we will also look at the nonlinear optical effects that can modify the laser pulse during its propagation at the relativistic laser intensities used, which also affects the trapping and acceleration of the electron bunches. Chapter 5 investigates the injection of an electron bunch in front of the laser pulse [38], which is also the scheme that is in progress for a proof-of-principle experiment of external injection at the University of Twente [42]. In this chapter the experimental setup is discussed and calculations for its conceptual design are presented. In chapter 6, we will show via calculations that, instead of femtosecond bunches, also attosecond electron bunches could be obtained from a laser wakefield accelerator. Such bunches are of great interest, because they might be used to study physical, chemical and biological processes with unprecedented temporal resolution. In the final chapter the results are summarized and discussed.

2

Theoretical foundations

Acceleration of electrons to high energies (GeV's) requires huge electromagnetic fields. Conventional accelerators are constrained by an upper limit of around 100 megavolt-per-meter, beyond which the field becomes unstable due to the electrical breakdown of the cavity walls. It has been known for a long time that plasmas can sustain much larger electromagnetic fields via large-amplitude electron density waves [1]. Such plasma waves can be initiated by a powerful source, for example, an electron bunch or an ultrashort high-intensity laser pulse, that can drive the collective oscillations of the plasma electrons. Enormous fields, as large as several hundreds of gigavolts-per-meter, are formed due to the charge separation. Such fields are of great interest for particle acceleration and might be a viable alternative to conventional cavity-based radio-frequency (rf) accelerators.

In this chapter we explore the theoretical foundations of laser wakefield acceleration and give an outline of the physics involved, which comprises special relativity, and laser, plasma and acceleration physics. In section 2.2 we start with some basic plasma physics and look at the interaction of plasma with light. Expressions for the laser wakefield in the one-dimensional and the three-dimensional case are derived in section 2.3. To get some insight in the trapping and acceleration process, section 2.4 studies the motion of electrons in the wakefield using a one-dimensional Hamiltonian analysis. In section 2.6 we discuss guiding and the nonlinear dynamics of a high-intensity laser pulse in a plasma. Finally, in section 2.7, an introduction will be given on external electron bunch injection schemes, which will be treated more extensively in the following chapters.

2.1 The Maxwell equations in the cgs system

In the field of laser and plasma physics we will need to use the Maxwell equations extensively. It is useful to express the Maxwell equations in Gaussian cgs (centimeter-gram-second system) instead of SI units. In this system of measurement the electric and magnetic field have the same units. The cgs system uses less constants, makes $4\pi\varepsilon_0$ equal to 1, and eliminates the permittivity ε_0 and the permeability μ_0; this simplifies the equations for a better view on their essence. In the cgs system, the only dimensional constant appearing in the Maxwell equations is c, the velocity of light in vacuum. In cgs units they take the following form

$$\boldsymbol{\nabla} \cdot \boldsymbol{D} = 4\pi\varrho \qquad \text{(Gauss's law or Poisson equation)} \qquad (2.1)$$

$$\boldsymbol{\nabla} \cdot \boldsymbol{B} = 0 \qquad \text{(Gauss's law for magnetism)} \qquad (2.2)$$

$$\boldsymbol{\nabla} \times \boldsymbol{E} = -\frac{1}{c}\frac{\partial \boldsymbol{B}}{\partial t} \qquad \text{(Faraday's law)} \qquad (2.3)$$

$$\boldsymbol{\nabla} \times \boldsymbol{H} = \frac{1}{c}\frac{\partial \boldsymbol{D}}{\partial t} + \frac{4\pi}{c}\boldsymbol{J} \qquad \text{(Ampère's law)} \qquad (2.4)$$

where ϱ and $\boldsymbol{J}$ are the charge and current densities. The relation between the electric displacement field ($\boldsymbol{D}$), electric field ($\boldsymbol{E}$) and polarization density ($\boldsymbol{P}$) is

$$\boldsymbol{D} = \boldsymbol{E} + 4\pi\boldsymbol{P}. \qquad (2.5)$$

The magnetic induction ($\boldsymbol{B}$), often referred to as the magnetic field, the (auxiliary) magnetic field ($\boldsymbol{H}$) and the magnetization ($\boldsymbol{M}$) are related as follows

$$\boldsymbol{B} = \boldsymbol{H} + 4\pi\boldsymbol{M}. \qquad (2.6)$$

In this work we will use the Maxwell equations for fully ionized plasmas where $\boldsymbol{P}$ and $\boldsymbol{M}$ are zero. In this case $\boldsymbol{D} = \boldsymbol{E}$ and $\boldsymbol{B} = \boldsymbol{H}$.

2.2 Basic plasma physics

Plasmas are media in which enormous electric fields (wakefields) can be generated, which can be used for the acceleration of electrons. The unique properties of plasmas make this possible. In order to understand the principle of the generation of these wakefields, we need to get some basic understanding of plasma physics. That is why we will discuss some basic plasma physics in this section.

2.2.1 What is a plasma?

The Nobel prize winning American chemist Irving Langmuir first used the term plasma for an ionized gas in 1927, because it reminded him of blood plasma which carries red and white corpuscles just like a plasma carries electrons and ions. In Greek πλασμα means "moldable substance" or "jelly". Plasma is the

most common form of non-dark matter[1]. It is estimated that plasmas constitute more than 99 percent of the visible universe. Examples of plasmas are the sun and other stars, fluorescent light bulbs, very hot flames, lightning, aurora borealis (northern polar lights), the solar wind and the earth's ionosphere.

A plasma is a collection of neutral particles, and mobile ions and electrons which are no longer bound to each other and exhibit collective behavior. Collective behavior means that the average motions of the particles depend not only on local conditions but also on the state of the plasma in remote regions. This is because the strong electric and magnetic fields generated by the motion of a charged particle can affect the motion of other particles far away in the plasma. The particles in a plasma mainly interact through these strong long-range electromagnetic fields. The weaker short-range interactions, like collisions, are often assumed to be negligible. This approximation is known as "collisionless" plasma. The collective behavior gives plasmas unique physics compared to solids, liquids and gases. For this reason, they are considered a distinct "fourth state of matter".

2.2.2   Debye shielding

In order to verify that, for the purpose of describing laser wakefield acceleration, the standard approximation of plasma within a hydrodynamic approach can be used, one has to look at a fundamental property: the ability of plasma to act as a shield for electric fields [43]. When isolated, the electric field of a charged particle diminishes as the square of the distance to the particle. However, this is not the case in a plasma, where the electrons are free to move into the vicinity of positive ions and away from other electrons. Thus, if a positive (or negative) charge is inserted into a plasma, it will change the local charge distribution by attracting (or repelling) electrons. The field of each isolated particle is thus partially shielded by its immediate neighbors. In a cold plasma with no thermal motions, this shielding would be perfect and their would be no electric field outside the cloud that shields the inserted particle. However, when there is a finite temperature this is no longer the case.

We will compute the characteristic distance for this shielding. Consider an electron distribution on a uniform and immobile background of positive ions in thermal equilibrium with the electric potential, ϕ, of the plasma. The energy of an electron in this potential is $e\phi$, which is independent of its momentum, so the electron density distribution, n_e, is given by the Boltzmann relation

$$n_e = n_0 \exp\left(\frac{e\phi}{k_B T_e}\right), \tag{2.7}$$

where e is the elementary charge, k_B is the Boltzmann constant, T_e is the temperature of the plasma electrons in Kelvin and n_0 is the density of the

---

[1]The current scientific consensus is that more than 95% of the total energy density in the universe is not plasma or any form of ordinary matter, but a combination of dark matter and dark energy, which is invisible to our current methods of detection.

fixed background of positive ions. Let us insert a test particle of charge Ze at the origin. The electrostatic potential is now given by Poisson's equation

$$\nabla^2\phi = -4\pi Ze\delta(r) - 4\pi en_0\left[1 - \exp\left(\frac{e\phi}{k_BT_e}\right)\right]. \tag{2.8}$$

The perturbation due to a single test particle is very small and one can safely assume that $e\phi/k_BT_e \ll 1$. In this case one can expand the exponential to find

$$\nabla^2\phi - \frac{4\pi n_0e^2}{k_BT_e}\phi = -4\pi Ze\delta(r). \tag{2.9}$$

Because we assume an isotropic plasma, the electrostatic potential is spherically symmetric. This equation can be solved by Fourier-transforming and then inverting to obtain the exponential decay length we are seeking,

$$\phi(r) = \frac{Ze}{r}\exp\left(\frac{-r}{\lambda_D}\right), \tag{2.10}$$

where r is the radial distance. This result shows an important feature of plasmas. Plasma electrons shield out the field of a charge beyond a characteristic distance λ_D, which is called the Debye length

$$\lambda_D = \sqrt{\frac{k_BT_e}{4\pi n_0e^2}} \approx 6.9\sqrt{\frac{T_e}{n_0}}. \tag{2.11}$$

For large Debye lengths ($\lambda_D \gg r$) the exponential in equation 2.10 becomes about unity and the potential falls off like $1/r$. For short Debye lengths the charge is shielded by nearby and mobile charges in only a few Debye lengths, because in this case the potential drops exponentially to zero. A comparison of the Debye potential and the Coulomb potential is plotted in figure 2.1.

This theory of Debye shielding is only valid if there are enough particles ($\gg 1$) in the shielding charge cloud. The average number of electrons contained in a "Debye sphere" is called the plasma parameter, Λ. It is defined as

$$\Lambda = \frac{4\pi n_0\lambda_D^3}{3} \approx 1380\frac{T_e^{3/2}}{n_0^{1/2}}. \tag{2.12}$$

2.2.3   Definition of a plasma

Including the Debye shielding, a more correct definition of a plasma can be formulated that can be used to justify varies simplifications in the modeling of the laser wakefield. The term plasma is generally reserved for a system of charged particles large enough to show collective behavior, excluding microscopically small collections of charged particles. There are two main criteria a collection of charged particles has to obey before it is termed a plasma:

- The Debye screening length should be short compared to the physical size (L) of the plasma ($\lambda_D \ll L$).
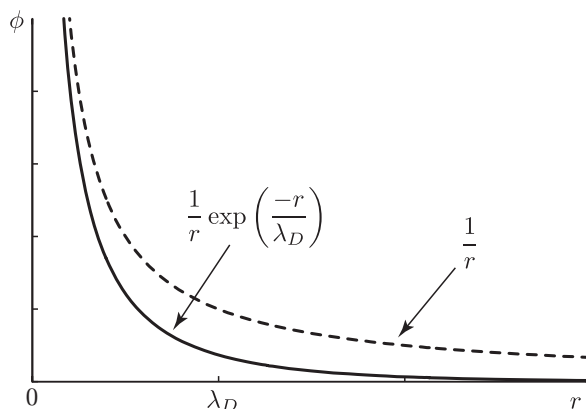
Figure 2.1: A comparison of the Debye potential (solid line) with the classical Coulomb potential (dashed line) for a negative charge.

- There should be a large number of particles in a Debye sphere ($\Lambda \gg 1$).

When these criteria are met, collective electrostatic interactions dominate over binary collisions, and the plasma particles can be treated as if they only interact with a smooth background field, rather than through pairwise interactions (collisions).

In the typical laser wakefield accelerator used in this thesis, we use a plasma created by a discharge in a capillary with an electron density of approximately 1×10^{18} cm^{-3} and an electron temperature of approximately 10 eV (1.16×10^5 K). This obeys the definition of a plasma and thus will show collective behavior, because it has a Debye length of around 23 nm and around 54 electrons in the Debye sphere.

2.2.4   Waves in cold uniform plasmas

Due to the collective behavior of the plasma particles, plasmas can support a wide variety of wave motions. In order to understand the formation of the laser wakefield, it is important to look at the behavior of these waves in a plasma. To calculate the propagation of waves in a cold plasma, one can use the cold plasma model, which greatly simplifies the equations. In the cold plasma model the particles are initially at rest. In other words, they have no kinetic thermal motion of their own. While the temperature of the typical plasma used for laser wakefield acceleration is of the order of 110,000 K ($\approx$ 10 eV), the cold plasma model can still be used, because the phase velocity of the excited waves, which is approximately the speed of light, is much larger than the thermal velocity of the electrons ($|\boldsymbol{v}_e| \approx 1.3 \times 10^6$ m/s $\ll c$).

In this section we will consider the propagation of electromagnetic waves in a plasma by deriving the wave equation governing the propagation of such

waves. One can derive the wave equation from the Maxwell equations and
Newton's second law. The Maxwell equations describe the relationship between
the electric field, $\boldsymbol{E}$, the magnetic field, $\boldsymbol{B}$, and the electric current density, $\boldsymbol{J}$,

$$\boldsymbol{\nabla} \times \boldsymbol{E} = -\frac{1}{c}\frac{\partial \boldsymbol{B}}{\partial t}, \tag{2.13}$$

$$\boldsymbol{\nabla} \times \boldsymbol{B} = \frac{1}{c}\frac{\partial \boldsymbol{E}}{\partial t} + \frac{4\pi}{c}\boldsymbol{J}. \tag{2.14}$$

One can convert the Maxwell equations to the wave equation by taking the curl
in equation 2.13 and substituting it into equation 2.14

$$\boldsymbol{\nabla}^2 \boldsymbol{E} - \boldsymbol{\nabla}(\boldsymbol{\nabla} \cdot \boldsymbol{E}) = \frac{4\pi}{c^2}\frac{\partial \boldsymbol{J}}{\partial t} + \frac{1}{c^2}\frac{\partial^2 \boldsymbol{E}}{\partial t^2}. \tag{2.15}$$

For cold plasmas one can use the single-particle model. The response of an
electron of mass m_e and charge $-e$ to an electric field $\boldsymbol{E}(t)$ is in the linear case
$(|\boldsymbol{v}_e|/c \ll 1)$ described by Newton's second law

$$m_e \frac{\partial \boldsymbol{v}_e}{\partial t} = -e\boldsymbol{E}, \tag{2.16}$$

with $\boldsymbol{v}_e$ the velocity of the electron. The ions are considered as fixed, which
is justified because of their relatively large mass, so the current density comes
approximately entirely from the electron motion

$$\boldsymbol{J} = -en_e\boldsymbol{v}_e. \tag{2.17}$$

To obtain the source term in equation 2.15, one can take the time derivative of
this equation and substitute equation 2.16 to get

$$\frac{\partial \boldsymbol{J}}{\partial t} = \frac{e^2 n_e}{m_e}\boldsymbol{E}. \tag{2.18}$$

By substituting this equation in expression 2.15, one gets the wave equation
for waves in a cold plasma

$$\boldsymbol{\nabla}^2 \boldsymbol{E} - \boldsymbol{\nabla}(\boldsymbol{\nabla} \cdot \boldsymbol{E}) = \frac{4\pi n_e e^2}{m_e c^2}\boldsymbol{E} + \frac{1}{c^2}\frac{\partial^2 \boldsymbol{E}}{\partial t^2}. \tag{2.19}$$

In the next two sections we will use this equation to investigate more details
of the propagation of electromagnetic waves in a plasma. First we will derive
the frequency of plasma waves, which is a longitudinal wave on which laser
wakefield acceleration is based. Next the propagation of light in plasma is
investigated and the dispersion relation is derived.

2.2.5   Plasma frequency

Small deviations from the quasi-neutrality in a plasma result in electron density
perturbations in space and time called plasma waves also known as Langmuir

waves. Irving Langmuir together with Lewi Tonks first discovered these oscillations in the 1920s. In equilibrium a plasma is neutral on the whole, because the number of ions and electrons are approximately equal. However one can create a local imbalance by taking a bunch of electrons and pulling them away from their equilibrium position. This will lead to an electric field that tries to pull the electrons back to their equilibrium position. Because of their higher mass, the ions will stay almost at the same position in this time, so one can consider them as fixed. When the electrons reach their equilibrium position they will overshoot because of their momentum. This process repeats itself and the electrons will perform simple harmonic oscillations around their equilibrium position. The formed density modulations are called plasma waves and are characterized by a natural frequency of oscillation known as the electron plasma frequency, which can be easily determined as follows. For plasma waves, the electromagnetic waves are longitudinal. In the one-dimensional case the electric field can be written as

$$\boldsymbol{E} = E_0 \exp i(kz - \omega t)\hat{\boldsymbol{z}}, \tag{2.20}$$

where i is the imaginary unit, k is the wave number, ω is the angular frequency and E_0 is the amplitude. Therefore, from equation 2.19 one gets

$$\left(\frac{4\pi n_e e^2}{m_e c^2} - \frac{\omega^2}{c^2} \right) E_z = 0, \tag{2.21}$$

which gives the dispersion relation for plasma waves,

$$\omega = \omega_p, \tag{2.22}$$

where

$$\omega_p = \sqrt{\frac{4\pi n_e e^2}{m_e}} \approx 5.64 \times 10^4 \sqrt{n_e}, \tag{2.23}$$

is the electron plasma frequency depending only on the electron density, n_e, as parameter. In a similar way we can define the ion plasma frequency,

$$\omega_{pi} = \sqrt{\frac{4\pi n_i Z^2 e^2}{m_i}}, \tag{2.24}$$

where m_i and Ze are respectively the mass and charge of an ion and n_i is the ion density. The ion plasma frequency, in a plasma with $n_e = n_i$, is much lower than the electron plasma frequency, due to the large mass of the ions compared to that of the electrons. The relatively high electron plasma frequency is, by far, the most important and normally called "the plasma frequency". It is one of the most fundamental parameters of a plasma and will play a central role in the interaction of a laser pulse with a plasma. In the following chapters the term plasma frequency will be exclusively used for the plasma electron frequency.

The dispersion relation tells us that ω does not depend on k, so the plasma wave can have an arbitrary wavelength and propagate with arbitrary phase velocity. The group velocity, defined as $\partial\omega/\partial k$, is zero, which means that the disturbance does not propagate.

2.2.6   Propagation of light in plasmas

In order to understand how the wakefield is generated by the laser pulse, it is useful to know how light propagates through a plasma. The propagation of light through a plasma can be calculated by using the fact that the electromagnetic waves are transverse. The wave equation derived in section 2.2.4 becomes for transverse waves

$$\boldsymbol{\nabla}^2 \boldsymbol{E} = \frac{\omega_p^2}{c^2}\boldsymbol{E} + \frac{1}{c^2}\frac{\partial^2 \boldsymbol{E}}{\partial t^2}. \tag{2.25}$$

In order to find the group and phase velocity of light traveling in a plasma, the dispersion relation has to be derived. One can do this by noting that each electromagnetic wave can be expressed as a sum of harmonic traveling waves. One such a longitudinal wave can be written like

$$\boldsymbol{E} = E_0 \exp\left[i(kz - \omega t)\right]\hat{\boldsymbol{x}}. \tag{2.26}$$

The differentials of equations 2.25 can be eliminated by taking this solution. This gives us the dispersion relation

$$\omega^2 = \omega_p^2 + k^2 c^2, \tag{2.27}$$

which relates the temporal frequency of the wave to its wave number and to other parameters of the plasma. The dispersion relation is plotted in figure 2.2. The group velocity, v_g, which describes the propagation of the envelope of a wave packet and is connected to the energy flow is defined in the usual manner

$$v_g = \frac{\partial\omega}{\partial k} = c\sqrt{1 - \frac{\omega_p^2}{\omega^2}}. \tag{2.28}$$

Also a phase velocity, v_ϕ, which describes the speed at which the phase of any frequency component of the wave travels, can be associated with a light wave propagating through plasma. The phase velocity of a light wave in plasma is always larger than the speed of light. From the dispersion relation its value is given by

$$v_\phi = \frac{\omega}{k} = \sqrt{c^2 + \frac{\omega_p^2}{k^2}} = \frac{c}{\eta}, \tag{2.29}$$

which means that η, the index of refraction of a plasma, is smaller than one. The refractive index is given by

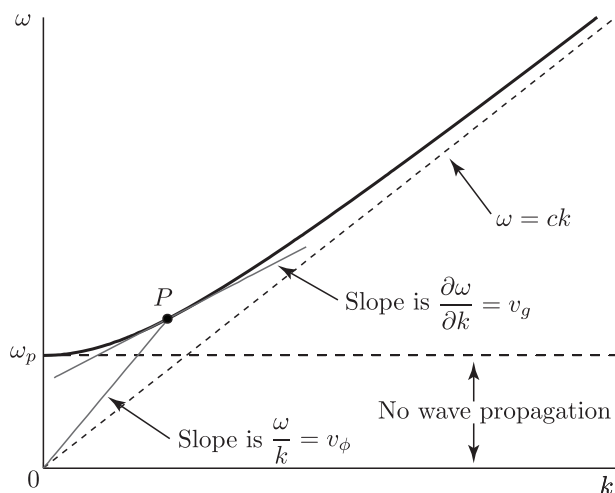$$\eta = \sqrt{1 - \frac{\omega_p^2}{\omega^2}}. \tag{2.30}$$

Figure 2.2: Dispersion relation $\omega(k)$ for electromagnetic waves in plasma. Notice how the phase (v_ϕ) and group velocity (v_g) can be geometrically represented at point P.

It can be seen that η becomes imaginary when $\omega < \omega_p$, which means that a plasma is only transparent for light with a frequency greater than the plasma frequency. In case it is lower, the pulse will be reflected, because the response time of the electrons ω_p^{-1} is fast enough and able to shield out the field of the light wave. For a given light frequency or wavelength, the critical plasma density, n_c, gives the transition between reflection and transmission

$$n_c[\text{cm}^{-3}] = \frac{m_e \omega^2}{4\pi e^2} \approx \frac{1.1 \times 10^{21}}{\lambda[\mu\text{m}]^2}, \tag{2.31}$$

with $\lambda = 2\pi c/\omega$ the free-space wavelength of the light in units of microns. For a drive laser wavelength of about 800 nm, which is typical for a laser wakefield accelerator experiment, the critical plasma density has a value of 1.7×10^{21} cm^{-3}. The critical density separates two different regimes of light-plasma interaction. If $n_e < n_c$, the plasma is called underdense, because the light can propagate through it. If $n_e > n_c$, equation 2.27 leads to a purely imaginary wavenumber, k, and besides strong reflection, as named above, the electromagnetic wave decays as an evanescent wave beyond the critical surface, where n_c occurs. Such a plasma is called overdense and the high density may provide a very strong interaction, though at a short interaction length [44].

2.3   Laser wakefield

In section 2.2.5 we saw that a disturbance of the quasi-neutrality of the plasma can excite a plasma wave. This is the main ingredient of the working principle of plasma accelerators, where one can use either a relativistic electron beam (plasma wakefield acceleration) or a high intensity drive laser pulse (laser wakefield acceleration) to excite relativistically moving electron density waves in plasmas. Here we will focus on the laser wakefield acceleration scheme. The electromagnetic field associated with the plasma wave driven by the laser pulse is called a laser wakefield, in analogy to a water wake wave excited by a boat sailing across a water surface. In this analogy the drive laser can be compared with a powerful motorboat and the plasma with the water. The boat displaces the water which results in a water wave behind it. The same thing happens when a laser pulse moves through a plasma. The radiation pressure of a laser pulse propagating inside a plasma displaces the plasma electrons. The ions remain at an almost fixed position, due to their higher mass. When the laser pulse has passed, the plasma electrons are pulled back by the ions. They overshoot their original position and create an electron density modulation behind the laser pulse. The charge separation creates very strong electric fields that propagate with the velocity of the laser pulse. When an electron bunch is injected in the proper location and time with a certain minimum velocity, it can be accelerated to high energies by this electric field.

2.3.1   Normalized vector potential

So far we have recalled only the linear response of a plasma to incident light pulses, i.e., the dispersion of light and plasma waves. However if a laser pulse of sufficiently high intensity travels through a plasma, the plasma starts to show a nonlinear response. Specifically, beyond a certain strength of the oscillating light field, it is able to drive the oscillations of the plasma electrons to velocities near the speed of light. In this case relativistic effects start to play a role, in particular the mass of the electrons grow, which lowers the plasma frequency to $\omega_p/\sqrt{\gamma}$, where

$$\gamma \equiv \frac{1}{\sqrt{1 - \frac{v_e^2}{c^2}}}, \tag{2.32}$$

is the Lorentz factor. A characteristic parameter for high intensity laser pulses, which can be used to express the importance of these relativistic effects, is the normalized vector potential. This dimensionless quantity is defined as

$$a = \frac{eA_\perp}{m_e c^2}, \tag{2.33}$$

where $A_\perp$ is the transverse vector potential. The peak amplitude of the normalized vector potential, a_0, is called the laser strength parameter. To provide an impression of the order of magnitude of this quantity, one can relate the

laser strength parameter to the peak electric field strength of the laser by considering a monochromatic electromagnetic wave in vacuum. In the Weyl gauge, the scalar potential is set equal to zero and $\boldsymbol{E} = -c^{-1}\partial\boldsymbol{A}/\partial t$, which gives

$$E_0 = \frac{m_e c \omega}{e} a_0, \tag{2.34}$$

i.e., $E_0[\text{TV/m}] \approx 3.21 a_0/\lambda[\mu\text{m}]$. For a linearly polarized laser beam with a Gaussian radial profile, the laser strength parameter can be related to the peak laser intensity, I_0, in the following way

$$I_0 = \frac{\pi c}{2} \left(\frac{m_e c^2 a_0}{e\lambda} \right)^2, \tag{2.35}$$

i.e., $I_0[\text{W/cm}^2] \approx 1.35 \times 10^{18} \left(a_0/\lambda[\mu\text{m}] \right)^2$ and the peak power, $P_0 = \pi w_0^2 I_0/2$, can then be expressed as

$$P_0[\text{GW}] \approx 21.5 \left(\frac{a_0 w_0}{\lambda} \right)^2, \tag{2.36}$$

where w_0 is the waist size, which is the distance from the beam axis to the point where the intensity has dropped to $1/e^2$ ($\approx 13.5\%$) of the maximum value.

Conservation of the transverse canonical momentum in one-dimensional systems shows that $a = \gamma v_\perp/c$ (derivation can be found in section 2.3.3, equation 2.52), where $v_\perp$ is the transverse quiver velocity of the electron in the laser field. Therefore, the electrons become relativistic for $a_0 \gtrsim 1$. The force induced by the magnetic field of the laser pulse, $\boldsymbol{v}/c \times \boldsymbol{B}$, then becomes comparable to the electric force and has to be taken into account, as the electrons can get a considerable longitudinal momentum from this field. The condition $a_0 \gtrsim 1$ corresponds to an intensity greater than 2.1×10^{18} W/cm^2 for a typical wavelength of 800 nm. Nowadays such intensities are routinely produced by many laboratories worldwide.

2.3.2 Ponderomotive force in the nonrelativistic case

In order to explain how an intense laser pulse provides a traveling perturbance as discussed in the analogy with a water wake, we will describe the force that is able to displace the electrons in the plasma. The radiation pressure of light is usually very weak. However when an intense light pulse travels through a plasma it can displace the electrons. The force associated with the radiation pressure of light in a plasma is called the ponderomotive force [45] and is what drives the laser wakefield. It was derived in 1957 by Boot and Harvie [46], who showed that an electron in a non-uniform electric field experiences an acceleration towards the position of least electric field strength. When a laser pulse travels through a plasma, the electrons will experience a rapidly oscillating electric field. In the case of a homogeneous field, the electrons perform oscillations driven by the field, but they return to their initial position after each

period. The time-averaged force exerted by the light on the electrons is then zero. However, in the case of an inhomogeneous field, for example a laser pulse, the quivering electrons will feel a non-zero average net force, the ponderomotive force, that drives them away from regions of high field-amplitude towards lower field-amplitude areas. To derive the strength of the ponderomotive force, the motion of an electron in the oscillating $\boldsymbol{E}$ and $\boldsymbol{B}$ field is considered. This motion is described by the Lorentz equation

$$m_e \frac{d\boldsymbol{v}_e}{dt} = -e \left[\boldsymbol{E}(\boldsymbol{r}) + \frac{\boldsymbol{v}_e}{c} \times \boldsymbol{B}(\boldsymbol{r}) \right], \qquad (2.37)$$

with $\boldsymbol{v}_e$ the velocity ($|\boldsymbol{v}_e|/c \ll 1$) and $\boldsymbol{r}$ the location of the electron. For simplicity, consider the case of a harmonic electric field

$$\boldsymbol{E} = \boldsymbol{E}_0(\boldsymbol{r}) \cos \omega t, \qquad (2.38)$$

where $\boldsymbol{E}(\boldsymbol{r})$ contains the spatial inhomogeneity of the electric field. We assume that this dependence is sufficiently slow and can be neglected in the lowest order. The particle coordinate is written as $\boldsymbol{r} = \boldsymbol{r}_0 + \Delta \boldsymbol{r}$, where $\boldsymbol{r}_0$ is the time average over one oscillation period and $\Delta \boldsymbol{r}$ is a small perturbation. First make a Taylor expansion of the electric field about a location $\boldsymbol{r}_0$

$$\boldsymbol{E} = \boldsymbol{E}_0(\boldsymbol{r}) \cos \omega t = \boldsymbol{E}_0(\boldsymbol{r}_0) \cos \omega t + (\Delta \boldsymbol{r} \cdot \boldsymbol{\nabla}) \boldsymbol{E}_0(\boldsymbol{r}_0) \cos \omega t + \dots \qquad (2.39)$$

For nonrelativistic electrons the $\boldsymbol{v}_e/c \times \boldsymbol{B}$ term is smaller than the $\boldsymbol{E}$ term. Therefore, to first order, the Lorentz equation is

$$m_e \frac{d\boldsymbol{v}_1}{dt} = -e\boldsymbol{E}_0(\boldsymbol{r}_0) \cos \omega t, \qquad (2.40)$$

which gives

$$\boldsymbol{v}_1 = -\frac{e}{m_e \omega} \boldsymbol{E}_0(\boldsymbol{r}_0) \sin \omega t, \qquad (2.41)$$

and

$$\Delta \boldsymbol{r} = \boldsymbol{r} - \boldsymbol{r}_0 = \frac{e}{m_e \omega^2} \boldsymbol{E}_0(\boldsymbol{r}_0) \cos \omega t. \qquad (2.42)$$

This lowest order motion is just the quiver motion of an electron in an oscillating electric field. At second order there is also a contribution from the magnetic field. The magnetic field can be derived from Faraday's law (2.3). For the lowest order component one can write $\boldsymbol{B}_1(\boldsymbol{r}_0) = -c/\omega \left[\boldsymbol{\nabla} \times \boldsymbol{E}_0(\boldsymbol{r}_0) \right] \sin \omega t$. The second order part of the Lorentz equation gives

$$m_e \frac{d\boldsymbol{v}_2}{dt} = -e \left[(\Delta \boldsymbol{r} \cdot \boldsymbol{\nabla})\boldsymbol{E}_0 + \frac{\boldsymbol{v}_1}{c} \times \boldsymbol{B}_1 \right]. \qquad (2.43)$$

If one cycle-averages this motion one obtains a motion, which is relatively slow compared to the quiver velocity (2.41) and to which one can associate the

so-called ponderomotive force

$$
\begin{aligned}
\boldsymbol{F}_p &= \left\langle m_e \frac{d\boldsymbol{v}_2}{dt} \right\rangle = -\frac{e^2}{2m_e\omega^2}\left[(\boldsymbol{E}_0\cdot\boldsymbol{\nabla})\boldsymbol{E}_0 + \boldsymbol{E}_0\times(\boldsymbol{\nabla}\times\boldsymbol{E}_0)\right] \\
&= -\frac{e^2}{4m_e\omega^2}\boldsymbol{\nabla}\boldsymbol{E}_0^2(\boldsymbol{r}) = -\frac{m_ec^2\boldsymbol{\nabla}a_0^2(\boldsymbol{r})}{4},
\end{aligned}
\tag{2.44}
$$

where the identity $\boldsymbol{E}_0\times(\boldsymbol{\nabla}\times\boldsymbol{E}_0) = \frac{1}{2}\boldsymbol{\nabla}\boldsymbol{E}_0^2 - \boldsymbol{E}_0\cdot\boldsymbol{\nabla}\boldsymbol{E}_0$ and the relation between E_0 and a_0 of equation 2.34 has been used. The factor $\frac{1}{2}$ in the first line of equation 2.44 comes from averaging $\cos^2\omega t$ over the laser period. This equation gives the ponderomotive force for a linearly polarized laser pulse. In the case of circular polarization, one has to replace a_0^2 by $2a_0^2$.

It can be seen that, independent of the polarization of the laser field, the magnitude of the ponderomotive force is proportional to the gradient of the intensity of the laser pulse ($\boldsymbol{F}_p\propto\boldsymbol{\nabla}a_0^2\propto\boldsymbol{\nabla}I_0$). The force is directed opposite to the gradient of the intensity and thus pointing away from regions of high intensity such as in the center of the laser pulse, towards low-intensity regions. If the laser pulse is sufficiently short in time, sharply focused in the transverse direction, and if the intensity is high enough, the ponderomotive force will transiently push plasma electrons aside and will thus act as a pulsed perturbation of the otherwise steady-state plasma. As a result the laser excites the type of plasma wave, described above, with an associated wakefield.

2.3.3 1D laser wakefield in the relativistic case

In this section we will present the physics of the interaction of an intense laser pulse with a plasma and calculate the generated wakefield by developing a nonlinear one-dimensional cold fluid model. This model neglects the transverse variations of the laser field and plasma properties, which means that the model will only be valid close to the laser pulse axis. However it can help us to understand certain basic properties of the wakefield. A three-dimensional model will be developed later. In our one-dimensional model, the plasma ions are assumed immobile, because of their much greater mass and the fast propagation of the laser pulse. The plasma will again be treated as an electron fluid with zero temperature. This assumption means that the particles are initially at rest, thereby allowing us to neglect the effects due to the thermal motion of the electrons. The nonlinear differential equation for the electrostatic potential, which describes the one-dimensional laser wakefield, will be derived. Our starting point is the general wave equation, that can easily be derived from the Maxwell equations

$$
\boldsymbol{\nabla}^2\boldsymbol{A} - \frac{1}{c^2}\frac{\partial^2\boldsymbol{A}}{\partial t^2} = -\frac{4\pi}{c}\boldsymbol{J} + \frac{1}{c}\frac{\partial}{\partial t}(\boldsymbol{\nabla}\phi).
\tag{2.45}
$$

For convenience we describe the laser field with the scalar electrostatic potential, ϕ, and the vector potential, $\boldsymbol{A}$, together with the Coulomb gauge,

$\nabla \cdot \boldsymbol{A} = 0$, instead of the electric, $\boldsymbol{E}$, and magnetic field, $\boldsymbol{B}$. The electric and magnetic fields can then be retrieved from the potentials in the usual way, via

$$\boldsymbol{E} = -\nabla\phi - \frac{1}{c}\frac{\partial \boldsymbol{A}}{\partial t}, \tag{2.46}$$

$$\boldsymbol{B} = \nabla \times \boldsymbol{A}. \tag{2.47}$$

The goal of the following is then to find the potentials in the presence of the laser pulse traveling through the plasma in order to discuss the conditions under which injected electrons can be accelerated. The laser pulse is assumed to propagate through the plasma along the z-direction. Hence, the vector potential only has a transverse component, $A_\perp$. In the one-dimensional description, the scalar electrostatic potential, ϕ, does not vary in the transverse direction, so one can write $\nabla\phi = \partial\phi/\partial z$. Using this one can expand the wave equation into two scalar differential equations

$$\left(\frac{\partial^2}{\partial z^2} - \frac{1}{c^2}\frac{\partial^2}{\partial t^2}\right) A_\perp = \frac{4\pi}{c}en_ev_\perp, \tag{2.48}$$

$$\frac{1}{c}\frac{\partial^2\phi}{\partial t\partial z} = -\frac{4\pi}{c}en_ev_z. \tag{2.49}$$

The second equation needed for deriving the wake potential is the Lorentz equation, which describes the motion of plasma electrons due to the presence of electromagnetic fields

$$\frac{d\boldsymbol{p}}{dt} = -e\left(-\nabla\phi - \frac{1}{c}\frac{\partial \boldsymbol{A}}{\partial t} + \boldsymbol{v}_e \times \nabla \times \frac{\boldsymbol{A}}{c}\right), \tag{2.50}$$

with $\boldsymbol{p}$ the momentum of a single electron. The fundamental law of conservation of momentum states that the total momentum of the system, $\boldsymbol{\Pi}$, remains constant. In this case the mechanical momenta of the electrons, $\boldsymbol{p}$, plus the momenta of the electromagnetic field should be constant

$$\boldsymbol{\Pi} = \boldsymbol{p} - e\frac{\boldsymbol{A}}{c} = \text{constant}. \tag{2.51}$$

Using the Lorentz equation and that $d\boldsymbol{\Pi}/dt = 0$ one can derive equations for the longitudinal and transverse velocity components

$$v_\perp = \frac{e}{m_e\gamma c}A_\perp, \tag{2.52}$$

$$m_e\frac{d(\gamma v_z)}{dt} = -\frac{e^2}{2m_ec^2\gamma}\frac{\partial A_\perp^2}{\partial z} + e\frac{\partial\phi}{\partial z}. \tag{2.53}$$

The transverse motion, which is the quiver motion of the electrons, is described by equation 2.52, which gives the quiver velocity of the electron. The longitudinal motion is described by equation 2.53. The first term on the RHS of this equation describes the ponderomotive force. Electrons can gain or lose

momentum due to this force and due to a gradient in the potential. Locations where the intensity increases with z (i.e., at the trailing edge of the laser pulse traveling in the $+z$-direction) will decelerate plasma electrons and a falling intensity (such as in front of a pulse) will accelerate electrons. One can rewrite equation 2.53 by using the quiver velocity and the definition of γ

$$\frac{dv_z}{dt} = -\frac{1}{2\gamma^2} \left(\frac{e^2}{m_e^2 c^2} \frac{\partial A_\perp^2}{\partial z} + \frac{e^2 v_z}{m_e^2 c^4} \frac{\partial A_\perp^2}{\partial t} \right) + \frac{1}{\gamma} \left(c^2 - v_z^2 \right) \frac{e}{m_e c^2} \frac{\partial \phi}{\partial z}. \quad (2.54)$$

The third equation needed is the Poisson equation which relates the scalar potential to the electron density, n_e,

$$\nabla^2 \phi = 4\pi e (n_e - n_0), \quad (2.55)$$

with n_0 the equilibrium electron density. In hydrogen plasma, when fully ionized, n_0 is equal to the ion-density n_i. In one dimension ∇^2 can be simplified and replaced with $\partial^2 / \partial z^2$.

To describe the properties of waves in fluids, one can normally make use of the conservation of mass in the form of a continuity equation. In plasma waves, however, the mass may not be conserved due to the presence of relativistically high velocities ($v \approx c$, $\gamma \neq 1$). Instead for the case of plasma, one can write a continuity equation for the charge density, which is conserved as long as there is no ionization and recombination

$$\frac{\partial n_e}{\partial t} + \boldsymbol{\nabla} \cdot (n_e \boldsymbol{v}) = 0. \quad (2.56)$$

In the one-dimensional case the $\boldsymbol{\nabla}$ operator can be replaced with $\partial / \partial z$.

For an easier discussion of the wakefield over a wider range of parameters, it is useful to introduce a scaling to make all variables dimensionless. For an easier illustration of the results, it is also convenient to make a mathematical transformation from the laboratory frame coordinates (z, t) to the frame that moves with the group velocity of the laser pulse, v_g, because in the moving frame the wake potentials and fields appear to stand still. We assign the moving frame coordinate as ξ and τ, where $\xi = k_p(z - v_g t)$ and $\tau = \omega_p t$. Here $k_p = \omega_p / v_g$, with ω_p the plasma frequency and v_g the group velocity of the laser pulse. The spatial and temporal derivatives are transformed as $\partial / \partial z = k_p \partial / \partial \xi$ and $\partial / \partial t = \omega_p \partial / \partial \tau - k_p v_g \partial / \partial \xi$. Then in the moving frame equation 2.48 can be rewritten by using equation 2.52 for the quiver velocity

$$\left[\frac{1}{\gamma_g^2} \frac{\partial^2}{\partial \xi^2} + 2\beta_g^2 \frac{\partial^2}{\partial \xi \partial \tau} - \beta_g^2 \frac{\partial}{\partial \tau^2} \right] a = \frac{\beta_g N}{\gamma_g} a, \quad (2.57)$$

where $\gamma_g = (1 - \beta_g^2)^{-1/2}$ is the Lorentz factor, $\beta_g = v_g / c$, $a = e A_\perp / m_e c^2$ and $N = n_e / n_0$. After normalization, equation 2.53 becomes

$$\frac{\partial}{\partial \xi} \left[\gamma (1 - \beta_g \beta_z) - \Phi \right] = -\beta_g \frac{\partial(\gamma \beta_z)}{\partial \tau}, \quad (2.58)$$

where the dimensionless potential is given by $\Phi = e\phi/m_e c^2$ and $\beta_z = v_z/c$. The same can be done for the Poisson equation

$$\frac{\partial^2 \Phi}{\partial \xi^2} = \beta_g^2 (N - 1), \tag{2.59}$$

and the continuity equation

$$\beta_g \frac{\partial N}{\partial \tau} = \frac{\partial}{\partial \xi} [N(\beta_g - \beta_z)]. \tag{2.60}$$

A further simplification is obtained by introducing the so-called quasi-static approximation [47]. In this approximation the evolution of the laser pulse envelope in the moving frame is assumed to be much slower than the plasma response. That is, if the laser pulse is sufficiently short, the fields a and Φ that drive the plasma are expected to not significantly evolve during a transit time of a plasma electron through the laser pulse. In other words $\tau_l \ll \tau_e$, where τ_l is the laser pulse duration and τ_e is the laser pulse evolution time. Thus, the plasma electrons experience a static, i.e., independent of τ, laser field and one can neglect $\partial/\partial\tau$ in the fluid equations that relate the plasma response to the fields, which are the equation for the longitudinal momentum (2.58) and the continuity equation (2.60). However, the $\partial/\partial\tau$ derivatives have to be retained in the wave equation (2.57), because it describes the evolution of the laser pulse. If one sets $\partial/\partial\tau = 0$ in equation 2.58 and integrates one gets the following conservation relation

$$\gamma(1 - \beta_g\beta_z) - \Phi - 1 = 0, \tag{2.61}$$

since $\Phi = 0$ and $\gamma = 1$ in the absence of a plasma wave. The same can be done for equation 2.60. Here one gets

$$N = \frac{\beta_g}{\beta_g - \beta_z}, \tag{2.62}$$

because $N = 1$ for $\xi \to \infty$. By taking the square of equation 2.61 one obtains

$$\begin{aligned}
(1 + \Phi)^2 &= \gamma^2(1 - \beta_g\beta_z)^2 \\
&= \gamma^2 \left[2(1 - \beta_g\beta_z) + \beta_g^2\beta_z^2 - 1 \right] \\
&= \gamma^2 \left[\frac{2(1 + \Phi)}{\gamma} + \beta_g^2\beta_z^2 - 1 \right].
\end{aligned} \tag{2.63}$$

By using the definition of γ and the relation between the quiver velocity and the normalized amplitude ($\beta_\perp = a/\gamma$), one can write β_z as a function of γ and a

$$\gamma = \frac{1}{1 - a^2/\gamma^2 - \beta_z^2} \quad \Rightarrow \quad \beta_z^2 = 1 - \frac{1 + a^2}{\gamma^2}. \tag{2.64}$$

Inserting this expression for β_z in equation 2.63 and solving for γ yields the following expression

$$\gamma = \gamma_g^2(1 + \Phi) \left(1 - \beta_g \sqrt{1 - \frac{1 + a^2}{\gamma_g^2(1 + \Phi)^2}} \right). \tag{2.65}$$

By substituting this expression for γ in equation 2.61 one can write β_z as a function of a and Φ as follows

$$\beta_z = \frac{1}{\beta_g} \left[1 - \frac{1}{\gamma_g^2(1 - \beta_g Y)} \right] = \frac{\beta_g - Y}{1 - \beta_g Y}, \tag{2.66}$$

where

$$Y = \left(1 - \frac{1 + a^2}{\gamma_g^2(1 + \Phi)^2} \right)^{1/2}. \tag{2.67}$$

Equation 2.66 can be used to eliminate β_z in equation 2.62,

$$N = \beta_g \gamma_g^2 \left(\frac{1}{Y} - \beta_g \right). \tag{2.68}$$

One can now substitute this expression for the normalized density, N, in the Poisson equation to arrive at the final differential equation that describes the one-dimensional laser wakefield through the wake potential, Φ,

$$\begin{aligned}
\frac{\partial^2 \Phi}{\partial \xi^2} &= \beta_g^2 \gamma_g^2 \left(\frac{\beta_g}{Y} - 1 \right) \\
&= \beta_g^2 \gamma_g^2 \left\{ \beta_g \frac{(1 + \Phi)/(1 + a^2)^{1/2}}{\left[(1 + \Phi)^2/(1 + a^2) - \gamma_g^{-2} \right]^{1/2}} - 1 \right\}. \tag{2.69}
\end{aligned}$$

For the derivation of this expression the laser pulse was assumed to be circular polarized. For a laser pulse with a linear polarization a^2 has to be replaced with $a^2/2$. The normalized electric field $\mathcal{E}_z = eE_z/m_e v_g \omega_p$ corresponding to the wake potential Φ, can be found from the following equation

$$\mathcal{E}_z = -\left(\frac{1}{\beta_g} \right)^2 \frac{\partial \Phi}{\partial \xi}. \tag{2.70}$$

Equation 2.69 is a nonlinear differential equation that generally needs to be solved numerically. However, 2.69 can also be solved analytically for low intensities ($a \ll 1$), which is called the regime of a linear laser wakefield. In the limit for $\beta_g \to 1$ equation 2.69 simplifies into

$$\frac{\partial^2 \Phi}{\partial \xi^2} = \frac{1}{2} \left[\frac{1 + a^2}{(1 + \Phi)^2} - 1 \right]. \tag{2.71}$$

Behind the laser pulse ($a = 0$) this can be written as

$$\frac{\partial^2 \Phi}{\partial \xi^2} = \frac{1}{2} \left[\frac{1}{(1 + \Phi)^2} - 1 \right] = \frac{1}{2} \left(1 - 2\Phi + 3\Phi^2 - \ldots - 1 \right) \approx -\Phi, \tag{2.72}$$

where the last term is an approximation for small Φ, which occurs at small drive intensities ($a \ll 1$). This approximation yields a sinusoidally perturbed plasma wave with wavelength $\lambda_p = 2\pi/k_p$. This case is depicted in figure 2.3a, for which we numerically calculated the laser wakefield using equation 2.69 for a linear polarized Gaussian laser pulse described by the following normalized amplitude

$$a = a_0 \exp\left(\frac{-\xi^2}{\sigma_z^2}\right), \tag{2.73}$$

where σ_z is the normalized pulse length. The shape of the wakefield changes when the laser amplitude is increased. This can be seen in figure 2.3b, where non-sinusoidal (nonlinear) perturbations occur and where the plasma perturbations are much stronger. In the nonlinear regime, where the normalized amplitude of the pulse is high ($a_0 \gtrsim 1$), the wakefield transforms into a sawtooth type of shape and the electron density becomes spiky. Simultaneously, as can be seen by comparing figure 2.3a and b, the spatial period increases with a and yields a longer plasma wavelength. The latter can be explained with an increasing quiver velocity ($v_e \to c$, $\gamma > 1$) that increases the relativistic mass of the plasma electrons ($m_e \to \gamma m_e$) and thereby lowers the plasma frequency according to equation 2.23.

The ponderomotive force of a high intensity laser pulse drives the wakefield by displacing plasma electrons from the path of the pulse. The following electron dynamics show a resonant frequency, the plasma frequency. As with any driven system exhibiting a resonance, there should be a maximum amplitude of the wakefield [3]. This maximum depends on the pulse length and occurs when it is of the order of the plasma wavelength. Figure 2.4 shows the maximum value of the wakefield amplitude, $\mathcal{E}_z$, as a function of the pulse duration, σ_z, calculated for several different laser amplitudes and by assuming a Gaussian laser pulse. Notice that the wakefield amplitude is driven most efficiently for a resonant pulse length of $\sigma_z = 2$. Thus, in order to excite a wakefield with the highest amplitude, it is important to match the laser pulse duration with the plasma density. It is, however, fairly tolerable to changes in the pulse length. One can also see that for larger laser amplitudes, the curve becomes broader, because of an increase in the nonlinear plasma wavelength.

2.3.4   Wavebreaking

To obtain the maximum acceleration one would like to make the longitudinal plasma oscillations as large as possible, such as by increasing the intensity of the laser pulse. However, it turns out that there are limits to the dynamics of a plasma wave as we described it, specifically, a plasma wave can break similar to the breaking of ocean waves when attaining too high an amplitude. Wavebreaking of plasma waves can be explained as follows. When the oscillation amplitude of the plasma electrons becomes too large, the restoring force due to the plasma wave is no longer large enough to let them continue their longitudinal oscillation. At this point the maximum oscillation is reached and
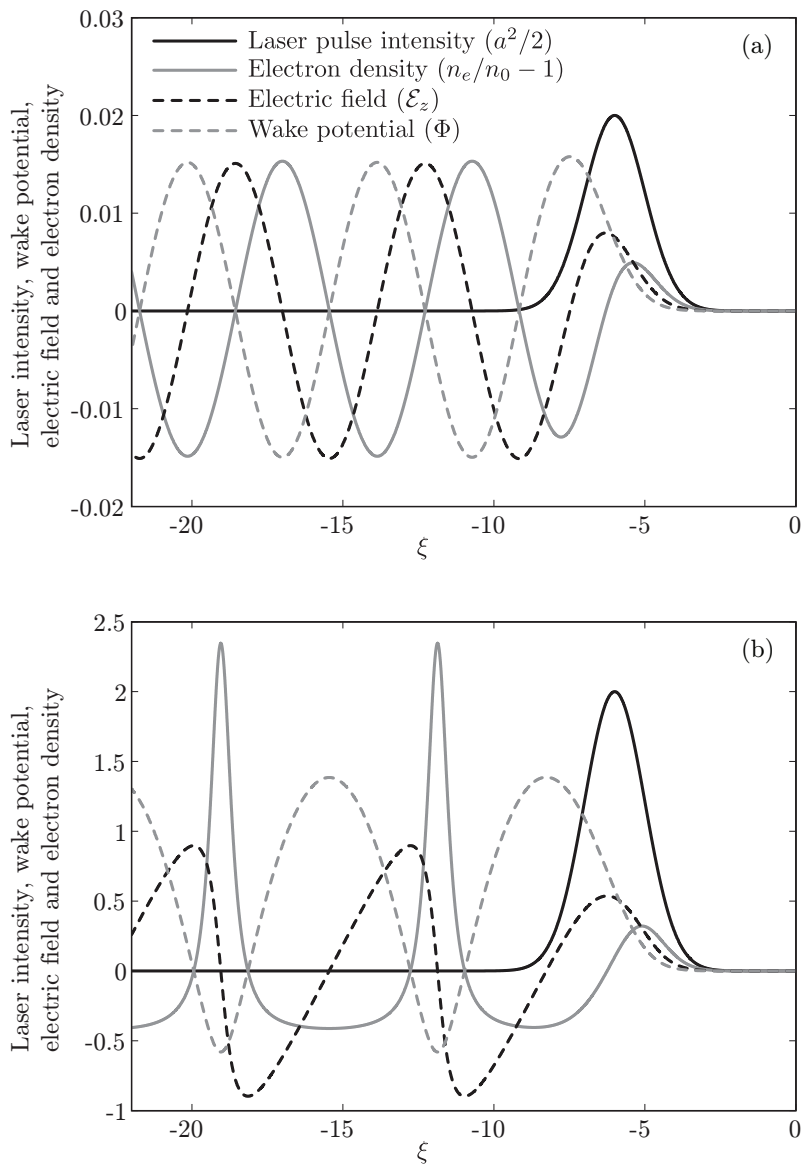
Figure 2.3: One-dimensional laser wakefield excited by a linearly polarized laser pulse with peak normalized amplitudes of $a_0 = 0.2$ (a) and $a_0 = 2$ (b). Shown are the wake potential, the electric field and the density profile created by a Gaussian laser pulse with a length ($1/e$) of $\sigma_z = 2$. and centered at $\xi = -6$ in a plasma channel with $\gamma_g = 50$.
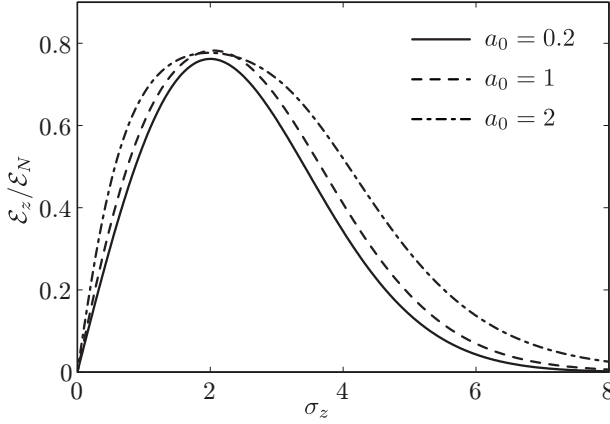
Figure 2.4: Normalized amplitude of the electric field $\mathcal{E}_z$ as a function of the normalized laser pulse length σ_z and normalized to the maximum amplitude of a flat-top pulse $\mathcal{E}_N = (a_0^2/2)/(1+a_0^2/2)^{1/2}$. The laser pulse is assumed Gaussian as described by equation 2.73.

the wave starts to decompose in shape. Much of the wave energy will then be converted into thermal energy of the electrons. Another, more detailed, explanation can be given by comparing the velocity of the individual electrons, v_e, with the velocity of the plasma wave, which is equal to the group velocity of the laser pulse, v_g. When the amplitude of the plasma wave increases, the electron velocity also increases. At the limit $v_e \to v_g$ this leads to a plasma density with singularities. Wavebreaking occurs then because, with $v_e > v_g$, electrons start to overtake the traveling wake wave.

In order to obtain a qualitative number for the maximum field as an estimate for an upper limit of wave dynamics without wavebreaking, the so-called nonrelativistic wavebreaking limit [48], we proceed as follows. In the one-dimensional linear case, considered here, one can write the accelerating electric field of the wakefield as

$$E = E_0 \exp{(k_p z - \omega_p t)}, \tag{2.74}$$

where E_0 is the field amplitude. By making the assumption that all plasma electrons oscillate with wavenumber $k_p = \omega_p/v_g$, one can find the maximum amplitude of the wakefield, $E_{\max}$. Poisson's equation then gives

$$\boldsymbol{\nabla} \cdot \boldsymbol{E}_{\max} = k_p E_{\max} = 4\pi e n_e, \tag{2.75}$$

which yields as the nonrelativistic wavebreaking field

$$E_{\mathrm{WB}} = \frac{m_e \omega_p v_g}{e} \approx \frac{m_e \omega_p c}{e}, \tag{2.76}$$

or, in units more suitable for an experimental description,

$$E_{\text{WB}}[\text{V/cm}] \approx 0.96\sqrt{n_e[\text{cm}^{-3}]}. \tag{2.77}$$

This equation shows that plasmas can indeed support extremely large fields without breaking, i.e., without loosing control over the shape of the wakefield. For example a typical plasma density of $n_0 = 1 \times 10^{18}$ cm^{-3} can support a plasma wave with an accelerating field of 96 GV/m, which is three orders of magnitude above what can be achieved by conventional rf accelerators.

The maximum amplitude of a plasma wave can exceed the nonrelativistic wavebreaking field when relativistic effects become important. The maximum amplitude or relativistic wavebreaking field can be calculated using equation 2.69, which includes relativistic effects. This equation will become complex if the potential, Φ, becomes below a certain minimum value defined by

$$(1 + \Phi_{\text{min}})^2 = (1 + a^2)/\gamma_g^2. \tag{2.78}$$

At this minimum the velocity of the electrons equals the group velocity of the laser pulse and wavebreaking occurs. One can use the principle of the first integral[2] to write equation 2.69 as follows

$$
\begin{aligned}
\left(\frac{d\Phi}{d\xi}\right)^2 &= 2\beta_g^2\gamma_g^2 \int \left(\beta_g \frac{1 + \Phi}{\sqrt{(1 + \Phi)^2 - (1 + a^2)\gamma_g^{-2}}} - 1 \right) d\Phi + C \\
&= 2\beta_g^2\gamma_g^2 \left(\beta_g \sqrt{(1 + \Phi)^2 - \frac{1 + a^2}{\gamma_g^2}} - (1 + \Phi) \right) + C. \tag{2.79}
\end{aligned}
$$

Only the wakefield behind the laser pulse, where $a = 0$ is considered. The normalized longitudinal electric field reaches its maximum strength, $\mathcal{E}_{\text{max}}$, when $\Phi = 0$ and $d^2\Phi/d\xi^2 = 0$. The constant C can be extracted by substituting these values into equation 2.79, which gives $C = (\beta_g^2\mathcal{E}_{\text{max}})^2 + 2\beta_g^2$. In the wavebreaking limit Φ is equal to $1/\gamma_g - 1$ and $d\Phi/d\xi = 0$. Thus in this limit one can write equation 2.79 as

$$0 = 2\beta_g^2\gamma_g^2 \left(-\frac{1}{\gamma_g} \right) + (\beta_g^2\mathcal{E}_{\text{max}})^2 + 2\beta_g^2, \tag{2.80}$$

which gives the normalized relativistic wavebreaking field [49]

$$E_{\text{RWB}} = E_{\text{WB}}\mathcal{E}_{\text{max}} = \frac{m_e\omega_p v_g}{e}\frac{\sqrt{2(\gamma_g - 1)}}{\beta_g}. \tag{2.81}$$

When relativistic effects are included, a plasma density of $n_0 = 1 \times 10^{18}$ cm^{-3} can support plasma waves with an accelerating field up to 862 GV/m.

---

[2]By substituting $z = \frac{dy}{dx}$ into $\frac{d^2y}{dx^2} = f(y)$ one can obtain that $\left(\frac{dy}{dx}\right)^2 = 2\int f(y)dy + C$

2.3.5   3D linear laser wakefield

In the previous sections we looked at the wakefield in the one-dimensional case by neglecting the transverse variation and an analytical expression could be found in the linear case. It turns out that for a three-dimensional geometry, one can find analytical expressions for the linear wakefield as well, provided that the wakefield is axially symmetric about the propagation direction and the initial transverse variation in plasma density is small. The latter is, e.g., fulfilled in a uniform plasma as well as in a wide plasma channel. The equations that are derived here will be used in the following chapter for the calculation of the wakefield.

The derivation starts with the Maxwell equations. From Faraday's law (2.3) and Ampère's law (2.4) the wave equation can be derived

$$\boldsymbol{\nabla} \times \boldsymbol{\nabla} \times \boldsymbol{E} = -\frac{1}{c^2} \left(4\pi \frac{\partial \boldsymbol{J}}{\partial t} + \frac{\partial^2 \boldsymbol{E}}{\partial t^2} \right). \tag{2.82}$$

The large mass of the ions and the short time scale of the process allows us to assume that the ions remain immobile. The next step is to insert the current density, $\boldsymbol{J} = -en_e\boldsymbol{v}_e$, into this wave equation. Because here only the linear wakefield is considered, nonlinear terms can be neglected, resulting in

$$\boldsymbol{\nabla} \times \boldsymbol{\nabla} \times \boldsymbol{E} = \frac{1}{c^2} \left(4\pi en_e \frac{\partial \boldsymbol{v}_e}{\partial t} - \frac{\partial^2 \boldsymbol{E}}{\partial t^2} \right). \tag{2.83}$$

From the Lorentz equation one gets the following expression for $\boldsymbol{v}_e$ by again only taking the linear terms

$$\frac{\partial \boldsymbol{v}_e}{\partial t} = -\frac{1}{m_e} \left(e\boldsymbol{E} - \boldsymbol{F}_p \right), \tag{2.84}$$

where $\boldsymbol{F}_p$ is the ponderomotive force exerted by the laser pulse on the plasma electrons. Combining this equation with equation 2.83 we obtain

$$\boldsymbol{\nabla} \times \boldsymbol{\nabla} \times \boldsymbol{E} = -\frac{4\pi e^2 n_e}{m_e c^2} \boldsymbol{E} + \frac{4\pi en_e}{m_e c^2} \boldsymbol{F}_p - \frac{1}{c^2} \frac{\partial^2 \boldsymbol{E}}{\partial t^2}. \tag{2.85}$$

For a cylindrically symmetric laser pulse envelope, which is usually present in experiments, the wakefield will be cylindrically symmetric as well, which makes it useful to use cylindrical coordinates, because then the θ-component becomes zero. The remaining r and z components are

$$-\frac{\partial}{\partial z} \left(\frac{\partial E_r}{\partial z} - \frac{\partial E_z}{\partial r} \right) = \frac{4\pi en_e}{m_e c^2} \left(F_{p,r} - eE_r \right) - \frac{1}{c^2} \frac{\partial^2 E_r}{\partial t^2}, \tag{2.86}$$

$$\nabla_\perp \left(\frac{\partial E_r}{\partial z} - \frac{\partial E_z}{\partial r} \right) = \frac{4\pi en_e}{m_e c^2} \left(F_{p,z} - eE_z \right) - \frac{1}{c^2} \frac{\partial^2 E_z}{\partial t^2}, \tag{2.87}$$

where $\nabla_\perp = \partial/\partial r + 1/r$.

In the same way one can write a wave equation for $\boldsymbol{B}$ by combining Faraday's and Ampère's law, and inserting the equation for the current

$$\boldsymbol{\nabla} \times \boldsymbol{\nabla} \times \boldsymbol{B} = -\frac{4\pi e}{c}\left(\boldsymbol{\nabla} \times (n_e \boldsymbol{v})\right) - \frac{1}{c^2}\frac{\partial^2 \boldsymbol{B}}{\partial t^2}. \tag{2.88}$$

One can treat $\boldsymbol{\nabla} \times \boldsymbol{\nabla} \times \boldsymbol{B}$ as a regular double vector product and write it like $\boldsymbol{\nabla}(\boldsymbol{\nabla} \cdot \boldsymbol{B}) - \boldsymbol{\nabla}^2\boldsymbol{B}$. In the latter, the first term vanishes, because Gauss's law for magnetism (2.2) states that the magnetic field, $\boldsymbol{B}$, has a divergence equal to zero ($\boldsymbol{\nabla} \cdot \boldsymbol{B} = 0$). Hence

$$\boldsymbol{\nabla}^2\boldsymbol{B} = \frac{4\pi e}{c}\left(n_e(\boldsymbol{\nabla} \times \boldsymbol{v}_e) - \boldsymbol{v}_e \times (\boldsymbol{\nabla} n_e)\right) + \frac{1}{c^2}\frac{\partial^2 \boldsymbol{B}}{\partial t^2}, \tag{2.89}$$

where $\boldsymbol{\nabla} \times (n_e\boldsymbol{v}_e)$ is written as $n_e(\boldsymbol{\nabla} \times \boldsymbol{v}_e) - \boldsymbol{v}_e \times (\boldsymbol{\nabla} n_e)$. By taking the rotation of equation 2.84 and inserting Faraday's law, one gets

$$\frac{\partial(\boldsymbol{\nabla} \times \boldsymbol{v}_e)}{\partial t} = \frac{e}{m_e c}\frac{\partial \boldsymbol{B}}{\partial t} + \frac{1}{m_e}\boldsymbol{\nabla} \times \boldsymbol{F}_p. \tag{2.90}$$

Because $\boldsymbol{F}_p \propto \boldsymbol{\nabla}a^2$ and $\boldsymbol{\nabla} \times \boldsymbol{\nabla}f = 0$ for every scalar f, one obtains

$$\boldsymbol{\nabla} \times \boldsymbol{v}_e = \frac{e}{m_e c}\boldsymbol{B}. \tag{2.91}$$

One can insert this into equation 2.89 to arrive at the wave equation for the magnetic field

$$\boldsymbol{\nabla}^2\boldsymbol{B} = \frac{4\pi e^2 n_e}{m_e c^2}\boldsymbol{B} - \frac{4\pi e}{c}\left(\boldsymbol{v}_e \times \boldsymbol{\nabla}n_e\right) + \frac{1}{c^2}\frac{\partial^2 \boldsymbol{B}}{\partial t^2}. \tag{2.92}$$

The only source term in equation 2.92 is the $\boldsymbol{v}_e \times \boldsymbol{\nabla}n_e$ term. One can conclude from this that $\boldsymbol{B} = 0$ for a uniform density ($\boldsymbol{\nabla}n_e = 0$). For cylindrical coordinates, the θ-component of Faraday's law (2.3) becomes

$$\frac{\partial E_r}{\partial z} - \frac{\partial E_z}{\partial r} = -\frac{1}{c}\frac{\partial B_\theta}{\partial t} = 0. \tag{2.93}$$

If we insert this into equation 2.86 and 2.87 we get

$$\frac{1}{c^2}\frac{\partial^2 E_r}{\partial t^2} + \frac{4\pi e^2 n_e}{m_e c^2}E_r \quad = \quad \frac{4\pi e n_e}{m_e c^2}F_{p,r} = -\pi e n_e \frac{\partial a^2}{\partial r}, \tag{2.94}$$

$$\frac{1}{c^2}\frac{\partial^2 E_z}{\partial t^2} + \frac{4\pi e^2 n_e}{m_e c^2}E_z \quad = \quad \frac{4\pi e n_e}{m_e c^2}F_{p,z} = -\pi e n_e \frac{\partial a^2}{\partial z}, \tag{2.95}$$

where we have inserted the ponderomotive force given by equation 2.44. It is useful to transform the equations from laboratory frame coordinates (z, t) to moving frame coordinates (ξ, ζ), where $\xi = k_p(z - v_g t)$ and $\zeta = k_p z$ and to introduce dimensionless variables. The equations now take the following form

$$\frac{\partial^2 \mathcal{E}_r}{\partial \xi^2} + N\mathcal{E}_r \quad = \quad N\mathcal{F}_{p,r} = -\frac{N}{4\beta_g^2}\frac{\partial a^2}{\partial \rho}, \tag{2.96}$$

$$\frac{\partial^2 \mathcal{E}_z}{\partial \xi^2} + N\mathcal{E}_z \quad = \quad N\mathcal{F}_{p,z} = -\frac{N}{4\beta_g^2}\left(\frac{\partial a^2}{\partial \xi} + \frac{\partial a^2}{\partial \zeta}\right), \tag{2.97}$$

where $\rho = k_p r$ and $N = n_e/n_0$ is the normalized plasma density. One can solve these integrals in the complex plane, using contour integration (see appendix A). The solution for these equations is

$$\mathcal{E}_{z,r}(\xi, \rho) = - \int_\xi^\infty \sqrt{N} \mathcal{F}_{p,z,r}(\xi', \rho) \sin\left[\sqrt{N}\left(\xi - \xi'\right)\right] d\xi'. \qquad (2.98)$$

If one assumes a Gaussian laser pulse in space and time

$$a = a_0 \exp\left(\frac{-\xi^2}{\sigma_z^2}\right) \exp\left(\frac{-\rho^2}{\sigma_r^2}\right), \qquad (2.99)$$

with σ_z and σ_r respectively the normalized length and spot size of the pulse, one can solve this integral and get a solution for the accelerating and focusing component of the wakefield

$$\mathcal{E}_z = \frac{a_0^2 N \sigma_z \sqrt{2\pi}}{16\beta_g^2} \left[\cos\left(\sqrt{N}\xi\right) - \mathrm{Re}(g)\right] \exp\left(\frac{-2\rho^2}{\sigma_r^2}\right) \exp\left(\frac{-N\sigma_z^2}{8}\right), \quad (2.100)$$

and

$$\mathcal{E}_r = \frac{a_0^2 \sqrt{2\pi N} \sigma_z \rho}{4\beta_g^2 \sigma_r^2} \left[\mathrm{Im}(g) - \sin\left(\sqrt{N}\xi\right)\right] \exp\left(\frac{-2\rho^2}{\sigma_r^2}\right) \exp\left(\frac{-N\sigma_z^2}{8}\right), \quad (2.101)$$

where g is

$$g = \exp\left(i\sqrt{N}\xi\right) \mathrm{erf}\left[\frac{\sqrt{2}(4\xi + i\sqrt{N}\sigma_z^2)}{4\sigma_z}\right], \qquad (2.102)$$

and $\mathrm{erf}(x)$ is the error function. The solution presented here describes the wakefield both inside and behind the laser pulse and is also a very good approximation for the linear wakefield in a wide plasma channel. Behind the laser pulse g can be simplified when $\xi \lesssim -3\sigma_z$. In this case one can write $\mathrm{Re}(g) = -\cos(\sqrt{N}\xi)$ and $\mathrm{Im}(g) = -\sin(\sqrt{N}\xi)$.

Equations 2.100 and 2.101 will be used in chapter 3 to calculate the effect of the transition from vacuum to plasma on the trapping of external injected electrons.

2.3.6   3D nonlinear laser wakefield

In the previous section an analytical expression for a linear laser wakefield in a uniform plasma and a wide plasma channel was derived. In the case of a nonlinear wakefield or a narrow plasma channel a set of nonlinear equations has to be solved numerically. The following system of equations, with their derivation briefly described below, gives the steady nonlinear laser wakefield in a radially nonuniform plasma by assuming axial symmetry in a cylindrical

geometry

$$\beta_g \frac{\partial P_z}{\partial \xi} - \frac{\partial \gamma}{\partial \xi} - \beta_g \mathcal{E}_z = 0, \tag{2.103}$$

$$\beta_g \frac{\partial P_r}{\partial \xi} - \frac{\partial \gamma}{\partial \rho} - \beta_g \mathcal{E}_r = 0, \tag{2.104}$$

$$-\frac{\partial \mathcal{B}_\theta}{\partial \xi} + \beta_g \frac{\partial \mathcal{E}_r}{\partial \xi} + \beta_r N_e = 0, \tag{2.105}$$

$$\nabla_\perp \mathcal{B}_\theta + \beta_g \frac{\partial \mathcal{E}_z}{\partial \xi} + \beta_z N_e = 0, \tag{2.106}$$

$$\beta_g \frac{\partial \mathcal{B}_\theta}{\partial \xi} - \frac{\partial \mathcal{E}_r}{\partial \xi} + \frac{\partial \mathcal{E}_z}{\partial \rho} = 0, \tag{2.107}$$

$$\nabla_\perp \mathcal{E}_r + \frac{\partial \mathcal{E}_z}{\partial \xi} + N_e - N_p(\rho) = 0. \tag{2.108}$$

In these equations $\nabla_\perp = \partial/\partial r + 1/r$ and $\mathcal{E}_z$, $\mathcal{E}_r$ and $\mathcal{B}_\theta$ are the longitudinal and radial components of the electric field and the azimuthal component of the magnetic field, normalized to the on-axis wavebreaking field $E_{\mathrm{WB}}(r = 0)$ which was derived in section 2.3.4. Further one has the relativistic factor, $\gamma = (1 + P_z^2 + P_r^2 + a^2/2)^{1/2}$ (for circular polarization a^2 has to be multiplied by 2) with $P_{z,r} = \beta_{z,r}\gamma$, the normalized density of the plasma electrons, $N_e = n_e(\xi, \rho)/n_p(0)$, and the unperturbed plasma density, $N_p = n_p(r)/n_p(0)$.

Equation 2.103 and 2.104 are derived from the relativistic equation of motion for plasma electrons

$$\frac{\partial \boldsymbol{p}}{\partial t} + (\boldsymbol{v} \cdot \boldsymbol{\nabla}) \boldsymbol{p} = -e \left(\boldsymbol{E} + \frac{\boldsymbol{v}}{c} \times \boldsymbol{B} \right). \tag{2.109}$$

Using the well-known vector identity

$$\begin{aligned} \boldsymbol{v} \times (\boldsymbol{\nabla} \times \boldsymbol{p}) &= \frac{1}{m_e \gamma} \boldsymbol{p} \times \boldsymbol{\nabla} \times \boldsymbol{p} \\ &= \frac{1}{2m_e \gamma} \boldsymbol{\nabla} |p|^2 - \frac{1}{m_e \gamma} (\boldsymbol{p} \cdot \boldsymbol{\nabla}) \boldsymbol{p}, \end{aligned} \tag{2.110}$$

one can rewrite this equation as

$$\frac{\partial \boldsymbol{p}}{\partial t} + e\boldsymbol{E} + m_e c^2 \boldsymbol{\nabla} \gamma = \boldsymbol{v} \times \left(\boldsymbol{\nabla} \times \boldsymbol{p} - \frac{e}{c} \boldsymbol{B} \right). \tag{2.111}$$

Taking the curl of this equation and using Faraday's equation (2.3) gives

$$\frac{\partial \boldsymbol{\Omega}}{\partial t} - \boldsymbol{\nabla} \times (\boldsymbol{v} \times \boldsymbol{\Omega}) = \boldsymbol{0}, \tag{2.112}$$

where $\boldsymbol{\Omega} \equiv \boldsymbol{\nabla} \times \boldsymbol{p} - e\boldsymbol{B}/c$ is called the generalized vorticity. For an unmagnetized plasma $\boldsymbol{\Omega}$ is zero at $t = 0$ and this equation implies that it then will remain

zero for $t > 0$. This gives $\boldsymbol{\nabla} \times \boldsymbol{p} - e\boldsymbol{B}/c = 0$. In a cylindrically symmetric wakefield $\boldsymbol{B} = (0, B_\theta, 0)$ and

$$\frac{\partial p_r}{\partial z} - \frac{\partial p_z}{\partial r} = \frac{e}{c} B_\theta. \tag{2.113}$$

Equation 2.111 now becomes

$$\frac{\partial \boldsymbol{p}}{\partial t} + e\boldsymbol{E} + m_e c^2 \boldsymbol{\nabla}\gamma = 0. \tag{2.114}$$

Equations 2.103 and 2.104 are the normalized versions of the z and r components of this equation. The last four expressions that describe the nonlinear wakefield can be derived from the Maxwell equations. Equations 2.105 and 2.106 are the r and z components of Ampère's law, where the current density, $\boldsymbol{J} = -en_e\boldsymbol{v}_e$, was substituted, equation 2.107 is the θ-component of Faraday's law and equation 2.108 comes from Gauss's law with $\varrho = -e(n_e - n_p)$.

Using these six equations the nonlinear wakefield can be calculated numerically. An example of a calculated wakefield is plotted in figure 2.5. The first figure (a) shows the accelerating field, in which the blue regions are the accelerating and the red regions the decelerating parts of the wakefield. The second figure (b) shows the focusing field, in which blue on top and red below means focusing and vice versa means defocusing. In this example the wakefield is generated in a plasma channel with a parabolic density profile, which is used for guiding the laser pulse. More about plasma channels can be found in section 2.6.1. As can be seen in figure 2.5, the wakefield shows a curvature of its wavefronts, which can be attributed to the use of the plasma channel in which the plasma density radially increases, yielding a longer plasma wavelength on the axis. In the nonlinear regime, curvature can also be formed due to the relativistic increase of the plasma wavelength. The curvature of the wakefield extends the overlap between the focusing and accelerating regions, which allows electrons to be accelerated over a longer distance. For the case of external bunch injection, a large overlap between focusing and accelerating regions is very important for the trapping of electrons and the use of a plasma channel is advantageous, in this case the overlap becomes larger than in a homogeneous plasma.

2.4   The Hamiltonian and separatrix

The acceleration of electrons in a laser wakefield can be studied by examining the motion of a single electron in the laser wakefield, represented by the electrostatic potential, ϕ. The one-dimensional Hamiltonian analysis of the dynamics of electrons in a wakefield can give some insight in the trapping and acceleration process. In this case we neglect the transverse variation of the wakefield, which is only valid for electrons moving along the pulse axis. For a relativistic electron in an electromagnetic field with scalar potential, ϕ, and
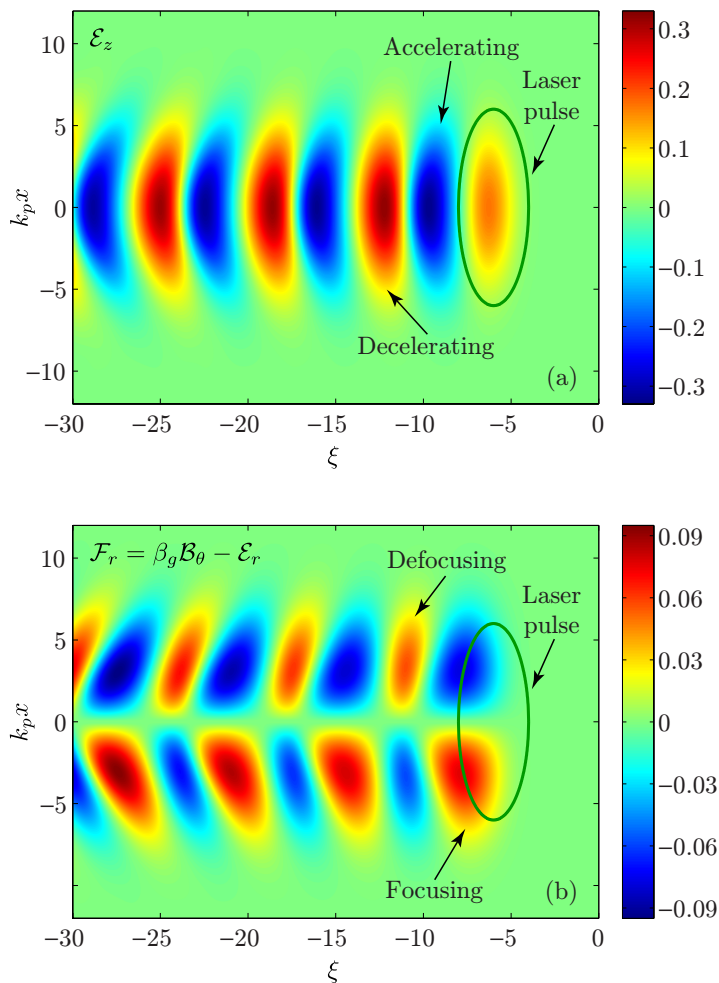
Figure 2.5: The normalized longitudinal electric field, $\mathcal{E}_z$ (a), and the transverse focusing force, $\mathcal{F}_r = \beta_g \mathcal{B}_\theta - \mathcal{E}_r$ (b), of the wakefield generated in a plasma channel. The laser pulse is centered at $\xi = -6$ and depicted by the ellipse. The parameters for the laser pulse are: $a_0 = 1$, $\sigma_r = 6$ ($w_0 = 38$ μm) and $\sigma_z = 2$ ($\sigma_z/k_p = 12.7$ μm, corresponding to a FWHM pulse duration (of the intensity) of 50 fs).

vector potential, $\boldsymbol{A}$, the Lagrangian becomes [50]

$$L = -mc^2 \sqrt{1 - \frac{\dot{\boldsymbol{x}}^2}{c^2}} + e\phi - \frac{e\dot{\boldsymbol{x}} \cdot \boldsymbol{A}}{c}. \tag{2.115}$$

The canonical momentum of the electron, $\boldsymbol{\Pi}$, can be obtained from the Lagrangian as follows

$$\boldsymbol{\Pi} = \frac{\partial L}{\partial \dot{\boldsymbol{x}}} = \frac{m\dot{\boldsymbol{x}}}{\sqrt{1 - \dot{\boldsymbol{x}}^2/c^2}} - \frac{e\boldsymbol{A}}{c}. \tag{2.116}$$

The Hamiltonian is the Legendre transform of the Lagrangian

$$H = \dot{\boldsymbol{x}} \cdot \boldsymbol{\Pi} - L = \gamma m \dot{\boldsymbol{x}}^2 + \frac{mc^2}{\gamma} - e\phi = \gamma mc^2 - e\phi. \tag{2.117}$$

The Hamiltonian for an electron in a laser wakefield depends on the position and the time coordinate only through the potentials. In the case of a laser wakefield accelerator, however, as is depicted, e.g., in figure 2.3, the potential moves along the z-coordinate with the group velocity of the laser pulse, v_g. Thus, whatever the particular form of the potential or field distribution, U, in a laser wakefield accelerator, it has the following relation between its z and t partial derivatives

$$\frac{\partial U}{\partial t} = -v_g \frac{\partial U}{\partial z}. \tag{2.118}$$

In this case the Hamiltonian has to follow the same relation

$$\begin{aligned}
\frac{\partial H}{\partial t} &= \frac{\partial H}{\partial A} \frac{\partial A}{\partial t} + \frac{\partial H}{\partial \phi} \frac{\partial \phi}{\partial z} \\
&= -v_g \frac{\partial H}{\partial A} \frac{\partial A}{\partial z} - v_g \frac{\partial H}{\partial \phi} \frac{\partial \phi}{\partial z} \\
&= -v_g \frac{\partial H}{\partial z}.
\end{aligned} \tag{2.119}$$

According to the Noether theorem, the constant of motion for such a system is $H - v_g \Pi_z$, where $\Pi_z = p_z - eA_z/c$ is the longitudinal component of the canonical momentum, which gives for the constant of motion

$$H - v_g \Pi_z = \gamma mc^2 - v_g p_z - e\phi + e\beta_g A_z = \text{constant}. \tag{2.120}$$

In the one-dimensional case $A_z = 0$. In normalized form the constant of motion becomes

$$\mathcal{H}(\gamma, \xi) = \gamma - \beta_g P_z - \Phi(\xi), \tag{2.121}$$

where $\mathcal{H}(\gamma, \xi)$ is a constant along a given electron orbit that can be used to describe the orbits of electrons in phase space (γ, ξ).

This constant of motion provides an explanation of the physics of the trapping and acceleration of an electron in a one-dimensional laser wakefield, by
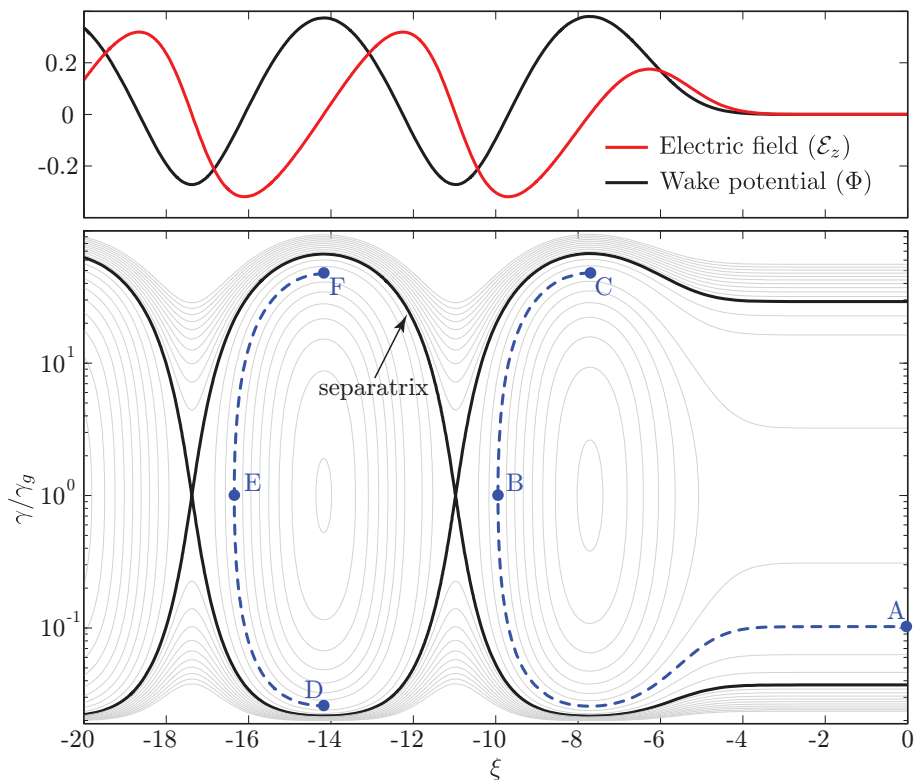
Figure 2.6: Phase space diagram for $\mathcal{H}(\gamma, \xi)$. The top graph plots the scalar potential and the electric field of the wakefield. The phase space is plotted below, where the solid black line defines the separatrix and the solid grey lines define several possible single particle orbits, described by curves of constant $\mathcal{H}(\gamma, \xi)$. The separatrix divides the phase space into two distinct areas. Within the separatrix the particle is trapped and moves on a closed orbit, whereas outside of the separatrix the particle is untrapped and moving on an open trajectory. The shown wakefield was calculated using a laser pulse with $a_0 = 1$, $\sigma_z = 2$ and $\gamma_g = 50$, which is centered at $\xi = -6$. The two blue curves show two trajectories of an injected electron. The first blue curve shows an electron injected in front of the laser pulse (at A). The second blue curve shows an electron injected behind the laser pulse (at D).

examining the electron trajectory in phase space. In figure 2.6 a phase space diagram is shown, where several electron trajectories are plotted. One can distinguish three different types of trajectories, which are separated by a phase curve called the separatrix (solid black line). Trajectories below the separatrix describe the motion of the electrons that do not have enough momentum to be captured by the wakefield. These electrons show a periodically changing kinetic energy and are slipping backwards, because they always have a lower velocity than the wakefield. Orbits above the separatrix describe the motion of electrons that have too much momentum and outrun the wakefield. These electrons always have a higher velocity than the wakefield and also have a periodically changing kinetic energy. Finally, inside the separatrix one finds closed trajectories (orbits) which describe the motion of electrons that are trapped in the wakefield. These electrons will always stay in a certain region of the wakefield, again with a periodically changing velocity.

Two of the possible trajectories of injected electrons, that correspond to trapped electrons, are shown by the blue curves. The first blue curve, starting at point A, shows an electron injected in front of the laser pulse, which means that this electron is starting from outside the wakefield, from zero potential. The laser pulse will overtake the electron, due to its higher velocity. This electron will follow the blue curve and first lose some energy, but after a while it will start to gain energy. At point B (where $\gamma/\gamma_g = 1$), which is called the turning or trapping point, the velocity of the electron, v_e, becomes equal to the velocity of the wakefield, v_g. From this point on, the electron's velocity is becoming larger than the wakefield's velocity and the electron starts to outrun the wakefield. At point C the electron has gained the maximum possible energy, because from this point on it would move into the decelerating phase of the field. This is the point where the plasma should end and the electrons should move into the vacuum. More about the injection of electrons in front of the laser pulse can be found in chapter 5.

The second blue curve, starting at point D, shows the injection of an electron behind the laser pulse. In this case the electron starts in the wakefield at point D and is accelerated. At the turning point E, the velocity of the electron becomes equal to the velocity of the wakefield. The electron is accelerated to its maximum energy at point F, from where it starts moving into the decelerating phase of the field. More about the injection of electrons behind the laser pulse can be found in chapter 3.

For an electron to become trapped, it is actually required to have a relativistic velocity initially, which could be understood as follows. The phase velocity of the wakefield is close to the speed of light. The electron has to stay in the accelerating phase of the wakefield long enough to gain enough energy to be trapped. The constant of motion, $\mathcal{H}$, allows us to also find a relationship between the initial energy of the electron, γ_0, and the wake potential at the trapping point, where γ becomes equal to γ_g. To find this relationship one has

to solve the equation

$$\gamma_0 - \beta_g \sqrt{\gamma_0^2 - 1} - \Phi_{\text{init}} = \frac{1}{\gamma_g^2} - \Phi_{\text{tr}}, \tag{2.122}$$

which has the following solution

$$\gamma_0 = \gamma_g^2 \left(\mathcal{S} - \beta_g \sqrt{\mathcal{S}^2 - \frac{1}{\gamma_g^2}} \right), \tag{2.123}$$

where $\mathcal{S} = 1/\gamma_g + \Phi_{\text{init}} - \Phi_{\text{tr}}$ with Φ_{init} the wake potential at the injection point and Φ_{tr} the wake potential at the trapping point. We will use this equation in the following chapters to study the trapping of electrons for the different external injection schemes.

2.5 Dephasing

Because the wakefield is driven by the laser pulse, its phase velocity is approximately equal to the group velocity of the laser pulse in the plasma. This can be assumed constant as long as there are no significant nonlinear effects acting on the pulse. Equation 2.28 shows that the group velocity of the laser pulse depends on the plasma density and is close to the speed of light for low plasma densities ($\omega_p \ll \omega$). However electrons that are accelerated in the wakefield over a sufficiently long distance will eventually obtain a velocity (v_e) higher than the phase velocity of the wake ($v_p \approx v_g$). The accelerated electrons will "outrun" the plasma wave and eventually slip from the accelerating phase into the decelerating phase of the wake wave. This process is called dephasing and it limits the acceleration length to the so-called dephasing length and thus dephasing forms a fundamental limitation to the maximum energy the electrons can gain. Note that the existence of a dephasing length is not a specific property of a laser wakefield accelerator, but also of all standard rf accelerators. The dephasing length can be estimated in a simplified approach when assuming a sinusoidal plasma wave. The electrons will cease to accelerate once they phase advance a distance of $(v_e - v_g)t \approx \pi/k_p$, which is half of a plasma wavelength. If we assume that $v_e \approx c$, as is usually required for trapping, the dephasing length, L_d, is given by $(1 - \beta_g)L_d \approx \lambda_p/2$ or

$$L_d \approx \gamma_g^2 \lambda_p, \tag{2.124}$$

assuming that $\gamma_g = \omega/\omega_p \gg 1$, which is fulfilled at sufficiently low plasma density (see section 2.2.5). Electrons will gain maximum energy when the acceleration length is matched to this dephasing length. To accelerate the electrons to their maximum energy we will normally choose a suitable length for the plasma. This choice will not only give the maximum possible energy, but will also often result in electron bunches with a small energy spread as we will see in the following chapters. From equation 2.124 one finds that a high

wake velocity (v_g) will give a long dephasing length, which can result in higher maximum energy for the electrons. However it requires a higher initial energy for the injected electrons (see section 2.4). The dephasing length limits the energy gain the most in high density plasmas.

2.6   Optical guiding

As was explained, the optimum acceleration is reached when the acceleration length is matched to the dephasing length. However, when calculating the typical acceleration lengths required, it turns out that an optical guiding of the drive pulse is required as well. For example, for a typical electron density of $n_e = 1 \times 10^{18}$ cm^{-3} one obtains a dephasing length of around 5.8 cm, which means that one has to maintain a high laser intensity over the same distance.

Providing a high intensity is certainly no problem when tightly focusing a laser pulse from a terawatt laser system down to a spot size of tens of micrometers. However, if behind the focus the laser pulse is not guided, the light will diverge again due to diffraction and the acceleration length will be limited by the Rayleigh length of the laser focus with the result of a less than maximized end energy of the electrons. To illustrate the need for increasing the acceleration length, let us provide some typical parameters. For a Gaussian beam propagating in free space, the beam radius, w, and therefore the intensity varies along the laser propagation axis, z, as

$$w(z) = w_0 \sqrt{1 + \left(\frac{z}{z_R}\right)^2},\tag{2.125}$$

where w_0 is the waist size and z_R is the Rayleigh length, which is given by

$$z_R = \frac{\pi w_0^2}{\lambda}.\tag{2.126}$$

The expressions show that the Rayleigh length is the distance over which the laser intensity decreases by a factor 2 relative to the intensity in the waist of the focal spot. When inserting typical experimental numbers, the Rayleigh length for a Gaussian laser pulse with a wavelength of 800 nm and focused down to a spot size of 30 μm is about 3.5 mm. This is more than a factor of 10 less than the desired acceleration length of several centimeters and would limit the maximum output energy of the accelerated electrons to at least an order of magnitude less than that which could be obtained with a matched (optimum) acceleration length. In order to reach the optimum acceleration length some guiding mechanism for the high intensity laser pulse is crucial. This requires that the refractive index of the plasma is given some suitable spatial distribution, e.g., as for low-intensity light is done in conventional graded index glass fibers.

In section 2.2.6 we derived the refractive index of a plasma. However this equation is only valid for low intensity laser pulses and homogeneous plasmas.

Variations of the plasma density due to a plasma wave or a pre-formed structure in the plasma can be incorporated into the equation by making the plasma density spatially dependent. A laser pulse with sufficient intensity will drive the oscillations of the electrons to velocities near the speed of light which will increase the relativistic mass of the electrons. This can be incorporated into the equation by replacing the on-axis plasma frequency ω_{p0} with $\omega_{p0}/\sqrt{\gamma}$. When one includes these effects into equation 2.30, which describes the refractive index, one gets

$$\eta(\mathbf{r}) = \sqrt{1 - \frac{\omega_{p0}^2}{\omega^2} \frac{n_e(\mathbf{r})}{n_{e0}\gamma(\mathbf{r})}}. \tag{2.127}$$

The density can become spatially modified due to contributions from a pre-formed plasma channel, Δn_p, or a plasma wave, δn, which modifies it to $n = n_0 + \Delta n_p + \delta n$. The relativistic factor of the electrons in the laser field is mainly given by their quiver motion, $\boldsymbol{p}_\perp = mc\boldsymbol{a}$, so $\gamma \approx \gamma_\perp = (1 + a^2)^{1/2}$. For small a, one can write $\gamma \approx 1 + a^2/2$. For a small normalized amplitude $a^2 \ll 1$, and small changes in density $|\Delta n_p/n_0| \ll 1$, $|\delta n/n_0| \ll 1$, the refractive index becomes [47]

$$\eta \approx 1 - \frac{\omega_{p0}^2}{2\omega^2} \left(1 - \frac{a^2}{2} + \frac{\Delta n_p}{n_0} + \frac{\delta n}{n_0}\right). \tag{2.128}$$

2.6.1 Plasma channel guiding

Guiding of a laser pulse becomes possible when the radial profile of the refractive index, $\eta(r)$, exhibits a maximum on axis, i.e., $\partial\eta/\partial r < 0$. In this way the diffractive divergence of the beam will be compensated by the the focusing effect of a lower phase velocity on axis. Specifically, if the refractive index shows a parabolic shape, a Gaussian intensity profile forms an eigen solution of the guided-wave equation [51]. This means that a beam with a transverse width matching the strength of the transverse index variation can be guided, without disturbances and with zero divergence, in a parabolic plasma channel over distances much longer than the Rayleigh length. It was thus an important contribution to all high intensity laser plasma experiments to discover that such a parabolic index variation can be produced in a rather simple manner, as follows [52–54]. When filling a thin capillary with neutral gas (e.g., H_2) and ionizing the gas fully with a so-called slow pulsed discharge. The heating of the plasma by the discharge current and cooling of the plasma at the walls of the capillary provides a parabolic plasma density with the required parabolic density profile. Plasma channel guiding was recently successfully used to guide the laser pulse and to accelerate electrons over distances in the order of centimeters [29, 55, 56]. This is why we have decided to base our analysis of various acceleration schemes on wave guiding in capillary discharge plasma channels. Its technological simplicity and the absence of any requirement for the intensity to achieve guiding makes it the most attractive technique for the different external injection schemes in the main part of this thesis.

For the unperturbed guiding of the laser pulse, its spot size has to be matched to the plasma channel. One can derive the required matched spot size from the wave equation for transverse waves which is given by equation 2.25,

$$\boldsymbol{\nabla}^2 \boldsymbol{E} = \frac{\omega_p^2}{c^2}\boldsymbol{E} + \frac{1}{c^2}\frac{\partial^2 \boldsymbol{E}}{\partial t^2}. \tag{2.129}$$

As a trial solution, consider the propagation of a plane electromagnetic wave with a radially decreasing amplitude, $E_0(r)$,

$$\boldsymbol{E} = E_0(r)\exp i(k_z z - \omega t)\hat{\boldsymbol{E}}, \tag{2.130}$$

with k_z the wave number in the propagation direction. Inserting this solution in the wave equation and using cylindrical coordinates yields an ordinary differential equation for the radial profile, $E_0(r)$,

$$\frac{1}{r}\frac{\partial}{\partial r}r\frac{\partial}{\partial r}E_0(r) = \left(\frac{\omega_p^2}{c^2} - \frac{\omega^2}{c^2} + k_z^2\right)E_0(r) = \left(-k^2\eta^2 + k_z^2\right)E_0(r), \tag{2.131}$$

where $\eta(r)$ is the radial refractive index distribution to be determined for guiding a given transverse field distribution. As the beam to be guided here we choose a Gaussian beam profile with a beam waist, w_0, and an amplitude,

$$E_0(r) = E_0\exp\left(\frac{-r^2}{w_0^2}\right), \tag{2.132}$$

in equation 2.131. This gives the following expression

$$-\frac{4}{w_0^2} + \frac{4r^2}{w_0^4} = -k^2\eta^2 + k_z^2, \tag{2.133}$$

showing that $\eta(r) \sim r^2$ is an index profile with the desired guiding property. As named above, the thermodynamical equilibrium of heating and cooling can provide a parabolic electron density profile. This profile can be described by

$$n_e = n_0 + \Delta n_e\left(\frac{r}{r_{\rm ch}}\right)^2, \tag{2.134}$$

where Δn_e is called the channel depth and $r_{\rm ch}$ the channel radius. The refractive index can now be written as

$$\eta^2 = 1 - \frac{4\pi e^2}{m_e\omega^2}\left(n_0 + \Delta n_e\frac{r^2}{r_{\rm ch}^2}\right). \tag{2.135}$$

By inserting this into equation 2.133 and equating the terms that are quadratic in r, one obtains the condition where matched guiding occurs. The matched spot size is

$$w_0 = \left(\frac{r_{\rm ch}^2}{\pi r_e\Delta n_e}\right)^{1/4}, \tag{2.136}$$

where $r_e = e^2/m_e c^2$ is the classical electron radius. If we take $r_{\rm ch} = w_0$, we can calculate the critical depth, which is the change in density required to guide a Gaussian beam with a spot size w_0. It is given by,

$$\Delta n_c = \frac{1}{\pi r_e w_0^2}. \tag{2.137}$$

In convenient units,

$$\Delta n_c[\mathrm{cm}^{-3}] = \frac{1.1 \times 10^{20}}{w_0^2[\mathrm{\mu m}]}. \tag{2.138}$$

Note that, if the laser spot size is not matched to the channel radius, i.e., for $\Delta n \neq \Delta n_c$, equation 2.129 yields that the laser spot size will oscillate about its matched value upon propagation through the channel.

The Gaussian beam profile turns out to be the zeroth order mode of a whole family of modes that can be guided in a parabolic plasma channel [51]. These higher order modes can become important when the laser pulse is not correctly matched to the plasma channel [57].

The propagation of a high intensity laser pulse in a plasma channel can be disturbed by two undesirable effects, namely relativistic self-focusing and plasma wave guiding. In the next two sections we will discuss these disturbances.

2.6.2 Relativistic self-focusing

A high intensity laser pulse moving through a plasma can self-focus, because the refractive index of the plasma is locally increased when the quiver velocity of the electrons approaches the speed of light. This results in an intensity dependent increase in the relativistic mass of the electrons and thus of the refractive index, which has a perturbing effect on the propagation of a laser pulse in a plasma channel. Consider a laser pulse in the weakly relativistic limit ($a^2 \ll 1$) propagating in an undisturbed plasma, where the density modulation due to the generated wave can be neglected. The refractive index of the plasma is in this case given by [47]

$$\eta = 1 - \frac{\omega_{p0}^2}{2\omega^2}\left(1 - \frac{a^2}{2}\right). \tag{2.139}$$

The equation shows that guiding of the laser pulse can take place, because the refractive index has a maximum on-axis $\partial\eta/\partial r < 0$ for the case of a laser pulse with an intensity profile that is maximum on-axis $\partial a^2/\partial r < 0$, which is a self-focusing, intensity-dependent, type of guiding. A Gaussian beam, for example, produces a Gaussian-shaped refractive index distribution suitable for self-focusing. Notice that equation 2.139 is of the form $\eta = \eta_0 + \eta_2 I$, which is similar to the case of a third-order nonlinearity in standard nonlinear optics, where such self-focusing is called Kerr self-focusing or Kerr lensing. A disadvantage of Kerr self-focusing is that shape-invariant guiding is restricted

to the so-called critical power for self-focusing, where the natural diffraction of the laser pulse is exactly balanced by the self-focusing effect. In the same way one can define the critical power for relativistic self-focusing in a plasma [58, 59]

$$P_c = \frac{m_e c^5 \omega^2}{e^2 \omega_p^2} \approx 17.4 \left(\frac{\omega}{\omega_p}\right)^2 \text{ GW}, \quad (2.140)$$

where a Gaussian laser beam profile, $a(z, r) = a_0(z) \exp\left(-r^2/w^2\right)$, was assumed. Self-focusing can be beneficial for certain laser-plasma accelerators where an increase of the interaction length between the laser and the plasma is desirable, but where no preformed plasma channel can be realized to increase the interaction length. However for schemes where the laser is guided by a plasma channel, self-focusing makes the laser beam radius oscillate during propagation through the preformed channel.

In this section we looked at self-focusing as a separate effect, where the electron density response, ∂n, was neglected. However the evolution of the laser pulse can also be strongly influenced by the plasma response. Relativistic guiding does not, for example, work if the temporal duration of the pulse becomes too short ($l \lesssim \lambda_p/\gamma_\perp$) [60, 61]. In such a case the refractive index is modified by the laser pulse on the time scale of the plasma frequency and not on the laser frequency time scale.

2.6.3 Plasma wave guiding

Besides the effect of the self-focusing of the laser pulse, the excited plasma wave also has an effect on the guiding. The plasma wave is, in part, located inside the laser pulse and the refractive index associated with the density modulation of the plasma wave affects the propagation of the pulse. The effective index of refraction for a low power ($P/P_c \ll 1$) and low intensity ($a^2 \ll 1$) laser pulse propagating in a plasma wave is given by [47]

$$\eta \approx 1 - \frac{\omega_{p0}^2}{2\omega^2} \left(1 + \frac{\delta n}{n_0}\right). \quad (2.141)$$

In order to show how the density is varying inside the laser pulse, figure 2.7 shows the electron density wave excited by a typical pulse. In the first half of the laser pulse the electron density has increased, because the ponderomotive force of the laser pulse pushes the electrons forward. There, the plasma channel is becoming less deep, which will make this part of the pulse defocus. In the second part of the laser pulse the density has decreased and the plasma channel becomes deeper, which will make this part of the pulse focus. Similarly, the variation of the electron density and the corresponding refractive index also causes a temporal deformation of the pulse. Group velocity dispersion (the group velocity at the front of the pulse is lower than the group velocity at the back) will compress the pulse and increase the peak intensity.
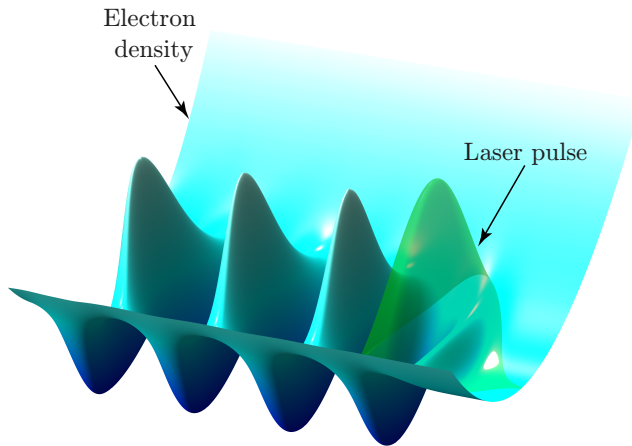
Figure 2.7: Electron density perturbation excited by a Gaussian laser pulse in a parabolic (waveguiding) plasma density with $a_0 = 1$, $\sigma_z = 2$, $k_p w_0 = 6$ and $\gamma_g = 50$.

Of course all these different dynamic processes, which will be called "the laser pulse dynamics" in the rest of this thesis, will affect the laser pulse simultaneously. This makes it impossible to give a closed analytical expression for the spatial-temporal evolution of high-intensity laser pulses. However the laser pulse evolution and the generated wakefield can be calculated numerically, which we have done with the code WAKE [62]. This code will be used extensively in the following chapters to ensure that our assumptions for the laser pulse and plasma parameters do not lead to undesired reshaping and modification of the pulse propagation.

2.7 External injection schemes

An important aspect we have not yet dealt with is the injection of the electrons into the laser wakefield. From the Hamiltonian analysis we saw that the electrons must have some minimum initial velocity and that injection has to occur at certain range of phases (i.e., combination of time and location) before electrons can be trapped in the accelerating phase of the wake. Also, the details of the injection, e.g., the initial energy and momentum distribution or duration of the bunch of injected electrons, will strongly determine the properties of the accelerated electron bunch(es), such as duration, energy spread and emittance, which comprises the so-called quality of the bunch after acceleration. Thus the injection of electrons in a laser wakefield accelerator forms a crucial part and is receiving central interest.

In internal injection schemes some electrons from the background plasma

are trapped and accelerated in a proper phase of the wakefield that yields femtoseconds relativistic bunches. An example of internal injection is the recently demonstrated "bubble" injection method [19–21]. This method provided electron bunches with energies of the order of 100 MeV and with a few percent relative energy spread. However this method still suffers from a poor shot-to-shot stability. The use of a 3.3 cm long plasma channel to extend the acceleration length led to the generation of an unprecedented 1 GeV electron bunch with 2.5% energy spread [29]. More recently the shot-to-shot stability was considerably improved by employing a second, counterpropagating laser pulse [30].

It was also proposed that external injection of a long (longer than the plasma wavelength), low energy (typically a few MeV's), electron bunch in the laser wakefield can lead to the generation of good quality femtosecond relativistic bunches [37, 38, 40, 63–70]. The injected bunch can be generated by a state-of-the-art radio-frequency (rf) photo-cathode linear accelerator (linac). This approach promises better control over the trapping and acceleration process.

The first demonstrations of the acceleration of external injected electrons by a laser wakefield accelerator was done by Clayton *et al.* [18], Nakajima *et al.* and [12] Amiranoff *et al.* [71]. In these experiments a long electron beam (20 ps [18], 200 ps [12] and continuous [71]) of several MeV was injected into a plasma wave and energy gain was demonstrated. However, the quality of the accelerated electron beam was not satisfactory, due to a non-optimum choice of parameters resulting in an enormous energy spread of one hundred percent. We will show in this thesis that external injection schemes are able to deliver high quality bunches when the right parameters are chosen and that such parameters lie in the range of what can be realized with existing technology.

Because of the small structure of the wakefield, i.e., its micron-scale longitudinal and transverse size, it was long believed that bunches with a duration less than one plasma wavelength had to be injected into a laser wakefield in order to get high quality electron bunches. The extremely high precision that seemed to be required to make laser wakefield acceleration a viable concept, namely external bunch injection with femtosecond duration and precision, made it appear an almost unsolvable challenge. However we have theoretically shown and explored the idea that a relatively long (longer than the plasma wavelength) and low energy (with a kinetic energy in the order of one or a few MeV) electron-bunch can be injected into a laser wakefield and still deliver high quality electron bunches. This prediction opens the possibility of injecting electron bunches even from conventional rf photo-cathode linacs, although such linacs can produce bunches of only relatively long duration in the order of 100 fs. These possibilities and also our exploration of such an approach have generated great interest in external electron bunch injection schemes for laser wakefield acceleration. Note however that, although the required electron bunch is long in terms of laser wakefield acceleration, it is actually short in terms of conventional accelerator physics and the generation of such bunches is not a trivial task. There are three different schemes for the external injection

of an electron bunch longer than the plasma wavelength into a laser wakefield. The electron bunch can be injected behind, in front or at an angle in relation to the drive laser pulse. These schemes will be introduced in the following chapters and for convenience sake, we will often call them "injection behind", "injection in front" and "injection at an angle".

3

Injection behind the laser pulse

It has long been believed that the only way to deliver high quality electron bunches was to inject an electron bunch with a length much smaller than the plasma wavelength ($\ll$ 100 µm). One expected that bunches in the order of or longer than the plasma wavelength would be spread over all the phases of the wakefield, resulting in an energy spread of 100% for the trapped electrons. Producing electron bunches much shorter than the plasma wavelength in a conventional accelerator is almost impossible and it appeared that the long bunches from such an accelerator were not suitable for injection into a laser wakefield. However, Gordon *et al.* [37] realized that such short electron bunches are not always necessary. The accelerating structure of the wakefield can, under certain conditions, act like a "chopper" or "slicer" when the electron bunch is injected behind the drive pulse in the wakefield. By carefully choosing the injection energy, this can result in a train of extremely short bunches of a few microns in size which are accelerated at almost the same phase of the wakefield to high energy (hundreds of MeV) with a relatively low energy spread (of the order of one or a few percents). This opens the possibility of using conventional radio-frequency (rf) accelerators, capable of generating electron bunches with sub-picosecond duration, to provide the injected electron bunches.

Several calculations have been carried out that proved the feasibility of this scheme [37, 65–67, 69, 72–75]. However, we found that two important perturbing effects which can severely hinder the trapping of electrons have been overlooked in these calculations thus far. The first effect is ponderomotive scattering in vacuum. When the electron bunch is injected into the laser wakefield, it is important to take into account the interaction of the injected electron bunch with the laser pulse in the vacuum region located in front of the plasma.

The second effect is the transition from vacuum to plasma. Previous calculations assumed a sharp plasma boundary, however, in reality there is always a finite transition region. The plasma wavelength in this region changes continuously, which means that the injected electrons see an altering wakefield. Both, ponderomotive scattering and the vacuum-plasma transition can result in strong scattering of the injected bunch even before it reaches the regular wakefield.

In this chapter we study the importance of these effects and how they modify the properties of the external injection of an electron bunch behind the drive pulse. The following section discusses the mechanism of the trapping of electrons using this scheme with an analysis based on the Hamiltonian dynamics developed in section 2.4. In the next two sections, we describe and study the two problems connected to this scheme. First, ponderomotive scattering in vacuum and second, the transition from vacuum to plasma. In section 3.4, we examine the properties of injection behind the laser pulse in some more detail. The final section gives a summary and conclusion.

3.1   The injection scheme

Before the properties and the perturbing effects of injection behind the laser pulse can be discussed, some basic introduction of the injection scheme is useful. The injection scheme is schematically shown in figure 3.1. An electron bunch, accelerated in a conventional accelerator to several MeV's, is focused into a plasma channel immediately behind a high-intensity drive laser pulse. Once the electron bunch enters the plasma channel, it will immediately experience the wakefield created there by the laser pulse. As will be shown in this chapter, the bunch, which is generally several times longer than the plasma wavelength, will be sliced into several smaller bunches with a duration of a few femtoseconds and a transverse size of a few micrometer in the wakefield. These small bunches are formed in the phases of the wakefield where the focusing and accelerating parts overlap because this is where the electrons can be trapped and bunch compression takes place. The phases, where trapping can occur are separated by one plasma wavelength and thus the trapped bunches will also be separated by one plasma wavelength. Electrons that are not injected in the proper phase are scattered by the wakefield.

However, there are two problems connected to this scheme that appear to have been overlooked so far and which we address here for the first time. First there is the problem of ponderomotive scattering [40]. Before acceleration, the electron bunch propagates more slowly than the laser pulse in the vacuum, which means that, at some distance in front of the plasma channel, the bunch is situated ahead of the laser pulse. Therefore the electron bunch has to propagate through the laser pulse in the vacuum and the interaction between the laser pulse and the electron bunch at that point has to be taken into account. This interaction can lead to strong scattering of the bunch in the vacuum, especially in the case of low injection energies. Section 3.2 will give a detailed analysis of
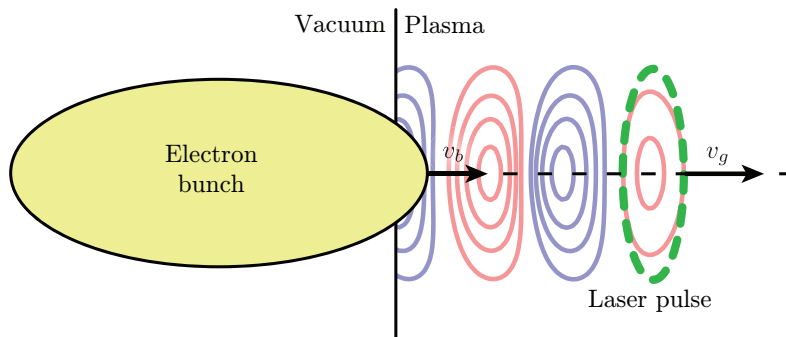
Figure 3.1: Schematic drawing of injection behind the laser pulse into a laser wakefield. An electron bunch with velocity v_b is injected into a laser wakefield.

ponderomotive scattering.

Second, there is the problem of the vacuum-plasma transition [41]. At the entrance of the plasma channel, there is a transition region in which the electron density grows from zero to the constant density in the channel. For a capillary-discharge plasma channel, the transition length is typically a few mm [76]. The growing electron density in this region can severely perturb the trapping process because, in this case, the plasma wavelength is not constant (as was assumed in the previous chapter), but changes continuously. The electrons will experience an altering wakefield, which can result in strong defocusing of the injected bunch. This effect becomes important for strong wakefields, long transition lengths and low injection energies, as will be explained in section 3.3, where we thoroughly investigate this effect.

For the injection of electron bunches behind the driving laser pulse to work, the above mentioned effects have to be minimized by taking a sufficiently low drive laser intensity ($a_0 < 0.5$) and by injecting the bunch with a relatively high energy. In the next section we will show, with the help of Hamiltonian dynamics, that the injection of a long electron bunch can indeed provide high quality bunches.

3.1.1 One-dimensional theory

It has always been thought that an externally injected electron bunch has to be much shorter than one plasma wavelength in order to acquire high quality (i.e., low energy spread) electron bunches. This would require extremely short electron bunches with a maximum of a few tens of femtoseconds duration, which are very difficult to obtain from a conventional rf accelerator. In this section we question this paradigm and show that bunches with such a short duration are not necessary [37]. We will estimate the basic properties, such as the minimum trapping energy and the length of the trapped bunches, for the
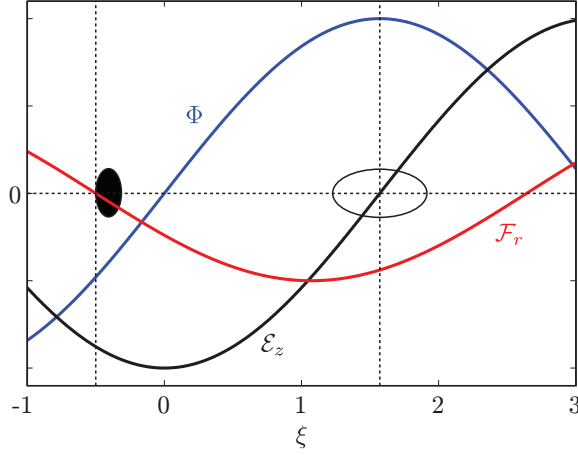
Figure 3.2: The wake potential Φ, the longitudinal $\mathcal{E}_z$ and transverse $\mathcal{F}_r = \beta_g \mathcal{B}_\theta - \mathcal{E}_r$ components of the wakefield versus the injection phase. The dashed vertical lines mark out the trapping region ($\mathcal{E}_z < 0$ and $\mathcal{F}_r < 0$). The black ellipse represents the trapped bunch and the white ellipse shows the initial phase range for the trapped electrons.

injection of a long ($\gg \lambda_p$) electron bunch behind the laser pulse.

To illustrate the basic working principle of this scheme, we first choose the one-dimensional approach based on Hamiltonian dynamics, before three-dimensional calculations are presented later. Suppose that a mono-energetic electron beam is injected with a length much longer than the plasma wavelength, which is equivalent to simultaneous injection in all phases of the wakefield. Suppose also that we operate at such a low laser power that the wakefield is linear and can be described by the on-axis wake potential $\Phi = \Phi_m \sin(\xi)$, where $\xi = k_p(z - v_g t)$ with $k_p(\omega_p)$ the plasma wavenumber (frequency). Figure 3.2 shows the typical behavior of the wakefield components near the axis, where, under certain conditions, part of the injected bunch is trapped. The phase region suitable for trapping and accelerating electrons is depicted by two dotted vertical lines and is given by $\xi_- \leq \xi \leq \pi/2$. In a uniform plasma $\xi_- = 0$; however, in a plasma channel the focusing region shifts somewhat to the left [37, 64, 77], and $\xi_- < 0$. Suppose that an electron with a relativistic factor $\gamma_0 < \gamma_g = (1 - \beta_g^2)^{-1/2}$ is injected at $\xi = \xi_0$. Because the injected electron travels slower than the laser pulse ($v_e < v_g$), it slips backward relative to the pulse and can gain energy in the accelerating region. If the wake amplitude is sufficiently large and the electron is injected at the proper phase, it can reach $\gamma = \gamma_g$ at the trapping (turning) point and can then be accelerated to high energy. The trapping phase, ξ_t, can be found from the constant of motion

derived in the previous chapter (equation 2.121)

$$\sin{(\xi_t)} = \sin{(\xi_0)} - \frac{\gamma_0 - 1/\gamma_g - \beta_g\beta_0\gamma_0}{\Phi_m} = \sin{(\xi_0)} - q(\gamma_0). \qquad (3.1)$$

Taking into account that $\xi_- \leq \xi_t \leq \pi/2$ and $q \geq 0$, one has the following trapping condition for the initial phase of the injected particles

$$\sin{(\xi_0)} \geq q(\gamma_0) + \sin{(\xi_-)}. \qquad (3.2)$$

Obviously, when $S \equiv q(\gamma_0) + \sin(\xi_-) > 1$ no electrons can be trapped in the wakefield, because the initial energy of the injected beam is too low for the chosen wakefield. For a higher injection energy, when $S = 1$, only electrons injected at $\xi_0 = \pi/2$ can be trapped, and the trapping point is at $\xi_t = \xi_-$. Here, the minimum relativistic factor for trapping, $\gamma_{\min}$, can be found from the equality $S = 1$. When $\gamma_g^2 \gg \gamma_0^2 \gg 1$ we get the following expression for $\gamma_{\min}$

$$\gamma_{\min} \approx \frac{1}{2\left[(1 - \sin{(\xi_-)})\,\Phi_m + \gamma_g^{-1}\right]}, \qquad (3.3)$$

which is in good agreement with numerical calculations. When $\gamma_0 > \gamma_{\min}$ (in the case $S < 1$) the region of initial phases for trapped electrons becomes $\pi/2 - \delta\xi_0/2 \leq \xi_0 \leq \pi/2 + \delta\xi_0/2$, where $\delta\xi_0$ is the width of the region. This region is depicted in figure 3.2 by the white ellipse. The trapped electrons occupy the phase region $\xi_- \leq \xi_t \leq \xi_- + \delta\xi_t$, depicted by the black ellipse in figure 3.2. One can show that electrons at the borders of the initial trapping region, with $\xi_0 = \pi/2 \pm \delta\xi_0/2$, are trapped at the same point, namely at $\xi_t = \xi_-$, and electrons with $\xi_0 = \pi/2$ are trapped at $\xi_t = \xi_- + \delta\xi_t$. The width of the initial region for trapped electrons, $\delta\xi_0$, is determined by the equality $\sin{(\pi/2 + \delta\xi_0/2)} = S$ [37], from which we find

$$\delta\xi_0 = 2\arccos{(S)}. \qquad (3.4)$$

The collection efficiency, i.e., the ratio of the number of trapped electrons to the total number of injected particles, is $\delta\xi_0/2\pi$. The width of the trapping region, $\delta\xi_t$, can be calculated by taking into account that $\xi_t = \xi_- + \delta\xi_t$, corresponds to $\xi_0 = \pi/2$. In this case, from equation 3.1, we have $\delta\xi_t = \arcsin{(1-q)} - \xi_-$. This gives for the trapped bunch a length of

$$l_t = \frac{\lambda_p\delta\xi_t}{2\pi} = \left(\frac{\lambda_p}{2\pi}\right)[\arcsin{(1-q)} - \xi_-], \qquad (3.5)$$

where λ_p is the plasma wavelength. The most interesting case is that of a short trapped bunch ($\delta\xi_t \ll 1$). In this case a small energy spread in the accelerated bunch can be achieved

$$\delta\xi_t \approx \frac{q(\gamma_{\min}) - q(\gamma_0)}{\cos{(\xi_-)}}, \qquad (3.6)$$

and, if additionally $\gamma_g^2 \gg \gamma_{0,\min}^2 \gg 1$

$$\delta\xi_t \approx \frac{1/\gamma_{\min} - 1/\gamma_0}{2\Phi_m \cos(\xi_-)}.$$

(3.7)

For example, when $\xi_- = -0.75$, $\lambda_p = 40$ μm, $\gamma_g = 50$, $\Phi_m = 0.1$ and the injection energy is 1.6 MeV ($\gamma_0 \approx 4.13$), this expression predicts a trapped bunch length of approximately 5 μm, which is in good agreement with simulations. Thus, when the injection energy is close to the minimum trapping energy, the trapped bunch length can be much smaller than the plasma wavelength. The reason for this is that, in this case, the trapped electrons experience almost the same accelerating force leading to a small energy spread in the accelerated bunch [37]. Increasing the initial bunch energy increases the collection efficiency and, also, the trapped bunch length. However, this results in a greater energy spread of the accelerated bunch. Hence, there is a trade-off between the collection efficiency and the energy spread of an accelerated bunch. The above estimations confirm that a long (unphased) electron bunch injected into a laser wakefield can lead to very short accelerated bunches with small energy spread, although with a low trapping efficiency.

The presented one-dimensional theory gives some basic insight into the injection process. However, it is only valid for on-axis electrons. The three-dimensional properties of the wakefield play an important role as well, especially for off-axis electrons. In the next two sections we will investigate two important perturbing effects that, mainly, off-axis electrons will experience: ponderomotive scattering [40] and the vacuum-plasma transition [41].

3.2   Ponderomotive scattering

At high intensity, a laser pulse can create a wakefield in a plasma, because it can push the electrons in the plasma away through the ponderomotive force (see section 2.3.2). As we have pointed out above, the ponderomotive force can also form a serious problem. Ponderomotive scattering of electrons can also take place in vacuum, when a laser pulse and an electron bunch meet, even before the acceleration in the wakefield can begin. This can be a problem when the electron bunch is injected in the wakefield just behind the laser pulse because, for this scheme, the laser pulse has to overtake the electron bunch at a certain distance before the plasma channel. In this section we will present our calculations of such scattering and its undesired effect on the trapping and acceleration of the bunch in the wakefield [40].

When an electron bunch is injected into the laser wakefield behind the laser pulse, i.e., in the standard approach, one has to take into account the following. Because the electron bunch propagates slower than the laser pulse in vacuum, there will be a certain distance in front of the plasma (actually in the vacuum) where the bunch must be situated in front of the laser pulse. This situation is schematically depicted in figure 3.3. Therefore the bunch is

exposed to the laser pulse while traveling through the vacuum and one has to take into consideration the action of the pulse on the injected bunch before both enter the plasma. The distance from the plasma at which the laser pulse starts to overtake the electron bunch, L_c (catching distance), can be calculated with the following expression

$$L_c = \frac{\ell}{1 - v_b/c},\qquad(3.8)$$

where ℓ is the distance from the head of the laser pulse to the tail of the electron bunch at the entrance of the plasma channel, v_b is the bunch velocity and c is the speed of light in vacuum. When the relativistic factor of the injected bunch, γ_0, is much larger than one ($\gamma_0^2 = (1 - \beta_b^2)^{-1} \gg 1$), this equation can be approximated by

$$L_c \approx 2\gamma_0^2\ell,\qquad(3.9)$$

where $\beta_b = v_b/c$ is the normalized bunch velocity. If we take for example an electron bunch with a kinetic energy of 1.6 MeV ($\gamma_0 \approx 4.13$) and $\ell \approx 180$ μm, the catching distance is approximately 6.1 mm. For comparison, a laser pulse with a spot radius $w_0 = 30$ μm and a wavelength $\lambda = 0.8$ μm has a Rayleigh length $z_R = \pi w_0^2/\lambda$ of approximately 3.5 mm. This means that the intensity of the laser pulse when it overtakes the electron bunch is close to its value at the focus. For sufficiently high intensity in the focus, the ponderomotive force [78] could lead to strong scattering of the injected bunch. It is clear from equation 3.8, that as the initial energy of the electron bunch is increased, the major part of the bunch interacts with the laser pulse at a relatively longer distance from the focus (the entrance of the plasma channel), where the ponderomotive force would be weaker, due to the smaller spotsize of the laser beam at that location. The effect of ponderomotive scattering might be neglected in this case. However one should bear in mind that, to obtain an optimum laser wakefield acceleration, the injection energy, amplitude of the laser pulse and the wakefield, and the parameters of the accelerated bunches depend on each other.

Injection of the electron bunch into the plasma at a larger distance from the laser pulse could also weaken the effect of ponderomotive scattering, because the interaction in vacuum takes place at a larger distance from the focus, where the ponderomotive force is weaker. However, as we will explain now, the "quality" of the wakefield degrades at a larger distance from the focus. To prevent diffraction broadening of the laser pulse in the plasma, a preformed plasma channel with a minimum density on-axis is needed to guide the laser pulse in the wakefield accelerator [47]. The laser wakefield generated in a plasma channel has characteristic properties. Due to the radial profile of the unperturbed plasma density in the channel, and due to the nonlinearity of the wakefield (if the peak intensity of the laser pulse is sufficiently high), the wake phase front becomes curved [2, 77, 79, 80]. The radius of curvature decreases with the distance from the laser pulse. This leads to oscillations of the wakefield in the radial direction, and to transverse wave breaking [81] at some distance from the
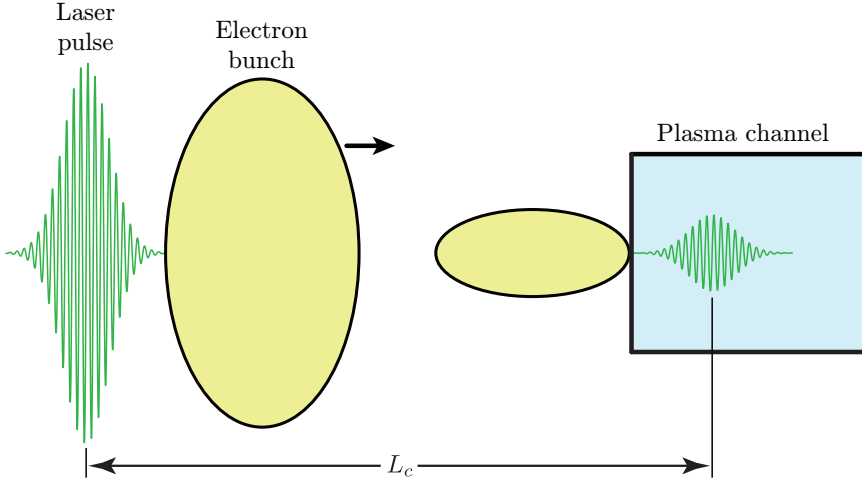
Figure 3.3: Schematic view of the injection of an electron bunch behind the drive laser pulse into a channel-guided laser wakefield. The electron bunch and the laser pulse are both focused into the plasma channel.

laser pulse. It is important to note that curvature of the phase front provides a broader phase region where electrons can be trapped and accelerated [77]. The amplitude of the accelerating (focusing) component of the wakefield decreases (increases) with the distance from the laser pulse [77]. Therefore, the "quality" of the wakefield degrades with distance from the pulse (in recent experiments [19–21] the electron bunch is accelerated in the first accelerating bucket behind the laser pulse). Our results show that the effect of the ponderomotive scattering can be weakened when injecting further behind the laser pulse, however, this comes at the cost of larger energy spread in the accelerated bunch making it undesirable for many potential applications.

In the next section we describe the model used to calculate the effect of ponderomotive scattering.

3.2.1   The model

For our modeling of the trapping and acceleration of injected electron bunches in a laser wakefield, we choose laser and bunch parameters close to those that can be realized in practice and are planned to be used in experiments on external bunch injection in laser wakefield acceleration [42, 74]. According to our modeling of the generation, transportation, and focusing of sub-picosecond electron bunches with an energy of several MeV [42], the bunch radius in the focus is of the order of 30 μm assuming that the bunch charge is below the beam loading limit [64] for the laser wakefield accelerator, which is typically of the order of 10-20 pC (see also [70, 75]). This is approximately equal to the

typical laser spot radius in channel-guided laser wakefield acceleration. The bunch diameter during transportation to the channel, before focusing, is typically of the order of a few millimeters [75]. We take these values into account in our calculations.

For our calculations, we assume an axially symmetric laser pulse with a Gaussian profile in both longitudinal (z) and transverse (r) directions. The normalized amplitude of the pulse is described as follows

$$a = a_0 \left(\frac{w_0}{w} \right) \exp \left(-\frac{r^2}{w^2} - \frac{(z - v_g t)^2}{l^2} \right), \tag{3.10}$$

where a_0 is the peak amplitude, l is the laser pulse length, w is the beam radius (spotsize) at which the intensity drops to $1/e^2$, and w_0 is the spotsize at the focus or waist size. For a Gaussian pulse the spotsize varies along the laser propagation axis as

$$w(z) = w_0 \sqrt{1 + \left(\frac{z}{z_R} \right)^2}, \tag{3.11}$$

where z_R is the Rayleigh length, which is a function of the laser wavelength, λ. It is given by

$$z_R = \frac{\pi w_0^2}{\lambda}. \tag{3.12}$$

The pulse is linearly polarized and is focused and matched to a preformed, fully ionized plasma channel, where it is guided with a constant radius. The unperturbed density of plasma electrons is, in this case [47]

$$n_p(r) = n_p(0) \left[1 + \left(\frac{2}{k_p w_0} \right)^2 \frac{r^2}{w_0^2} \right]. \tag{3.13}$$

In such a plasma channel, due to the associated quadratic decrease of the refractive index from the axis, the laser pulse spot size, w, remains constant upon guiding, $w(z) = w_0$, and the velocity of the laser pulse is v_g. While in front of the channel the pulse propagates in vacuum with $w = w_0 (1 + z^2/z_R^2)^{1/2}$ (see e.g., [78]) and velocity c, and where the ponderomotive force $\boldsymbol{F}_p = -(m_e c^2/4\gamma)\boldsymbol{\nabla} a^2$ is used to calculate the action of the laser pulse on the bunch. The ponderomotive force pushes charged particles towards the regions with lower intensity, i.e., outside the path of the laser pulse. The normalized ponderomotive force is given by

$$\frac{d\boldsymbol{P}}{d\tau} = -\frac{1}{4\gamma} \boldsymbol{\nabla} a^2, \tag{3.14}$$

with $\gamma = \sqrt{1 + \boldsymbol{P}^2 + a^2/2}$, where $\boldsymbol{P}$ is the normalized momentum of the electron. In cylindrical coordinates the components of the ponderomotive force

become

$$\frac{dP_z}{d\tau} = -\frac{1}{4\gamma}\frac{\partial a^2}{\partial \zeta}, \tag{3.15}$$

$$\frac{dP_r}{d\tau} = -\frac{1}{4\gamma}\frac{\partial a^2}{\partial \rho}, \tag{3.16}$$

where $\zeta = k_p z$ and $\rho = k_p r$. Combining

$$\frac{d\gamma}{d\tau} = \boldsymbol{\beta}\frac{d\boldsymbol{P}}{d\tau} + \frac{1}{4\gamma}\frac{da^2}{d\tau}, \tag{3.17}$$

with equation 3.14 gives

$$\frac{d\gamma}{d\tau} = \frac{1}{4\gamma}\left(\frac{da^2}{d\tau} - \boldsymbol{\beta}\boldsymbol{\nabla}a^2\right) = \frac{1}{4\gamma}\frac{\partial a^2}{\partial \tau}. \tag{3.18}$$

For the z-component we can write

$$\frac{dP_z}{d\tau} = \frac{d(\beta_z\gamma)}{d\tau} = \beta_z\frac{d\gamma}{d\tau} + \gamma\frac{d\beta_z}{d\tau} = \beta_z\frac{1}{4\gamma}\frac{\partial a^2}{\partial \tau} + \gamma\frac{d\beta_z}{d\tau} = -\frac{1}{4\gamma}\frac{\partial a^2}{\partial \zeta},$$

which gives

$$\frac{d\beta_z}{d\tau} = -\frac{1}{4\gamma^2}\left(\frac{\partial a^2}{\partial \zeta} + \beta_z\frac{\partial a^2}{\partial \tau}\right). \tag{3.19}$$

The same expression for the r-component yields

$$\frac{d\beta_r}{d\tau} = -\frac{1}{4\gamma^2}\left(\frac{\partial a^2}{\partial \rho} + \beta_r\frac{\partial a^2}{\partial \tau}\right). \tag{3.20}$$

Equations 3.19 and 3.20 are used to describe the interaction of the laser pulse with the electrons in the vacuum. Inserting the normalized amplitude for a Gaussian laser pulse, as is given by equation 3.10, into these equations gives the expressions used for the calculation of the trajectory of the electrons moving through the laser pulse.

The injected bunch is modeled numerically by a random Gaussian distribution (which is obtained from the standard uniform random-number generator by the Box-Muller transformation [82]) in both longitudinal and transversal directions, with an average electron concentration

$$n_b = n_{b0}\exp\left[-\frac{x^2 + y^2}{r_b^2} - \frac{(z - v_b t)^2}{\sigma_b^2}\right], \tag{3.21}$$

where r_b and σ_b are, respectively, the bunch size in transverse and longitudinal directions. The channel-guided laser wakefield is calculated with our fluid-Maxwell code [38, 83], which solves the set of equations derived in section 2.3.6. The electron motion in the wakefield is calculated with the corresponding

equation of motion, in the same way as described in [38]. For an axially symmetrical laser pulse the following electrical and magnetic fields are generated in a plasma channel: $\boldsymbol{E}(E_r, 0, E_z)$, $\boldsymbol{H}(0, H_\theta, 0)$. It should be mentioned that the slab geometry (when laser and bunch parameters depend on one transverse coordinate only, for example x) sometimes used in the literature gives different results in comparison to a, seemingly more realistic, axially symmetrical geometry. This is particularly important for simulations of the bunch-laser interaction in vacuum. Our simulations for both cases show that the difference in the results may be up to ten percent, because the slab geometry overestimates the number of electrons near the wakefield axis.

For our simulations we choose typical parameters for laser wakefield acceleration in a plasma channel: $\lambda = 0.8$ μm, $\lambda_p = 47$ μm (corresponding to a plasma electron concentration of approximately 5×10^{17} cm^{-3}), $w_0 = 30$ μm, $l = 15$ μm (that corresponds to full-width-at-half-maximum [FWHM] pulse duration of approximately 59 fs for the intensity profile), the spot-size-corrected gamma factor [2, 37], corresponding to the laser group velocity in the channel of $(\lambda_p/\lambda_L)[1 + (\lambda_p/\pi w_0)^2]^{-1/2} \approx 52.6$. The longitudinal, $\mathcal{E}_z$, and transverse, $\mathcal{F}_r = \beta_g \mathcal{B}_\theta - \mathcal{E}_r$, components of the wakefield generated in a matched plasma channel by a laser pulse with the above mentioned size and with $a_0 = 0.5$ are shown in figure 3.4. The wakefield is normalized to the wave-breaking field $E_{\mathrm{WB}} = m_e \omega_p(r=0)c/e$ [2], which in our case, is approximately 680 MV/cm. Figure 3.4 displays all the features of the calculated wakefield as generated in the plasma channel. The electron bunch is focused at the entrance of the channel to a radius $r_b = w_0 = 30$ μm and with a convergence angle of $0.42°$ ($\approx 7 \times 10^{-3}$ rad), so that the bunch radius is 1.5 mm 20 cm in front of the channel. The FWHM duration of the injected bunch is 250 fs, corresponding to $\sigma_b = 45$ μm. The full duration of the bunch can be estimated as 500 fs, which corresponds to a bunch length of 150 μm. Here it should be noted that during focusing, the bunch typically becomes somewhat longer because off-axis particles travel a longer distance to the focus as compared to the on-axis particles. This effect, though small for our parameters, is also taken into account in our simulations. The plasma channel length is fixed to 5 cm, which is a typical value for capillary plasma channels. The collection efficiency, energy spread and mean energy of the accelerated bunches are calculated for all trapped electrons.

3.2.2 The effect of ponderomotive scattering

In our calculations we consider the case where one attempts to inject the bunch into the wakefield just after the pulse. The bunch center is chosen to be 75 μm from the laser pulse center when the bunch enters the channel. Four trapped bunches are formed in this case.

To demonstrate the effect of ponderomotive scattering on the injected bunch in front of the plasma channel, we choose $a_0 = 0.5$ (corresponding to a peak intensity of 5.3×10^{17} W/cm^2; in this case $\Phi_{\max} \approx 0.1$) and an injection energy of the bunch of 2.6 MeV. Figure 3.5 shows the injected bunch at the entrance
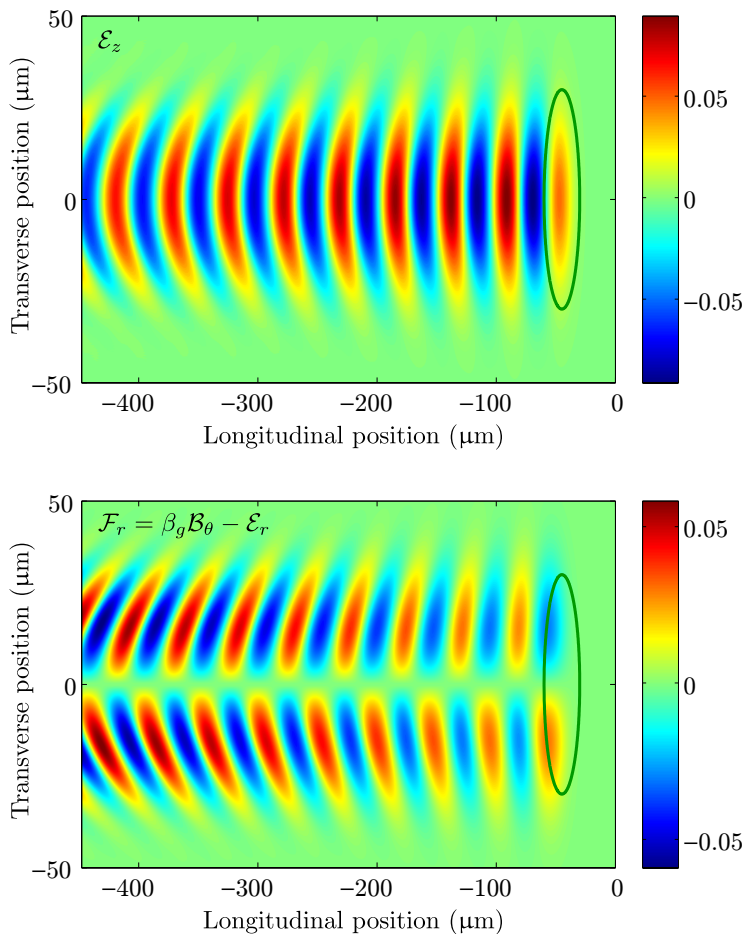
Figure 3.4: The normalized longitudinal, $\mathcal{E}_z$, and transverse, $\mathcal{F}_r$, components of the laser wakefield generated in a plasma channel. The laser pulse parameters are $a_0 = 0.5$, $w_0 = 30$ μm ($k_p w_0 = 4$), $l = 15$ μm ($\sigma_z = 2$, that corresponds to a FWHM duration of approximately 59 fs). The position of the laser pulse is depicted by the ellipse.
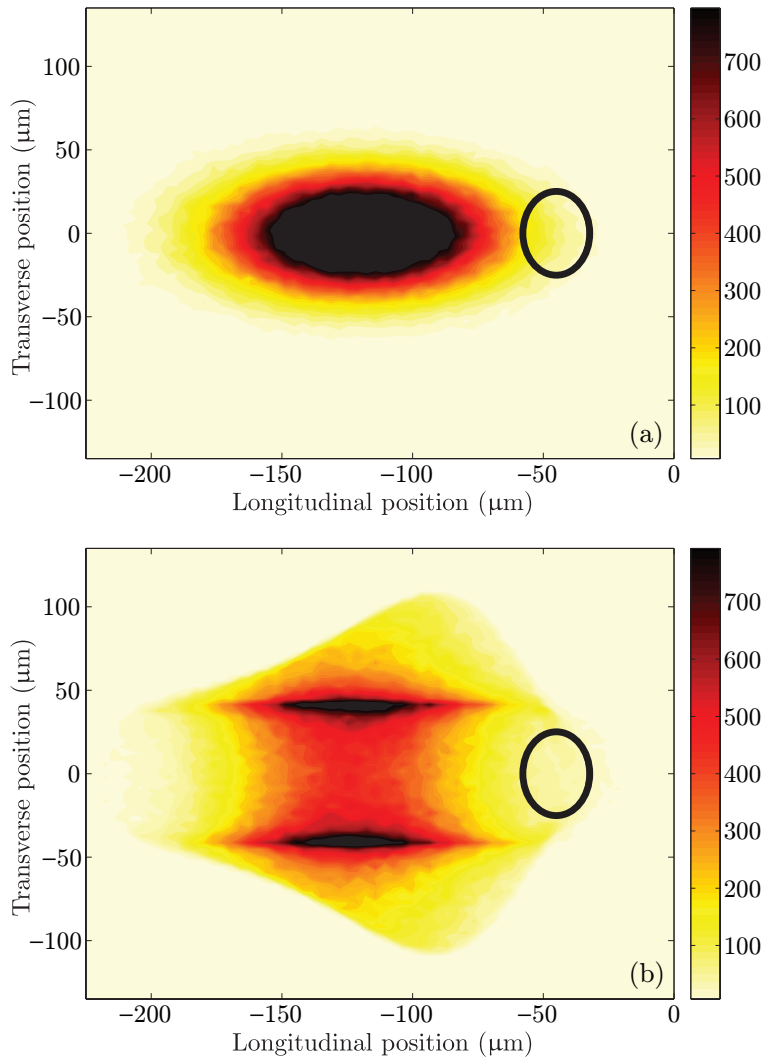
Figure 3.5: The electron concentration (in arbitrary units) in the injected bunch at the entrance of a plasma channel, without (a) and with (b) ponderomotive scattering by the laser pulse in front of the plasma channel. The initial kinetic energy of the bunch is 2.6 MeV, the normalized laser pulse amplitude at the focus is $a_0 = 0.5$. The ellipses depict the position of the laser pulse. Both the electron bunch and the laser pulse propagate to the right

of the plasma channel without and with the laser-bunch interaction in front of the channel. The energy of the electrons after interaction with the laser pulse in vacuum changes insignificantly. However, one can see, by comparing figure 3.5b with 3.5a, that strong ponderomotive scattering of most of the injected electrons occurs. The electrons are pushed in the transverse directions due to the radial component of the ponderomotive force. Most of the electrons are thereby injected into a region where the wakefield is weak. As a result the fraction of trapped particles (collection efficiency) can drop dramatically, in the shown example from 12.8% down to 0.19%.

To study the effect of ponderomotive scattering on the trapping and acceleration of the injected bunch in a laser wakefield accelerator more systematically, we calculated the dynamics of the bunch after its interaction with the pulse in front of a plasma channel, in the laser wakefield. Figure 3.6 compares the collection efficiency, the root-mean-square (rms) relative energy spread and the mean energy of the accelerated bunches as a function of the injection energy, with and without the interaction in front of the channel. It can be seen that, by taking into account the ponderomotive scattering, the collection efficiency drops considerably at low injection energies. In this case the collection efficiency is close to zero for injection energies below 3 MeV. At higher injection energies the effect of the scattering becomes weaker, as mentioned above. However, in this case, the energy spread of the accelerated bunches becomes larger. It is remarkable that ponderomotive scattering can lead to a smaller energy spread, (compared to the case when the scattering is off) due to a smaller contribution from the off-axis electrons. Therefore, because of ponderomotive scattering, the compromise between the energy spread and the collection efficiency is reached at higher injection energies. The mean energy of the accelerated bunch is about 250 MeV for practically interesting injection energies.

In figure 3.7 we plot the calculated collection efficiency and the relative energy spread of the accelerated bunches for the case of lower laser intensity, $a_0 = 0.2$ (peak intensity of $\approx 8.4 \times 10^{16}$ W/cm^2), for which $\Phi_{max} \approx 0.015$ and the minimum trapping energy is approximately 5.5 MeV ($\gamma_{min} \approx 12$). It can be seen that both values grow monotonically with the injection energy. The calculations show that the effect of ponderomotive scattering is negligible due to the lower pulse intensity and longer catching distance (remember that $L_c \propto \gamma_0^2$). Most of the injected electrons interact with the laser pulse at a large distance from the focus, where the ponderomotive force is weak. For the range of injection energies used for figure 3.7, the mean energy of the accelerated bunches lies between 37 and 51 MeV's.

3.2.3   Different injection positions

As we have already discussed above, the structure of the laser wakefield in a plasma channel changes with the distance from the laser pulse: the wake phase front becomes more curved and the accelerating (focusing) field becomes weaker (stronger) as the distance from the pulse increases. The effect of the
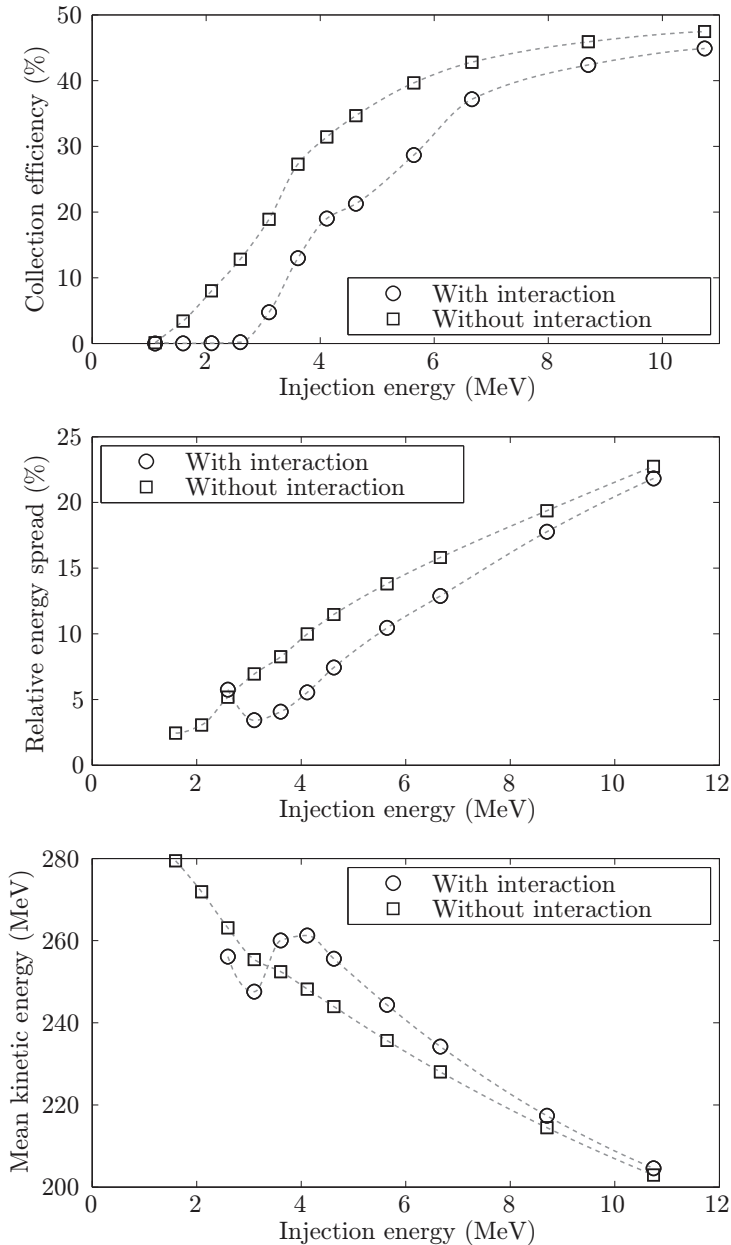
Figure 3.6: The collection efficiency, relative energy spread and mean energy of the accelerated bunches vs. the kinetic energy of the injected bunch. The lines show the values obtained with and without scattering of the injected electron bunch by the laser pulse in front of the plasma channel.
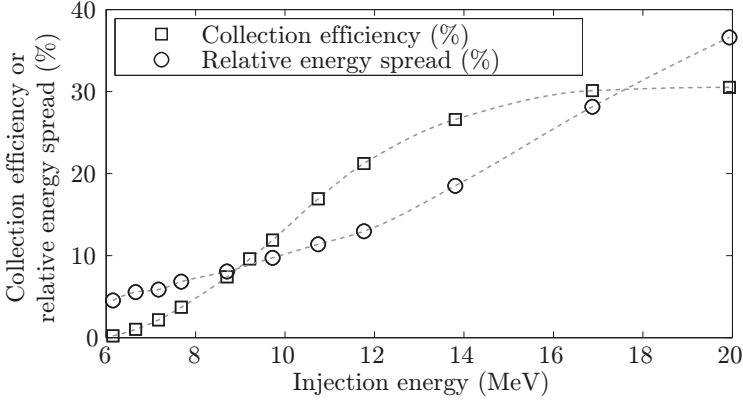
Figure 3.7: The collection efficiency and the relative energy spread in the case of a lower intensity laser pulse, $a_0 = 0.2$. Other parameters are the same as in figure 3.6.

ponderomotive scattering may be weakened when an electron bunch is injected into the laser wakefield at a larger distance from the laser pulse. This is because the laser-bunch interaction in vacuum will take place at a larger distance from the focus where the ponderomotive force is weaker. To study the effect of different injection positions in the wakefield on the dynamics of the injected bunch, we increased the distance between the bunch and the laser pulse, such that the bunch center is now at a distance of 275 μm (this corresponds to about 6 plasma wavelengths) from the pulse center when the bunch enters the channel (see figure 3.4). The other parameters are the same as before. In figure 3.8 we present the simulation results for the collection efficiency and relative energy spread for $a_0 = 0.5$. One can see that ponderomotive scattering still plays a significant role at low injection energies, although the catching distance in this case is approximately two times longer than in the previous case. In general the collection efficiency is larger if the bunch is injected at a longer distance from the laser pulse; however, the energy spread also becomes larger (compare figures 3.6 and 3.8), which is an undesirable effect. One can also see that, in this case, the energy spread does not change monotonically with the injection energy. This is apparently caused by the features of the wakefield described above. Simulations show that for lower laser power ($a_0 = 0.2$) and for the same injection position the ponderomotive scattering can be neglected. In this case the collection efficiency and the relative energy spread are again higher when compared with the case where the bunch is injected closer to the laser pulse (compare figures 3.7 and 3.9).
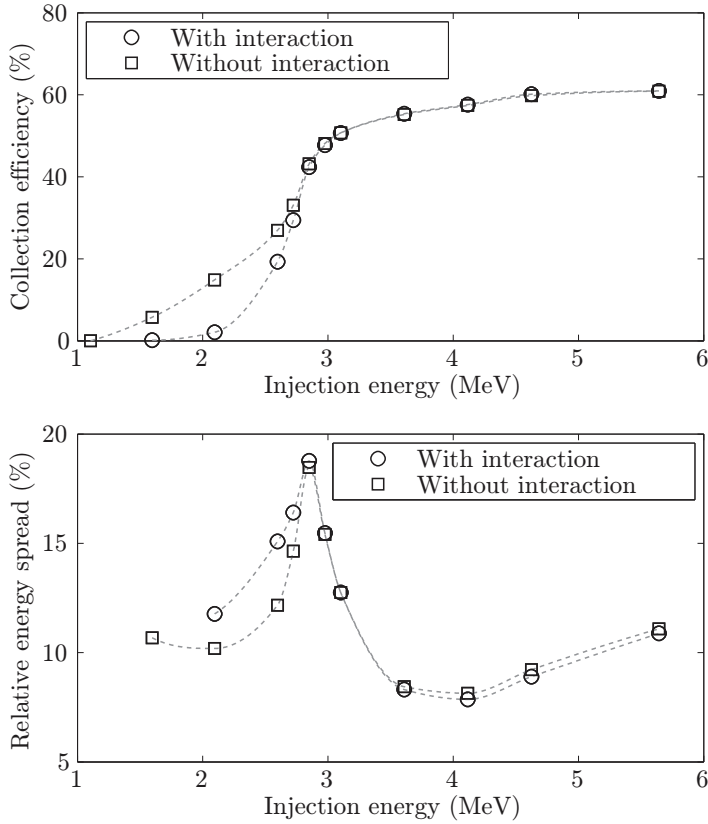
Figure 3.8: The collection efficiency and relative energy spread of the acceler-ated bunches as a function of the injection energy. The curves show the results with and without ponderomotive scattering. All the parameters except the injection position are the same as in figure 3.6. In this case the center of the injected bunch is 275 μm from the center of the laser pulse (see figure 3.4)
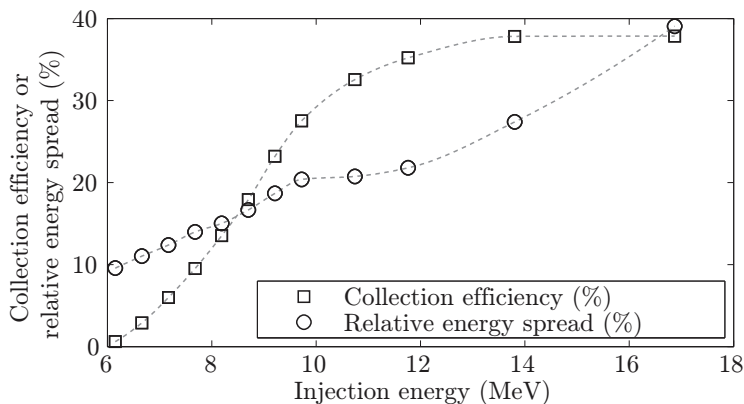
Figure 3.9: The collection efficiency and relative energy spread in the case of $a_0 = 0.2$. Other parameters are the same as in figure 3.8.

3.2.4   Summary of ponderomotive scattering

In summary, we have studied the effect of ponderomotive scattering on injection of an electron bunch behind the laser pulse. We have found that, in the most practically interesting cases, where the accelerated bunches have a small energy spread, the collection efficiency may decrease considerably due to the laser-bunch interaction in front of the plasma channel. For certain injection energies the ponderomotive scattering can provide a relatively small (few percent) energy spread at the cost of reduced collection efficiency. When a relatively low power laser pulse is used in combination with higher injection energies, the scattering of the bunch in front of the channel can be neglected. The energy gain in this case is typically of the order of a few tens of MeV [74]. We also found that the injection position in the laser wakefield plays an important role. When the bunch is injected into a plasma channel at larger distances from the laser pulse, the effect of the ponderomotive scattering is weaker and the collection efficiency is higher due to the changed structure of the wakefield. However, the energy spread in this case is undesirably larger than that found when injecting the bunch just behind the laser pulse.

When the collection efficiency is small, one can try to increase the number of accelerated electrons by increasing the charge of the injected bunch. However, calculations show that, at higher charges, the bunch sizes from a conventional linear accelerator become larger. This is due to the increasing influence of Coulomb repulsion, especially at lower bunch energies. This lowers the collection efficiency and increases the energy spread. Another approach that can be taken to increase the collection efficiency and keep the energy spread small is to choose a laser spot size much larger than the injected bunch size. In this case the effect of ponderomotive scattering could be weak, because the electrons propagate near the pulse axis where the transverse component of the

ponderomotive force is small. Such an approach however, would require very high laser powers in the petawatt range.

In the next section we will study another problem for the injection of an electron bunch behind the laser pulse, namely the effect of the transition from vacuum to plasma at the entrance of the plasma channel.

3.3 The vacuum-plasma transition

In the previous section we saw how the laser pulse can scatter the injected electron bunch when it is injected behind the pulse. This is not the only problem for this scheme. We found that the transition region from vacuum to plasma can also have a significant perturbing effect on the injected electron bunch. Others who have carried out calculations so far have assumed a sharp plasma boundary. However, in reality there is always a finite length transition region from vacuum to plasma: the plasma density, n_p, grows monotonously along the longitudinal axis to the level at which a regular laser wakefield, suitable for the synchronous acceleration of electrons, is excited. In the transition region, the wake wavelength, λ_p, becomes space dependent and decreases with z, because $\lambda_p(z) \propto [n_p(z)]^{-1/2}$. Therefore, at a fixed distance from the laser pulse in the transition region, the wakefield is not stationary, but changes as a function of time while the laser pulse travels. Correspondingly, a relativistic electron injected into the wake may experience a wakefield that changes from accelerating to decelerating and from focusing to defocusing, or vice versa. Such electrons may then be scattered before reaching the regular stationary wakefield. Thus the transition region may have a large effect on the trapping and acceleration process.

In literature several measurements of this longitudinal electron density profile can be found. For gas jets, with a typical plasma density of around 10^{19} cm^{-3}, transition regions of 200 µm [24] and 400 µm [30] were measured. However, for the capillary-discharge plasma channel with a density around 10^{18} cm^{-3} considered here, transition lengths of 2 to 8 mm were measured [76].

We will now investigate what effect this vacuum-plasma transition region can have on the collection efficiency, the energy spread and the mean energy of the accelerated bunches. We will study the effect of the transition region for the case of a channel-guided wakefield and for the case of a wakefield created by a wide laser pulse in a transversely uniform plasma. First we present the model used for the calculations.

3.3.1 The model

We again consider an axially symmetrical Gaussian laser pulse described by the normalized amplitude, $a = eE_0/(m_e c \omega)$ (here E_0 is the amplitude of the laser field, c is the speed of light, ω is the laser frequency and m_e and e are the

mass and charge of an electron)

$$a = a_0 \left(\frac{w_0}{w} \right) \exp \left(-\frac{r^2}{w^2} - \frac{(z - v_g t)^2}{l^2} \right), \qquad (3.22)$$

where a_0 is the peak amplitude, l is the laser pulse length, v_g is the group velocity of the laser pulse and z and r are the cylindrical coordinates. In vacuum or in a uniform plasma the spot size is $w(z) = w_0 (1 + z^2/z_R^2)^{1/2}$ (where $z_R = \pi w_0^2/\lambda$ is the Rayleigh length, λ is the laser wavelength and w_0 is the spot size in the waist) and in a plasma channel, where the laser pulse is waist-matched, i.e., w does not vary with z, $w(z) = w_0$.

We model the vacuum-plasma transition region ($z < z_0$) with a Gaussian function using a characteristic length L, in which the normalized unperturbed plasma density is given by

$$N_p(z, r) = \begin{cases} N_{p0}(r) \exp\left[-(z - z_0)^2/L^2 \right] & \text{for } z < z_0 \\ N_{p0}(r) & \text{for } z > z_0, \end{cases} \qquad (3.23)$$

where $N_p = n_p(z, r)/n_p(z_0, 0)$. For a transversely uniform plasma $N_{p0} = 1$, and in a plasma channel suitable for guiding the laser pulse [47],

$$N_{p0}(r) = 1 + \left(\frac{2}{k_{p0} w_0} \right)^2 \frac{r^2}{w_0^2}, \qquad (3.24)$$

where $k_{p0} = 2\pi/\lambda_{p0}$ and λ_{p0} is the on-axis plasma wavelength at $z > z_0$.

To find a solution for the laser wakefield excited in a plasma, including the transition region, it is convenient to normalize the wakefield components to the wavebreaking field ($E_{\text{WB}} = m_e c \omega_{p0}/e$, where $\omega_{p0} = k_{p0} c$) [2], the spatial coordinates to $1/k_{p0}$ and introduce the normalized time $\tau = \omega_{p0} t$. For the sake of simplicity, we assume that the group velocity of the laser pulse is equal to the speed of light in vacuum, c, over the entire plasma region (which implies that $\omega \gg \omega_{p0}$). Although the excited wakefield is not sensitive to the exact value of the group velocity, v_g, in this regime, this is not the case for the trapping and acceleration and here one needs to take into account the exact value of the relativistic factor associated with the group velocity, $\gamma_g = (1 - v_g^2/c^2)^{-1/2}$. From the Maxwell equations one finds that, for an axially symmetrical laser pulse in cylindrical coordinates, the following components of the electric and magnetic field are generated in the wakefield: $\boldsymbol{E}(E_r, 0, E_z)$, $\boldsymbol{H}(0, H_\theta, 0)$. We are interested in the linear wakefield, where $|\boldsymbol{E}| \ll 1$ and $|\boldsymbol{H}| \ll 1$. We can calculate the linear wakefield with the equations derived in section 2.3.5 of the previous chapter. Comparison with numerical calculations of the wakefield in a plasma channel, $N_p = N_{p0}(r)$, shows that this analytical solution describes the wakefield correctly for $a_0 < 0.5$, $w_0 > 5$ and for at least a few oscillations of the wakefield behind the laser pulse. This is sufficient for the study of the dynamics of injected electrons. For these parameters the curvature of the phase front and the overlap between the focusing and accelerating component of the wakefield can be accurately described.

For our calculations we take parameters which are typical for a corresponding experiment: a laser wavelength $\lambda = 0.8$ μm, a plasma wavelength $\lambda_p = 40$ μm (corresponding to a plasma electron concentration of 7×10^{17} cm^{-3}) and a laser pulse duration of 30 fs. The electrons in the injected bunch are assumed to possess a Gaussian distribution with a FWHM duration of 212 fs, which corresponds to 63.6 μm. The length of this bunch is larger than the plasma wavelength in the channel, which means that multiple bunches may be formed and accelerated. The motion of the electrons through the wakefield is calculated using the equation of motion as described in [38], which also yields the collection efficiency, the energy, and the energy spread of the trapped particles. In our calculations we fix the length of the plasma channel to 5 cm.

We will now study the effect of the vacuum-plasma transition on the dynamics of an electron bunch injected just after the laser pulse for the wakefields found in two typical situations. The first is that which is found in a channel-guided laser wakefield. We will look at the effect of the transition for two different intensities of the laser pulse. The second situation is found when a wide laser pulse enters a transversely uniform plasma. In this case the radius of the laser pulse is assumed to be sufficiently large, so that the Rayleigh length is of the order of the dephasing length. In all calculations the ponderomotive scattering in front of the plasma channel is neglected, in order to study how the vacuum-plasma transition will perturb the injection of electrons separately from other perturbing effects.

3.3.2 Injection into a channel-guided laser wakefield

It is experimentally possible to maintain a high peak intensity over long interaction lengths using a plasma channel with a minimum density on-axis to prevent diffraction of the laser pulse [47]. The radial plasma density variation in the channel has an effect on the created wakefield, in particular, it causes the phase fronts of the wakefield to become curved. In the wakefield, the farther from the laser pulse, the stronger this curvature becomes. This curvature plays an important role. It improves the collection efficiency, as it enlarges the region where electrons can be trapped [77]. To calculate the shape of this field, we use equations 2.100 and 2.101. The plasma density is described by equation 3.23 with $N_{p0}(r)$ given by equation 3.24. The FWHM width of the injected bunch at the entrance of the channel is chosen as 42 μm in both x and y directions. The FWHM bunch duration is chosen as 212 fs and is the same in all cases. We choose a normalized waist spotsize, $w_0 = 6$ (corresponding to a dimensional waist spotsize of 38 μm). This gives a spot-size-corrected gamma factor of $\gamma_g \approx (\lambda_p/\lambda_L)[1 + (\lambda_p/\pi w_0)^2]^{-1/2} = 47.4$ [2, 37] in the channel.

To study the effect of the vacuum-plasma transition, we first choose a normalized laser pulse amplitude $a_0 = 0.4$ (corresponding to a peak intensity of 3.4×10^{17} W/cm^2, which gives $\mathcal{E}_{z,\max} = 0.061$ for the maximum normalized accelerating amplitude in the channel). The dynamics of the injected electrons are calculated while they move through the density transition region and then

are trapped and accelerated in the wakefield. To illustrate the dynamics, figure 3.10 shows six snapshots of the distribution of an electron bunch with an initial kinetic energy of 3.6 MeV in the wakefield in a vacuum-plasma transition region with $L = 1.9$ mm. The bunch is seen at several positions in the transition region. The transverse component of the wakefield is plotted in the background. The first snapshot shows the initial bunch. The second snapshot shows the bunch at 3.7 mm in front of the plasma channel, where there is a non-zero plasma density, although very low, $N_p = 0.03$. The low value of the plasma density leads to a long plasma wavelength and the whole bunch experiences a relatively weak focusing force. The next snapshots show how the plasma wavelength decreases and the field strength increases. It can be seen that an injected electron sees the force changing from focusing to defocusing and back again. From this example it can be clearly seen that the transition region gives the effect of strongly scattering of the bunch. In the shown case only 0.7% of the injected electrons are trapped in the wakefield, while the collection efficiency is 16% with an infinitely sharp vacuum-plasma transition.

We have calculated the dynamics of the electron bunch for a range of injection energies and transition lengths. Because the bunch is several plasma wavelengths long, multiple bunches are formed (in this case 3 to 4). The collection efficiency, energy, and root-mean-square (rms) relative energy spread, as calculated for all trapped particles after propagation in a 5 cm long plasma channel, are plotted in figure 3.11. One can see that the size of the transition region can have a large effect on the collection efficiency. The longer the transition length, the smaller the collection efficiency. For a transition length longer than 1 mm almost no electrons can be trapped. This effect is strongest for bunches with a low kinetic energy. However, some improvement can be seen in collection efficiency for transition lengths around 0.7 mm. The energy spread increases until a transition length of 0.7 mm. For $L > 0.7$ mm, it decreases and one sees that a longer transition length can improve the energy spread. Though, in this case, almost no electrons are trapped. Furthermore, one can see that the transition region has no significant effect on the energy, except that the energy increases only slightly for longer transitions.

For investigating the bunch dynamics with a lower laser intensity, we consider the same parameters as for the previous case but with a laser peak intensity that is four times lower ($a_0 = 0.2$, $I_0 = 0.84 \times 10^{17}$ W/cm^2 and $\mathcal{E}_{z,\mathrm{max}} = 0.015$). The results are shown in figure 3.12. It can be seen that the effect of the transition region is not as large as for the previous, stronger, wakefield. Essentially, one observes the same behavior shifted to longer transition lengths L. In this case, for $L \approx 1.7$ mm, the collection efficiency increases and, until $L \approx 2$ mm, the effect on the collection efficiency is small. The same applies for the relative energy spread and the energy. This can be explained by the higher injection energies needed for the trapping of electrons, which makes them less sensitive to the fields generated in the transition region and by the weaker field generated with a lower intensity laser pulse.
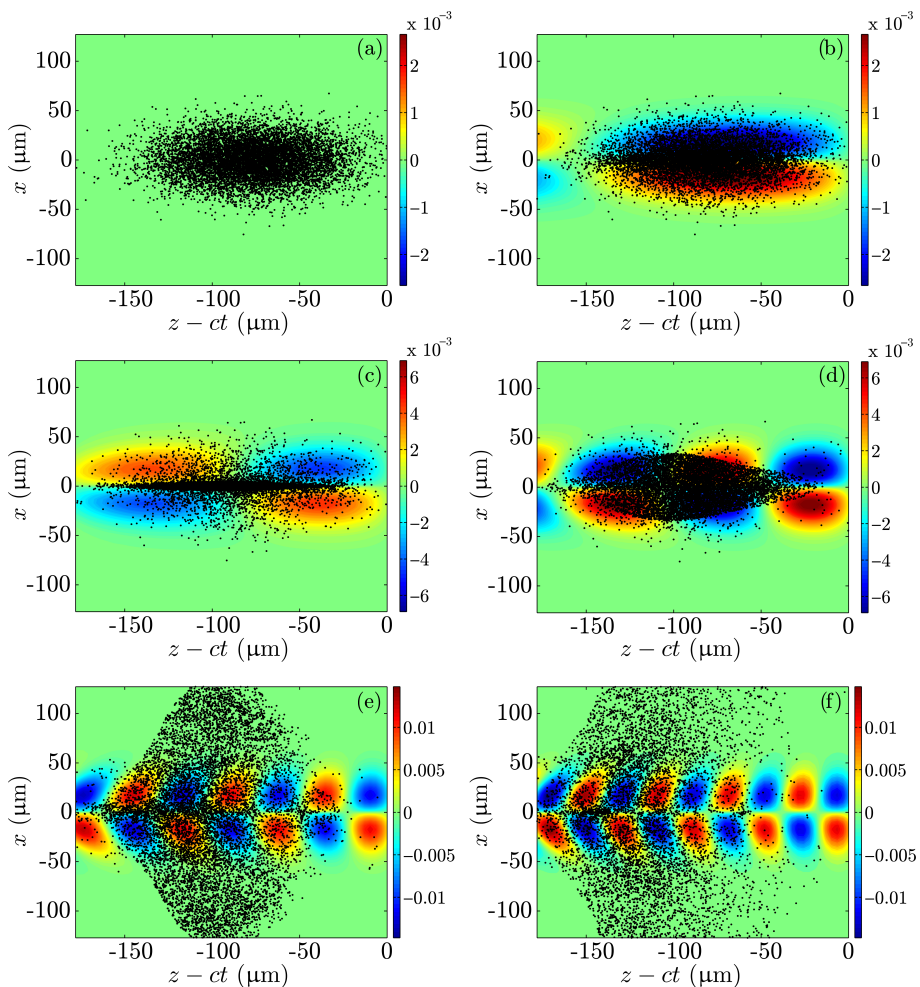
Figure 3.10: Six snapshots of the calculated dynamics of an electron bunch moving through a vacuum-plasma transition with a transition length of 1.9 mm. The electron bunch is plotted on top of the normalized transverse component of the wakefield, $\mathcal{F}_r = -\mathcal{E}_r$. It is shown in the frame moving with the laser pulse at 6 (a), 3.7 (b), 3.2 (c), 2.5 (d), 1.3 (e) and 0 (f) mm from the plasma channel entrance (z_0). The laser pulse (not shown) is positioned at around $z - ct = 0$. The kinetic energy of the injected bunch is 3.6 MeV.

3.3.3   Injection into a laser wakefield generated in a transversely uniform plasma

Current technology enables the generation of petawatt ultrashort pulses which can be used for laser wakefield acceleration [65, 67]. Such high powers then enable the use of a weak focusing to wide pulses (relatively large spot radius), which can be of the order of 100 μm. In this case the Rayleigh length grows to several centimeters ($z_R = 3.9$ cm for a laser wavelength of 800 nm and waist size of 100 μm) for propagation in a uniform plasma. Thus, high intensities are maintained over lengths comparable to the dephasing length, which makes it obsolete to prepare a guiding plasma channel. A second advantage of such pulses is that more charge can be trapped with a wider bunch of electrons. The vacuum-plasma transition can, however, still play a big role. In this section we show what the effect of the density transition is for trapping and acceleration of electrons in wakefields generated with wide laser pulses in transversely uniform plasmas.

For the calculation of the wakefield we take into account the changing radius and intensity of the laser pulse as described by expression 3.22. We assume that the laser pulse is focused to $k_{p0}w_0 = 16$ (corresponding to 100 μm) at the point where the vacuum-plasma transition has ended, at z_0, where N_p reaches unity. We will use the same peak intensities as for the case of the plasma channel and start again with a laser peak amplitude, $a_0 = 0.4$. We take the same ratio of transverse bunch size to laser pulse radius as for the plasma channel, which means that the FWHM bunch width is 111 μm in both x- and y-directions. The dynamics of the bunch are again calculated for a range of injection energies and transition lengths. The results are shown in figure 3.13.

It can be noticed that the rms energy spread is considerably higher than we calculated previously for the plasma channel. This can be attributed to the change in the properties of the laser wakefield in this regime. First, the laser pulse radius and its peak intensity change during propagation in the plasma. Although the Rayleigh length in this case is as large as 3.9 cm, there is still a noticeable change in normalized amplitude, a_0, from an initial amplitude of 0.4 to 0.25 after 5 cm of pulse propagation in the plasma. Therefore, in our case, the wakefield becomes weaker while the laser pulse propagates in the plasma, with a corresponding effect on the dynamics of the electrons. Second, because $\partial E_r/\partial r$ scales as $1/w^2$, the ratio of the transverse size of the accelerated bunch to the radius of the laser pulse will be larger for wider pulses. Thus the energy spread in the accelerated bunches increases since off-axis electrons see a weaker accelerating field.
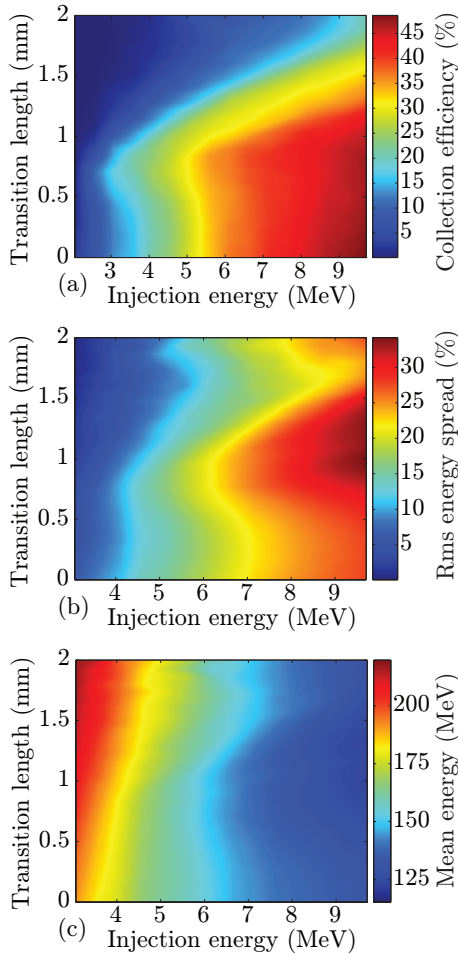
Figure 3.11: The collection efficiency (a) and rms relative energy spread (b) given in percent and the mean kinetic energy in MeV (c) of all accelerated bunches as a function of the injection energy and the transition length. In this case $a_0 = 0.4$ and $k_{p0}w_0 = 6$.
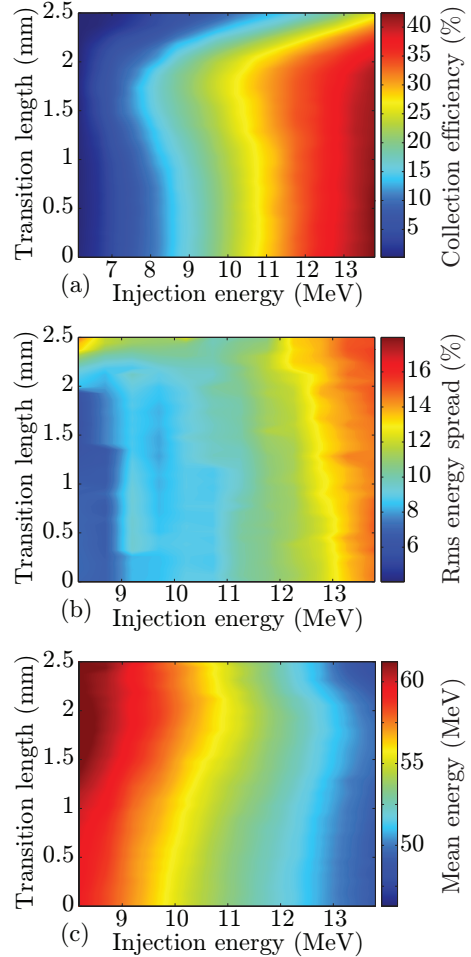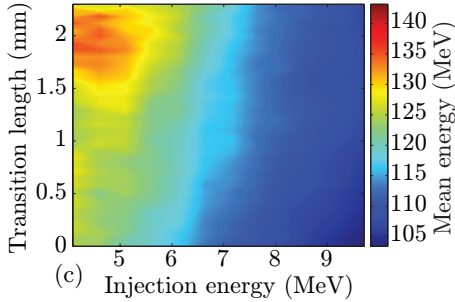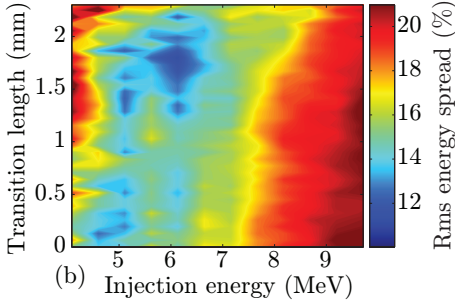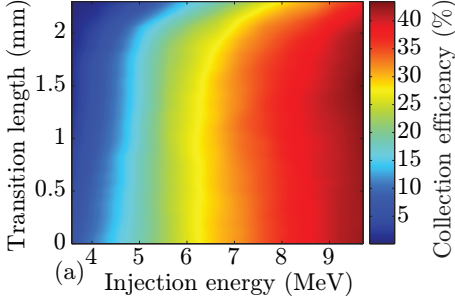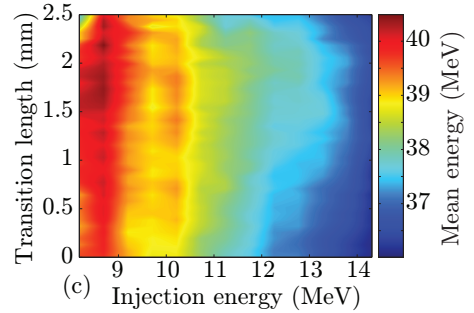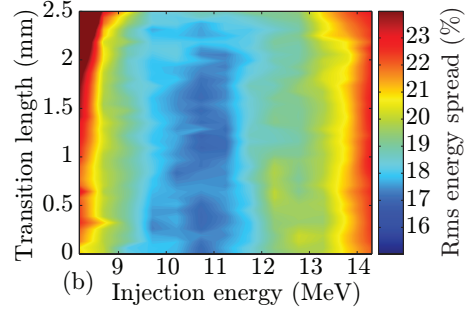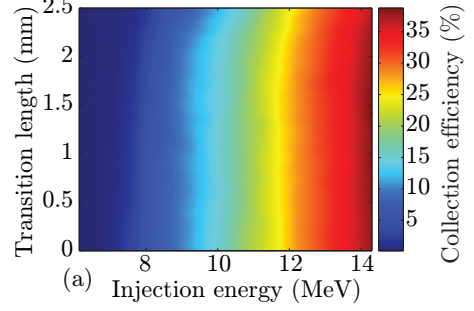
Figure 3.12: The collection efficiency (a) and rms relative energy spread (b) given in percent and the mean kinetic energy in MeV (c) of all accelerated bunches as a function of the injection energy and the transition length. In this case $a_0 = 0.2$ and $k_{p0}w_0 = 6$.

(a)
(b)
(c)

Figure 3.13: The collection efficiency (a) and rms relative energy spread (b) given in percent and the mean kinetic energy in MeV (c) of all accelerated bunches as a function of the injection energy and the transition length for the case of a radially uniform plasma. In this case $a_0 = 0.4$ and $k_{p0}w_0 = 16$.

Figure 3.14: The collection efficiency (a) and rms relative energy spread (b) given in percent and the mean kinetic energy in MeV (c) of all accelerated bunches as a function of the injection energy and the transition length for the case of a radially uniform plasma. In this case $a_0 = 0.2$ and $k_{p0}w_0 = 16$.

When looking at the effect of the vacuum-plasma transition, one sees that the effect is less that found in the case of a narrower laser pulse in a plasma channel. Until a transition length of 2 mm the effect on the collection efficiency is very weak. The effect on the energy spread is a bit larger, and one can also see that certain transition lengths can decrease the energy spread a bit. The mean energy is not much influenced by the density transition, however, one sees that longer transitions can lead to a somewhat larger mean energy. The weaker effect of the vacuum-plasma transition in the case of wider pulses can be explained by the weaker transverse field generated by such pulses; the effect of the transition seems to be mainly caused by the transverse force and a weaker force gives a weaker effect.

We have performed a second set of calculations for a wide laser pulse, with the same parameters as described above, but again with a four times lower intensity ($a_0 = 0.2$). The results are shown in figure 3.14. In this case one sees that the effect is even smaller than in the case of $a_0 = 0.4$, which means that there is almost no visible effect. The difference between a gradual transition and a sharp transition is negligible, especially for the collection efficiency and energy spread. There is a small effect for the mean energy only. A somewhat higher energy can be obtained for transition lengths of around 1.8 mm and injection energies of about 12.5 MeV.

3.3.4   Summary of the vacuum-plasma transition effects

We have shown that the transition between the vacuum and the plasma, where the laser pulse and the injected electron bunch enter, can have a strong effect on the trapping and acceleration of the electron bunches in the laser wakefield. The effect is stronger for stronger laser wakefields, lower injection energies, and with bigger lengths of the transition. Because the injected electrons see an altering laser wakefield in the transition region, some of the electrons are scattered once they see a defocusing force. This may considerably reduce the collection efficiency. Our calculations have shown that, even for a relatively low intensity ($a_0 = 0.4$), the effect of the vacuum-plasma transition can be rather large, especially for long transition lengths. One can expect that for pulses with high intensities this effect will become even stronger, which means that the collection efficiency can become small even for short transition lengths.

3.4   Properties of injection behind the laser pulse

As we saw in the previous sections, ponderomotive scattering and the vacuum-plasma transition can have a strong effect on the external injection of an electron bunch behind the laser pulse into a laser wakefield. These effects make this injection scheme only suitable for linear wakefields and, as we will show in the following chapters, it is the only external injection scheme that works well for these linear wakefields. In this case one would use a relatively low laser

Table 3.1: Parameters used to study injection behind the laser pulse

On-axis electron density	7×10^{17} cm^{-3}
On-axis plasma wavelength	40 μm
Bunch duration (FWHM)	200 fs
Bunch radius in the focus (FWHM)	64 μm
Bunch energy spread	1%
Bunch emittance	1 μm
Laser normalized amplitude	0.3
Laser power	2.7 TW
Laser pulse energy	145 mJ
Laser intensity	1.9×10^{17} W/cm^2
Laser central wavelength	0.8 μm
Laser pulse duration (FWHM)	50 fs
Laser pulse waist size	30 μm

intensity and preferably inject the electrons with a relatively high energy, in order to suppress ponderomotive scattering and the effect of the vacuum-plasma transition. In this section we will look at how this scheme performs for such parameters.

For the calculation of the wakefield we use the equations derived in section 2.3.5. We choose a relatively low normalized amplitude of 0.3 for the laser pulse, so that the effects of ponderomotive scattering and the vacuum-plasma transition, which are included in this calculation, are minimized. The used plasma, bunch, and laser parameters are tabulated in table 3.1. In figure 3.15 and 3.16 the electron dynamics are shown for an electron bunch injected with a high kinetic energy of 6.8 MeV, an energy spread of 1% and a transverse emittance of 1 μm. The first snapshot in figure 3.15 shows the injected electron bunch in front of the channel, where it will experience ponderomotive scattering and a vacuum-plasma transition with a length of 2 mm. The remaining snapshots, all of them in front of the channel, show that these effects seem to be relatively weak for the chosen parameters. The bunch arrives almost intact at the entrance of the plasma channel, which corresponds to $t = 0$ ps and $z = 0$ cm. Figure 3.16 shows six subsequent snapshots of the trapping of this bunch in the wakefield starting with $t = 0$ ps and $z = 0$ cm. The trapping process is clearly visible. Part of the electrons are focused towards the axis, at places where the bunch overlaps the focusing areas, while other electrons are scattered in the defocusing areas. In this example, the plasma wavelength is 40 μm, so the electron bunch is overlapping with about five trapping regions and five separate bunches are formed. The distance between the formed bunches is approximately equal to the plasma wavelength. After tens of picoseconds several bunches are formed and compressed in radial and longitudinal directions. The fast trapping process helps to minimize the energy spread, because all electrons
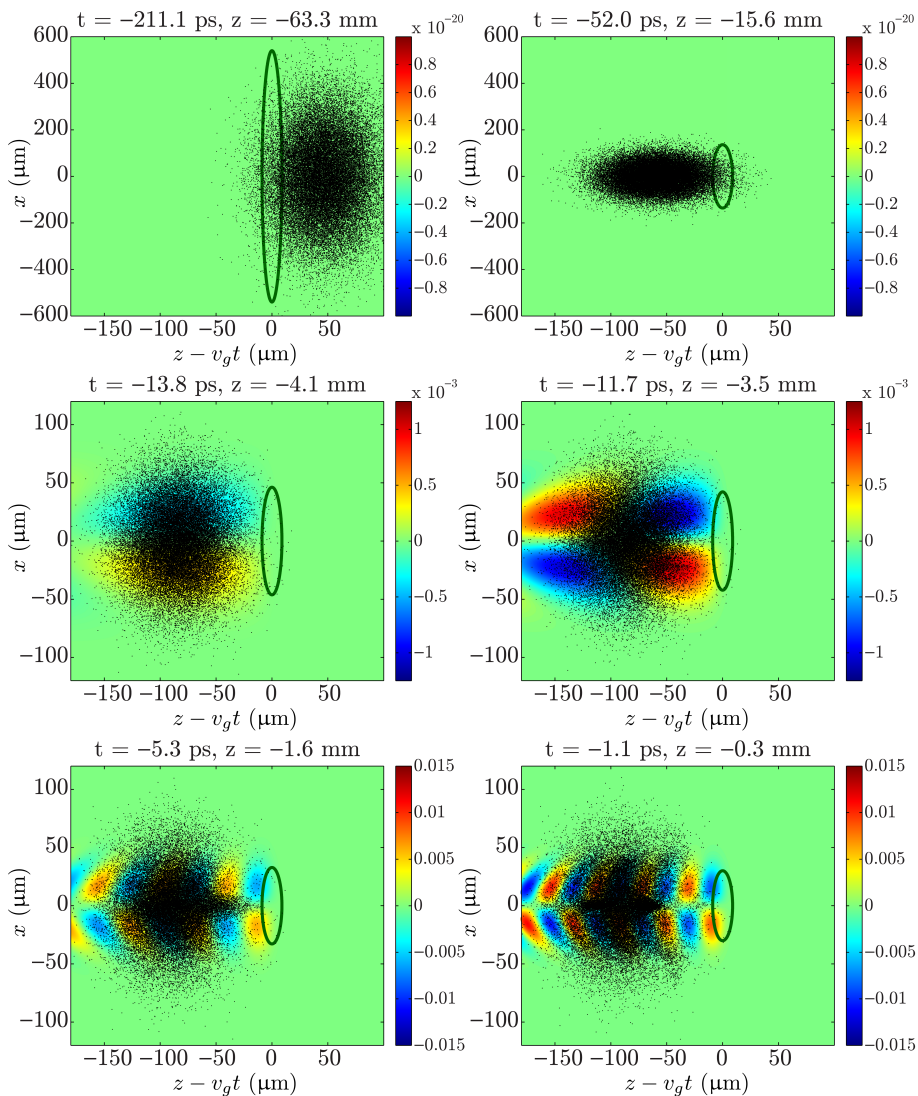
Figure 3.15: Six snapshots of the simulation of the dynamics of an electron bunch experiencing ponderomotive scattering and moving through a vacuum-plasma transition with a transition length of 2 mm. The electron bunch is plotted on top of the normalized transverse component of the wakefield, $\mathcal{F}_r = -\mathcal{E}_r$. It is shown in the frame moving with the laser pulse at 63.3, 15.6, 4.1, 3.5, 1.6 and 0.3 mm in front of the plasma channel entrance. The laser pulse (depicted by the ellipse) is positioned at around $z - v_g t = 0$. The kinetic energy of the injected bunch is 6.8 MeV.
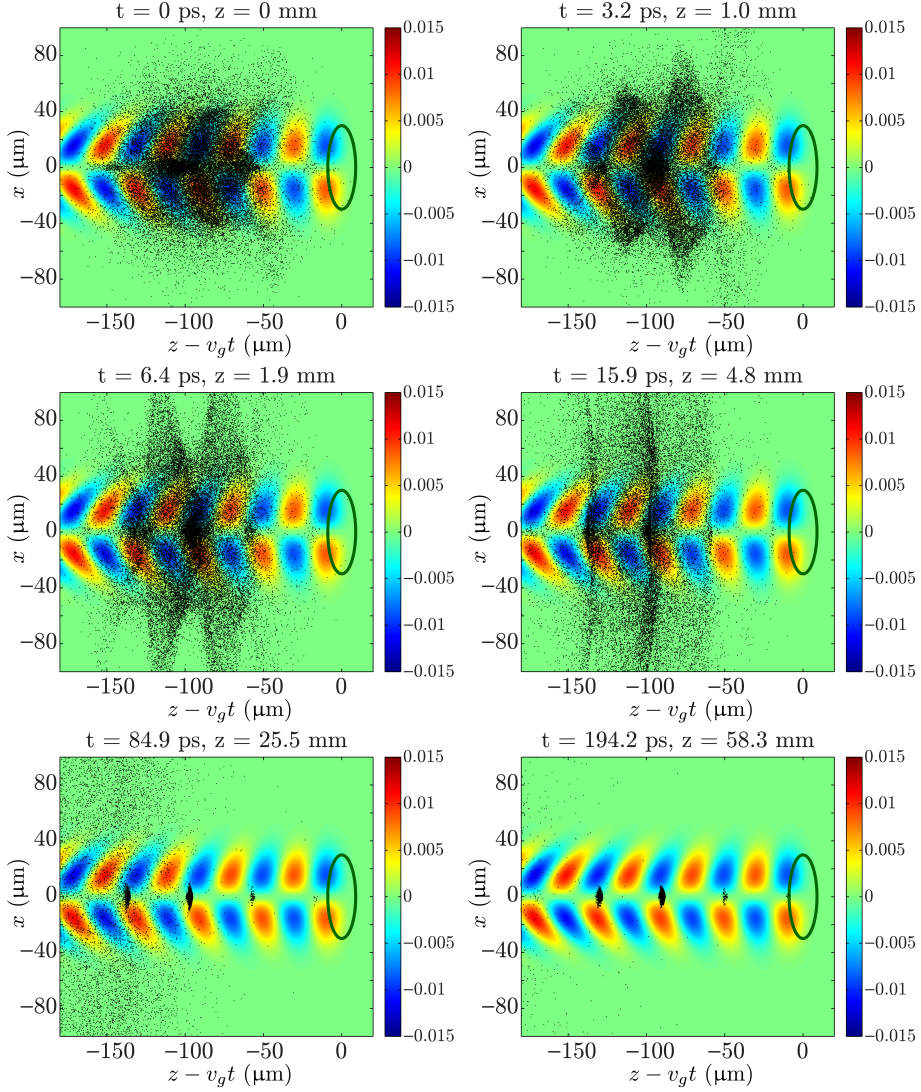
Figure 3.16: Six snapshots of the simulation of the dynamics of an electron bunch injected behind the laser pulse in a plasma channel. The dynamics in front of the channel are plotted in figure 3.15. The electron bunch is plotted on top of the normalized transverse component of the wakefield, $\mathcal{F}_r = -\mathcal{E}_r$. It is shown in the frame moving with the laser pulse at 0, 1.0, 1.9, 4.8, 25.5 and 58.3 mm from the plasma channel entrance. The laser pulse (depicted by the ellipse) is positioned at around $z - v_g t = 0$. The kinetic energy of the injected bunch is 6.8 MeV.
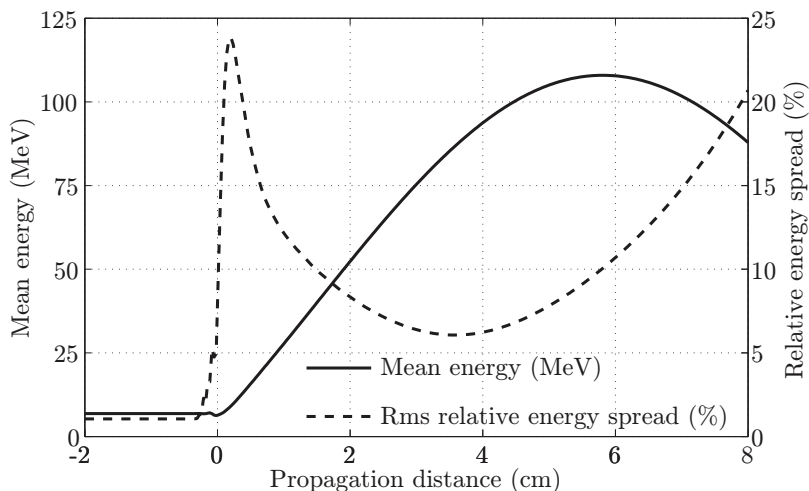
Figure 3.17: The mean energy (solid line) and rms relative energy spread (dashed line) for an electron bunch injected with a kinetic energy of 7.4 MeV into the wakefield with a normalized amplitude of $a_0 = 0.3$.

will experience almost the same accelerating field. The collection efficiency is for this example 4.6%. However, when neglecting ponderomotive scattering and the vacuum-plasma transition, we obtain a collection efficiency of 9.6%. Thus, while it looks as if the electron bunch is almost unaffected by these perturbing effects, they still have an impact on the collection efficiency, because they alter the transverse momentum of the electrons. After the electrons are trapped in the wakefield, they are accelerated by the longitudinal electric field. After propagating 5.8 cm in the plasma channel, the electron bunches reach the maximum energy of 108 MeV as can be seen in figure 3.17, which plots the energy and the relative rms energy spread for the electron bunch as a function of the propagation distance. The energy spread at this distance is 10%. However this is not the minimum energy spread. The minimum energy spread of 6% is reached after a propagation distance of 3.6 cm, where the bunches have reached an energy of 87 MeV. Hence, the minimum energy spread does not coincide with maximum energy for this scheme. One can also see this in figure 3.18, which plots one of the trapped electron bunches in phase space at several positions in the plasma channel. It can be seen that, initially, the bunch is small in the P_z (momentum) direction for propagation distances up to 3.6 cm, where minimum relative energy spread is reached. However when the bunch propagates further, it starts to lengthen in the P_z direction, indicating an increase in energy spread. The rms transverse size of the accelerated bunches is 2.8 µm in x- and y-direction, and their normalized transverse emittance is 1.5 µm. The rms duration of each bunch after acceleration is about 3.1 fs.
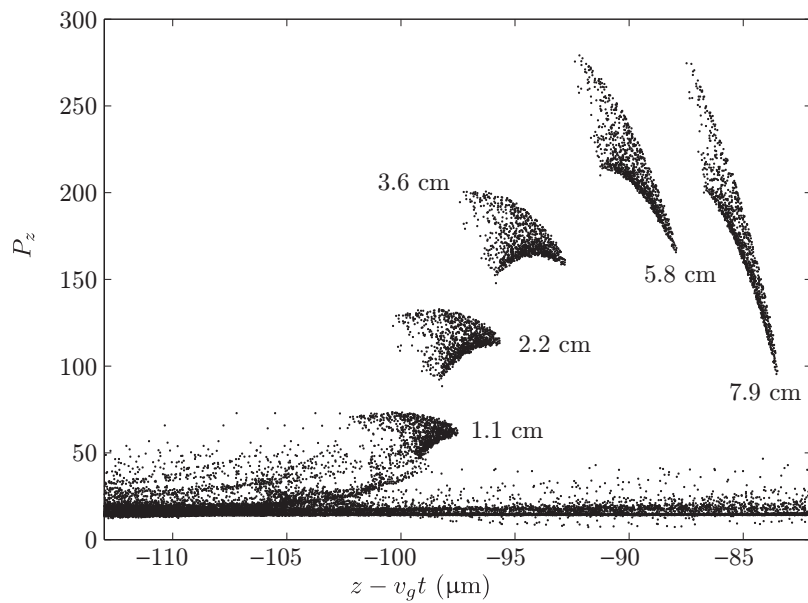
Figure 3.18: The accelerated electron bunch in phase space at subsequent positions in the plasma channel for an injection energy of 7.4 MeV and the wakefield with a normalized amplitude of $a_0 = 0.3$.

Figure 3.19a shows the collection efficiency as a function of the injection energy when the scattering effects are taken into account, in comparison to neglecting them. It can be seen that ponderomotive scattering and the vacuum-plasma transition do still play a role, although a relatively high injection energy and low laser intensity was used. The collection efficiency increases when the initial kinetic energy of the electrons increases. Figure 3.19b shows the rms relative energy spread as a function of the kinetic injection energy. The relative energy spread increases in an almost linear fashion, when the injection energy is increased. In order to obtain a low energy spread, the injection energy has to be close to the minimum trapping energy and a trade-off has to be made between the charge and the energy spread of the trapped electron bunch. The scattering effects do reduce the energy spread a bit, when compared to no scattering.

3.5   Summary and conclusion

External injection of an electron bunch from a conventional accelerator behind the laser pulse into a laser wakefield can lead to high-quality electron bunches. However, one has to take into account the effect of ponderomotive scattering and the vacuum-plasma transition. Because of these effects, injection behind the laser pulse will only work for linear wakefields in which electrons with a relatively high initial energy are injected. Also a trade-off has to be made between low energy spread and high collection efficiency.
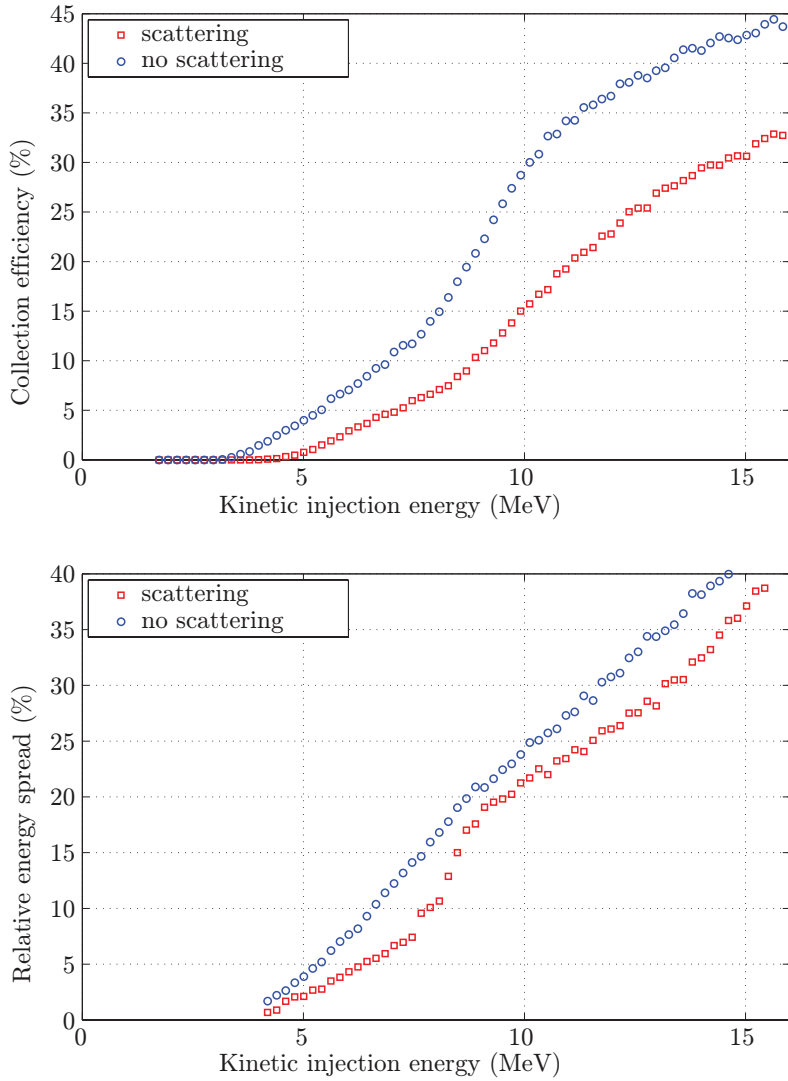
Figure 3.19: The collection efficiency (a) and rms relative energy spread (b) as a function of the kinetic injection energy for injection behind the laser pulse into the wakefield with a normalized amplitude of $a_0 = 0.3$ with (red square) and without (blue circle) ponderomotive scattering and the vacuum-plasma transition.

4

Injection at an angle

In the previous chapter, external injection behind the laser pulse was discussed. We found that this scheme suffers from two important disturbing effects that cause scattering of the electron bunch before it even reaches the regular wakefield for acceleration.

In this chapter we will present a novel alternative scheme for external bunch injection where scattering as described in chapter 3 does not play a role, although the injection still takes place behind the laser pulse. We propose to inject the electron bunch at a small angle into the plasma channel directly behind the laser pulse, where the wakefield is generated.

Injecting at an angle was also proposed by Kalmykov *et al.* [69] to avoid ponderomotive scattering, but in their case the bunch is first positioned behind the laser pulse before it enters the plasma. Therefore the bunch would still have to propagate through the transition from vacuum to plasma and experience scattering. We propose the injection of the bunch into the laser wakefield at an angle, in the region of the regular plasma channel, in such a way that the bunch enters the wakefield from the side. The bunch will start from a zero field and then experience a wakefield of constant wavelength, but increasing in strength, where it can be trapped and accelerated. This way, the bunch will not experience any wakefield in the transition region: it only approaches the wakefield where the plasma density is already at its full value and where the regular wakefield is generated. This approach completely avoids the bunch overlapping the wakefield in the transition region so that both the ponderomotive scattering and the effect of the vacuum-plasma transition region are avoided.

In this chapter we present a detailed investigation of such an injection at
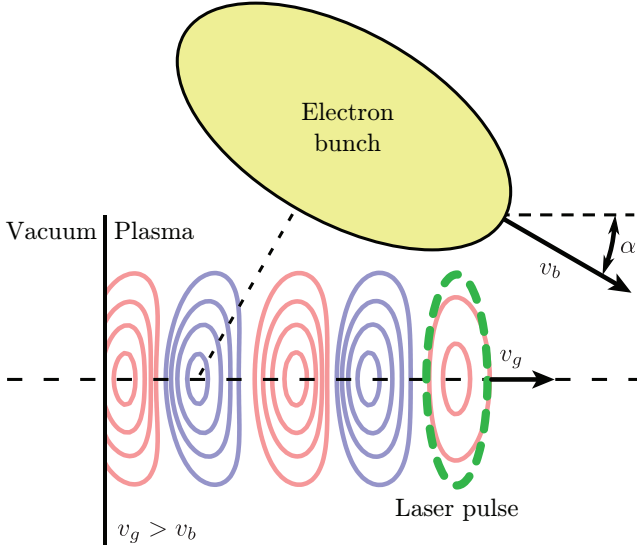
Figure 4.1: Schematic drawing of injection at an angle into a laser wakefield. In this novel scheme, a relatively low energy (typically a few MeV's) electron bunch is injected behind the laser pulse at a small angle, α, with respect to the laser propagation axis.

an angle into the laser wakefield. The basic working principle of this novel injection scheme is given in section 4.1. The effect of the injection angle will be discussed in section 4.2. In section 4.3 the properties of the injection scheme are investigated. Sections 4.4 to 4.6 describe the effect of the laser pulse dynamics on the properties of the accelerated bunch. The last section gives a summary and conclusion.

4.1   The injection scheme

In this section the working principle of the injection of electron bunches at an angle into a laser wakefield is explained, for which we refer to figure 4.1. A low-energy electron bunch, with an energy of a few MeV, is generated by a radio frequency (rf) photocathode linac and injected at a small angle, α, directly behind a high-intensity laser pulse in a plasma with some offset relative to the laser propagation axis. This causes the electron bunch to enter the wakefield from the transverse direction. It is preferable to inject the bunch into the wakefield close to the laser pulse because the accelerating field is the largest and generates bunches with the highest quality at that point, as shown in the previous chapter. The velocity of the electron bunch, v_b, is lower than the group velocity of the laser pulse, v_g. Thus, the electron bunch slips backward

in the frame moving with the pulse. The dotted line in figure 4.1 indicates the trajectory that the bunch will follow in this frame. When the longitudinally accelerating and transversely focusing forces of the generated wakefield are sufficiently strong (and when other parameters are suitably chosen) a large fraction of the injected bunch might be trapped, compressed and accelerated in the wakefield. This scheme avoids ponderomotive scattering [40] and the vacuum-plasma density transition [41], as described in chapter 3. The dynamics of injection at an angle look much like the dynamics of injection in front of the laser pulse [38, 64, 70], a third external injection scheme which will be discussed in the next chapter. In both cases the injected electrons move gradually into the wakefield. In contrast, electrons injected on-axis behind the laser pulse enter the wakefield abruptly so that the strength of the experienced wakefield depends on the injection phase [37, 40].

The avoidance of ponderomotive scattering and the vacuum-plasma transition could also be achieved by injecting the electron bunch on-axis in front of the laser pulse (see next chapter). However, we show that there are additional advantages that make injection at an angle interesting. It is, for example, possible to use electron bunches of a wider transverse size, which allows the entrapment of bunches with a higher charge in the wakefield. The longitudinal length of the electron bunch is not a critical issue when a low energy spread is required. The injected bunch from an rf linac is typically several times longer than the plasma wavelength, λ_p [42, 74]. Similar to injection behind, the electrons of such a bunch will be trapped into several bunches separated by the plasma wavelength, λ_p. A low energy spread can be obtained in the accelerated bunches by careful choosing of the injection energy and injection angle. The trapping distance (an important quantity that determines the final energy spread of the bunch) can be made relatively small (~ 1 mm [41]) by choosing larger angles. However, the wakefield should also be strong enough to be able to transversely trap electrons which are injected at larger angles. In the following section we will study how the injection angle influences the collection efficiency, energy spread, and energy of the accelerated bunches.

4.2 Effect of the angle

Low-energy electrons injected at an angle in a strong laser wakefield can be trapped and accelerated [38], however, the maximum allowable angle depends on the strength of the wakefield and the injection energy of the electrons. The explanation for this is that, for bigger injection angles, the transverse momentum of the electrons becomes too large and the bunch propagates through the wakefield without trapping. Correspondingly, for a successful trapping under a given angle and with a given energy, the wakefield should be sufficiently strong.

Except for the amplitude of the laser pulse, we have simulated the described injection at an angle for the same parameters of the plasma channel and the laser pulse as in section 3.3.2 of the previous chapter. Here we choose a stronger laser pulse with $a_0 = 1$ (corresponding to a peak intensity of 2.1×10^{18} W/cm^2,
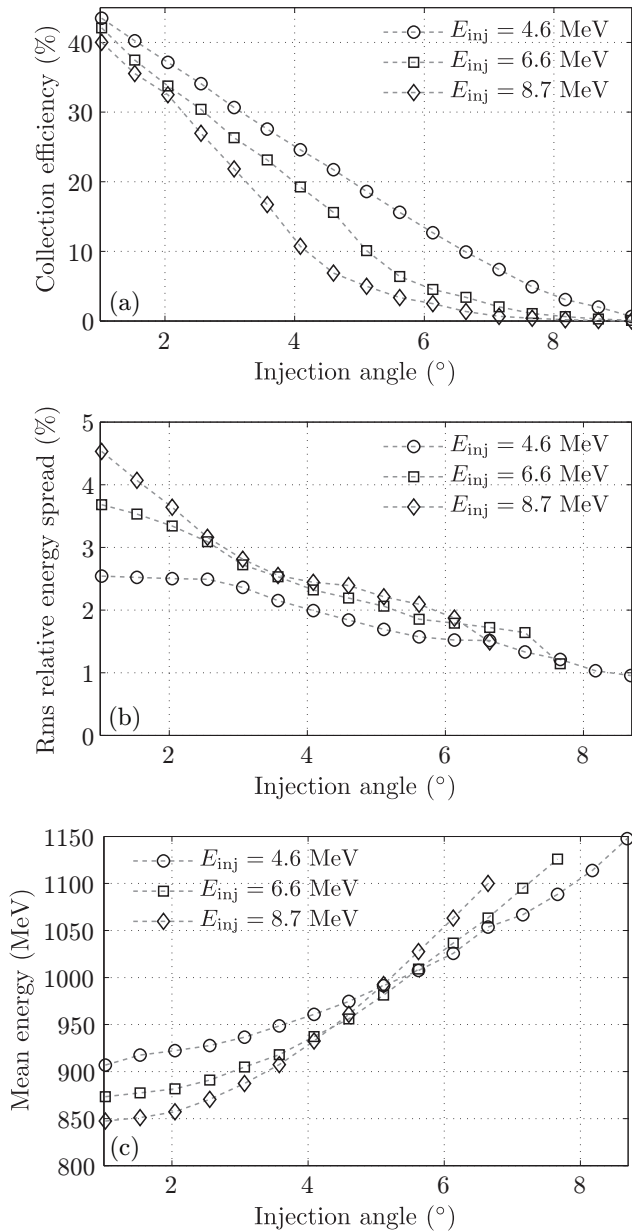
Figure 4.2: The collection efficiency (a), rms relative energy spread (b) and mean energy (c) of the accelerated bunches versus the injection angle of the electron bunch for a channel-guided laser wakefield. In this case $a_0 = 1$, $k_{p0}w_0 = 6$ and the plasma channel has a length of 6 cm. The curves are shown for injection energies of 4.6, 6.6 and 8.7 MeV.

which gives $\mathcal{E}_{z,\mathrm{max}} = 0.38$). The linear theory is no longer valid in this case, so we have included the wakefield nonlinearities in full via the calculation of the wakefield numerically with our numerical fluid code [38, 83] (see section 2.3.6). To give a typical example for the basic working of the scheme, we investigate the injection of an electron bunch the same size as that used in section 3.3.2. We used three different kinetic energies (4.6, 6.6 and 8.7 MeV) and several injection angles for the investigation. The collection efficiency, relative energy spread, and mean energy are plotted in figure 4.2 versus the injection angle of the electron bunch. It can be seen that the collection efficiency decreases monotonously with the injection angle, that, for small injection angles about 40% of the injected electrons are trapped and that this wakefield cannot trap electrons injected with angles larger than 9 degrees. It can further be seen that, for a given injection angle, the collection efficiency is larger for lower injection energies. The dependence of the collection efficiency on the injection angle becomes stronger for larger injection energies. In general one can obtain a better combination of collection efficiency and energy spread with injection at an angle than with bunch injection behind the laser pulse [37, 40, 66]. The rms energy spread after acceleration in a 6 cm long channel is relatively low and decreases with the injection angle, while the mean energy after acceleration in the wakefield grows with the angle.

For small injection angles ($\alpha \ll 1$ rad), one can estimate the trapping distance (L_{tr}), which we define as the distance traveled by the pulse before the electron meets the trapping point, located close to the wake axis. The trapping distance can be approximated by the time (t_{tr}) it takes for an electron bunch to reach the trapping point multiplied by the speed of the pulse (which is close to c). This gives $L_{tr} \approx t_{tr} c$. Obviously $t_{tr} \approx d/v_r$, where d is the diameter and v_r is the transverse velocity of the electron bunch. Taking into account that v_r/c is approximately the injection angle, α, one can estimate the trapping distance for a bunch injected at an angle as

$$L_{tr} \sim \frac{d}{\alpha}. \tag{4.1}$$

This trapping distance does not depend on the energy and the length of the bunch (which is the case for injection in front of the laser pulse [64]). When the bunch is injected parallel to the laser pulse, that is $\alpha \to 0$, the trapping distance becomes infinity and the bunch will not be trapped when it starts off-axis. From a practical point of view, the trapping distance, L_{tr}, should be a small fraction of the acceleration distance, because the bunch not only needs to be trapped but it also needs to be accelerated to high energies. This determines the minimum angle, α_{min}, at which injection at an angle is a useful scheme. Hence, one can estimate the minimum angle as $\alpha_{\mathrm{min}} \sim d/L_*$, where L_* is a small fraction of the length of the plasma channel. This minimum angle, along with the maximum angle discussed above, form a range of angles at which the scheme works. According to our simulations, injection at 1 to 3 degrees gives an acceptable combination of collection efficiency and energy spread. In this

Table 4.1: Parameters used to study injection at an angle

On-axis electron density	7×10^{17} cm^{-3}
On-axis plasma wavelength	40 μm
Bunch duration (FWHM)	200 fs
Bunch radius in the focus (FWHM)	64 μm
Bunch energy spread	1%
Bunch emittance	1 μm
Laser normalized amplitude	0.7 & 0.9
Laser power	14.8 & 24.5 TW
Laser pulse energy	790 & 1306 mJ
Laser intensity	1.0×10^{18} & 1.7×10^{18} W/cm^2
Laser central wavelength	0.8 μm
Laser pulse duration (FWHM)	50 fs
Laser pulse waist size	30 μm

section we saw the angle dependence of this scheme. Other dependencies are investigated in the next section.

4.3   Properties of injection at an angle

In this section we will look at the properties of injection at an angle for typical parameters. The used plasma channel, electron bunch, and laser parameters are tabulated in table 4.1. As can be seen in this table, we will look at two wakefields with normalized amplitudes, a_0, of 0.7 and 0.9. The wakefields are calculated using the WAKE code [62, 84], which includes the full laser pulse dynamics such as intensity-dependent self-focusing and self-shortening. More about the effects of the laser pulse dynamics can be found in section 4.4.

To illustrate the transverse trapping with injection at an angle, figure 4.3 shows six snapshots of an electron bunch injected with a kinetic energy of 3.6 MeV at an angle of 4 degrees into the wakefield with $a_0 = 0.9$ at several positions and times in the plasma channel. The first snapshot is obtained at the entrance of the plasma channel, $z = 0$ mm. Here one can see the electron bunch coming from the side, just before it starts to enter the wakefield. The next four snapshots show how a part of the electron bunch, in this case 14%, is trapped in the wakefield. The other electrons either: become scattered by the defocusing part of the wakefield, go through the wakefield, or become "reflected" by the wakefield. The last frame shows the trapped electrons at the end of the plasma channel, which is 5.3 cm long. Four bunches separated by one plasma wavelength are formed. Here the bunches have reached a mean energy of 721 MeV.

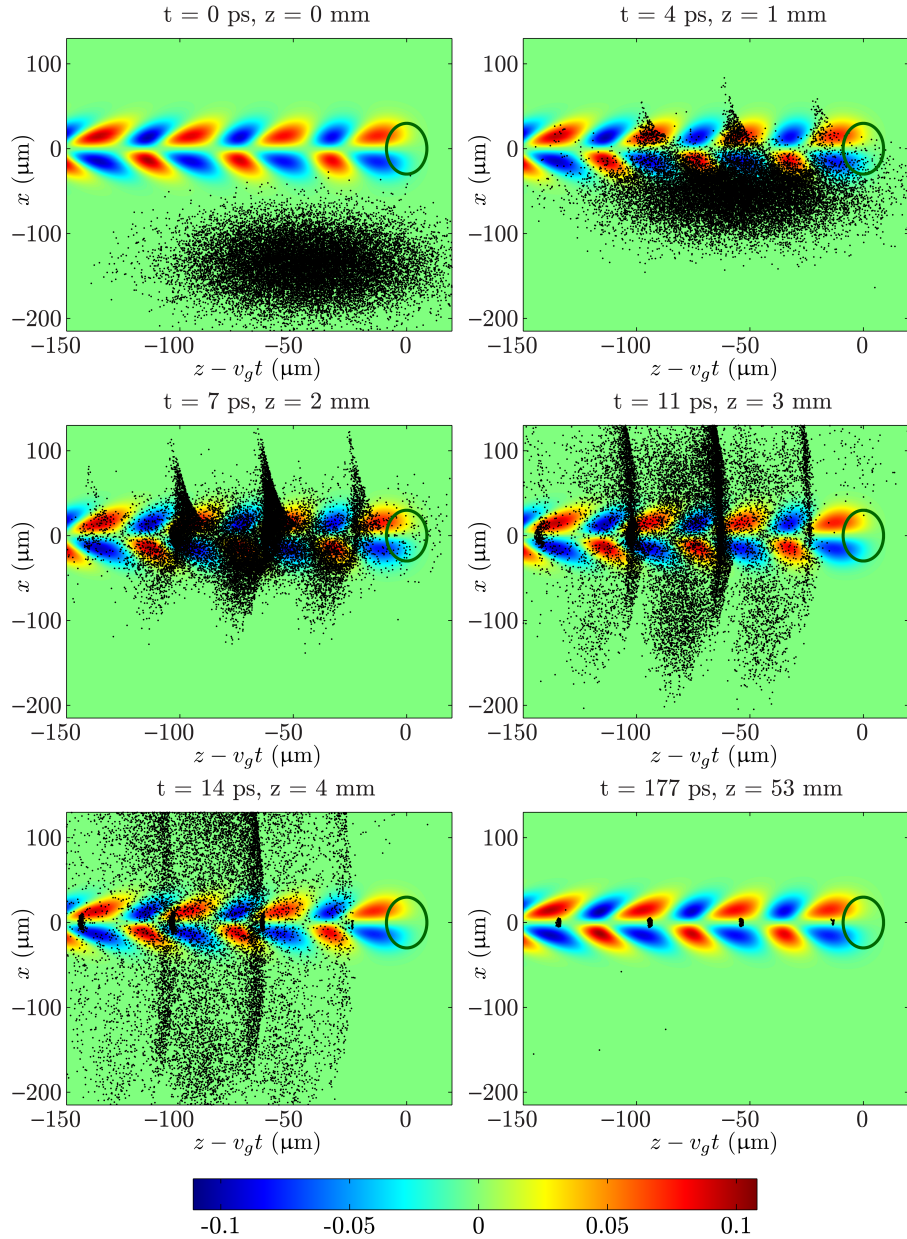The energy and rms relative energy spread, averaged over all the trapped

Figure 4.3: Six snapshots of the dynamics of external injection at an angle. The electron bunch is plotted on top of the transverse component of the wakefield. The snapshots are shown in the frame moving with the laser pulse at 0, 1, 2, 3, 4 and 53 mm from the plasma channel entrance. The laser pulse is positioned at $z - v_g t = 0$. The electron bunch is injected into the wakefield at an angle of $4°$ with $a_0 = 0.9$ with a kinetic energy of 3.6 MeV.
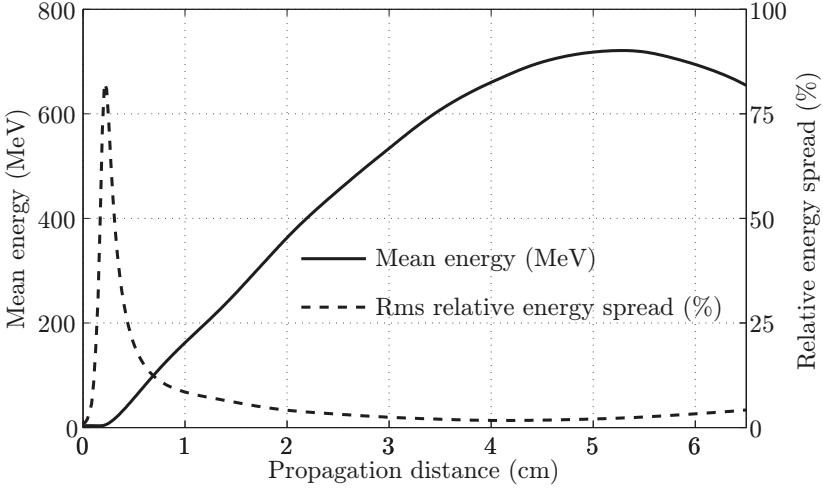
Figure 4.4: The mean energy (solid line) and rms relative energy spread (dashed line) for an electron bunch injected with a kinetic energy of 3.6 MeV at an angle of 4° into the wakefield with a normalized amplitude of $a_0 = 0.9$.

electrons in all bunches, are plotted as a function of the propagation distance in figure 4.4. One can notice that the relative energy spread initially shows a quick growth to high values. Two groups of electrons contribute to this: trapped electrons which quickly gain high energy, and electrons which are not yet trapped and remain at low energy. After the trapping process is completed, the relative energy spread of the trapped bunches decreases considerably and reaches a low value of about 1.6%. The rms transverse size of the bunches after trapping becomes 2 μm in x and y-direction. Their rms duration is 1.2 fs. These values stay approximately constant during the acceleration process. The normalized transverse emittance of the bunches is 2 μm in both directions.

In figure 4.5 one of the electron bunches is shown in phase space at several positions in the plasma channel (the other bunches behave in a similar way). In phase space one can see why the relative energy spread is decreasing (as was shown in figure 4.4). After the bunch is trapped and while it is accelerating, it starts to rotate in phase space in such a way that the size in the P_z-direction decreases. Such rotation appears because, initially, the electrons in front of the accelerating electron bunches possess a higher energy than the electrons in the back, since they were trapped first and have been accelerating for the longest time. However, at a certain moment, the electrons in front enter the weaker part of the accelerating field, while the electrons in the back are still in the strong part.

Finally, we have calculated how injection at an angle depends on the injection energy. The collection efficiency and the relative energy spread for a
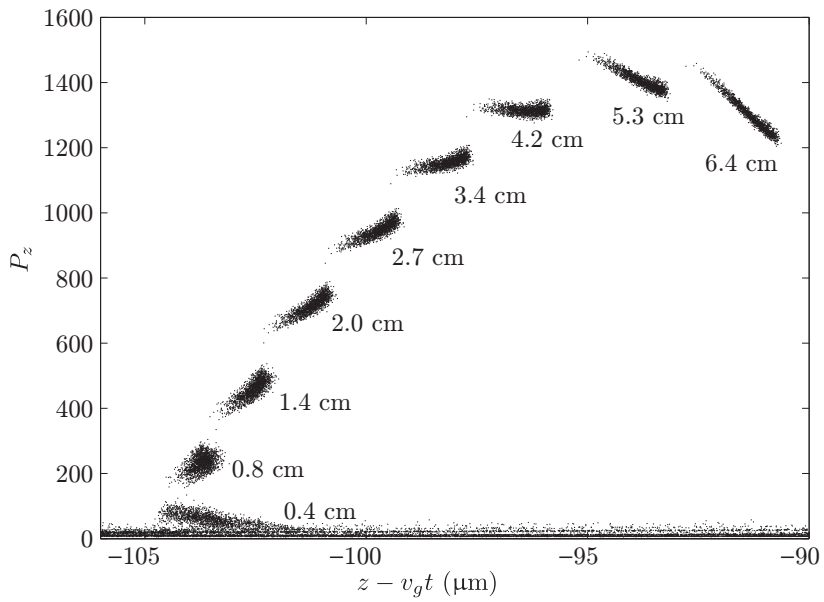
Figure 4.5: The accelerated electron bunch in phase space at subsequent positions in the plasma channel for an injection energy of 3.6 MeV and the wakefield with a normalized amplitude of $a_0 = 0.9$.
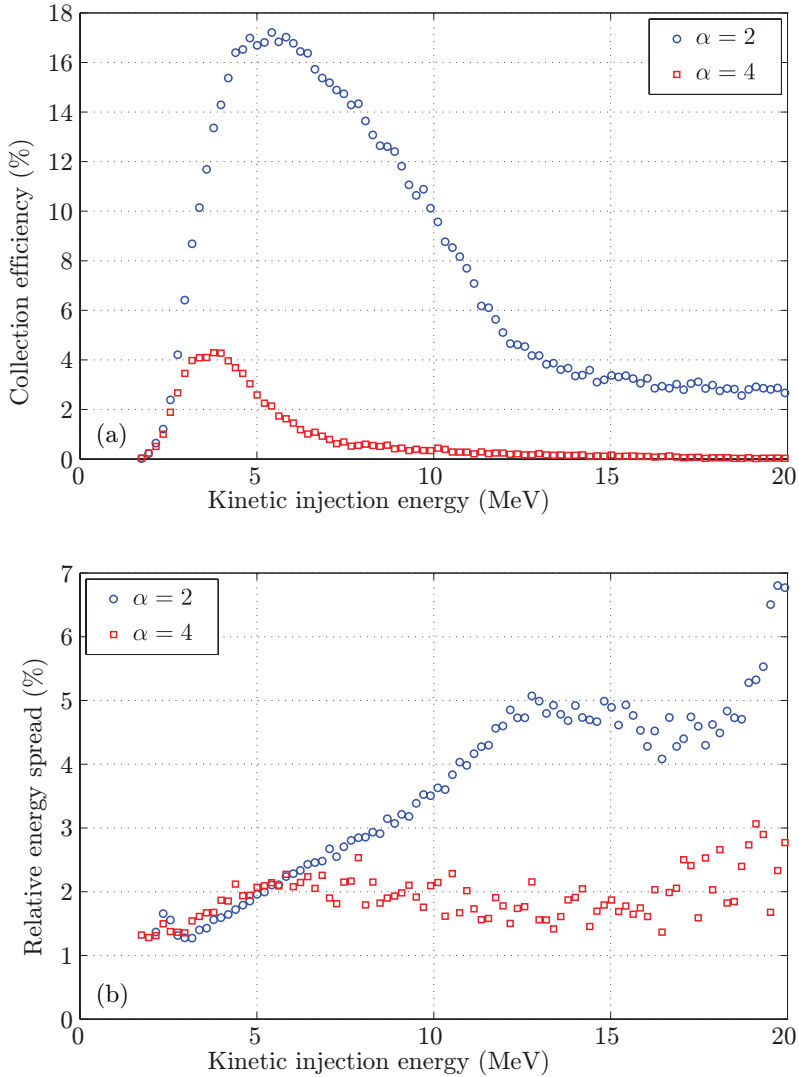
Figure 4.6: The collection efficiency (a) and rms relative energy spread (b) as a function of the kinetic injection energy for injection at an angle of 2 (blue circle) and 4 degrees (red square) into the wakefield with a normalized amplitude of $a_0 = 0.7$.
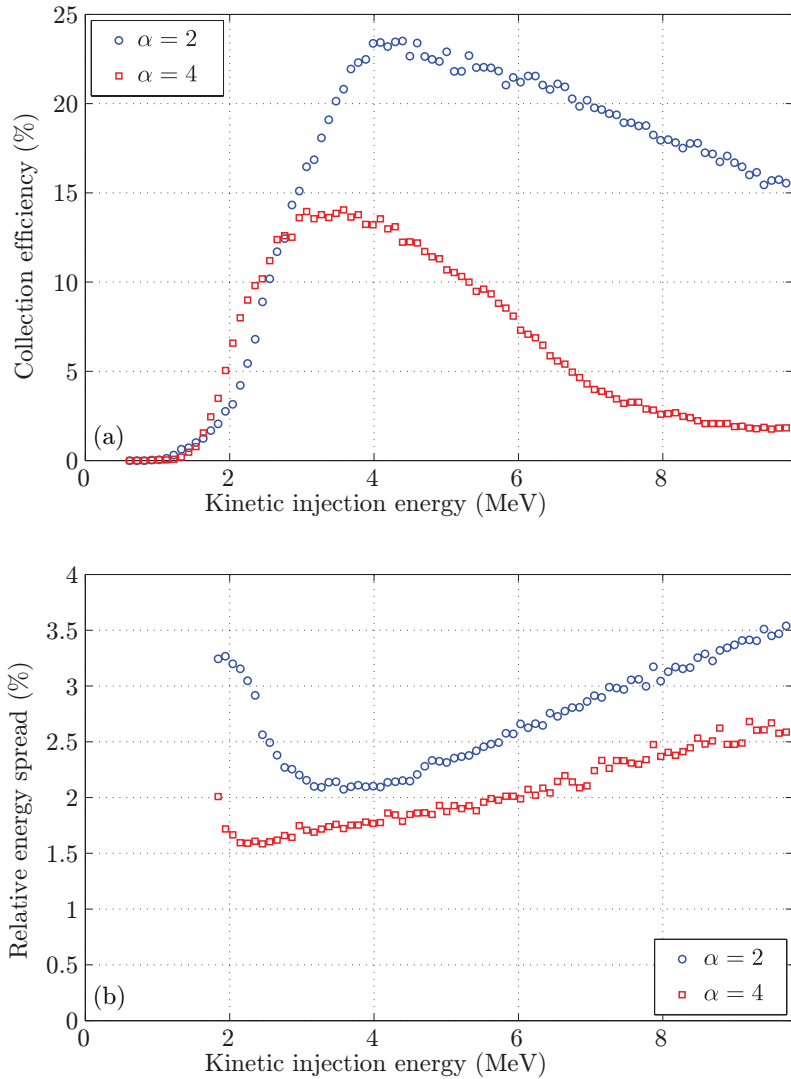
Figure 4.7: The collection efficiency (a) and rms relative energy spread (b) as a function of the kinetic injection energy for injection at an angle of 2 (blue circle) and 4 degrees (red square) into the wakefield with a normalized amplitude of $a_0 = 0.9$.

wakefield with $a_0 = 0.7$ are plotted in figure 4.6 for an angle of 2 and 4 degrees as a function of the injection energy. It shows that the minimum required injection energy for both angles is approximately 2.5 MeV. It can be seen that, depending on the injection angle, there is an "optimum" injection energy where a maximum collection efficiency is acquired. For an angle of 2 degrees a maximum collection efficiency of 17% is obtained for an injection energy of 6 MeV and for an angle of 4 degrees a maximum of 4% is obtained for 4.5 MeV. For higher injection energies, the collection efficiency drops strongly: for an angle of 4 degrees it drops to almost zero, while for an angle of 2 degrees it drops until approximately 14 MeV, followed by a slower decrease.

A second calculation has been done for the same angles, but using a stronger wakefield driven with $a_0 = 0.9$. The result is plotted in figure 4.7. One can see a similar behavior, but the maximum collection efficiency is higher than in the previous case: 23% for 5 MeV and an angle of 2 degrees and 14% for 4 MeV and an angle of 4 degrees. The minimum injection energy required for both angles is approximately 1.6 MeV, which is lower than in the previous case where it was 2.5 MeV. In all these calculations, the laser pulse dynamics were taken into account. In the following sections, we will investigate the effect of these dynamics in more detail.

4.4 Laser pulse dynamics

At relativistic intensities, the plasma starts to behave in a nonlinear fashion, which has an effect on the propagation of the laser pulse and, also, on the generated wakefield (see section 2.6). In the following, we will investigate these dynamics, while the laser pulse is also guided by a plasma channel. In the next section, this is used to calculate the effect of the laser pulse dynamics on injection at an angle. In our calculations we use a linearly polarized axially-symmetrical Gaussian laser pulse with the normalized amplitude, $a = eE_L/(m_e c\omega)$ [2], described as

$$a = a_0 \exp\left(-\frac{r^2}{w_0^2} - \frac{(z - v_g t)^2}{l^2}\right), \tag{4.2}$$

where a_0 is the normalized peak amplitude, l is the length of the pulse, v_g is the group velocity of the pulse and z and r are the cylindrical coordinates. Initially the laser pulse has a full-width-at-half-maximum (FWHM) duration for the intensity of 50 fs (corresponding to $l = 12.7$ μm) and is focused to a waist spotsize, w_0, of 30 μm. The Rayleigh length, $z_R = \pi w_0^2/\lambda$, for such a pulse, with a wavelength, λ, of 800 nm, is 3.5 mm. A preformed plasma channel is used to prevent diffraction of the pulse, so that it can be guided over several centimeters (see section 2.6.1). We take a typical plasma density of 7×10^{17} cm^{-3}, which corresponds to a plasma wavelength, λ_p, of 40 μm. Depending on the chosen peak amplitude, the peak power of the pulse is

$$P[\text{TW}] \approx 21.5 \times 10^{-3} \left(\frac{a_0 w_0}{\lambda}\right)^2 \approx 30.2 a_0^2. \tag{4.3}$$

In comparison, the critical power for relativistic self-focusing is given by [47],

$$P_c[\text{TW}] \approx 17.4 \times 10^{-3} \left(\frac{\lambda_p}{\lambda} \right)^2 \approx 43.5. \qquad (4.4)$$

Here we will restrict ourself to weakly relativistic pulses with a normalized peak amplitude, a_0, of 0.6 and 0.8. The power corresponding to these pulses is, 10.9 TW and 19.3 TW respectively, which is well below the critical power for self-focusing. However, the dynamics of the laser pulse can still play an important role when the pulse has to travel several centimeters through a preformed plasma channel. The plasma channel is assumed to be created by a capillary discharge which generates a parabolic electron density, n_p, profile of the form [47]

$$n_p(r) = n_p(0) \left[1 + \left(\frac{2}{k_p r_{\text{ch}}} \right)^2 \frac{r^2}{r_{\text{ch}}^2} \right], \qquad (4.5)$$

where $k_p = 2\pi/\lambda_p$ is the plasma wavenumber and r_{ch} is the channel radius. A Gaussian laser pulse of nonrelativistic intensity ($a_0^2 \ll 1$) and low peak power ($P \ll P_c$) is guided in such a plasma channel with constant radius w_0, if w_0 is matched to the channel, which means that $r_{\text{ch}} = w_0$. Without such matching, the spot size of the pulse will oscillate during propagation. However, when the power of the laser pulse is of the order of the critical power, as considered here, the refractive index becomes a function of the intensity through the gamma-factor of the plasma electrons. This leads to self-focusing [47]. Additionally, the plasma wave generated by the laser pulse has a focusing and defocusing effect on the pulse. The front of the pulse, where the electron density has increased, experiences a weakening of the total focusing, while the back of the pulse, where the density has decreased, experiences an enhancement of the total focusing [47]. In this case, self-focusing and plasma wave guiding would cause the pulse radius to oscillate even when it was initially matched to the channel. As a result, the peak intensity of the pulse and the peak amplitude of the generated wakefield also oscillate upon propagation. This leads to a larger energy spread in the trapped electron bunch as shown in the next section. Therefore it is desirable that the named oscillations are as small as possible. We found that this can be obtained by choosing a channel radius slightly larger than that required from the matching condition, $r_{\text{ch}} = w_0$, such that self-focusing is compensated for with a reduced focusing (guiding) effect of the channel.

We calculated the dynamics for laser pulses with $a_0 = 0.6$ and $a_0 = 0.8$ and the formed wakefields with the fully relativistic particle code WAKE [62, 84]. The normalized peak intensity, as a function of the propagation distance, is plotted in figure 4.8. The dashed lines represent the case of a matched channel radius and the solid lines represent the case of a channel with a somewhat larger (optimized) radius. One can see that, for a channel with a certain (slightly larger) radius than that used for exact matching, the amplitude of the
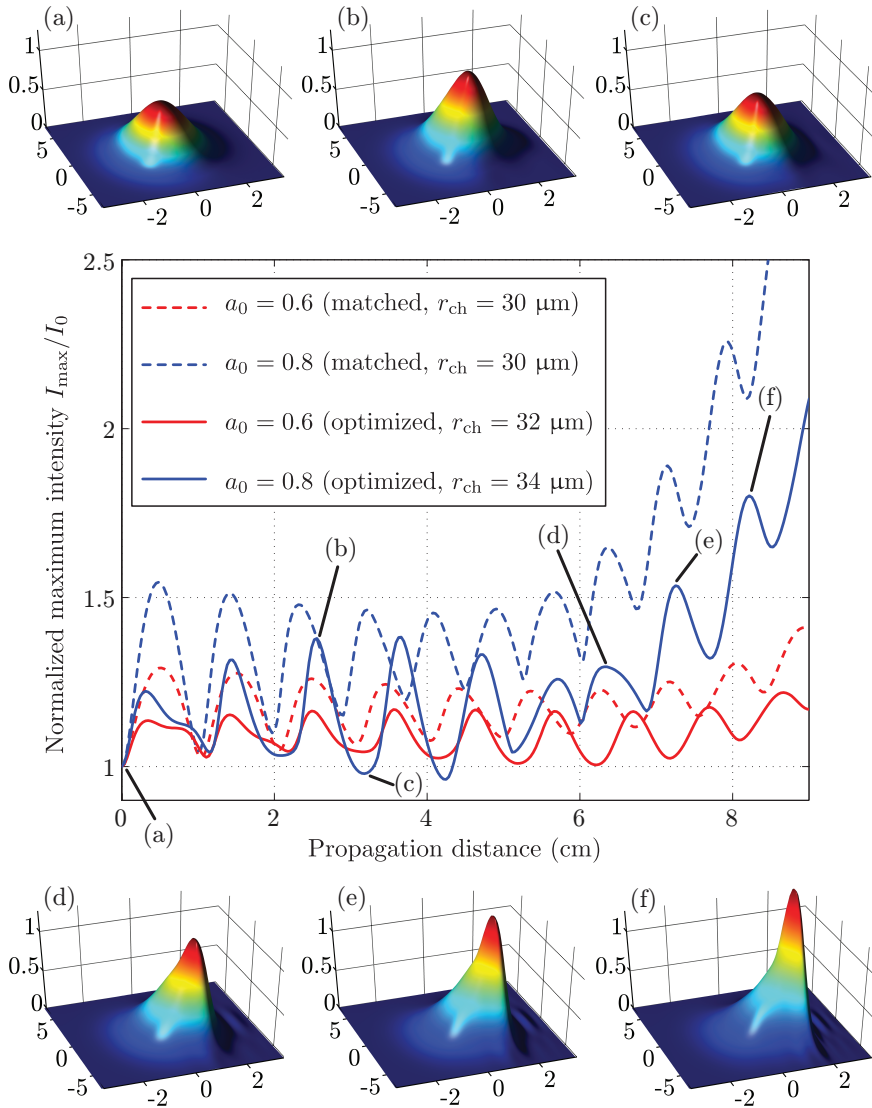
Figure 4.8: The maximum laser pulse intensity, I_{max}, normalized to its initial value I_0, as a function of the propagation distance of the laser pulse through the plasma channel. The calculations were done with the WAKE code. The initial duration of the laser pulse is 50 fs (FWHM) and the plasma density is 7×10^{17} cm^{-3} ($\lambda_p = 40$ μm).

oscillations in laser intensity are the smallest and that the average intensity remains approximately constant (e.g., the trace with $a_0 = 0.8$ and $r_{ch} = 34$ μm). We found that even wider channels increase the amplitude of the oscillations again. As expected, the oscillations become stronger when the peak intensity is increased and the power comes closer to the critical power.

In the region of the laser pulse, both the plasma density and the refractive index vary, which causes an additional temporal deformation of the pulse [85]. Specifically, the laser pulse is compressed and its peak intensity increases due to the group velocity dispersion. This pulse compression is responsible for the gradual increase of the peak intensity as can be seen in figure 4.8, and for longer propagation distances the intensity increase is stronger. A drawback of pulse shortening on the wakefield is that it decreases the dephasing length. This is due to the fact that pulse shortening lets the laser pulse slip backwards, which also causes the wakefield to slip backwards such that the maximum energy an accelerated electron bunch can potentially obtain decreases.

Another effect which needs to be considered, and which was observed in the calculations, is that, during propagation of the laser pulse through the plasma, the pulse loses some of its energy, due to the generation of the wakefield. We observed that for $a_0 = 0.6$ this loss amounts to about 4% after 6 cm of propagation through the plasma channel. For $a_0 = 0.8$ we found a loss of about 10% over the same propagation distance.

Before we present the effect of the laser pulse dynamics, we first calculate the minimum trapping energy for the described wakefields.

4.5 Minimum trapping energy

Electrons injected at an angle are transversely trapped in the accelerating phases of the wakefield near the axis by the focusing component of the wakefield at the position where the accelerating field is at maximum. When an electron is injected into a laser wakefield, there is a minimum energy for the electron below which it cannot be trapped (see e.g., [38, 40, 64]). We calculated the minimum trapping energy for the second accelerating region of the wakefield. The second accelerating region was chosen, because electrons injected at small angles can still be trapped here without going through the laser pulse which, essentially, forms a combination of injection at an angle and injection in front of the laser pulse. A description and analysis of injection in front of the pulse will be given in the next chapter. The same parameters as were used in the previous section were chosen for the laser pulse and the plasma channel. The calculations have been done for three different normalized peak amplitudes, namely $a_0 = 0.6$, $a_0 = 0.8$ and $a_0 = 1.0$, and $r_{ch} = w_0 = 30$ μm. For this set of calculations, the laser pulse dynamics were not taken into account because the trapping time for an electron is much shorter than the typical time in which the laser pulse evolves towards a different intensity. However, trapping of an electron bunch takes place during a time period in which laser dynamics may play an important role, as we will see below. The minimum trapping energy
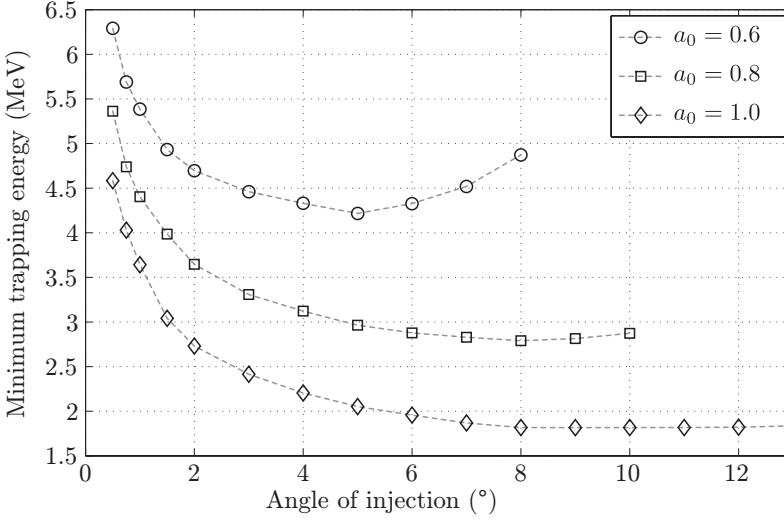
Figure 4.9: The minimum kinetic trapping energy for the second accelerating region of the wakefield as a function of the injection angle.

is plotted as a function of the injection angle in figure 4.9. One can see that the minimum trapping energy decreases when the laser pulse amplitude is increased, i.e., a stronger field allows the trapping of less energetic electrons. One also sees that the minimum trapping energy decreases for larger angles. However, for $a_0 = 0.6$, the minimum trapping energy increases again when the angle becomes larger than 5 degrees and a weak increase can also be seen for $a_0 = 0.8$ beyond 8 degrees. The injected electrons are slower than the laser pulse and will slip backwards relative to the wakefield. If the injection angle is too small, the electrons will only approach the wakefield axis slowly while slipping backwards and this slow approach increases the chance of the electrons being scattered away from the wakefield in the defocusing region. Therefore, for a given laser wakefield and injection energy, there is a minimum injection angle for trapping. For larger injection angles the transverse momentum of the electrons is also larger and the faster approach to the axis avoids much of this scattering. However, beyond a certain angle the transverse momentum becomes too large for a transverse trapping and the electrons will pass through the wakefield and are not trapped longitudinally and accelerated. Therefore, there is also a maximum injection angle for trapping. That an electron requires a minimum longitudinal momentum to be trapped in the wakefield can explain the increase in minimum trapping energy for a normalized amplitude of $a_0 = 0.6$ and $a_0 = 0.8$ when the angle is larger. A larger angle for the same injection energy means that the transverse momentum increases and the longitudinal momentum decreases. To compensate for the decrease in longitudinal

momentum the injection energy has to be increased, which explains why at a certain angle the minimum trapping energy increases again.

4.6 Effect of the laser pulse dynamics

In this section we will present the dynamics of an electron bunch injected at an angle, while also including the full dynamics of the laser pulse. We consider wakefields generated by the laser pulses with the parameters chosen in the section 4.4.

For the calculations of the dynamics of an electron bunch we use a bunch with a Gaussian density distribution in both longitudinal (z) and transverse (x and y) directions. The bunch has a FWHM duration of 250 fs (75 µm). The FWHM size of the bunch is 67 µm in both transverse directions. The parameters of the bunch are chosen in such a way that its center would move through the wakefield axis at about 120 µm behind the laser pulse. In this case electrons can be trapped simultaneously in the first, second, third and fourth accelerating regions of the wakefield. The bunch dynamics are calculated for several injection positions in the plasma channel. The longitudinal injection position of the bunch in the plasma channel is defined as the distance from the channel entrance at which the edge of the bunch enters the wakefield. More specifically, the position where the bunch center is located at a distance $2\sigma_b + w_0$ from the wakefield axis, when σ_b is the rms bunch radius. As we saw in section 4.4, the laser pulse dynamics make the wakefield change as a function of injection position. This means that an electron bunch entering the wakefield at a different laser propagation distance in the channel (see section 4.4) will experience a different wakefield. In the following, we present the results of our calculations of the electron dynamics in the wakefield with the parameters described in section 4.4. We will vary several parameters of the problem and focus on the behavior of the collection efficiency and minimum relative energy spread.

First we present the results obtained with the initial normalized amplitude of the laser pulse being $a_0 = 0.6$ and the plasma channel radius set to a value of 32 µm, which is a bit larger than the matched radius. The length of the plasma channel is chosen such that the accelerated electron bunch has minimum relative energy spread, which typically occurs after 5 to 7 cm propagation. The collection efficiency and minimum rms relative energy spread are plotted as a function of the injection position (that is for different laser propagation distances, see figure 4.8) for several different injection energies and for angles of 2 and 6 degrees in figure 4.10 and 4.11.

One can see that the laser pulse dynamics play an important role, because the energy spread and the collection efficiency depend on the injection position. Specifically, the relative energy spread oscillates as a function of the injection position. The explanation for this is based on the intensity oscillations described in section 4.4. For an injection position where the gradient of the laser peak intensity (see figure 4.8) is low, one obtains a low energy spread. For in-
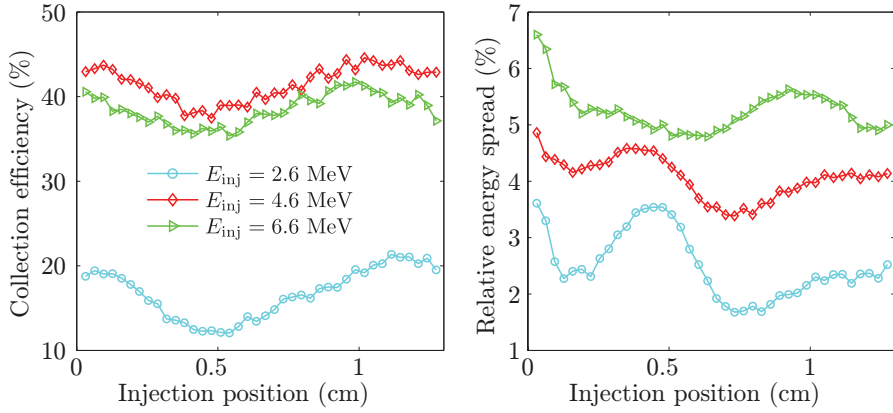
Figure 4.10: The minimum rms relative energy spread and collection efficiency of the accelerated bunches versus the injection position of the externally injected electron bunch. In this case $a_0 = 0.6$ and $\alpha = 2°$. The curves are shown for kinetic injection energies of 2.6, 4.6 and 6.6 MeV.
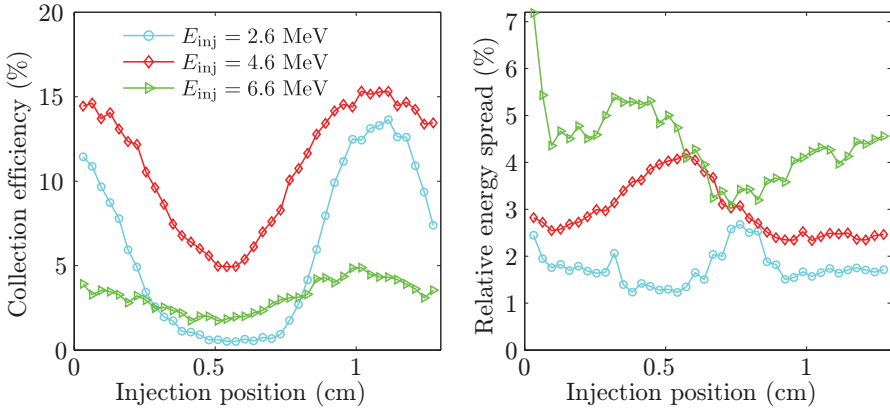

Figure 4.11: The minimum rms relative energy spread and collection efficiency of the accelerated bunches versus the injection position of the externally injected electron bunch. In this case $a_0 = 0.6$ and $\alpha = 6°$. The curves are shown for kinetic injection energies of 2.6, 4.6 and 6.6 MeV.

jection positions with a high gradient of the peak intensity, the energy spread becomes larger. The phase of the wakefield, where an electron is trapped depends particularly on the wakefield amplitude [37, 40], which is given by the peak intensity and duration of the laser pulse. If the strength of the wakefield changes while the bunch is being trapped, the electrons are trapped at different phases in the wakefield. This leads to a larger energy spread compared to the case where there are no laser dynamics. Correspondingly, for a low energy spread, either the laser pulse dynamics should be kept weak while the electron bunch is trapped, or the trapping time should be kept small. It can be seen that the collection efficiency also depends in a similar, oscillating manner on the position where the electron bunch is injected into the plasma channel. The explanation is that, at positions where the laser intensity is higher, a stronger wakefield is generated, which can trap more electrons.

The collection efficiency is at its best when the injection energy is not too high and, also, not too low, depending on the injection angle. For injection energies that are too low, electrons cannot be trapped because their initial energy is below the minimum trapping energy. When the injection energy is too large, the transverse momentum of the electrons is too large to be trapped by the transverse focusing forces.

The figures show that a lower energy spread is obtained for lower injection energies and that a larger injection angle can also give a lower energy spread. We observed that the trapping distance for an electron bunch, defined as the distance traveled by the laser pulse from the point where the first electron is trapped to the point where the last electron is trapped, decreases for larger injection angles. This explains the lower energy spread for injection with a larger angle because, the longer it takes to trap the bunch, the larger the energy spread becomes [64]. On the other hand, lower injection energies and larger angles decrease the collection efficiency as there are less positions where electrons can be trapped. Thus, a compromise has to be made between collection efficiency and energy spread. For example: an angle of 6 degrees, an injection energy of 2.6 MeV and, an injection position of 1 cm, gives a relatively low energy spread of approximately 1.6% and a reasonably high collection efficiency of 13%.

The rms transverse size of the accelerated bunches lies in the range of 1.5 to 3 µm for an angle of 2 degrees and 1.5 to 6 µm for an angle of 6 degrees. For both angles, the final energy is in the range between 300 and 500 MeV, where the final energy grows monotonically with decreasing injection energy.

A second calculation has been done with the same parameters as above, but with the higher laser pulse intensity, namely for $a_0 = 0.8$ and a plasma channel radius of 34 µm.

The results are plotted in figures 4.12 and 4.13, where we show again the collection efficiency and energy spread for different injection energies and for injection angles of 2 and 6 degrees. In general, because the wakefield in this case is stronger than in the previous case, it can be seen that more electrons can be trapped for the same injection energy. It is also noticed that the minimum
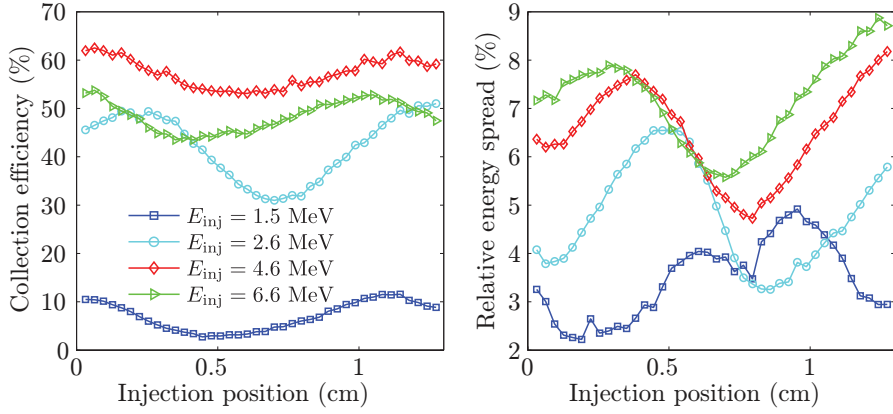
Figure 4.12: The minimum rms relative energy spread and collection efficiency of the accelerated bunches versus the injection position of the externally injected electron bunch. In this case $a_0 = 0.8$ and $\alpha = 2°$. The curves are shown for kinetic injection energies of 1.5, 2.6, 4.6 and 6.6 MeV.
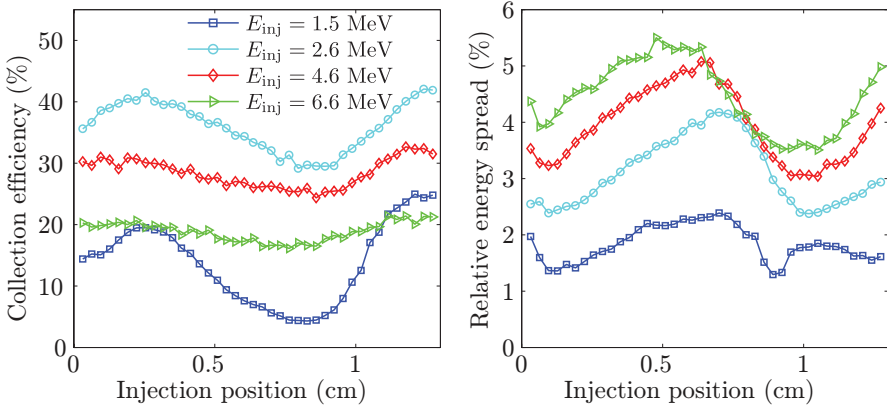

Figure 4.13: The minimum rms relative energy spread and collection efficiency of the accelerated bunches versus the injection position of the externally injected electron bunch. In this case $a_0 = 0.8$ and $\alpha = 6°$. The curves are shown for kinetic injection energies of 1.5, 2.6, 4.6 and 6.6 MeV.

trapping energy is lower than in the previous case (with $a_0 = 0.6$). This means that even electrons with the rather low initial kinetic energy of 1.5 MeV can be trapped.

Qualitatively, one can observe the same behavior as in the previous case, however, because the dynamics of the laser pulse are stronger, some differences can be seen. The variations in the collection efficiency and the energy spread are larger, which makes it even more important to inject at an optimum position in the plasma channel. By choosing the right angle, injection energy and injection position, one can obtain accelerated bunches with less than 2% energy spread and a good collection efficiency of 20 to 30%.

A clear difference from the previous case ($a_0 = 0.6$) is the behavior of the energy spread for an injection angle of 2 degrees (figure 4.12) and an injection energy of 1.5 MeV. We found that this is caused by a combination of injection in front of the laser pulse and injection at an angle; the electron bunch goes partly through the laser pulse. Electrons are trapped about 120 μm behind the laser pulse and, because the injection energy is low and the angle is small, part of the bunch goes through the laser pulse in the plasma.

The energy of the accelerated bunches with $a_0 = 0.8$ is generally higher than with $a_0 = 0.6$, values between 500 and 800 MeV are obtained. Also in this case, a lower final energy corresponds to a higher injection energy. The rms transverse size of the accelerated bunches is in the range of 1 to 3 μm for $\alpha = 2°$ and $\alpha = 6°$.

4.7 Summary and conclusion

In this chapter we have studied the external injection of an electron bunch at an angle into the channel-guided laser wakefield including the dynamics of the laser pulse in the plasma channel. It turns out that the dynamics of the laser pulse have a large influence on the final energy spread of the accelerated electron bunches. Wakefields created with higher power laser pulses have stronger dynamics and the effect on the trapping and acceleration of the electrons is also stronger. However, by varying the injection position, injection energy and injection angle, the energy spread can be minimized, while higher collection efficiencies can be achieved. This shows that, even when the laser pulse dynamics become important, micron-sized electron bunches accelerated to several hundreds of MeV's can be generated by injection at an angle. In particular, minimizing the energy spread can be achieved by injecting the electron bunch into the channel where the wakefield is as constant as possible. Minimizing the trapping distance by increasing the injection angle and decreasing the injection energy can lower the energy spread even more.

The energy spread is calculated by averaging over all electrons in all the bunches that are formed and accelerated behind a single laser pulse. However the energy spread for one of these bunches can be considerably lower. The energy and energy spread of a bunch depends on how far behind the laser pulse it is formed. The farther from the pulse, the weaker the accelerating field and

the stronger the focussing field becomes. The wakefield also develops a curve [2, 83]. In general the bunches that are accelerated at a greater distance from the pulse have a lower energy and a higher energy spread, which means that the total energy spread will increase when more bunches are formed. Thus, the injected bunch should be kept short to minimize the number of formed bunches.

We conclude that external injection at an angle into the laser wakefield is an important alternative when the scattering of the injected bunch by a laser pulse or by the wakefield in the vacuum-plasma transition needs to be avoided.

Injection in front of the laser pulse

External injection at an angle (as discussed in the previous chapter) has shown to be a scheme that can provide accelerated electron bunches of high quality (low energy spread). A special case of that scheme is the injection with a zero angle on-axis, which means that the electron bunch is injected in front of the laser pulse. In this case the laser pulse does not overtake the electron bunch in the vacuum (unlike injection behind). The laser pulse overtakes the electron bunch inside the plasma so that the wakefield compensates for the ponderomotive scattering. Khachatryan [38] proposed this scheme and showed that, in this way, an externally injected electron bunch can be effectively trapped, compressed and accelerated to a short bunch with a high quality. At the University of Twente we have been refining this scheme and are currently preparing a proof-of-principle experiment [42]. A sub-picosecond electron bunch with an energy of a few MeV will be injected into a plasma channel just before a high intensity ultrashort laser pulse. In this chapter we study the injection scheme and look at the experimental design.

5.1   The injection scheme

The central idea of the injection scheme is schematically depicted in figure 5.1. An electron bunch is focused into a plasma channel ahead of a terawatt drive laser pulse, which generates a strong wake wave in the plasma. The duration of the injected bunch can be relatively long (sub-picosecond). The kinetic energy of this bunch should be in the order of a few MeV. Inside the plasma channel
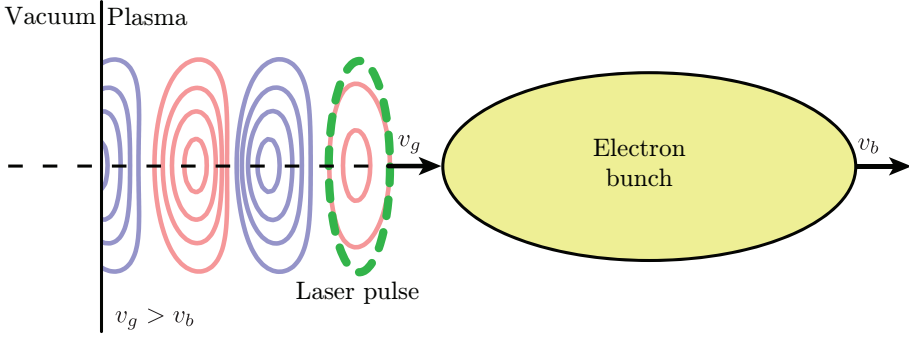
Figure 5.1: Schematic drawing of injection in front of the laser pulse into a laser wakefield. An electron bunch with velocity v_b is injected into a laser wakefield.

the laser pulse travels with the group velocity, as derived in section 2.2.6,

$$v_g = c\sqrt{1 - \frac{\omega_p^2}{\omega^2}}. \tag{5.1}$$

The wake wave generated by the laser pulse will propagate with a phase velocity equal to the laser group velocity and, of course, to enable the wakefield to overtake the bunch, the bunch velocity v_b has to be smaller than the group velocity of the laser pulse ($v_b < v_g$). The travel distance of the laser pulse needed to overtake the bunch is called the trapping distance and will be derived in the next section.

We will show that when the laser pulse overtakes the electron bunch, a large fraction of the electrons can be trapped at the accelerating slope of the wake immediately behind the laser pulse. These electrons are all collected in the first accelerating phase of the wakefield where a compressed bunch builds up. When suitable parameters are chosen the trapped and compressed electron bunch can become much shorter than the plasma wavelength. To illustrate these properties in the simplest-possible situation we will first describe a one-dimensional case using Hamiltonian dynamics. This yields an analytical description for the duration of the trapped bunch and also for several other properties.

5.1.1 One-dimensional theory

By investigating injection in front with a one-dimensional theory [64], the transverse variations of the laser wakefield are neglected. This is only valid for electrons moving along the pulse axis. However this case is of interest because, in the three-dimensional case, the trapped electrons will also become concentrated close to the axis and their longitudinal dynamics are well described by the one-dimensional theory. The one-dimensional theory also allows a more detailed description and helps clarify the underlying physics.
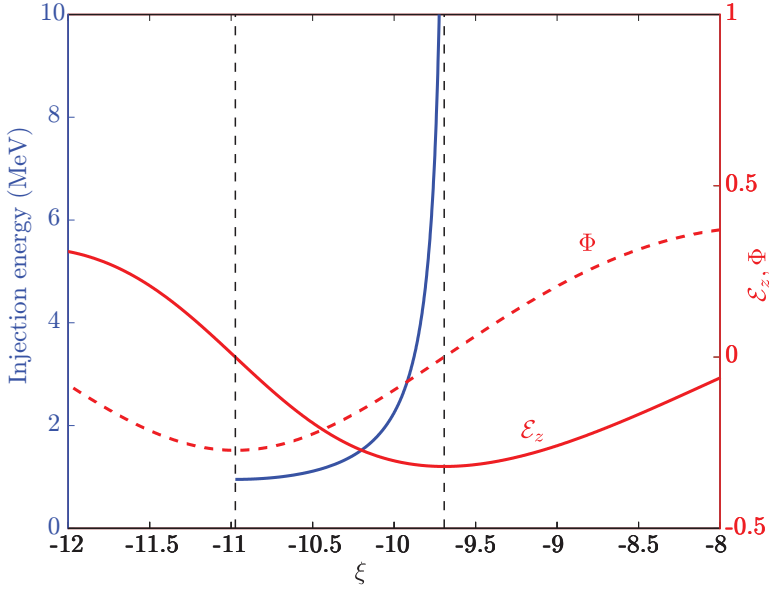
Figure 5.2: Relationship between the injection energy (in MeVs) and the trapping position for $a_0 = 1$, $\gamma_g = 50$ and $\sigma_z = 2$. Also the normalized electric field ($\mathcal{E}_z$) and the normalized wake potential (Φ) are plotted. The trapping region lies between the dashed lines.

In section 2.4 we derived the relationship between the initial energy of the electron, γ_0, and the wake potential at the trapping point from the constant of motion of the system. For injection in front of the laser pulse, where the electron is initially at zero potential ($\Phi_{\text{init}} = 0$), this relationship is

$$\gamma_0 = \gamma_g^2 \left(S - \beta_g \sqrt{S^2 - \frac{1}{\gamma_g^2}} \right), \tag{5.2}$$

where $S = 1/\gamma_g - \Phi_{\text{tr}}$ and Φ_{tr} the wake potential at the trapping point. The given relationship between injection energy and trapping position is plotted in figure 5.2. The parameters for the wakefield are the same as those for the plot of the separatrix in figure 2.6 with $a_0 = 1$, $\sigma_z = 2$ and $\gamma_g = 50$. Electrons with an initial energy $\gamma_{\text{min}} < \gamma_0 < \gamma_g$ can be trapped in the region between the dashed lines, where the normalized potential is in the range $\Phi_{\text{min}} < \Phi < 0$. The width of this region is less than a quarter of the linear plasma wavelength. While the nonlinear plasma wavelength will increase for increasing wake amplitude $E_{z,\text{max}}$, the length of the trapping region will reduce, because of the steepening of the plasma wave.

For this scheme the laser pulse has to overtake the electron bunch in the plasma which requires a certain propagation distance. This distance is called
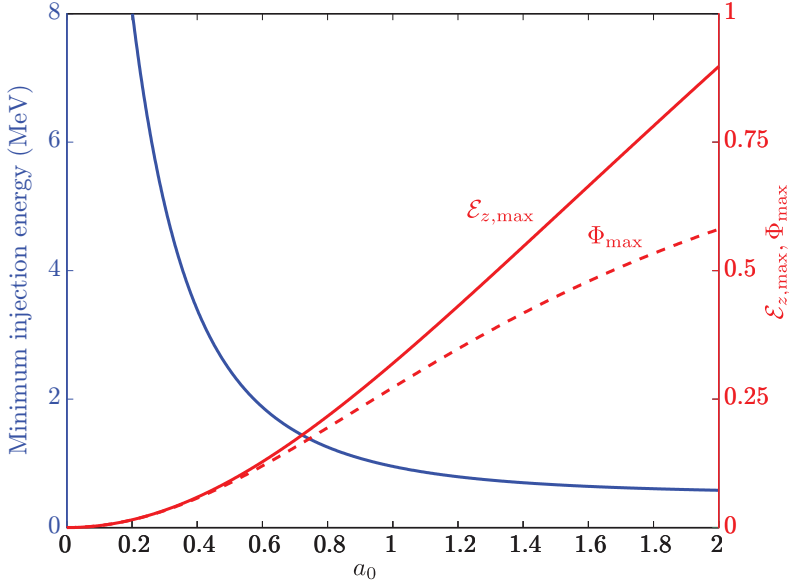
Figure 5.3: The minimum trapping energy (in MeVs) and the amplitude of the accelerating field (expressed in $\mathcal{E}_{z,\mathrm{max}}$ and Φ_{max})

the trapping distance and can be estimated as follows. When the injected bunch has a length L_0 and is approximately mono-energetic and $1 \ll \gamma_0^2 \ll \gamma_g^2$, we get for the trapping distance

$$L_{\mathrm{tr}} \approx \frac{L_0}{1 - \beta_b/\beta_g} \approx 2\gamma_0^2 L_0, \tag{5.3}$$

with β_b and β_g the normalized electron and laser velocity respectively. Thus the trapping distance will quickly grow when the initial bunch energy is increased, because the difference in velocity between the laser pulse and the electron bunch becomes smaller. This increases the time necessary for the pulse to overtake the bunch.

To estimate the length of the trapped bunch, we consider the following. Once an electron is trapped it will start to dephase (see section 2.5). An electron at the back of the injected bunch will be trapped slightly earlier than an electron at the front of the bunch. During this time the electron that was trapped first has already propagated some distance in the wakefield and away from the trapping point. This can be cast into the expression

$$L \approx L_{\mathrm{tr}}\left(1 - \beta_g\right) \approx \frac{L_{\mathrm{tr}}}{2\gamma_g^2}. \tag{5.4}$$

By inserting the trapping distance, one obtains the following expression for the

Table 5.1: Parameters used to study injection in front

On-axis electron density	7×10^{17} cm^{-3}
On-axis plasma wavelength	40 µm
Bunch duration (FWHM)	200 fs
Bunch radius in the focus (FWHM)	64 µm
Bunch energy spread	1%
Bunch emittance	1 µm
Laser normalized amplitude	0.7 & 0.9
Laser power	14.8 & 24.5 TW
Laser pulse energy	790 & 1306 mJ
Laser intensity	1.0×10^{18} & 1.7×10^{18} W/cm^2
Laser central wavelength	0.8 µm
Laser pulse duration (FWHM)	50 fs
Laser pulse waist size	30 µm

trapped bunch length

$$L \approx \left(\frac{\gamma_0}{\gamma_g} \right)^2 L_0 \ll L_0. \tag{5.5}$$

This equation shows that the trapped bunch length is considerably shorter than the initial bunch length. This statement sounds simple, but it is extremely important. This statement actually declares that with the injection in front of the laser pulse, the injection phase of the electrons will be almost the same, despite the bunch not satisfying the condition $L_0 \ll \lambda_p$. In other words, the injection of a relatively long bunch ($L_0 > \lambda_p$) can also generate an extremely short bunch. If we take, for example, an electron bunch with $\gamma_0 = 8$ ($E_0 \approx$ 3.6 MeV) and a duration of 250 fs (which corresponds to a bunch length of 75 µm) and inject this into a wakefield with $\gamma_g = 50$, we find a trapped bunch length of only 1.9 µm (or a duration of 6.4 fs). Of course these one-dimensional calculations do not give us the full picture. In the next section we investigate the injection scheme in the three-dimensional case with numerical calculations.

5.2 Properties of injection in front

Let us now investigate the properties of injection in front for typical parameters with numerical calculations. The parameters used for this calculation are the same as those used for injection at an angle, which was studied in section 4.3 of the previous chapter. For convenience, the parameters are given once more in table 5.1. We examine the scheme for two wakefields with normalized amplitudes, a_0, of 0.7 and 0.9, which are calculated with the WAKE code [62, 84].

In figure 5.4 six snapshots of an electron bunch, injected with a kinetic energy of 2 MeV into the wakefield generated with a laser pulse with $a_0 = 0.9$, are
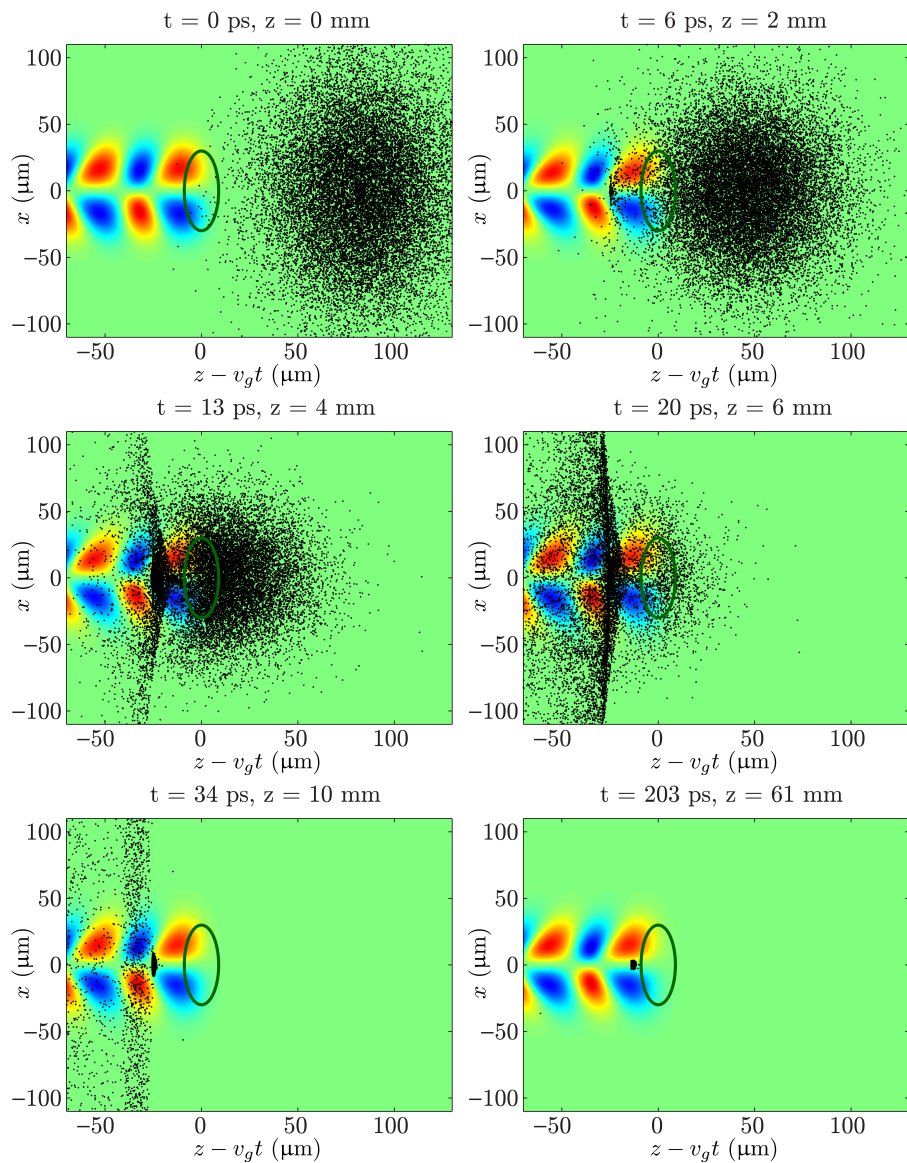
Figure 5.4: Six snapshots of the dynamics of external injection in front of the laser pulse. The electron bunch (slightly converging due to standard magnetic focusing) is plotted on top of the transverse component of the wakefield. It is shown in the frame moving with the laser pulse at 0, 2, 4, 6, 10 and 61 mm from the plasma channel entrance. The laser pulse is positioned at $z - v_g t = 0$. The electron bunch is injected into the wakefield with $a_0 = 0.9$ with a kinetic energy of 2 MeV.

Figure 5.5: The mean energy (solid line) and rms relative energy spread (dashed line) for an electron bunch injected with a kinetic energy of 2 MeV in front of the laser pulse into the wakefield with a normalized amplitude of $a_0 = 0.9$.
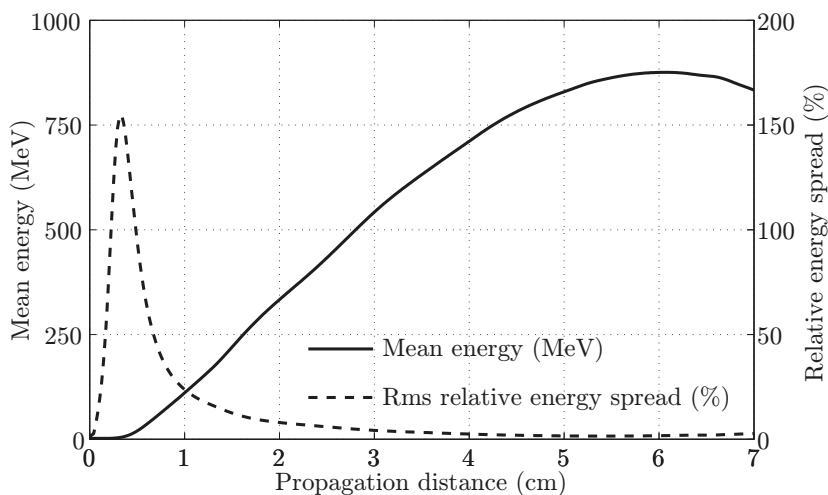
shown at subsequent positions in the plasma channel. In the first snapshot one can see the electron bunch still located in front of the laser pulse. The next four snapshots show how this bunch converges further by e.g., standard magnetic focusing techniques, and is overtaken by the laser pulse in the plasma channel. About 30% of the electrons are trapped in the first accelerating and focusing part of the wakefield. Thus, in contrast to injection behind and injection at an angle, only one bunch is formed. The final snapshot shows the accelerated electron bunch at the end of the plasma channel after 61 mm of propagation. At this position the electron bunch has reached its maximum energy, which is, in this case, 876 MeV.

In figure 5.5 the energy and relative energy spread are plotted as a functions of the propagation distance. One can see that the energy of the trapped electron bunch gradually increases during propagation through the plasma channel. The maximum of 876 MeV is reached after a propagation distance of 61 mm. This is where the plasma channel should stop, as further propagation through the channel would result in a decrease in energy and an increase in energy spread. The reason of this is that, beyond this position, the bunch would be entering the decelerating part of the wakefield due to dephasing (see section 2.5). We note that this plot looks quite similar to the plot for injection at an angle in figure 4.4. In both cases the electron bunch "gradually" enters the wakefield from the front or from the side while, for injection behind, the bunch enters the wakefield all at once.

In figure 5.6, the electrons are plotted in phase space in several positions in
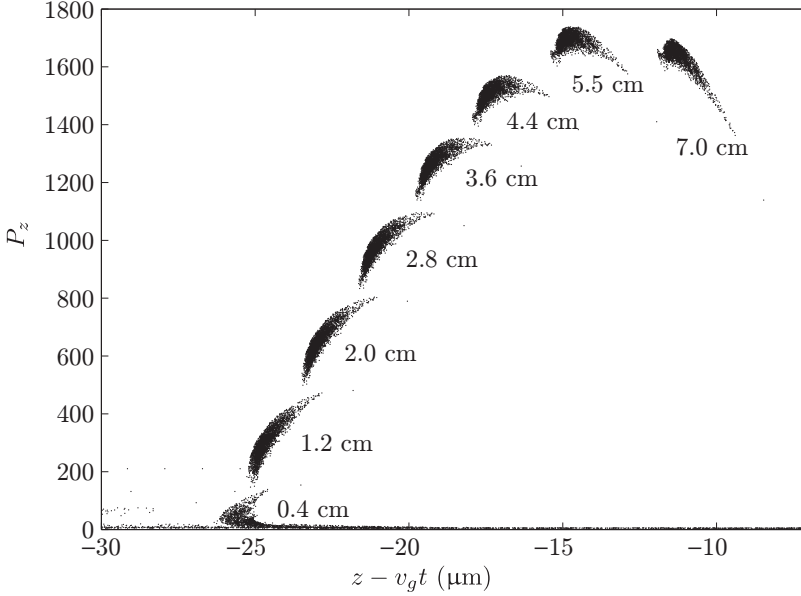
Figure 5.6: The accelerated electron bunch in phase space at subsequent positions in the plasma channel for an injection energy of 2.6 MeV and the wakefield with a normalized amplitude of $a_0 = 0.9$.

the plasma channel to show the behavior of the energy spread. One can see that when the bunch is just trapped, after propagating 1.2 cm, the energy spread is high because the extension in the P_z-direction is large. The electrons that were trapped first have already accelerated to high energy, while the electrons that were overtaken and trapped last still have a low energy. However, when the electron bunch comes close to the maximum possible energy, the energy spread decreases. The reason for the decreasing spread is that the wakefield does not have a constant acceleration gradient. Electrons at the front of the trapped bunch will approach the decelerating part of the wakefield earlier and experience a weaker accelerating force, while electrons at the rear still experience a strong accelerating force. Thus, the electrons at the rear gain more energy than the electrons at the front of the trapped bunch. This decreases the size of the bunch in the P_z-direction in phase space and consequently decreases the energy spread.

In figure 5.7 the collection efficiency (a) and energy spread (b) is shown for injection in front for wakefields with $a_0 = 0.7$ and $a_0 = 0.9$. There is a minimum injection energy below which no electrons can be trapped. For the wakefield with $a_0 = 0.7$ this minimum trapping energy is approximately 2.5 MeV and for the wakefield with $a_0 = 0.9$ the minimum trapping energy is about 1.3 MeV. Above this minimum trapping energy the collection efficiency gradually
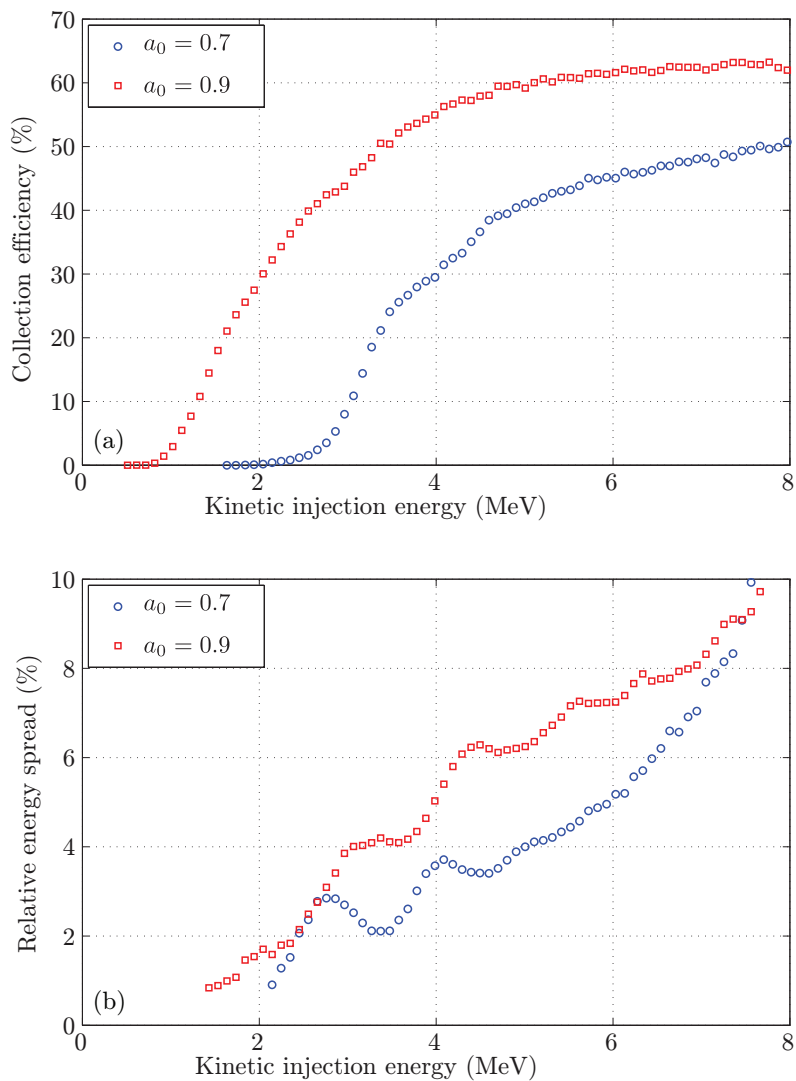
Figure 5.7: The collection efficiency (a) and rms relative energy spread (b) as a function of the kinetic injection energy for injection in front of the laser pulse into the wakefield with a normalized amplitude of $a_0 = 0.7$ (blue circle) and $a_0 = 0.9$ (red square).

increases and saturates at a value of 50% for $a_0 = 0.7$ and 65% for $a_0 = 0.9$. We note that these are actually extremely high values for the rather large dimensions of the injected bunch. What can also be noted in figure 5.7b is that the energy spread is slightly oscillating. This oscillation is caused by the laser pulse dynamics with their oscillating peak intensity. Looking at the general trend of the energy spread, it can be seen that it increases with increasing injection energy. This means that, if a lower energy spread is required, this will be accompanied with a lower collection efficiency.

5.2.1   Comparison with injection at an angle

When looking at the dynamics of the trapped electron bunches, one can see that they looks very similar to those found with injection at an angle. This is not surprising because in both cases the injected electrons initially propagate through a region in the plasma where there is no wakefield and only move gradually into a stronger wakefield. As a result, the trapping conditions which can be derived from the Hamiltonian are largely the same. This differs from the case when electrons are injected behind the laser pulse [37, 66] and suddenly enter the wakefield. In this case, the injection phase will determine the strength of the wakefield the electrons suddenly experience. Calculations for a kinetic injection energy of 3 MeV and a wakefield with $a_0 = 0.9$, as described above, for the three different injection schemes show that, after full acceleration, the energy spread amounts to 1.7% for injection in front, 2.2% for injection at an angle of 4 degrees, and 20% for injection behind (without ponderomotive scattering and transition region). The parameters chosen in this direct comparison are not the most optimum for injection behind the drive pulse, but the example demonstrates that injection at an angle can be viewed as a modification of injection in front.

5.3   Experimental design

We are currently preparing a proof-of-principle experimental demonstration of external injection of a sub-picosecond electron bunch from a conventional radio-frequency (rf) accelerator into a laser wakefield. The initiation of the experimental activities started within the Dutch research program "Laser Wakefield Accelerator" and the design and assembly continued through additional funding by the Dutch ministry for Education, Culture and Science (OCW). Further support was provided by the Forschungszentrum Dresden-Rossendorf (FZD) in Germany and collaboration with FZD is planned to continue as they have a linear accelerator in combination with a high-power laser available as well. We plan to use injection of an electron bunch in front of the drive laser as the injection scheme. In this section, we will give a brief description of the experimental design being developed at the University of Twente. More detailed information can be found in the article concerning the design [42] and in the PhD thesis of Irman [86].
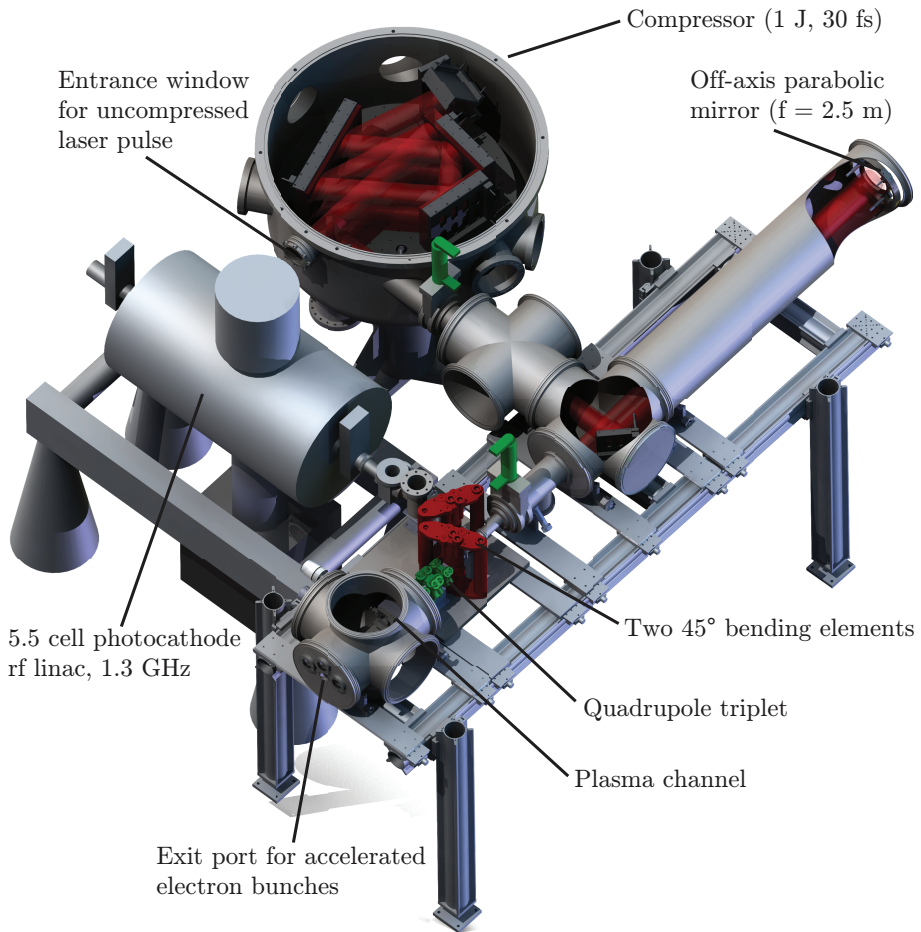
Figure 5.8: The laser wakefield accelerator at the University of Twente. The terawatt pulse is focused by an off-axis parabolic mirror onto the entrance of a plasma channel and enters the channel just after the electron bunch. The bunch, from the photocathode rf linear accelerator, is transported to the channel via a bending section, which consists of two subsequent 45° bending magnets with an intermediate quadrupole magnet, and is focused towards the plasma channel using a focusing section consisting of quadrupole magnets. An electron spectrometer is installed at the exit of the channel to measure the bunch energy and energy spread. The time delay between the bunch and the pulse is controlled by an optical delay and by the phase locking of the laser oscillator to the microwave drive frequency of the linear accelerator.

Our laser wakefield accelerator setup is shown in figure 5.8. A high power laser with a pulse energy of approximately 1 J and with a FWHM duration of 30 fs focused to a spot size of 30 μm, yielding an intensity of 2×10^{18} W/cm^2, excites the wakefield in a plasma channel. The injected electrons are emitted from a copper photocathode, illuminated by a short laser pulse, and are accelerated in a 5.5 cell linear accelerator. This accelerator can provide the required electron bunches of several pC charge and with an energy up to 6 MeV.

In order to have a small energy spread in the laser wakefield accelerated bunch, the trapping distance should be substantially shorter than the acceleration length, which, for a conventional capillary discharge plasma channel, is typically about 5 cm [52]. Accordingly, to employ a channel of such length, we intend to reduce the trapping distance by lowering the electron energy and shortening the injected bunch. Due to the required minimum electron energy for trapping in the plasma wake created with our laser parameters, which is approximately 1 MeV on-axis and increases to 2.5 MeV in the transverse wings of the laser pulse [64], we choose a total energy ($\gamma_0 m_e c^2$) of 3.4 MeV for the injected bunches. The Coulomb force and energy spread in the bunch are known as the natural lengthening sources. In our experiment, the Coulomb force effect is reduced by choosing electron bunches with a low charge of 5 pC. The lengthening due to the energy spread is reduced by having designed the electron beam line to be as short as possible. To reduce the duration of the bunch even more we have adopted a magnetic bunch compression scheme. This means that the trapping distance becomes considerably less than the length of the plasma channel. In the linear accelerator the electron bunch acquires a time-energy correlation (chirp) along the bunch length. We employ a magnetic compression section which is installed about 0.5 m downstream from the accelerator in order to compress the bunch. The compression section possesses a non-isochronous property. This means that it introduces an energy-dependent path length on the electrons such that higher-energy electrons follow a longer path than lower-energy electrons. Thus proper tuning of the parameters of the compression section should give the needed chirp compensation resulting in a compression of the bunch. In the actual design, the compression section consists of two subsequent 45° bending magnets with a quadrupole placed in the middle. The function of the quadrupole is to compensate for the increase in bunch transverse size in the bending plane behind the first bending magnet. The compression section is then followed by a set of quadrupole triplets for transversely focusing the electron bunches to match the spot size of the drive laser in the plasma channel and, thereby, increasing the number of electrons which will interact with the wakefield.

We performed simulations of the complete electron bunch dynamics up to the plasma channel with numerical codes TRANSPORT, PARMELA and the general particle tracer code (GPT [87]). The details of these calculation can be found in the concept article and the PhD thesis of Irman [42, 86]. Here we present only the properties of the bunch calculated at the entrance of the plasma
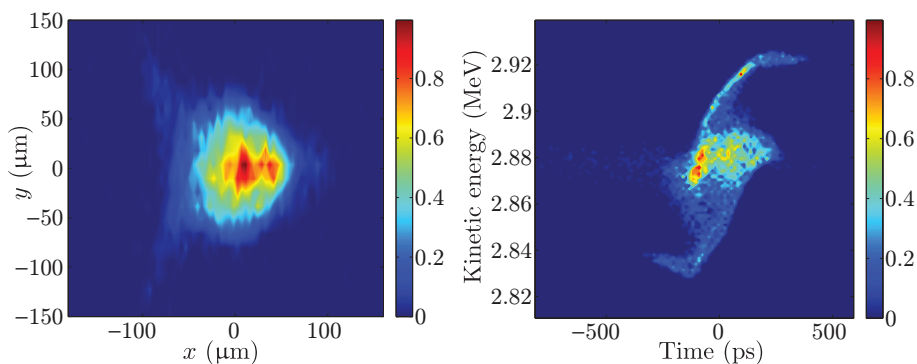
Figure 5.9: The cross section (a) and longitudinal phase space density (b) of the injected electron bunch at the focus. The colors represent the normalized electron density.

channel and the further acceleration in the laser wakefield. The cross-section, calculated in the focus, for the electron bunch that arrives at the entrance of the plasma channel is shown in figure 5.9a. It can be seen that the bunch size in the x- and y-directions is 35 μm (rms) and 40 μm (rms), respectively. The bunch durations are approximately 250 fs, as shown in figure 5.9b. The relative energy spread of the bunch is 0.56%. The normalized emittance is 0.9 μm in the x-direction and 1.6 μm in the y-direction. Fortunately, these parameters can be well accepted for our scheme of injection in front of the laser pulse.

The bunch parameters obtained from the GPT code were imported into our three-dimensional particle tracer code to calculate the trapping, compression and acceleration in the laser wakefield. The bunch focus is placed inside the channel, about 4 mm from the channel entrance, to maximize the number of trapped electrons. Figure 5.10 displays the energy and relative rms energy spread of the trapped electron bunch during acceleration. It can be seen that the energy of the electron bunch grows very rapidly (solid line) and reaches its maximum of 744 MeV after a propagation distance of 5.4 cm inside the plasma channel. The energy spread in the bunch, indicated by the dashed line, increases at the beginning of the process and then decreases strongly to a low value of 1.1% at the end of the channel. The increase of the energy spread in the early (trapping) process is due to the participation of two groups of electrons as explained in section 4.3.

The longitudinal and transverse compression of the bunch during trapping and acceleration is shown in figure 5.11. It can be seen that, after the trapping process is finished, at a propagation distance of about 1.8 cm, the bunch has an x and y size of 1.7 μm (rms) and 1.3 μm (rms), respectively. The duration of the bunch is 6 fs, corresponding to a bunch length of 1.8 μm.

In our calculations we find that a significant fraction of about 48% of the
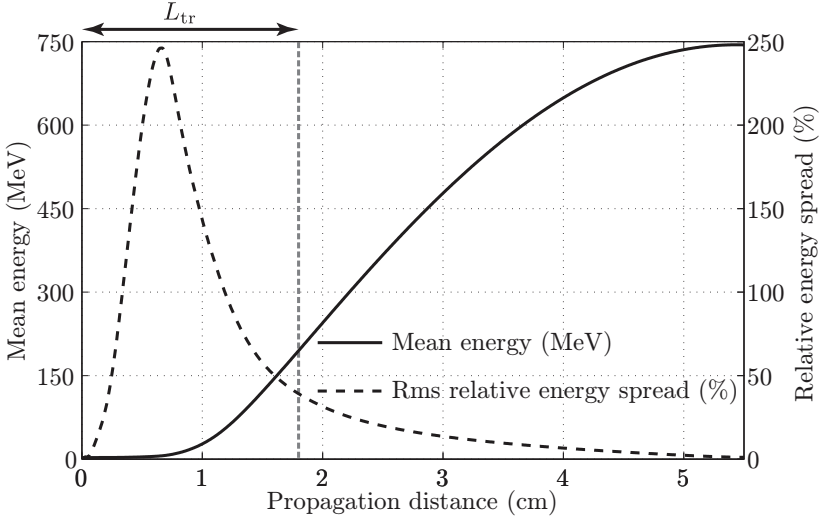
Figure 5.10: The mean energy and rms relative energy spread of the trapped electron bunch during trapping and acceleration in the laser wakefield. A maximum energy of 744 MeV and a lowest energy spread of 1.1% is reached at a propagation distance of 5.4 cm in the plasma channel.

injected electrons are trapped, which amounts to a total charge of 2.4 pC in the accelerated bunch. The transverse normalized emittances are 3.8 µm and 2.5 µm respectively for the x- and y-direction. As an overview, the input and output parameters for our laser wakefield experiment are summarized in table 5.2.

5.4   Summary and conclusion

In this chapter, injection of an electron bunch in front of the laser pulse into a laser wakefield has been presented. We have shown that the injection of relatively long electron bunches (sub-picosecond) can result in high quality accelerated bunches. In contrary to injection behind and injection at an angle, only one bunch is trapped in the wakefield. The dynamics of the trapping of the electrons turn out to be very similar to injection at an angle. For both schemes, electrons come from a zero wakefield and gradually move into a stronger wakefield. Also, for this scheme, a compromise has to be made between high collection efficiency and low energy spread.

   Injection in front is a very interesting scheme for experimental realization because the scattering of the injected bunch in front of the plasma channel does not take place and the required parameters can be realized. The design of a realistic laser wakefield acceleration experiment has been analyzed. In this
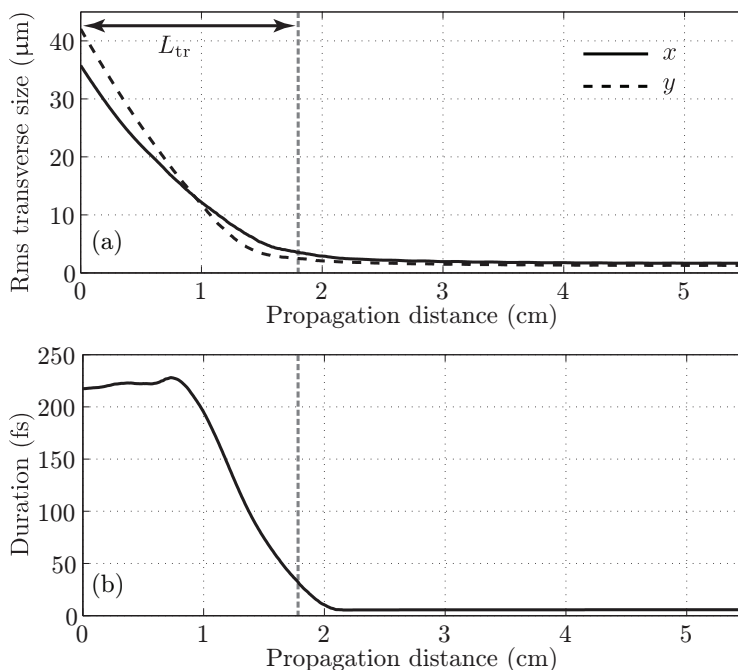
Figure 5.11: The compression of the injected electron bunch in the laser wakefield. After the trapping distance, $L_{tr} \approx 1.8$ cm, the bunch size shrinks considerably. At the exit of the plasma channel (after 5.4 cm), the bunch size (a) is 1.7 µm and 1.3 µm in the x and y directions respectively and the $2\times$ rms bunch duration (b) is 6 fs.

Table 5.2: Bunch parameters for the proof-of principle laser wakefield acceleration experiment with external injection. The injected bunch charge is 5 pC. The on-axis plasma density is 8.6×10^{17} cm^{-3}, the channel length is 5.4 cm, the laser spotsize is 30 µm, the peak intensity is 2×10^{18} W/cm^2.

Bunch parameters	Before compressor	Injected bunch	At exit of plasma channel
Energy (MeV)	2.88	2.88	744
Energy spread (%)	0.47	0.56	1.1
Emittance in x (µm)	0.3	0.9	3.8
Emittance in y (µm)	0.3	1.6	2.5
2 rms bunch duration (fs)	2000	250	6
Rms transverse size in x (µm)	330	35	1.7
Rms transverse size in y (µm)	330	40	1.3

proposed experiment, which is currently in the process of testing and alignment, an electron bunch generated by an rf photocathode linear accelerator is injected into a plasma channel just in front of the drive laser pulse. Simulations predict that bunches with an energy of about 0.7 GeV and with about 1% relative energy spread can possibly be obtained from our planned experiment.

6

Attosecond electron bunches

Attosecond electron bunches are of great interest as a new and unique tool for opening novel avenues of research and applications. Examples are electron microscopy with attosecond resolution or the generation of attosecond X-ray beams, for investigating physical, chemical and biological processes with unprecedented temporal resolution.

In the previous chapters we have shown that the external injection of an electron bunch into a laser wakefield can provide ultra-relativistic electron bunches with a duration of several femtoseconds. Recently it has also been experimentally shown for internal injection that laser wakefield accelerators [1] can provide ultra-relativistic femtosecond bunches for various parameters of the drive laser and the plasma [19–21, 27, 29, 30, 33, 88]. In this chapter we show that, due to a strong chirp of the betatron frequency along the direction of acceleration, laser wakefield acceleration can also provide attosecond bunches. The attosecond bunches propagate over significant distances (many tens of centimeters) without a significant increase in duration, due to their ultra-relativistic nature.

Several schemes for the generation of attosecond electron bunches have been suggested. These schemes include inverse free-electron-laser interactions [89], the interaction of intense laser pulses with over-dense plasma [90], the acceleration of electrons with tailored laser pulses [91], the slicing of electron bunches with intense, ultrashort laser pulses [92], the interaction of laser pulses with nanofilms [93], wires, sub-micron droplets [94, 95] or with a plasma slice [96].

However, all these schemes are of limited attractiveness because they require either large accelerator structures [89] or rather exclusive (petawatt) laser systems to provide extreme intensities in the order of 10^{20}-10^{22} W/cm^2 (nor-

malized amplitude, a_0, in the range of 10-100) [90–94, 96]. A second limitation is that these schemes deliver bunches with only a few to a few tens of MeV's. Then, even with sub-pC charge [89, 91, 94], Coulomb repulsion severely limits the life time of the bunches (e.g., to tens of femtoseconds [93]) which hinders the application of these schemes.

In this chapter we present a new method of generating attosecond bunches. Our approach is based on much lower intensities ($a_0 \sim 1$), such as those readily available from terawatt laser systems. The space charge dependent life time of the attosecond bunches is increased by several orders of magnitude beyond the nanosecond range, because the bunches emerge with ultra-relativistic energies (GeV-level).

6.1   The working principle

To explain the working principle of our scheme, we recall that in all accelerators with a radial focusing field the individual electrons perform transverse oscillations about the axis of acceleration (z) known as betatron oscillations. The amplitude and phase of the betatron oscillation is determined by the transverse coordinate and momentum of injection, and the betatron oscillation frequency, ω_β, is determined by the ratio of the particle mass to the focusing field [97]. The betatron motion of an entire bunch injected on axis with a certain transverse bunch radius and momentum (emittance, divergence) is rather similar. The bunch radius oscillates between maximum and minimum values [98], which depend on the so-called mismatch between the initial bunch radius and emittance on the one hand and the focusing field and particle mass on the other hand. The betatron oscillation frequency of the bunch radius, ω_R, is twice the single-particle betatron frequency [98]

$$\omega_R = 2\omega_\beta = 2\omega_p\sqrt{\frac{f}{\gamma}}, \tag{6.1}$$

where ω_p, f and γ are, respectively, the plasma frequency, the focusing gradient and the relativistic factor.

In standard rf accelerators, the described betatron dynamics are relatively simple because, typically, the focusing field and thus the betatron frequency is approximately constant along the length of the bunch. Also, the focusing fields are relatively weak such that the betatron oscillation period is much longer than the bunch duration. As a result, if one considers the bunch as being divided-up into shorter sub-slices along the propagation direction, the radius of each sub-slice performs its own betatron oscillation in phase (synchronized) with that of the other slices.

In a laser wakefield accelerator the circumstances are dramatically different, due to the huge wakefields that vary strongly over the length of the bunch. Here, injected bunches inevitably become mismatched, because the transverse focusing wakefield increases strongly along the bunch. Also, the relativistic

mass increases rapidly during acceleration such that a single bunch comprises of a wide range of masses. Our investigations show that these effects, even in the extremely short bunches present in a laser wakefield accelerator (few femtosecond and micrometer), generate a strong longitudinal increase (chirp) of the betatron frequency along the bunch. As a result, the radius oscillations of sub-slices acquire a relative phase which grows into a transverse density modulation with attosecond peaks in the on-axis electron density.

6.2 The model

To illustrate the formation of such attosecond peaks, we model the dynamics of a femtosecond electron bunch that has been generated via a particular injection mechanism (for example, in the bubble regime [29] or from a plasma density gradient [33]) and where further acceleration occurs in a channel-guided laser wakefield accelerator. Here one could think of injecting an initial femtosecond bunch from a gas jet into a plasma channel [98] for further acceleration.

We start using a typical set of parameters that can be experimentally realized, i.e., a gamma factor of 100 (51 MeV), an energy spread of 3%, a full-width-at-half-maximum (FWHM) duration of 7.5 fs, a root-mean-square (rms) width of 1.3 μm in both transverse (x and y) directions, and normalized transverse emittances of 1.1 μm, all in a Gaussian distribution. The plasma channel for waveguiding and the laser parameters were chosen in such a way that the laser pulse dynamics are kept to a minimum, while the wakefield is strong enough to accelerate electrons to several hundred MeV. As the waveguide for acceleration we consider a 48 mm long plasma channel provided by a capillary discharge. The unperturbed electron density profile, $n_p(r)$ typically has a parabolic profile [47] for which we assume a radius, r_{ch}, of 61 μm and an on-axis electron concentration of 7×10^{17} cm^{-3} (plasma wavelength of 40 μm). The drive laser pulse is assumed to be Gaussian-shaped and linearly polarized, with a central wavelength of 0.8 μm, a duration of 35 fs (FWHM), and focused to a waist radius of 30 μm, i.e., to a peak intensity of 1.7×10^{18} W/cm^2 ($a_0 = 0.9$). The calculations are carried out using the fully relativistic particle code WAKE [62] which can calculate the cylindrically symmetric wakefield in a plasma channel including the laser pulse dynamics. The calculation of the electron trajectories has been carried out using our own three-dimensional particle tracer code. In this calculation the effect of beam loading is neglected, which we find justified for a bunch charge of several pC.

6.3 Attosecond bunch formation

In figure 6.1 the formation of attosecond bunches is illustrated, by showing the electron distribution at four subsequent times. The strength of the transverse focusing field is encoded in colors and increases in the direction of the acceleration $(+z)$. At $t = 0$ ps the bunch, still possessing its initial Gaussian shape, is

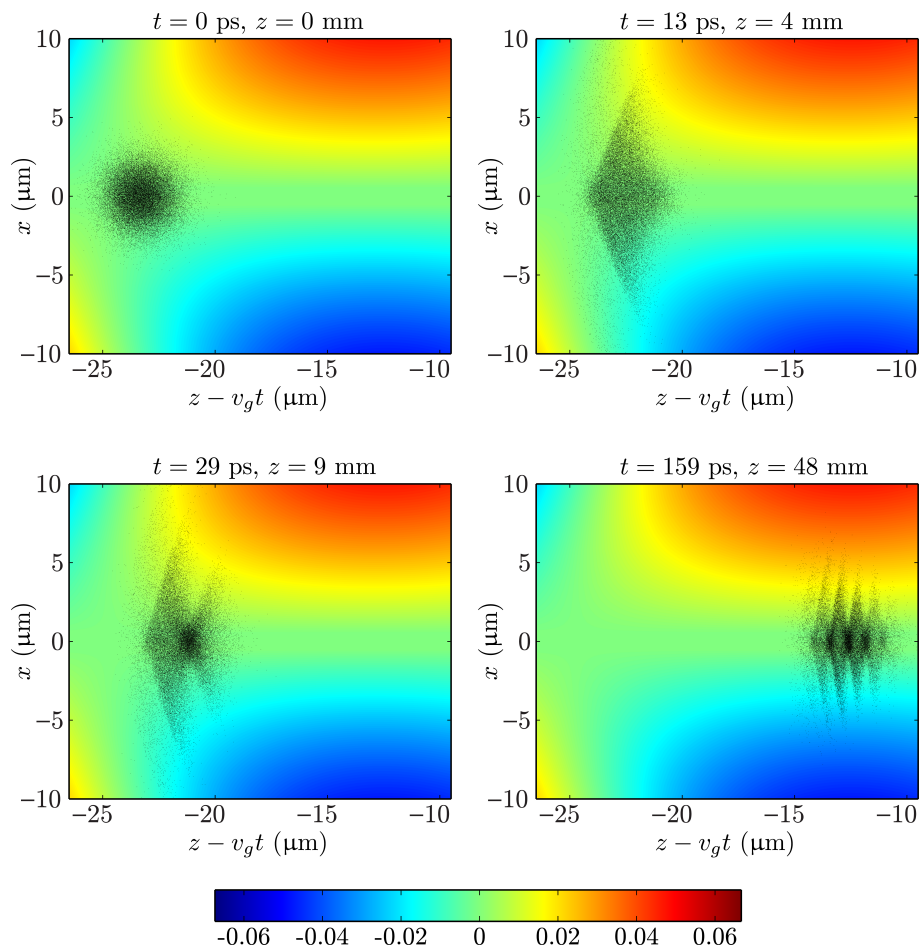Figure 6.1: Mechanism of attosecond bunch generation. The electron bunch is plotted on top of the transverse (focusing) component of the wakefield at 0, 4, 9 and 48 mm from the plasma channel entrance. Because the focusing field is stronger in the front of the bunch, the betatron oscillation of the radius is faster in the front than in the tail of the bunch (betatron chirp) which imposes a transverse modulation along the bunch.
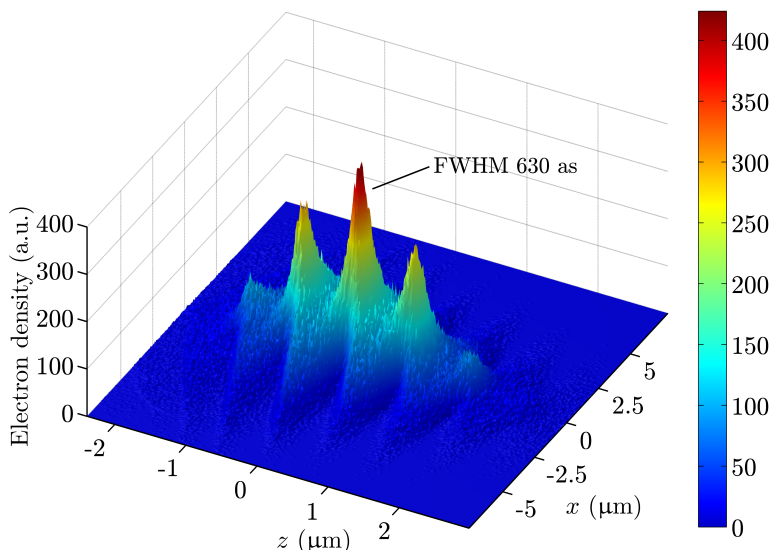
Figure 6.2: Electron density distribution of the accelerated femtosecond electron bunch (in arbitrary units) with attosecond bunching at the exit of a laser wakefield accelerator.

shown right after injection into the first acceleration phase in the focusing part of the wakefield. Thereafter, due to the mismatch with the focusing field, the transverse bunch radius starts to oscillate according to equation 6.1. However, later (at 13 ps) one can see that the radius in the front and at the tail of the bunch is smaller (higher density) than the radius at the center of the bunch (lower density). This is because f and γ vary strongly along the bunch such that the front has already performed an extra oscillation as compared to the tail. The modulation of the bunch radius progresses until, at the end of the accelerator ($t = 159$ ps, kinetic energy 655 MeV, energy spread 10%), several strong electron density peaks have formed. To display more details, figure 6.2 shows a separate plot of the electron density distribution for the last frame ($t = 159$ ps). As can be seen, several peaks of high electron density are formed on axis, approximately 800 nm apart, and each having a FWHM duration of approximately 630 as. We note that the initial bunch duration shows no influence on the duration of the sub-bunches but only on how many sub-bunches are formed.

In order to investigate of the described attosecond bunch formation is also present in other regimes of laser wakefield acceleration, we investigated the regime of external injection in front of the laser pulse [38], discussed in chapter
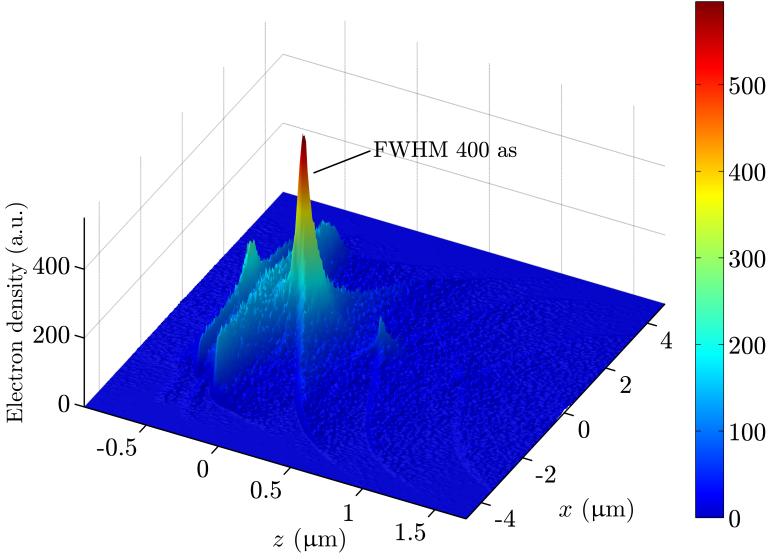
Figure 6.3: Electron density distribution of the accelerated femtosecond electron bunch (in arbitrary units) where the initial bunch is externally injected in front of the laser pulse.

5. Here, the injected electrons are overtaken by the laser pulse in the plasma and a considerable part of the bunch is trapped, compressed and accelerated in the first accelerating region behind the pulse [38]. The advantage of this scheme is that it allows the use of sub-picosecond electron bunches with an energy of several MeV such as those available from conventional rf accelerators. For our calculations we considered the initial bunches to have a duration of 250 fs FWHM, with an energy of 2.9 MeV and 0.7% energy spread, again, with a Gaussian shape. The electron bunch is focused into the plasma channel with an rms radius of 38 μm. The normalized emittance of the injected bunch is 0.6 μm in both transverse coordinates x and y. The plasma channel and the laser pulse parameters are taken as in the first example. Figure 6.3 shows the structure of the accelerated bunch immediately after leaving the plasma channel. There, the electrons are accelerated to an energy of 690 MeV with an energy spread of 5.5%. The rms radius of the accelerated femtosecond bunch is 1.4 μm and its transverse emittances are 2.4 μm. Again a fine-structure in the bunch, caused by the chirp of the betatron frequency, as described above, is present. However, due to the laser pulse dynamics, which plays an important role for the initial trapping of the bunch, a single and strong attosecond peak shows up in the electron density. The duration of the peak is approximately 400 as (FWHM).

In order to make use of the attosecond bunches at some distance behind the

plasma accelerator it is essential that the bunches maintain their attosecond duration after they have left the accelerator and travel, e.g., to a detector to measure the duration (such as via optical transition radiation [99]). To inspect the propagation of the bunches, we consider a slice of the bunch with a certain, fixed longitudinal position, z, relative to the center of the bunch. In the free propagation of the bunch through the vacuum after the acceleration, the radius of the slice (the local bunch radius), σ, evolves according to [98]

$$\sigma = \sigma_* \sqrt{1 + \frac{(z_{\mathrm{pr}} - z_*)^2}{Z_b^2}}, \tag{6.2}$$

where $Z_b = \gamma \sigma_*^2 / \varepsilon_n$ is the characteristic distance over which the radius grows and where z_{pr} is the propagation distance. The characteristic distance, Z_b, which is comparable to the Rayleigh length for a focused optical beam, depends on the spot size in the focus, σ_*, also called waist size, the relativistic factor, γ, and the normalized emittance, ε_n. The waist size of the considered slice is given by $\sigma_*^2 = \varepsilon_n^2 / \gamma^2 h$, where $h = \varepsilon_n^2 / \gamma^2 \sigma_p^2 + \sigma_p'^2$ with σ_p and $\sigma_p' = d\sigma_p / dz$ the bunch radius and the divergence at the exit of the plasma channel. Note that, when the bunch leaves the wakefield, the divergence can either be positive or negative, and in the latter case the slice will become focused at a distance behind the channel given by $z_* = \sigma_p \sigma_p' / h$.

The local radius in the structured bunch coming from the wakefield accelerator can be approximated by [98]

$$\sigma_p^2 = \sigma_0^2 + \sigma_1^2 \sin\left(\frac{2\pi z}{\lambda_b} + C\right), \tag{6.3}$$

where σ_0, σ_1 and C are constants and λ_b is the distance between neighboring sub-bunches. With the local bunch radius and its divergence at the exit of the plasma given by expression 6.3, equation 6.2 can be applied to predict the radius of each slice in vacuum. Simple analysis reveals that the Rayleigh length, Z_b, changes monotonically throughout the femtosecond bunch having minimum (maximum) for minimum (maximum) σ_p. This means that the parts of the bunch with smaller radii will diverge more strongly.

From this it can be concluded that there is a transition behind the accelerator where the structure of figure 6.2 is reversed, meaning that the parts with largest radii become the parts with smallest radii and vice versa. Another way to look at this is to consider the transverse momentum of the electrons when they undergo a betatron oscillation, which has a maximum for the parts with minimum radius and vice versa. Our simulations show that, typically, the reversal occurs within the first few millimeters of propagation behind the plasma channel. After this process the attosecond structure remains stable during further propagation in vacuum.

Using the data from figure 6.2 and the GPT code [87], we calculated the electron density after 10 cm propagation through vacuum behind the accelerator. It can be seen (figure 6.4) that the rms bunch radius has grown to 145 μm.
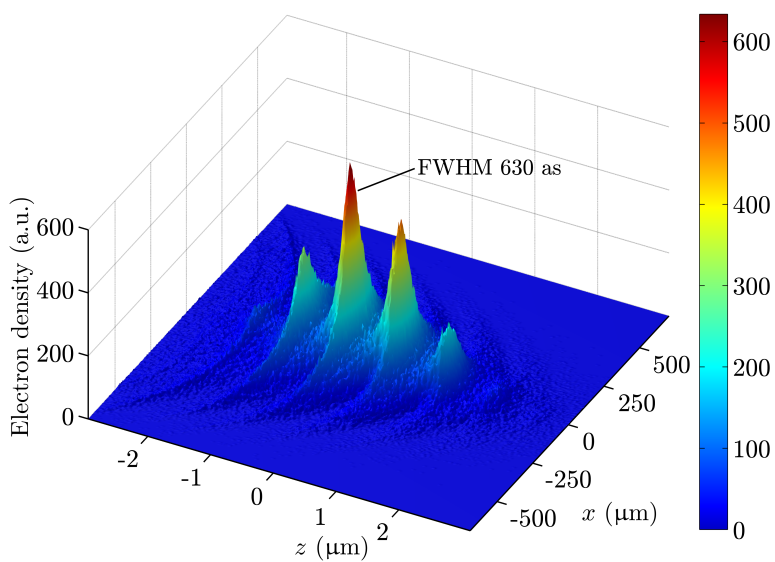
Figure 6.4: Electron density distribution of the accelerated femtosecond electron bunch (in arbitrary units), presented in Fig. 6.2, after propagating 10 cm in vacuum.
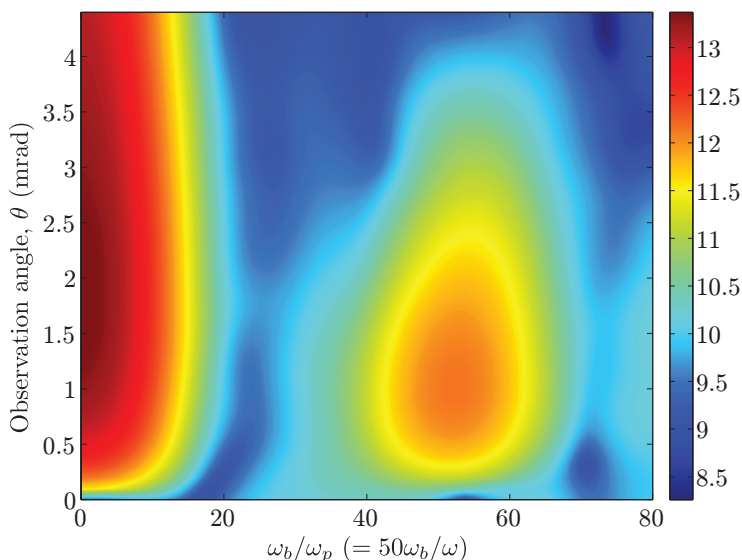
Figure 6.5: Coherent betatron radiation emitted by an electron bunch in a laser wakefield accelerator. The spectral and angular distribution of the normalized radiation energy is given on a logarithmic scale. Here ω is the laser frequency.

But, the main observation is that the attosecond structure is maintained, with the difference being that the maxima and minima of the electron density are now reversed. Our simulations show that for up to several tens of pC, space charge can be neglected. After the reversal the attosecond bunches remained stable during further propagation in vacuum over many tens of centimeters.

6.4 Betatron radiation

The described examples comprising of bunch injection behind and in front of the laser pulse, and our calculations over wider parameter ranges (see below) indicate that the described attosecond dynamics are a rather general and intrinsic feature of laser wakefield accelerators. However, the formation of such attosecond bunches is difficult to detect and thus can easily go unnoticed. A widely used technique for measuring the temporal structure of an electron bunch, that can be used here, is coherent transition radiation [99]. However, we will show that the attosecond bunches may also be identified via a non-destructive way by measuring their optical signature, i.e., by spectrally analyzing the coherent betatron radiation emitted during acceleration and formation. This radiation is confined to small emission angles, in the order of $1/\gamma_m$, where γ_m is the average relativistic factor of the electrons at the exit of the accelerator [100].

The results of a calculated radiation pattern, for the bunches presented in

figure 6.2, is shown in figure 6.5, which depicts the angular and spectral distri-
bution of the radiated energy normalized to $e^2/4\pi^2 c$ (here e is the elementary
charge and c is the speed of light) on a logarithmic scale (10^4 particles were
used for this particular calculation). The strong radiation at low frequencies
seen in figure 6.5 is the coherent betatron radiation from a femtosecond electron
bunch [100]. This radiation scales approximately as $\exp\left[-\left(\omega_b\sigma_b/c\right)^2\right]$ (here ω_b
is the radiated frequency and σ_b the rms bunch length). This agrees with the
form factor formalism [100], according to which the energy radiated by a bunch
is proportional to $N_e\left[1+(N_e-1)f\right]$, where N_e is the number of particles in
the bunch and f is the form factor. Note, however, that the radiation at fre-
quencies lower than ω_p will be absorbed in the plasma and cannot be observed
outside the plasma channel. Of more interest is the weaker emission occurring
at higher frequencies (see figure 6.5), because we found from our calculations
that this can be attributed to the attosecond structure of the bunch. To verify
this, we have calculated analytically the form-factor of the attosecond struc-
tured bunch, modeling it as a Gaussian bunch with a local radius that satisfies
expression 6.3. From this we have found that the emitted radiation comprises
of a second peak at the frequency

$$\omega_* \approx \frac{c\pi}{\lambda_b}\left(1+\sqrt{1+\frac{2\lambda_b^2}{\pi^2\sigma_b^2}}\right). \qquad (6.4)$$

If we apply this to the electron bunch depicted in figure 6.2, according to
equation 6.4, there should be a peak in the optical spectrum at a wavelength
of 0.77 μm, which corresponds to $\omega_* \approx 52\omega_p$. This agrees very well with the
value predicted by the numerical calculation (see figure 6.5). Detection of this
radiation can be difficult when the spectra of the betatron radiation and the
drive laser pulse overlap. However, one can look at the betatron radiation at a
different polarization from that of the drive laser.

6.5   Parameter study

In the remaining part we show that the described attosecond dynamics are
not an incidental effect but a general and intrinsic feature of laser wakefield
accelerators that occurs over a wide range of parameters. A different type of
sub-bunching has been observed and described by Glinec *et al.* [99] and Nemeth
et al. [101]. However, that scheme generates bunches with only a fixed period
(2.3 fs, corresponding to 700 nm) imposed by the spatial periodicity of the laser
field. In our scheme the bunch duration and bunch separation is scalable with
external parameters.

   To investigate such scaling, we started with a variation of the length of
the plasma channel with all other parameters chosen as above. The result
displayed in Fig. 6.6a shows that a longer channel provides shorter bunches,
with durations saturating to a value of about 600 as. It can be seen that the
bunches are mainly formed in the first part of the channel, where the gradient

of the focusing field varies the most and where the accelerating field is the largest.

Next we varied the peak intensity of the laser pulse. The result displayed in Fig. 6.6b shows that a higher intensity provides shorter bunches, towards a saturation of about 600 as for $a_0 > 0.9$. This scaling can be understood because a higher laser intensity induces a stronger wakefield and transverse focusing gradient along the bunch which imposes a wider chirp of the betatron frequency.

Similarly, we found that reducing the initial energy shortens the bunches as is displayed in Fig. 6.6c, because a lower initial Lorentz factor gives a wider betatron chirp.

The bunch duration can also be reduced by lowering the relative energy spread of the injected bunch, which is shown in Fig. 6.6d. It can be seen that, to obtain the smallest duration the energy spread should be as low as possible. An explanation for this is that the energy spread in the bunch causes a decoherence for a given longitudinal slice of the bunch. When the broadening of the frequency due to this energy spread becomes comparable to the longitudinal chirp of the betatron frequency, the duration of the sub-bunches will be effected.

The calculated dependence of the bunch on the initial emittance of the injected electrons is shown in Fig. 6.6e. An intermediate maximum duration is seen at around 0.4 μm emittance. This can be explained as some initial matching of the bunch to the focusing field which reduces the contrast of the on-axis electron density modulation. From there the bunches can be shortened with lower or higher emittance, but the shortest bunches are obtained with lower emittance.

Finally, the bunch duration can be reduced by injecting bunches with smaller radii, which is shown in Fig. 6.6f. However when the radius becomes smaller than 1 μm, some electrons get sufficient transverse momentum to escape the wakefield [98].

A further shortening of the bunches seems possible with a combined variation of parameters. The systematic exploration of this would require numerous additional calculations. As a first example of optimization, we obtained bunches as short as 100 as with an increased intensity ($a_0 = 1.5$), a low injection energy (10 MeV), close to zero emittance (< 0.05 μm) and a low energy spread ($< 0.5\%$).

6.6   Conclusion

In conclusion we note that the described attosecond bunch generation appears to be a general property of laser wakefield accelerators as the sub-bunching appears over a wide range of parameters and it is even independent of the selected injection mechanism. For example we have shown the generation of attosecond bunches when the electron bunch is injected behind the laser pulse in a second stage and also when injecting in front of the laser pulse. The independence from the injection scheme is further underlined by our observation of
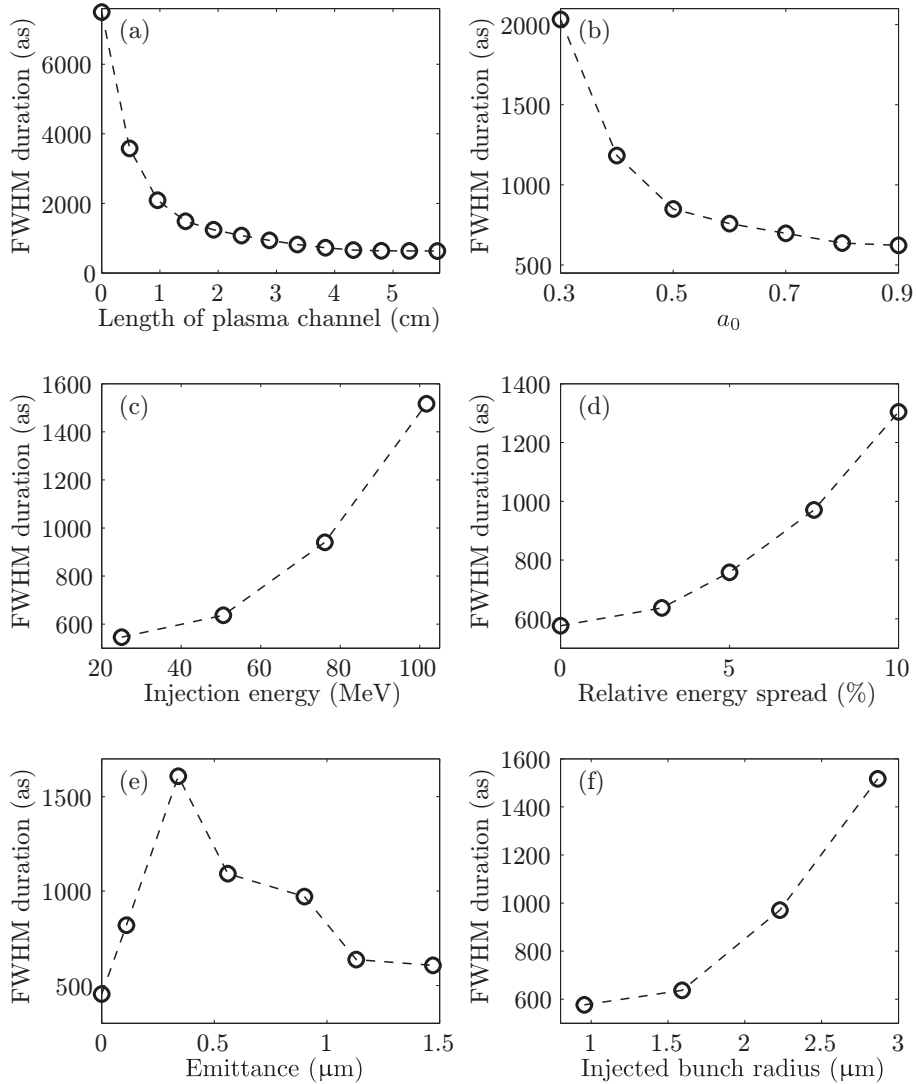
Figure 6.6: Duration of the sub-bunches as a function of the plasma channel length (a), the normalized amplitude, a_0, of the laser pulse (b), the initial energy (c), the initial energy spread (d), the initial normalized emittance (e), and the initial radius (f) of the injected bunch.

attosecond bunches for injection at an angle, the mechanism that we detailed in chapter 4. The described mechanism of attosecond bunch generation via a longitudinal chirp of the betatron frequency appears to be an intrinsic feature of laser wakefield accelerators and thus may well be present and observable in currently performed experiments.

7
Conclusions and discussion

Over the past few years, as the physics of the acceleration process has become better understood, laser wakefield accelerators have made tremendous progress. The construction of tabletop accelerators using plasma acceleration is now closer than ever. Some of the research is already heading for use in applications, such as the generation of X-rays for medical, biological and material science, which is currently based on large facilities, synchrotrons, and linear accelerators. The X-rays are generated by sending accelerated electron bunches with high energy and peak current through magnetic undulators [102–105]. The electron bunches produced by a laser wakefield accelerator seem to be ideal for the generation of X-rays because they possess an extremely short duration of less than 10 fs and, thereby, provide high peak currents. If the conventional accelerator could be replaced by a table-top plasma accelerator, these sources would become available to smaller institutions, such as universities or local research institutes. This could have great impact on the fundamental research and applications that use generated X-ray radiation.

However, such applications require an extremely stable and reliable output from the wakefield accelerator. Presently, experimental investigations of laser wakefield acceleration have focused primarily on internal injection, which requires to operate in the strongly nonlinear regime. This renders the injection and acceleration sensitive to fluctuations or drift of the experimental parameters and makes it difficult to control the electron beam properties and attain stable and reproducible electron bunches. Currently the main challenge is to explore approaches that stabilize the performance of the accelerator. In this thesis we investigated the use of external injection of an electron bunch from a conventional radio-frequency (rf) accelerator. This promises better stability

because the injection of electrons and the excitation of the wakefield can be fully separated. In this case we expect to get full control over the timing and spatial alignment of the injection and over the scaling of the output energy. Furthermore, one would be able to work in the linear or slightly nonlinear regime, with moderate laser intensities and relatively low plasma density, which is the regime of minimum sensitivity to fluctuations of the experimental parameters.

An issue that arises is the need for plasma channels which optically guide the drive laser pulse to increase the interaction length. External injection works best in a relatively low plasma density ($\sim 10^{18}$ cm^{-3}), however, in this case the electrons reach their maximum energy only after a large acceleration distance, the dephasing length, of several centimeters. When the laser pulse is not guided, diffraction of the pulse will limit the acceleration length to a few millimeters making it impossible to obtain high-energy electrons. Thus external injection schemes require a plasma channel to get optimal acceleration.

In this thesis we have studied two known schemes and one novel scheme for the external injection of electrons in a laser wakefield and acceleration in waveguiding plasma channels. Our results show that external injection in a laser wakefield accelerator can deliver highly relativistic electron bunches with an ultrashort duration of a few femtoseconds. These injection schemes defy expectation as they do not require that ultrashort bunches are already prepared before injection and injected with ultra-precise (femtosecond) timing, a technique that lies beyond current technology. In the schemes that we investigated it is sufficient to inject much longer bunches with a relaxed timing on the picosecond scale. Thereby a corresponding demonstration experiment seems feasible with current technology, where sub-picosecond electron bunches can be delivered by standard rf accelerators. External injection is very flexible and works over a relatively broad range of parameters. The three investigated schemes can be distinguished via the injection position of the electron bunch in relation to the laser pulse.

The first scheme, which was discussed in chapter 3, is the injection of an electron bunch behind the laser pulse directly into the plasma wave. We showed that a long electron bunch, injected behind the laser pulse and thus distributed over all the phases of the wakefield, will be sliced into a train of several separate bunches separated by the plasma wavelength. The reason for such slicing is that only the electrons which arrive in the proper phase are trapped and accelerated. By choosing the initial energy of the electron bunch to be close to the minimum injection energy, a compromise between reasonable collection efficiency and low energy spread electron bunches can be made.

However, when carefully looking at this scheme, we discovered two problems that had been overlooked in previous investigations. These problems were thoroughly studied in this thesis. First, before the injected electron bunch reaches the plasma, and is still traveling through vacuum, it can be scattered by the ponderomotive force of the laser pulse. This scattering in front of the plasma channel can not actually be avoided in this scheme because, in order to position the bunch behind the laser pulse before it enters the plasma

channel, the laser pulse has to overtake the electron bunch in the vacuum. We showed that under certain conditions the undesired scattering of the injected electron bunch can be quite strong, particularly for high laser intensities and low injection energies. Second, the injected bunch can be scattered in the region where the wakefield is spatially inhomogeneous at the entrance of the plasma channel. The incident drive laser pulse excites a wakefield while the plasma density increases, this lets the plasma wavelength decrease continuously from infinite towards its final, regular value which is constant throughout the rest of the channel. Correspondingly the injected bunch experiences a wakefield changing from accelerating to decelerating, from focusing to defocusing, or vice versa, and can be scattered before reaching the regular wakefield. Again, this effect is strongest for high laser intensities and low injection energies.

In spite of these perturbing effects, injection behind the laser pulse still offers good performance for the injection of a high energy bunch into a linear wakefield, where a relatively low laser intensity is used. While the final energy of the accelerated bunch will not be very high (~ 100 MeV), the use of a linear wakefield means that the stability and reproducibility of the laser wakefield accelerator can be very good.

The second external injection scheme, introduced in chapter 4, is a novel scheme that we proposed to circumvent the problems with ponderomotive scattering and the vacuum-plasma transition. The idea is still to inject behind the laser pulse, but at a small angle with regard to the laser and wakefield propagation axis. When injecting at an angle, such that the bunch experiences the wakefield only behind the vacuum-plasma transition, both the ponderomotive scattering and the scattering in the inhomogeneous wakefield at the entrance of the plasma channel are avoided. The electrons are, in a manner similar to standard (coaxial) injection behind the pulse, trapped and accelerated in a train of bunches separated by the plasma wavelength. However, this scheme has more advantages. One can, for example, inject more charge into the wakefield by using electron bunches of a wider transverse size. This is not possible with standard injection behind the pulse, because electrons that are far away from the wakefield axis can not be trapped. Compared to standard injection one has to work in the slightly nonlinear regime and inject with a higher energy in order to trap electrons. In this regime at high intensity, due to nonlinear optical interaction, the laser pulse can undergo significant spatial-temporal modifications called laser pulse dynamics. This is why we have also investigated the effect of the laser pulse dynamics on injection at an angle. It turns out that the dynamics of the laser pulse can increase the final energy spread of the accelerated bunches. However, this effect can be minimized by injecting the electron bunch at a specific position in the channel where the variations of the wakefield is lowest. Also the duration of the injected bunch only has a small effect on the energy spread. A longer bunch generates more accelerated bunches, separated by one plasma wavelength. Increasing the angle results in a lower energy spread, but at the cost of a lower collection efficiency.

The third injection scheme we discussed, is the injection in front of the laser

Table 7.1: Comparison of the three external injection schemes

	Behind	At an angle	In front
Number of accelerated bunches	σ_b/λ_p	σ_b/λ_p	1
Required wakefield	linear	nonlinear	nonlinear
Typical acquired energy	~ 100 MeV	~ 1 GeV	~ 1 GeV
Trapping distance	very short	d/α	$2\gamma_0^2 L_0$
Maximum energy and minimum energy spread coincide	no	yes	yes

pulse. For this scheme an electron bunch with a relatively low energy (a few MeV) is injected just ahead of the laser pulse into the plasma channel. Inside the channel, the laser pulse overtakes the electron bunch, because the velocity of the pulse is higher than the velocity of the bunch. Some of the injected electrons are trapped and strongly compressed in the first accelerating slope of the wakefield, immediately behind the laser pulse. Thus, in this case, a single electron bunch is formed in the wakefield. The dynamics of the electrons for this scheme are similar to the dynamics for injection at an angle. For both schemes the electrons start in a zero wakefield and gradually enter the wakefield.

At the University of Twente, we are currently preparing an experiment to demonstrate the injection in front of the laser pulse. In chapter 5, we analyzed the experimental design and predict that high quality electron bunches, with an energy of 0.7 GeV and an energy spread of about 1%, can be obtained.

Each of the described schemes has its own specific properties and requirements. Depending on the application, either one of these schemes can be chosen via only slight experimental modification regarding the injection timing and angle. Table 7.1 provides a direct comparison of the schemes. For injection behind the pulse and at an angle, the number of bunches formed and accelerated depends on the bunch duration and plasma wavelength. For injection in front a single bunch is always formed and accelerated. For injection behind one has to work in a linear wakefield, because otherwise ponderomotive scattering and the effect of the vacuum-plasma transition would be too strong and scatter the bunch. For injection at an angle and in front, a slightly nonlinear wakefield is required to trap electrons with a typical injection energy. Due to its limitation to the linear wakefield regime, injection behind has only a moderate energy gain of around 100 MeV, while the other schemes, due to their higher wakefield acceptability, can deliver energies of up to 1 GeV. The trapping distance for injection in front depends on the bunch duration, which should be as short as possible to obtain high quality bunches. The trapping distance for injection behind and at an angle does not depend on the bunch duration and is less important for the quality of the final bunches. However, the bunch duration determines how many bunches are formed. For injection in front and at an

angle, the maximum energy coincides approximately to the minimum energy spread, while this is generally not the case for injection behind.

External injection schemes can be controlled via several parameters. One can control the process by modifying the energy, charge and size of the injected electron bunch, the intensity and spotsize of the laser pulse or the length, density and radius of the plasma channel. The injection at an angle offers the largest amount of control parameters and thus the widest flexibility, because here the injection angle is a control parameter as well. In all three injection schemes, the energy spread can be controlled with the injection energy. Specifically, a lower injection energy yields a lower energy spread, but at a lower collection efficiency. In general, one has to find a balance between trapped charge, energy spread, and energy, depending on the desired application. The acceleration length for a fixed plasma channel length can be controlled (e.g., to maximize the energy or to minimize the energy spread) for injection in front and at an angle by tuning the injection position via the timing of the injection with regard to the drive laser pulse.

The current demonstrations of laser wakefield accelerators, also in theoretical investigations, in general, generate electron bunches with a duration in the order of several femtoseconds. However, as is described in chapter 6, we predict that laser wakefield accelerators can generate even shorter electron bunches with durations in the range of several hundred attoseconds. We have shown that such bunches are not only formed under very special conditions, but are formed in different regimes of laser wakefield acceleration via two examples, for a staged wakefield accelerator and for a single stage with external bunch injection in front of the laser pulse. From the investigation over a wider range of typical parameters and also for injection at an angle, we conclude that the observed formation of attosecond bunches is an intrinsic, general and important feature of laser wakefield accelerators. We have shown that the generated bunches stably propagate through vacuum, maintaining their attosecond structure over tens of centimeters, which is of high interest for applications.

In conclusion, we have shown that the external injection of an electron bunch from a conventional rf accelerator into a laser wakefield can provide femto- and even attosecond electron bunches of a high quality, comparable to current wakefield accelerators based on internal injection such as the bubble and colliding pulse regime. However, external injection promises a much better control over the acceleration process, because the application of lower laser intensities and use of lower plasma densities to keep the excited wakefield in the linear or slightly nonlinear regime is sufficient. A second fundamental advantage of external injection is the number of parameters that can be varied to optimize the properties of the accelerated bunches. A suitable external injection scheme can be chosen depending on the applications. The research in this thesis can offer a valuable aid in assisting laser wakefield acceleration live up to its huge potential.

A
Solution for a linear wakefield

In order to solve the equations for the three-dimensional linear wakefield one has to solve the general equation

$$\frac{\partial^2 \mathcal{E}}{\partial \xi^2} + N\mathcal{E} = N\mathcal{F}_p. \tag{A.1}$$

To solve this equation one first takes the Fourier transforms of $\mathcal{E}$ and $\mathcal{F}_p$, $\hat{\mathcal{E}}$ and $\hat{\mathcal{F}}_p$

$$\hat{\mathcal{E}} = \frac{1}{\sqrt{2\pi}} \int_{-\infty}^{\infty} \mathcal{E}(\xi) \exp{(i\lambda\xi)} d\xi, \tag{A.2}$$

$$\mathcal{E} = \frac{1}{\sqrt{2\pi}} \int_{-\infty}^{\infty} \hat{\mathcal{E}}(\lambda) \exp{(-i\lambda\xi)} d\lambda, \tag{A.3}$$

$$\hat{\mathcal{F}}_p = \frac{1}{\sqrt{2\pi}} \int_{-\infty}^{\infty} \mathcal{F}_p(\xi) \exp{(i\lambda\xi)} d\xi, \tag{A.4}$$

$$\mathcal{F}_p = \frac{1}{\sqrt{2\pi}} \int_{-\infty}^{\infty} \hat{\mathcal{F}}_p(\lambda) \exp{(-i\lambda\xi)} d\lambda, \tag{A.5}$$

for which equation A.1 gives

$$-\lambda^2 \hat{\mathcal{E}}(\lambda) + N\hat{\mathcal{E}}(\lambda) = N\hat{\mathcal{F}}_p. \tag{A.6}$$

The solution for $\hat{\mathcal{E}}$ of this equation is

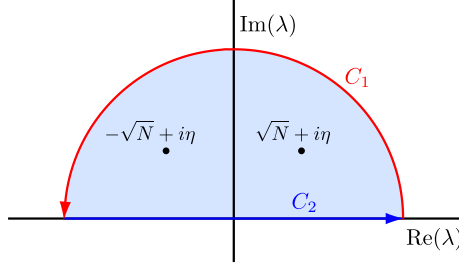$$\hat{\mathcal{E}}(\lambda) = \frac{N\hat{\mathcal{F}}_p}{N - \lambda^2}. \tag{A.7}$$

Figure A.1: The path C is a concatenation of paths C_1 and C_2.

One can now take the inverse tranform to get

$$
\begin{aligned}
\mathcal{E}(\xi) &= \frac{1}{\sqrt{2\pi}} \int_{-\infty}^{\infty} \frac{N\hat{\mathcal{F}}_p(\lambda)}{N - \lambda^2} \exp\left(-i\lambda\xi\right) d\lambda, \\
&= \frac{1}{2\pi} \int_{-\infty}^{\infty} \int_{-\infty}^{\infty} \frac{N\mathcal{F}_p(\xi')}{N - \lambda^2} \exp\left[i\lambda\left(\xi' - \xi\right)\right] d\lambda d\xi'. \qquad \text{(A.8)}
\end{aligned}
$$

The first integral

$$
\int_{-\infty}^{\infty} f(\lambda) d\lambda = \int_{-\infty}^{\infty} \frac{1}{N - \lambda^2} \exp\left[i\lambda\left(\xi' - \xi\right)\right] d\lambda, \qquad \text{(A.9)}
$$

can be solved using contour integrals and Cauchy's residue theorem. The function has two poles at $\lambda = -\sqrt{N}$ and $\lambda = \sqrt{N}$. Consider a closed contour C, which is a semicircle in the upper plane and a concatenation of two paths C_1 and C_2 (see figure A.1). First move the poles at $\lambda = \pm\sqrt{N}$ slightly in the upperplane. In this case their residues do not contribute at "negative times". This means one has to solve

$$
\int_{-\infty}^{\infty} \frac{1}{N - (\lambda - i\eta)^2} \exp\left[i\lambda\left(\xi' - \xi\right)\right] d\lambda, \qquad \text{(A.10)}
$$

with poles at $\lambda = \pm\sqrt{N} + i\eta$. The residues of the function at $\lambda = \pm\sqrt{N} + i\eta$ are

$$
\begin{aligned}
\text{Res}\left\{f(\lambda), \lambda = \sqrt{N} + i\eta\right\} &= -\frac{1}{2\sqrt{N}} \exp\left[i(\sqrt{N} + i\eta)(\xi' - \xi)\right], \\
\text{Res}\left\{f(\lambda), \lambda = -\sqrt{N} + i\eta\right\} &= \frac{1}{2\sqrt{N}} \exp\left[i(-\sqrt{N} + i\eta)(\xi' - \xi)\right].
\end{aligned}
$$

When one takes the contour as shown, Jordan's lemma tells that the factor $\exp\left[i\lambda\left(\xi' - \xi\right)\right]$ will make an integral over C_1 in the upper plane zero if $\xi' > \xi$, while for $\xi' < \xi$ an integral over C_1 in the lower plane will give zero. The

residue theorem together with Jordan's lemma tells that

$$
\begin{aligned}
\oint_C f(\lambda)d\lambda &= \int_{C_1} f(\lambda)d\lambda + \int_{C_2} f(\lambda)d\lambda \\
&= \int_{C_2} f(\lambda)d\lambda = 2\pi i \sum \text{Res.}
\end{aligned} \tag{A.11}
$$

This means that

$$
\int_{-\infty}^{\infty} \frac{1}{N - (\lambda - i\eta)^2} \exp\left[i\lambda\left(\xi' - \xi\right)\right]d\lambda =
$$

$$
\frac{\pi i}{\sqrt{N}} \exp\left[\eta\left(\xi - \xi'\right)\right]\left(\exp\left[i\sqrt{N}\left(\xi - \xi'\right)\right] - \exp\left[-i\sqrt{N}\left(\xi - \xi'\right)\right]\right) =
$$

$$
-\frac{2\pi}{\sqrt{N}} \exp\left[\eta\left(\xi - \xi'\right)\right]\sin\left[\sqrt{N}\left(\xi - \xi'\right)\right]. \tag{A.12}
$$

By taking the limit of η to zero one arrives at the final solution for $\xi' > \xi$

$$
\int_{-\infty}^{\infty} \frac{1}{N - \lambda^2} \exp\left[i\lambda\left(\xi' - \xi\right)\right]d\lambda = -\frac{2\pi}{\sqrt{N}} \sin\left[\sqrt{N}\left(\xi - \xi'\right)\right], \tag{A.13}
$$

and for $\xi' < \xi$ the solution is zero. Hence,

$$
\mathcal{E}(\xi, \rho) = -\int_{\xi}^{\infty} \sqrt{N}\mathcal{F}_p(\xi', \rho)\sin\left[\sqrt{N}\left(\xi - \xi'\right)\right]d\xi'. \tag{A.14}
$$

B
Electron beams

B.1 Definition of root-mean-square values

Quantities like energy spread, bunch duration, bunch width, etc. are in this thesis expressed with the standard deviation. The standard deviation is the root-mean-square (rms) deviation of its value from the mean. It is calculated with the following formula

$$\text{std}(x) = \sqrt{\overline{x^2} - \overline{x}^2} = \sqrt{\frac{1}{n}\sum_{i=1}^{n} x^2 - \frac{1}{n^2}\left(\sum_{i=1}^{n} x\right)^2},$$

where x denotes any of the previously named quantities, n is the number of electrons in a bunch and i is the number of the ith particle.

B.2 Transverse emittance

Emittance is a quantity that describes the parallelism of an electron beam. It is a conserved quantity in an ideal focusing system and therefore can be used to compare the quality of electron beams. Emittance is based on the effective six-dimensional volume occupied in phase space by the electron distribution. A high quality electron beam with high focusability will occupy a small area in phase space. For the calculation of the emittance in our computer codes, we use the normalized rms (root-mean-square) emittance defined as [106]

$$\epsilon_{n,\text{rms}} = \frac{1}{m_e c}\sqrt{\langle x^2\rangle\langle p_x^2\rangle - \langle xp_x\rangle^2}, \tag{B.1}$$

where $\langle\rangle$ defines the second central moment of the electron distribution

$$\langle x^2 \rangle = \frac{1}{n} \sum_{i=1}^{n} x^2 - \frac{1}{n^2} \left(\sum_{i=1}^{n} x \right)^2,$$

$$\langle p_x^2 \rangle = \frac{1}{n} \sum_{i=1}^{n} p_x^2 - \frac{1}{n^2} \left(\sum_{i=1}^{n} p_x \right)^2,$$

$$\langle x p_x \rangle = \frac{1}{n} \sum_{i=1}^{n} x p_x - \frac{1}{n^2} \sum_{i=1}^{n} x \sum_{i=1}^{n} p_x. \tag{B.2}$$

Bibliography

[1] T. Tajima and J. M. Dawson. Laser electron accelerator. *Phys. Rev. Lett.*, 43(4):267–270, 1979.

[2] E. Esarey, P. Sprangle, J. Krall, and A. Ting. Overview of plasma-based accelerator concepts. *IEEE Trans. Plasma Sci.*, 24(2):252–288, 1996.

[3] E. Esarey, C. B. Schroeder, and W. P. Leemans. Physics of laser-driven plasma-based electron accelerators. *Rev. Mod. Phys.*, 81(3):1229–1285, 2009.

[4] C. Joshi. The development of laser- and beam-driven plasma accelerators as an experimental field. *Phys. Plasmas*, 14(5):055501, 2007.

[5] P. Chen, J. M. Dawson, R. W. Huff, and T. Katsouleas. Acceleration of electrons by the interaction of a bunched electron beam with a plasma. *Phys. Rev. Lett.*, 54(7):693–696, 1985.

[6] J. B. Rosenzweig, D. B. Cline, B. Cole, H. Figueroa, W. Gai, R. Konecny, J. Norem, P. Schoessow, and J. Simpson. Experimental observation of plasma wake-field acceleration. *Phys. Rev. Lett.*, 61(1):98, 1988.

[7] D Strickland and G Mourou. Compression of amplified chirped optical pulses. *Opt. Comm.*, 56(3):219–221, 1985.

[8] P. Maine, D. Strickland, P. Bado, M. Pessot, and G. Mourou. Generation of ultrahigh peak power pulses by chirped pulse amplification. *IEEE J. Quantum Electron.*, 24(2):398 –403, 1988.

[9] K. Nakajima, T. Kawakubo, H. Nakanishi, A. Ogata, Y. Kato, Y. Kitagawa, R. Kodama, K. Mima, H. Shiraga, K. Suzuki, T. Zhang, Y. Sakawa, T. Shoji, Y. Nishida, N. Yugami, M. Downer, D. Fisher, B. Newberger, and T. Tajima. A proof-of-principle experiment of laser wakefield acceleration. *Phys. Scr.*, T52:61, 1994.

[10] D. Umstadter, S. Y. Chen, A. Maksimchuk, G. Mourou, and R. Wagner. Nonlinear optics in relativistic plasmas and laser wake field acceleration of electrons. *Science*, 273(5274):472–475, 1996.

[11] A. Modena, Z. Najmudin, A. E. Dangor, C. E. Clayton, K. A. Marsh, C. Joshi, V. Malka, C. B. Darrow, C. Danson, D. Neely, and F. N. Walsh.

Electron acceleration from the breaking of relativistic plasma-waves. *Nature*, 377(6550):606–608, 1995.

[12] K. Nakajima, D. Fisher, T. Kawakubo, H. Nakanishi, A. Ogata, Y. Kato, Y. Kitagawa, R. Kodama, K. Mima, H. Shiraga, K. Suzuki, K. Yamakawa, T. Zhang, Y. Sakawa, T. Shoji, Y. Nishida, N. Yugami, M. Downer, and T. Tajima. Observation of ultrahigh gradient electron acceleration by a self-modulated intense short laser pulse. *Phys. Rev. Lett.*, 74(22):4428–4431, 1995.

[13] C. A. Coverdale, C. B. Darrow, C. D. Decker, W. B. Mori, K-C. Tzeng, K. A. Marsh, C. E. Clayton, and C. Joshi. Propagation of intense sub-picosecond laser pulses through underdense plasmas. *Phys. Rev. Lett.*, 74(23):4659–4662, 1995.

[14] D. Gordon, K. C. Tzeng, C. E. Clayton, A. E. Dangor, V. Malka, K. A. Marsh, A. Modena, W. B. Mori, P. Muggli, Z. Najmudin, D. Neely, C. Danson, and C. Joshi. Observation of electron energies beyond the linear dephasing limit from a laser-excited relativistic plasma wave. *Phys. Rev. Lett.*, 80(10):2133–2136, 1998.

[15] V. Malka, S. Fritzler, E. Lefebvre, M.-M. Aleonard, F. Burgy, J.-P. Chambaret, J.-F. Chemin, K. Krushelnick, G. Malka, S. P. D. Mangles, Z. Najmudin, M. Pittman, J.-P. Rousseau, J.-N. Scheurer, B. Walton, and A. E. Dangor. Electron acceleration by a wake field forced by an intense ultrashort laser pulse. *Science*, 298(5598):1596–1600, 2002.

[16] C. I. Moore, A. Ting, K. Krushelnick, E. Esarey, R. F. Hubbard, B. Hafizi, H. R. Burris, C. Manka, and P. Sprangle. Electron trapping in self-modulated laser wakefields by raman backscatter. *Phys. Rev. Lett.*, 79(20):3909–3912, 1997.

[17] W. P. Leemans, P. Catravas, E. Esarey, C. G. R. Geddes, C. Toth, R. Trines, C. B. Schroeder, B. A. Shadwick, J. van Tilborg, and J. Faure. Electron-yield enhancement in a laser-wakefield accelerator driven by asymmetric laser pulses. *Phys. Rev. Lett.*, 89(17):174802, 2002.

[18] C. E. Clayton, K. A. Marsh, A. Dyson, M. Everett, A. Lal, W. P. Leemans, R. Williams, and C. Joshi. Ultrahigh-gradient acceleration of injected electrons by laser-excited relativistic electron plasma waves. *Phys. Rev. Lett.*, 70(1):37–40, 1993.

[19] J. Faure, Y. Glinec, A. Pukhov, S. Kiselev, S. Gordienko, E. Lefebvre, J. P. Rousseau, F. Burgy, and V. Malka. A laser-plasma accelerator producing monoenergetic electron beams. *Nature*, 431:541–544, 2004.

[20] C. G. R. Geddes, Cs. Toth, J. van Tilborg, E. Esarey, C. B. Schroeder, D. Bruhwiler, C. Nieter, J. Cary, and W. P. Leemans. High-quality

electron beams from a laser wakefield accelerator using plasma-channel guiding. *Nature*, 431:538–541, 2004.

[21] S. P. D. Mangles, C. D. Murphy, Z. Najmudin, A. G. R. Thomas, J. L. Collier, A. E. Dangor, E. J. Divall, P. S. Foster, J. G. Gallacher, C. J. Hooker, D. A. Jaroszynski, A. J. Langley, W. B. Mori, P. A. Norreys, F. S. Tsung, R. Viskup, B. R. Walton, and K. Krushelnick. Monoenergetic beams of relativistic electrons from intense laser-plasma interactions. *Nature*, 431:535–538, 2004.

[22] B. Hidding, K.-U. Amthor, B. Liesfeld, H. Schwoerer, S. Karsch, M. Geissler, L. Veisz, K. Schmid, J. G. Gallacher, S. P. Jamison, D. Jaroszynski, G. Pretzler, and R. Sauerbrey. Generation of quasimonoenergetic electron bunches with 80-fs laser pulses. *Phys. Rev. Lett.*, 96(10):105004, 2006.

[23] T. Hosokai, K. Kinoshita, T. Ohkubo, A. Maekawa, M. Uesaka, A. Zhidkov, A. Yamazaki, Hideyuki Kotaki, M. Kando, K. Nakajima, S. V. Bulanov, P. Tomassini, A. Giulietti, and D. Giulietti. Observation of strong correlation between quasimonoenergetic electron beam generation by laser wakefield and laser guiding inside a preplasma cavity. *Phys. Rev. E*, 73:036407, 2006.

[24] C. T. Hsieh, C. M. Huang, C. L. Chang, Y. C. Ho, Y. S. Chen, J. Y. Lin, J. Wang, and S. Y. Chen. Tomography of injection and acceleration of monoenergetic elecrons in a laser wakefield accelerator. *Phys. Rev. Lett.*, 96(095001), 2006.

[25] A. Maksimchuk, S. Reed, S. S. Bulanov, V. Chvykov, G. Kalintchenko, T. Matsuoka, C. McGuffey, G. Mourou, N. Naumova, J. Nees, P. Rousseau, V. Yanovsky, K. Krushelnick, N. H. Matlis, S. Kalmykov, G. Shvets, M. C. Downer, C. R. Vane, J. R. Beene, D. Stracener, and D. R. Schultz. Studies of laser wakefield structures and electron acceleration in underdense plasmas. *Phys. Plasmas*, 15(5):056703, 2008.

[26] E Miura, K Koyama, S Kato, N Saito, M Adachi, Y Kawada, T Nakamura, and M Tanimoto. Demonstration of quasi-monoenergetic electron-beam generation in laser-driven plasma acceleration. *Appl. Phys. Lett.*, 86(25):251501, 2005.

[27] J. Osterhoff, A. Popp, Zs. Major, B. Marx, T. P. Rowlands-Rees, M. Fuchs, M. Geissler, R. Horlein, B. Hidding, S. Becker, E. A. Peralta, U. Schramm, F. Gruner, D. Habs, F. Krausz, S. M. Hooker, and S. Karsch. Generation of stable, low-divergence electron beams by laser-wakefield acceleration in a steady-state-flow gas cell. *Phys. Rev. Lett.*, 101(8):085002, 2008.

[28] A. Pukhov and J. Meyer-ter Vehn. Laser wake field acceleration: the highly non-linear broken-wave regime. *Appl. Phys. B*, 74(4-5):355–361, 2002.

[29] W. P. Leemans, B. Nagler, A. J. Gonsalves, C. Tóth, K. Nakamura, C. G. R. Geddes, E. Esarey, C. B. Schroeder, and S. M. Hooker. Gev electron beams from a centimetre-scale accelerator. *Nature Phys.*, 2(10):696–699, 2006.

[30] J. Faure, C. Rechatin, A. Norlin, A. Lifschitz, Y. Glinec, and V. Malka. Controlled injection and acceleration of electrons in plasma wakefields by colliding laser pulses. *Nature*, 444:737–739, 2006.

[31] D. Umstadter, J. K. Kim, and E. Dodd. Laser injection of ultrashort electron pulses into wakefield plasma waves. *Phys. Rev. Lett.*, 76(12):2073–2076, 1996.

[32] E. Esarey, R. F. Hubbard, W. P. Leemans, A. Ting, and P. Sprangle. Electron injection into plasma wakefields by colliding laser pulses. *Phys. Rev. Lett.*, 79(14):2682–2685, 1997.

[33] C. G. R. Geddes, K. Nakamura, G. R. Plateau, Cs. Toth, E. Cormier-Michel, E. Esarey, C. B. Schroeder, J. R. Cary, and W. P. Leemans. Plasma-density-gradient injection of low absolute-momentum-spread electron bunches. *Phys. Rev. Lett.*, 100(21):215004, 2008.

[34] S. Bulanov, N. Naumova, F. Pegoraro, and J. Sakai. Particle injection into the wave acceleration phase due to nonlinear wake wave breaking. *Phys. Rev. E.*, 58(5):R5257–R5260, 1998.

[35] R. G. Hemker, N. M. Hafz, and M. Uesaka. Computer simulations of a single-laser double-gas-jet wakefield accelerator concept. *Phys. Rev. ST Accel. Beams*, 5(4):041301, 2002.

[36] H. Suk, N. Barov, J. B. Rosenzweig, and E. Esarey. Plasma electron trapping and acceleration in a plasma wake field using a density transition. *Phys. Rev. Lett.*, 86(6):1011–1014, 2001.

[37] D. F. Gordon, R.F. Hubbard, J. H. Cooley, B. Hafizi, A. Ting, and P. Sprangle. Quasimonoenergetic electrons from unphased injection into channel guided laser wakefield accelerators. *Phys. Rev. E*, 71(026404), 2005.

[38] A. G. Khachatryan. Trapping, compression and acceleration of an electron bunch in the nonlinear laser wakefield. *Phys. Rev. E*, 65(4):046504, 2002.

[39] M. J. H. Luttikhof, A. G. Khachatryan, F. A. Van Goor, K.-J. Boller, and P. Mora. Electron bunch injection at an angle into a laser wakefield. *Laser Part. Beams*, 27(1):69–77, 2009.

[40] A. G. Khachatryan, M. J. H. Luttikhof, F. A. van Goor, and K.-J. Boller. Effect of the ponderomotive scattering and injection on electron-bunch injection into a laser wakefield. *Appl. Phys. B*, 86(1):41–47, 2007.

[41] M. J. H. Luttikhof, A. G. Khachatryan, F. A. van Goor, and K.-J. Boller. The effect of the vacuum-plasma transition and an injection angle on electron-bunch injection into a laser wakefield. *Phys. Plasmas*, 14(8):083101, 2007.

[42] A. Irman, M. J. H. Luttikhof, A. G. Khachatryan, F. A. van Goor, J. W. J. Verschuur, H. M. J. Bastiaens, and K.-J. Boller. Design and simulation of laser wakefield acceleration with external electron bunch injection in front of the laser pulse. *J. Appl. Phys.*, 102(2):024513, 2007.

[43] F. F. Chen. *Introduction to plasma physics*. Plenum Press, New York, 1974.

[44] R. A. Loch. *High harmonic generation and ion acceleration with high-intensity laser pulses*. PhD thesis, University of Twente, Enschede, 2009.

[45] W. L. Kruer. *The physics of laser plasma interactions*. Westview Press, Oxford, 2003.

[46] H. A. H. Boot and R. B. R. S. Harvie. Charged particles in a non-uniform radio-frequency field. *Nature*, 180(4596):1187, 1957.

[47] E. Esarey, P. Sprangle, J. Krall, and A. Ting. Self-focusing and guiding of short laser pulses in ionizing gases and plasmas. *IEEE. J. Quantum Electron.*, 33:1879–1914, 1997.

[48] J. M. Dawson. Nonlinear electron oscillations in a cold plasma. *Phys. Rev.*, 113(2):383–387, 1959.

[49] A. I. Akhiezer and R. V. Polovin. Theory of wave motion of an electron plasma. *Sov. Phys. JETP*, 3(5):696–705, 1956.

[50] J. D. Jackson. *Classical electrodynamics*. John Wiley & Sons, Inc., New York, 1999.

[51] K. Okamoto. *Fundamentals of optical waveguides*. Academic Press, Burlington, 2006.

[52] A. Butler, D. J. Spence, and S. M. Hooker. Guiding of high-intensity laser pulses with a hydrogen-filled capillary discharge waveguide. *Phys. Rev. Lett.*, 89(18):185003, 2002.

[53] D. J. Spence and S. M. Hooker. Investigation of a hydrogen plasma waveguide. *Phys. Rev. E*, 63(1):015401, 2000.

[54] D. J. Spence, A. Butler, and S. M. Hooker. Gas-filled capillary discharge waveguides. *J. Opt. Soc. Am. B*, 20(1), 2003.

[55] S. Karsch, J. Osterhoff, A. Popp, T. P. Rowlands-Rees, Zs. Major, M. Fuchs, B. Marx, R. Hrlein, K. Schmid, L. Veisz, S. Becker, U. Schramm, B. Hidding, G. Pretzler, D. Habs, F. Grner, F. Krausz, and S. M. Hooker. Gev-scale electron acceleration in a gas-filled capillary discharge waveguide. *New J. Phys.*, 9(11):415, 2007.

[56] T. P. Rowlands-Rees, C. Kamperidis, S. Kneip, A. J. Gonsalves, S. P. D. Mangles, J. G. Gallacher, E. Brunetti, T. Ibbotson, C. D. Murphy, P. S. Foster, M. J. V. Streeter, F. Budde, P. A. Norreys, D. A. Jaroszynski, K. Krushelnick, Z. Najmudin, and S. M. Hooker. Laser-driven acceleration of electrons in a partially ionized plasma channel. *Phys. Rev. Lett.*, 100(10):105005, 2008.

[57] C. G. Durfee III, J. Lynch, and H. M. Milchberg. Mode properties of a plasma waveguide for intense laser pulses. *Opt. Lett.*, 19(23):1937–1939, 1994.

[58] P. Sprangle, Cha-Mei Tang, and E. Esarey. Relativistic self-focusing of short-pulse radiation beams in plasmas. *IEEE Trans. Plasma Sci.*, 15(2):145–153, 1987.

[59] G. Z. Sun, E. Ott, Y. C. Lee, and P. Guzdar. Self-focusing of short intense pulses in plasmas. *Phys. Fluids*, 30(2):526–532, 1987.

[60] P. Sprangle, E. Esarey, and A. Ting. Nonlinear interaction of intense laser pulses in plasmas. *Phys. Rev. A*, 41(8):4463–4469, 1990.

[61] P. Sprangle, E. Esarey, J. Krall, and G. Joyce. Propagation and guiding of intense laser pulses in plasmas. *Phys. Rev. Lett.*, 69(15):2200–2203, 1992.

[62] T. M. Antonsen and P. Mora. Self-focusing and raman-scattering of laser-pulses in tenuous plasmas. *Phys. Rev. Lett.*, 69(15):2204–2207, 1992.

[63] A. G. Khachatryan. Trapping, compression, and acceleration of an electron beam by the laser wake wave. *JETP Letters*, 74(7):371–374, 2001.

[64] A. G. Khachatryan, F. A. van Goor, K.-J. Boller, A. J. W. Reitsma, and D. A. Jaroszynski. Extremely short relativistic-electron-bunch generation in the laser wakefield via novel bunch injection scheme. *Phys. Rev. ST Accel. Beams*, 7(12):121301, 2004.

[65] L. M. Gorbunov, S. Yu. Kalmykov, and P. Mora. Laser wakefield acceleration by petawatt ultrashort laser pulses. *Phys. Plasmas*, 12(3):033101, 2005.

[66] R. F. Hubbard, D. F. Gordon, J. H. Cooley, B. Hafizi, T. G. Jones, D. Kaganovich, P. Sprangle, A. Ting, and A. Zigler. Trapping and acceleration of nonideal injected electron bunches in laser wakefield accelerators. *IEEE Trans. Plasma Sci.*, 33(2):712–722, 2005.

[67] A. F. Lifschitz, J. Faure, V. Malka, and P. Mora. Gev wakefield acceleration of low energy electron bunches using petawatt lasers. *Phys. Plasmas*, 12(9):093104, 2005.

[68] T. Esirkepov, S. V. Bulanov, M. Yamagiwa, and T. Tajima. Electron, positron, and photon wakefield acceleration: trapping, wake overtaking, and ponderomotive acceleration. *Phys. Rev. Lett.*, 96:014803, 2006.

[69] S. Yu. Kalmykov, L. M. Grobunov, P. Mora, and G. Shvets. Injection, trapping, and acceleration of electrons in a three dimensional nonlinear laser wakefield. *Phys. Plasmas*, 13(11):113102, 2006.

[70] A. G. Khachatryan, M. J. H. Luttikhof, A. Irman, F. A. van Goor, J. W. J. Verschuur, H. M. J. Bastiaens, and K.-J. Boller. Conceptual design of a laser wakefield acceleration experiment with external bunch injection. *Nucl. Instrum. Methods A*, 566(2):244–249, 2006.

[71] F. Amiranoff, S. Baton, D. Bernard, B. Cros, D. Descamps, F. Dorchies, F. Jacquet, V. Malka, J. R. Marquès, G. Matthieussent, P. Miné, A. Modena, P. Mora, J. Morillo, and Z. Najmudin. Observation of laser wakefield acceleration of electrons. *Phys. Rev. Lett.*, 81(5):995–998, 1998.

[72] W. van Dijk, S. B. van der Geer, M. J. van der Wiel, and G. J. H. Brussaard. Parameter study of acceleration of externally injected electrons in the linear laser wakefield regime. *Phys. Plasmas*, 15(9):093102, 2008.

[73] W van Dijk, J. M. Corstens, S. B. van der Geer, M. J. van der Wiel, and G. J. H. Brussaard. Effects of timing and stability on laser wakefield acceleration using external injection. *Phys. Rev. ST Accel. Beams*, 12(5):051304, 2009.

[74] W. H. Urbanus, W. van Dijk, S. B. van der Geer, G. J. H. Brussaard, and M. J. van der Wiel. Front-to-end simulations of the design of a laser wakefield accelerator with external injection. *J. Appl. Phys.*, 99(11):114501, 2006.

[75] M. J. van der Wiel, O. J. Luiten, G. J. H. Brussaard, S. B. van der Geer, W. H. Urbanus, W. van Dijk, and Th. van Oudheusden. Laser wakefield acceleration: the injection issue. overview and latest results. *Phil. Trans. R. Soc.*, 364(1840):679–687, 2006.

[76] M. Levin, A. Pukhov, R. F. Hubbard, D. Kaganovich, D. F. Gordon, P. Sprangle, A. Ting, B. Hafizi, and A. Zigler. Longitudinal profiles of plasma parameters in a laser-ignited capillary discharge and implications for laser wakefield accelerator applications. *Appl. Phys. Lett.*, 87:261501, 2005.

[77] N. E. Andreev, L. M. Gorbunov, V. I. Kirsanov, K. Nakajima, and A. Ogata. Structure of the wake field in plasma channels. *Phys. Plasmas*, 4(4):1145–1153, 1997.

[78] B. Quesnel and P. Mora. Theory and simulation of the interaction of ultraintense laser pulses with electrons in vacuum. *Phys. Rev. E*, 58(3):3719–3732, 1998.

[79] S. V. Bulanov, F. Pegoraro, and A. M. Pukhov. Two-dimensional regimes of self-focusing, wake field generation, and induced focusing of a short intense laser pulse in an underdense plasma. *Phys. Rev. Lett.*, 74(5):710–713, 1995.

[80] S. V. Bulanov and A. S. Sakharov. Induced focusing of electromagnetic-wave in a wake plasma-wave. *JETP Lett.*, 54(4):203–207, 1991.

[81] S. V. Bulanov, F. Pegoraro, A. M. Pukhov, and A. S. Sakharov. Transverse-wake wave breaking. *Phys. Rev. Lett.*, 78(22):4205–4208, 1997.

[82] W. H. Press, S. A. Teukolsky, W. T. Vetterling, and B. P. Flannery. *Numerical recipes in C++: The art of scientific computing*. Cambridge University Press, London, 2002.

[83] A. G. Khachatryan. Excitation of nonlinear two-dimensional wake waves in radially nonuniform plasma. *Phys. Rev. E*, 60(5):6210–6213, 1999.

[84] P. Mora and T.M. Antonsen. Electron cavitation and acceleration in the wake of an ultraintense, self-focused laser pulse. *Phys. Rev. E.*, 53(3):R2068–R2071, 1996.

[85] D. F. Gordon, B Hafizi, R. F. Hubbard, J. R. Penano, P Sprangle, and A Ting. Asymmetric self-phase modulation and compression of short laser pulses in plasma channels. *Phys. Rev. Lett.*, 90(21):215001, 2003.

[86] A. Irman. *Integral design of a laser wakefield accelerator with external bunch injection*. PhD thesis, University of Twente, Enschede, 2009.

[87] General Particle Tracer code (http://www.pulsar.nl/gpt).

[88] N. A. M. Hafz, T. M. Jeong, I. W. Choi, S. K. Lee, K. H. Pae, V. V. Kulagin, J. H. Sung, T. J. Yu, K.-H. Hong, T. Hosokai, J. R. Cary, D.-K. Ko, and J. Lee. Stable generation of gev-class electron beams from self-guided laser-plasma channels. *Nature Photon.*, 2(9):571–577, 2008.

[89] C. M. S. Sears, E. Colby, R. Ischebeck, C. McGuinness, J. Nelson, R. Noble, R. H. Siemann, J. Spencer, D. Walz, T. Plettner, and R. L. Byer. Production and characterization of attosecond electron bunch trains. *Phys. Rev. ST Accel. Beams*, 11(6):061301, 2008.

[90] N. Naumova, I. Sokolov, J. Nees, A. Maksimchuk, V. Yanovsky, and G. Mourou. Attosecond electron bunches. *Phys. Rev. Lett.*, 93(19):195003, 2004.

[91] G. V. Stupakov and M. S. Zolotorev. Ponderomotive laser acceleration and focusing in vacuum for generation of attosecond electron bunches. *Phys. Rev. Lett.*, 86(23):5274–5277, 2001.

[92] I. Y. Dodin and N. J. Fisch. Stochastic extraction of periodic attosecond bunches from relativistic electron beams. *Phys. Rev. Lett.*, 98(23):234801, 2007.

[93] V. V. Kulagin, V. A. Cherepenin, M. S. Hur, and H. Suk. Theoretical investigation of controlled generation of a dense attosecond relativistic electron bunch from the interaction of an ultrashort laser pulse with a nanofilm. *Phys. Rev. Lett.*, 99(12):124801, 2007.

[94] A. Karmakar and A. Pukhov. Collimated attosecond gev electron bunches from ionization of high-z material by radially polarized ultra-relativistic laser pulses. *Laser Part. Beams*, 25(3):371–377, 2007.

[95] T. V. Liseykina, S. Pirner, and D. Bauer. Relativistic attosecond electron bunches from laser-illuminated droplets. *Phys. Rev. Lett.*, 104(9):095002, 2010.

[96] Y.-Y. Ma, Z.-M. Sheng, Y.-T. Li, W.-W. Chang, X.-H. Yuan, M. Chen, H.-C. Wu, J. Zheng, and J. Zhang. Dense quasi-monoenergetic attosecond electron bunches from laser interaction with wire and slice targets. *Phys. Plasmas*, 13(11):110702, 2006.

[97] Jr. Humphries. *Charged particle beams.* John Wiley and Sons, New York, 1990.

[98] A. G. Khachatryan, A. Irman, F. A. van Goor, and K.-J. Boller. Femtosecond electron-bunch dynamics in laser wakefields and vacuum. *Phys. Rev. ST Accel. Beams*, 10(12):121301, 2007.

[99] Y. Glinec, J. Faure, A. Norlin, A. Pukhov, and V. Malka. Observation of fine structures in laser-driven electron beams using coherent transition radiation. *Phys. Rev. Lett.*, 98(19):194801, 2007.

[100] A. G. Khachatryan, F. A. van Goor, and K.-J. Boller. Coherent and incoherent radiation from a channel-guided laser wakefield accelerator. *New J. Phys.*, 10:083043, 2008.

[101] K. Németh, B. Shen, Y. Li, H. Shang, R. Crowell, K. C. Harkay, and J. R. Cary. Laser-driven coherent betatron oscillation in a laser-wakefield cavity. *Phys. Rev. Lett.*, 100(9):095002, 2008.

[102] Z. Huang and K.-J Kim. Review of x-ray free-electron laser theory. *Phys. Rev. ST Accel. Beams*, 10(3):034801, 2007.

[103] K. Nalkajima. Towards a table-top free-electron laser. *Nature Phys.*, 4(2):92–93, 2008.

[104] H. P. Schlenvoigt, K. Haupt, A. Debus, F. Budde, O. Jaeckel, S. Pfoten-
      hauer, H. Schwoerer, E. Rohwer, J. G. Gallacher, E. Brunetti, R. P.
      Shanks, S. M. Wiggins, and D. A. Jaroszynski. A compact synchrotron
      radiation source driven by a laser-plasma wakefield accelerator. *Nature
      Phys.*, 4(2):130–133, 2008.

[105] M. Fuchs, R. Weingartner, A. Popp, Zs. Major, S. Becker, J. Oster-
      hoff, I. Cortrie, B. Zeitler, R. Hoerlein, G. D. Tsakiris, U. Schramm,
      T. P. Rowlands-Rees, S. M. Hooker, D. Habs, F. Krausz, S. Karsch,
      and F. Gruener. Laser-driven soft-x-ray undulator source. *Nature Phys.*,
      5(11):826–829, 2009.

[106] K. Floettmann. Some basic features of the beam emittance. *Phys. Rev.
      ST Accel. Beams*, 6(3):034202, 2003.

Dankwoord

Dit proefschrift is een afsluiting van een periode van vier jaren onderzoek. Promotieonderzoek waar ik de afgelopen jaren met veel plezier aan heb gewerkt. Een promotie kun je echter niet alleen en ik wil daarom op deze plaats iedereen bedanken die mij op de een of andere manier heeft geholpen met het tot stand komen van dit proefschrift.

Om te beginnen wil ik mijn promotor, Klaus Boller, bedanken voor de mogelijkheid om dit promotieonderzoek te doen. Bedankt voor je wetenschappelijke begeleiding en je enthousiasme voor het onderzoek. Ook bedankt voor je kritische commentaren en suggesties voor het verbeteren van dit proefschrift.

Vervolgens wil ik mijn copromotor, Arsen Khachatryan, bedanken voor de plezierige samenwerking en dagelijkse begeleiding. Ik bewonder jouw enorme vakkennis. Ik heb veel van je geleerd in de vele discussies die we hadden en zonder jouw wetenschappelijke begeleiding zou dit proefschrift er niet zijn gekomen.
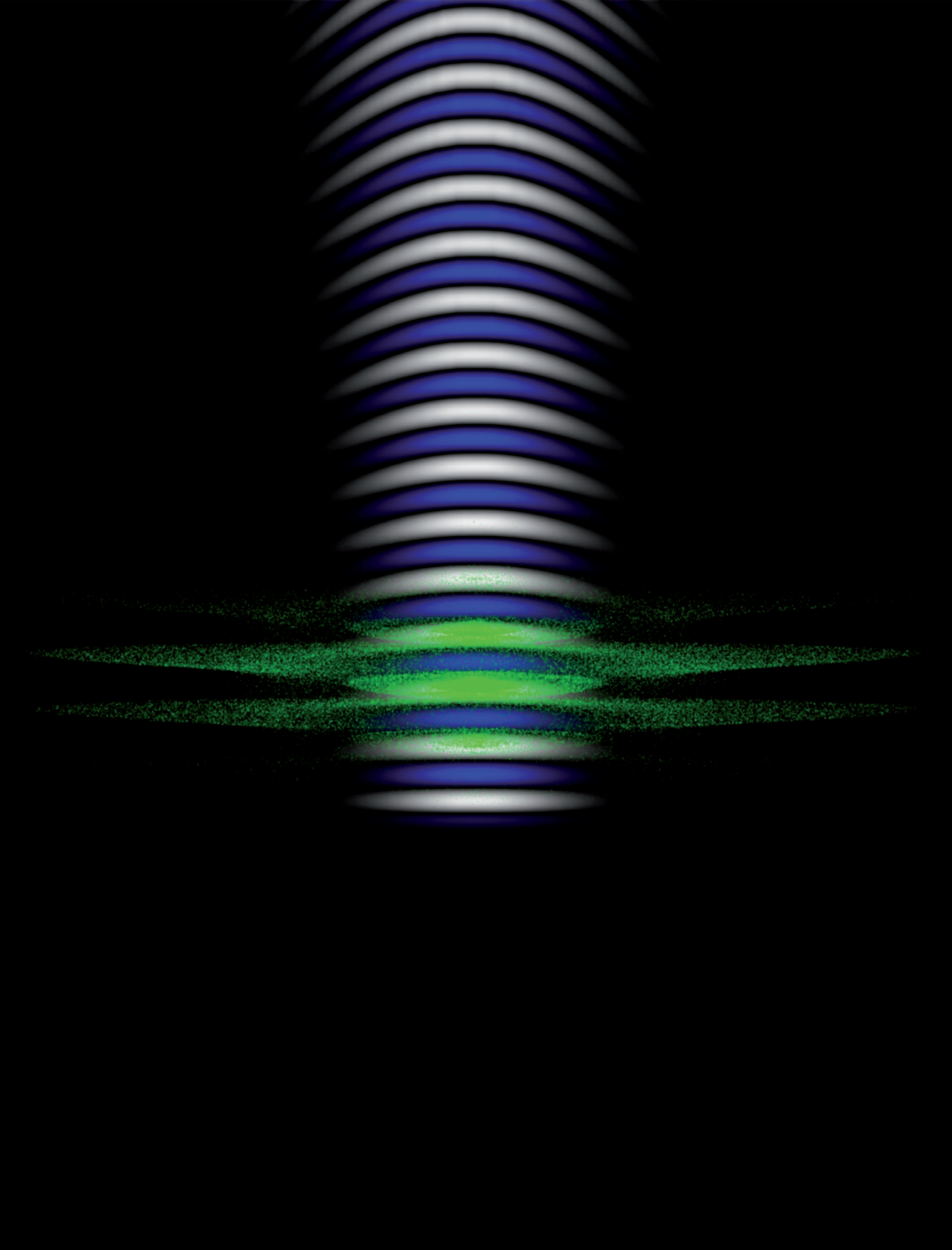
Verder wil ik Fred van Goor bedanken. Voor vragen of hulp kon ik ook altijd bij jou terecht. In het bijzonder wil ik Arie en Rolf bedanken voor de prettige samenwerking en de vele interessante discussies. Rolf en Thijs bedankt dat jullie mij als paranimfen willen bijstaan tijdens de verdediging. De leden van mijn promotiecommissie wil ik bedanken voor de tijd en moeite die ze gestoken hebben in het lezen en bestuderen van dit proefschrift. Ik wil Donna bedanken voor het controleren van het Engels in dit proefschrift en professor Patrick Mora voor het mogen gebruiken van de WAKE code en voor zijn uitgebreide uitleg van deze code.

Een goede werksfeer bepaalt voor een groot gedeelte of je plezier hebt in je werk. Daarom wil ik de hele vakgroep bedanken voor de fijne werksfeer en het plezier dat in overvloed aanwezig was. Tijdens de promotie heb ik veel groepsleden zien komen en gaan. Ik wil dan ook al mijn collega's bedanken: Ab, Anton, Arco, Balaji, Bas-Jan, Bert, Bob, Cees, Chris, Claudia, Denny, Denis, Dimitri, Edip, Elena, Feng, Fred, Gerald, Gerard, Ian, Isabel, Jacob, Jean, Jelle, Jeroen, Joan, Johan, Johan-Martijn, Hein, Kasper, Kees, Lantian, Lars, Leon, Lilian, Liviu, Marten, Martijn, Muharrem, Olivier, Peter, Petra, Piet, Ramon, Robert, Roel, Ronald, Ruud, Simone, Thomas, Tom en Willem.

Tenslotte wil ik mijn ouders, broer en zus bedanken voor hun onvoorwaardelijke steun gedurende mijn promotie en de voorafgaande studie.

Allemaal bedankt!

Mark Luttikhof